UNIVERSITÀ DELLA CALABRIA

UNIVERSITÀ DELLA CALABRIA

Dipartimento di Farmacia e Scienze della Salute e della Nutrizione

Dottorato di Ricerca in

MEDICINA TRASLAZIONALE

CICLO

XXXI

Genomics-based discovery and anticancer activity assessment of new Thioviridamide-like molecules produced by *Actinobacteria*

Settore Scientifico Disciplinare BIO/10

Coordinatore: Ch.mo Prof. Sebastiano Andò

Supervisore/Tutor: Ch.ma Prof.ssa Anna Rita Cappello

Dottorando: Dott. Luca Frattaruolo

Presentazione al Collegio dei Docenti del Dott. Luca Frattaruolo per il conseguimento del titolo di "Dottore di Ricerca in Medicina Traslazionale" (XXXI ciclo)

Il cancro è considerato, attualmente, una patologia che rappresenta la principale causa di morte in tutto il mondo. La resistenza alla chemioterapia e alle terapie mirate a livello molecolare insieme agli effetti collaterali dei chemioterapici ed alla loro tossicità nei confronti delle cellule sane costituiscono enormi minacce al trattamento della malattia. A tal proposito, la ricerca scientifica e l'innovazione tecnologica sono orientate verso lo sviluppo di nuovi approcci terapeutici mirati a superare questi problemi.

In questo contesto, si inserisce l'attività di ricerca svolta dal Dott. Luca Frattaruolo, durante il dottorato di Ricerca in "Medicina Traslazionale" (XXXI ciclo), rivolta allo studio di composti naturali, allo scopo di individuare nuove molecole con potenzialità antitumorali.

In particolare, il suo progetto di dottorato ha avuto l'obbiettivo di identificare, in *Actinobacteria*, nuovi prodotti naturali, analoghi della Thioviridamide, appartenenti ad una particolare classe di metaboliti secondari (RiPPs), di studiarne l'origine biosintetica e di effettuarne la caratterizzazione chimico-funzionale allo scopo di comprendere i meccanismi molecolari alla base del loro potenziale farmacologico.

Gli Attinomiceti sono batteri Gram-positivi aerobi che colonizzano principalmente il suolo, da cui ricavano molteplici componenti organici che utilizzano come fonte di energia. Sono microrganismi da molti anni al centro dell'interesse della ricerca biotecnologica e farmaceutica in quanto, grazie alla produzione di metaboliti secondari biologicamente attivi, rappresentano una delle principali fonti di composti naturali dotati di attività farmacologica, attualmente in fase di sperimentazione preclinica e clinica.

I RiPPs sono una classe di peptidi, sintetizzati a livello ribosomiale e modificati a livello post-traduzionale, caratterizzati da una profonda diversità chimica risultante dall'ampia gamma di processi di maturazione a cui un peptide precursore, codificato geneticamente, può andare incontro conferendo ai prodotti un'ampia varietà di attività biologiche.

La Thioviridamide è un RiPP biosintetizzato da *Streptomyces olivoviridis* NA005001 caratterizzato da una potente attività antiproliferativa e pro-apoptotica in diverse linee cellulari tumorali. La caratteristica peculiare della molecola è rappresentata dalla presenza di 5 gruppi tioammidici che sostituiscono quelli ammidici nello scheletro peptidico. Recentemente, il cluster genico responsabile della biosintesi della Thioviridamide è stato identificato e confermato mediante espressione eterologa.

In primo luogo, il lavoro svolto dal Dott. Frattaruolo ha permesso di identificare, mediante studi di bioinformatica, diversi microrganismi che nel loro genoma presentano cluster genici simili a quello responsabile della biosintesi della Thioviridamide, ma con leggere differenze che rendono tali organismi potenziali produttori di molecole analoghe. I batteri identificati, appartenenti al phylum degli *Actinobacteria*, sono stati studiati e l'analisi LC/MS dei prodotti del loro metabolismo secondario ha permesso di identificare 3 nuove molecole:

- la Thiostreptamide S4, prodotto da *Streptomyces* sp. NRRL S 4;
- la Thiostreptamide S87, prodotto da *Streptomyces* sp. NRRL S-87;
- la Thioalbamide, prodotto da *Amycolatopsis alba* DSM 44262.

La correlazione tra i cluster genici e i nuovi prodotti naturali identificati è stata confermata mediante due diversi approcci sperimentali, biologico-molecolari:

1. delezione del cluster genico nel ceppo batterico produttore, che ha portato alla generazione di mutanti incapaci di produrre i composti identificati;
2. espressione eterologa del cluster genico, che ha portato alla produzione dei composti precedentementi identificati in un microorganismo ospite, *Streptomyces coelicolor* M1146.

Questi risultati hanno permesso di stabilire che la Thioviridamide non è una molecola unica nel suo genere, ma fa parte di una famiglia di composti, identificati per la prima volta in questo studio, a cui, da oggi, è stato dato il nome di Thioviridamide-like molecules (TLMs).

Successivamente, è stato effettuato uno scale-up dei processi fermentativi degli *Actinobacteria* produttori dei TLMs che ha permesso la purificazione dei tre composti precedentemente identificati. I tre prodotti purificati sono stati caratterizzati chimicamente mediante studi di risonanza magnetica nucleare (NMR), monodimensionale e bidimensionale, ed analisi di spettrometria di massa tandem (MS2), ed è stata stabilita, con certezza, la loro struttura chimica. Gli studi strutturali hanno consentito, inoltre, di evidenziare le differenze tra i nuovi TLMs e la Thioviridamide, dovute a leggere difformità sia dei peptidi precursori che degli enzimi di maturazione che intervengono durante i processi biosintetici.

Tra i nuovi composti identificati, la Thioalbamide è stato purificato in maggiore quantità e sottoposto a studi *in vitro*, eseguiti su diversi modelli biologici procariotici ed eucariotici.

I risultati ottenuti hanno evidenziato un'intensa attività anti-proliferativa, già a concentrazioni nell'ordine del nanomolare, altamente selettiva nei confronti di diverse linee cellulari tumorali e migliore di quella evidenziata, nelle stesse condizioni sperimentali, dalla doxorubicina, antibiotico antitumorale utilizzato, in clinica, nel trattamento di diverse neoplasie.

Al contrario, non è stata riscontrata alcuna attività inibitoria nei confronti di batteri e lieviti.

Studi successivi di microscopia e citofluorimetria hanno permesso di indagare, per la prima volta, sugli eventi cellulari indotti dalla Thioalbamide, allo scopo di individuare i meccanismi molecolari alla base della attività anti-proliferativa riscontrata, in linee cellulari di carcinoma mammario, che riflettono la diversità biologica di diversi sottotipi molecolari di breast cancer. A tal fine, sono stati utilizzati diversi tipi di cellule di tumore mammario, capaci di esprimere o meno il recettore estrogenico (ER), quello progestinico (PR) e il recettore 2 per il fattore di crescita epidermico umano (HER2). In particolare, gli esperimenti sono stati condotti su cellule **MCF7** (ER+, PR+/-, HER2-); **T47 D** (ER+, PR+, HER2-); **MDA-MB-231** (ER-, PR-, HER2-); **SKBR3** (ER-, PR-, HER2+).
Dai risultati è emerso che Thioalbamide ha la capacità di determinare cambiamenti nella morfologia cellulare, di bloccare il ciclo cellulare in fase G1 e di innescare processi apoptotici, attraverso pathways estrinseci ed intrinseci. Inoltre, l'accumulo di specie reattive dell'ossigeno (ROS), nelle cellule trattate, ha permesso di ipotizzare la capacità del peptide di indurre stress ossidativo. Il co-trattamento delle cellule con Vitamina E, potente scavenger dei ROS, ha determinato la perdita dell'attività anti-proliferativa della molecola, dimostrando che lo stress ossidativo è il fenomeno scatenante la morte cellulare indotta dalla nuova molecola, in tutte le linee cellulari testate. L'aumento dei ROS è risultato essere, inoltre, accompagnato da un aumento dell'attività delle superossido dismutasi (SODs), enzimi deputati alla neutralizzazione dell'anione superossido, che ha permesso di escludere un fenomeno di stress ossidativo dovuto a deficit enzimatico. L'aumento dell'attività delle SODs, indotto dalla Thioalbamide, è risultato essere tuttavia limitato nel tempo e, dopo 72 ore di trattamento, l'effetto tamponante delle SODs non è stato più sufficiente a contrastare la produzione di ROS, con conseguente attivazione del processo apoptotico. L'analisi dei livelli di espressione delle due isoforme della superossido-dismutasi (SOD 1 e SOD2), ha evidenziato un incremento selettivo dell'isoforma mitocondriale (SOD2), suggerendo una overproduzione dei ROS a livello dei mitocondri e il loro coinvolgimento nel meccanismo d'azione del peptide.

Infine, mediante tecnologia Agilent Seahorse XF è stata valutata la capacità del composto di influenzare il metabolismo della cellula tumorale ed i risultati hanno evidenziato, dopo trattamento, un abbattimento del consumo di ossigeno (OCR) e dell'acidificazione extracellulare (ECAR), riflettendo la capacità della nuova molecola di influenzare negativamente le due principali vie di produzione energetica, la via glicolitica e la fosforilazione ossidativa. La riduzione di OCR, in particolare, rispecchia un'alterazione della funzionalità della catena di trasporto degli elettroni, mitocondriale. È noto che i processi metabolici mitocondriali sono indispensabili per la crescita e propagazione delle cancer stem-like cells (CSCs), una sottopopolazione di cellule tumorali responsabile della resistenza del tumore ai chemioterapici, della ricorrenza neoplastica e del processo di metastatizzazione. Pertanto, i risultati ottenuti hanno portato il Dott. Frattaruolo ad indagare su

un'eventuale coinvolgimento della Thioalbamide, nella formazione di *mammospheres* e a dimostrarne, dopo trattamento, un decremento nella efficienza della formazione e propagazione, delle CSCs, confermando così l'abilità del composto di interferire con la bioenergetica della cellula tumorale.

Attualmente, sono in corso:

- studi di proteomica, allo scopo di comprendere esattamente le vie metaboliche coinvolte per individuare l'esatto target molecolare della Thioalbamide;
- studi, *in vivo*, per valutare gli effetti anti-proliferativi su modelli xenograft e sullo sviluppo di metastasi, al fine di compiere un ulteriore step nel processo di traslazione dalla ricerca di base alla clinica.

Il Dott. Frattaruolo, durante il triennio del Dottorato in Medicina Traslazionale, ha frequentato assiduamente il laboratorio di Biochimica e Biotecnologie molecolari del Dipartimento di Farmacia e Scienze della Salute e della Nutrizione, sotto la supervisione della Prof.ssa Anna Rita Cappello ed ha svolto regolarmente le attività di studio e di ricerca previste per il corso di dottorato. Complessivamente, durante il triennio ha dimostrato entusiasmo e notevole attitudine alla ricerca. Dotato di spirito critico nella pianificazione dell'attività di ricerca e nell'elaborazione ed interpretazione dei risultati sperimentali, ha acquisito buona padronanza delle metodologie utilizzate che si evince dalla capacità di svolgere attività di ricerca in grande autonomia e con senso di responsabilità. Ha avuto modo di confrontarsi ed integrarsi al meglio con l'ambiente di lavoro, conseguendo una piena crescita sia sul piano scientifico che personale ed ha seguito e supportato studenti per lo svolgimento di tesi sperimentali con grande dedizione e diligenza.

Inoltre, il Dott. Frattaruolo ha accresciuto l'esperienza maturata durante il corso di dottorato con un periodo di formazione all'estero (01/03/2016–01/09/2016; 21/11/2016–01/03/2017), svolto presso il Department of molecular Microbiology, del John Innes Centre di Norwich (UK), sotto la guida del Dr. Andrew Truman.

Il contributo scientifico del Dott. Luca Frattaruolo è dimostrato dai lavori pubblicati su riviste peer-reviewed la cui rilevanza scientifica della collocazione editoriale è di buon livello.

Pertanto, si esprime un giudizio ampiamente positivo sull'attività svolta dal Dott. Luca Frattaruolo nel triennio di Dottorato.

Elenco Pubblicazioni

- Perri, F., Haworth, I., **Frattaruolo, L.**, Brindisi, M., El-magboub, A., Ferrario, A., Gomer, C., Aiello, F. & Adams, J.D. Naturally occurring sesquiterpene lactones and their semi-synthetic

derivatives modulate PGE2 levels by decreasing COX2 activity and expression. Helyion (UNDER REVISION).

- Santos-Aberturas, J., Chandra, G., **Frattaruolo, L.**, Lacret, R., Pham, T.H., Miguel-Vior, N., Eyles, T.H. & Truman, A.W. Uncovering the unexplored diversity of thioamidated ribosomal peptides in Actinobacteria using the RiPPER genome mining tool. Nucleic Acids Research (UNDER REVISION).
- **Frattaruolo, L.**, Aiello, F., Carullo, G., Fiorillo, M., Brindisi, M., Cappello, M.S., Pilco, G. & Cappello, A.R (2018). Polyunsaturated Fatty Acids and their Role in the Diet of Cancer Patients: An Overview. International Journal of Nutritional Sciences, 3(2): 1024.
- Tundis, R., **Frattaruolo, L.**, Carullo, G., Armentano, B., Badolato, M., Loizzo, M. R., ... & Cappello, A. R. (2018). An ancient remedial repurposing: synthesis of new pinocembrin fatty acid acyl derivatives as potential antimicrobial/anti-inflammatory agents. Natural product research, 1-7.
- Li, Y., Cappello, A. R., Muto, L., Martello, E., Madeo, M., Curcio, R., Lunetti, P., Raho, S., Zaffino, F., **Frattaruolo, L.**, Lappano, R., Malivindi, R., Maggiolini, M., Aiello, D., Piazzolla, C., Capobianco, L., Fiermonte, G., Dolce, V. R. (2018). Functional characterization of the partially purified Sac1p-independent adenine nucleotide transport system (ANTS) from yeast endoplasmic reticulum. The Journal of Biochemistry.
- **Frattaruolo, L.**, Lacret, R., Cappello, A. R., & Truman, A. W. (2017). A genomics-based approach identifies a thioviridamide-like compound with selective anticancer activity. ACS chemical biology, 12(11), 2815-2822.
- Carullo, G., Cappello, A. R., **Frattaruolo, L.**, Badolato, M., Armentano, B., & Aiello, F. (2017). Quercetin and derivatives: useful tools in inflammation and pain management. Future medicinal chemistry, 9(1), 79-93.
- Ozsvari, B., Fiorillo, M., Bonuccelli, G., Cappello, A. R., **Frattaruolo, L.**, Sotgia, F., Trowbridge, R., Foster, R., Lisanti, M. P. (2017). Mitoriboscins: Mitochondrial-based therapeutics targeting cancer stem cells (CSCs), bacteria and pathogenic yeast. Oncotarget, 8(40), 67457.

Poster communications

- **L. Frattaruolo**, M. Fiorillo, M. Brindisi, R. Curcio, R. Lacret, F. Zaffino, V. Dolce, A.W. Truman, F. Sotgia, M.P. Lisanti, A.R. Cappello, Elucidating Thioalbamide activity: new insights into TLMs anticancer Mechanism, V FISV CONGRESS • Rome, Italy - September 18-21, 2018 pag. 169

- M. Brindisi, M. Bonesi, B. Armentano, L. **Frattaruolo, R.** Curcio, G. Bedini, L. Peruzzi, R. Tundis, M.S. Cappello, Santolina corsica Jord. & Fourr. extracts exert pro-apoptotic activity and inhibit breast adenocarcinoma cell (MDA-MB-231) migration, XV FISV CONGRESS • Rome, Italy - September 18-21, 2018 pag. 167 R.
- Mancuso, B. Armentano, **L. Frattaruolo**, M. Brindisi, R. Curcio, V. Rago, R. Lappano, M. Fiorillo, V. Dolce, M. Maggiolini, B. Gabriele, A.R. Cappello, "In vitro antiproliferative and proapoptotic activities of new 2-oxazolidinone derivatives". CDCO• Milano, Italy – September 0913, 2018.
- A.R. Cappello, L. Muto, Y, Li, P. Scarcia, V. Rago, P. Lunetti, R.Curcio, R. Malivindi, F. Zaffino, F. Pezzuto, M. Fiorillo, V. Dolce, **L. Frattaruolo**, B. Armentano, E. Spagnolo, L. Capobianco, "Physiological role of membrane citrate transporters in prostate tumor progression". THE FUTURE OF CANCER THERAPY: THE GENOME EDITING ERA• Catanzaro, Italy – June 08-09, 2017.

Partecipazione a seminari e workshop

- Partecipazione al workshop "Novel strategies of translational medicine in oncology", 22 Giugno 2018, Sala Seminari Laboratorio di Medicina Traslazionale, Università della Calabria.
- Partecipazione al seminario "Nuovi farmaci antitumorali di derivazione virale", Prof. Arnaldo Caruso, 24 Aprile 2018, Aula 52 – Capannone F, Università della Calabria.
- Partecipazione al corso di "Advanced English", Dott.ssa Anna Franca Plastina, 2-23 Maggio 2018, Aula seminari Dipartimento FSSN, Università della Calabria.
- Partecipazione al corso di "Metabolomica", Dott. Amerigo Beneduci, 11-13 Luglio 2017, Aula Bucci - cubo 15D, Università della Calabria.
- Partecipazione al corso di "Capacità sequestrante di leganti naturali nei confronti di metalli biodisponibili", Dott.ssa Emilia Furia, 12-14 Luglio 2017,Aula Bucci - cubo 15D, Università della Calabria.
- Partecipazione al corso "Antioxidant Reaction Mechanisms and Oxidative Stress", Dott.ssa Gloria Mazzone, 27-28 Giugno 2017, Aula CH-17-7A-1T - Cubo 17/C, Università della Calabria.
- Partecipazione al seminario "Conditional targeted somatic mutagenesis in the mouse", prof. Daniel Metzger, 12 Giugno 2017, aula Seminari del Centro Sanitario, Università della Calabria.

- Partecipazione al seminario "Recent Advances Towards Personalized Chemotherapy", Prof. Tamer Shoeib, 4 Maggio 2017, aula Seminari del Dipartimento di Chimica e Tecnologie Chimiche, Università della Calabria.
- Partecipazione al corso di "informatica", Ing. Andrea Tagarelli, 18 Aprile – 23 Maggio 2017, Aula Seminari Dipartimento FSSN, Università della Calabria.
- Partecipazione al seminario "An Atomistic View of Human Diseases", Dott.ssa Alessandra Magistrato, 10 Dicembre 2015, Aula Terenzi – cubo 12c, Università della Calabria.
- Partecipazione al corso "NMR for organic and biological chemistry: Old experiments for new applications. Theoretical and practical overview", Dott. Ignacio Delso Hernàndez, 24 Novembre – 3 Dicembre 2015, Sala Terenzi cubo 12C, Università della Calabria.

Rende 25/02/2019

Il docente tutor

Prof. ssa Anna Rita Cappello

INDEX

ABSTRACT
(ITALIAN VERSION)

Fin dalla scoperta della penicillina da parte di Alexander Fleming nel 1928, i prodotti naturali microbici hanno rappresentato una risorsa essenziale per lo sviluppo di nuovi agenti farmacologici. All'interno dell'immenso panorama di microorganismi che popolano gli ecosistemi terrestri e marini, i batteri appartenenti al phylum *Actinobacteria* rappresentano la principale fonte di molecole naturali bioattive. Il metabolismo secondario di questi mircroorganismi, infatti, è complesso e molto variabile, ed è responsabile della produzione di molecole molto diverse dal punto di vista chimico, biosintetico e dell'attività biologica.

Una classe di metaboliti secondari relativamente recente ma in rapida espansione, è rappresentata dai peptidi sintetizzati a livello ribosomiale e modificati a livello post-traduzionale (RiPPs). Questi prodotti naturali peptidici sono dotati di diverse attività biologiche e un enorme potenziale farmacologico, con uno spettro di attività che include, tra le tante, quella antibatterica, antitumorale, ipolipidemizzante e immunomodulatrice. L'evidenza del potenziale biologico di queste molecole ha, pertanto, spinto l'interesse della ricerca biotecnologica e farmaceutica a concentrarsi su questa classe di metaboliti secondari. L'attenzione è rivolta, in particolare, all'identificazione di nuovi ceppi batterici produttori di RiPPs bioattivi e alla caratterizzazione dei pathway biosintetici, allo scopo di comprendere meglio gli aspetti biochimici alla base della loro biosintesi.

In questo scenario si colloca la thioviridamide, RiPP biosintetizzato da *Streptomyces olivoviridis* NA005001 e caratterizzato da una potente attività antiproliferativa e pro-apoptotica nei confronti di diverse linee cellulari tumorali. Questo composto peptidico, unico nel suo genere, presenta un gruppo 2-idrossi-2-metil-4-oxopentanoile all'estremità N-terminale, un residuo di β-idrossi-N_1,N_3-dimetilistidinio (hdmHis), un residuo di S-(2-aminovinil)-cisteina (AviCys) che fa parte di un macro-ciclo e cinque gruppi tioammidici che sostituiscono i gruppi ammidici nello scheletro peptidico. Recentemente, il cluster genico responsabile della biosintesi della thioviridamide è stato identificato, dimostrando l'origine ribosomiale di questa molecola, ma i processi biosintetici alla base della sua produzione non sono ancora completamente noti. La promettente attività antitumorale della thioviridamide, così come la sua peculiare struttura chimica e l'interessante pathway biosintetico, rendono questo composto estremamente interessante agli occhi della ricerca.

La prima parte di questo lavoro di tesi ha avuto l'obbiettivo di identificare, mediante un approccio genomico, nuovi prodotti naturali, analoghi della thioviridamide, biosintetizzati da *Actinobacteria*, e di effettuarne la caratterizzazione chimico-funzionale, allo scopo di valutarne il potenziale antitumorale.

Studi bioinformatici, basati sull'utilizzo di tools per l'analisi di omologie di sequenza, hanno permesso di individuare, all'interno del vasto panorama di batteri dal genoma noto, microorganismi contenenti nel proprio genoma cluster genici simili a quello responsabile della biosintesi della thioviridamide. I cluster genici identificati in questi microorganismi sono risultati essere leggermente difformi da quello presente in *S. olivoviridis*, con differenze sia a livello del peptide precursore e sia a livello dei sistemi enzimatici di maturazione che lo convertono in un RiPP maturo. Tali microorganismi, pertanto, appaiono essere potenziali produttori di molecole strutturalmente analoghe alla thioviridamide, con caratteristiche chimiche e biologiche sconosciute alla comunità scientifica.

Tre dei diversi ceppi batterici identificati si sono rivelati capaci di produrre, in determinate condizioni sperimentali, molecole analoghe alla thioviridamide:

- Thiostreptamide S4, prodotto da *Streptomyces* sp. NRRL S-4

- Thiostreptamide S87, prodotto da *Streptomyces* sp. NRRL S-87

- Thioalbamide, prodotto da *Amycolatopsis Alba* DSM 44262

La correlazione tra i cluster genici e i nuovi prodotti naturali identificati è stata confermata mediante due diversi approcci biologico-molecolari:

- la delezione del cluster genico nel ceppo batterico produttore, che ha portato alla generazione di mutanti incapaci di produrre i composti identificati.

- l'espressione eterologa del cluster genico, che ha portato alla produzione dei composti precedentemente identificati in un microorganismo ospite, *Streptomyces coelicolor* M1146.

I risultati ottenuti hanno permesso di stabilire che la thioviridamide non è una molecola unica nel suo genere, ma fa parte di una famiglia di composti, identificati in questo studio, a cui è stato dato il nome di thioviridamide-like molecules (TLMs).

Uno scale-up dei processi fermentativi ha permesso di purificare i tre nuovi prodotti naturali in quantità sufficenti per la loro caratterizzazione chimica, effettuata mediante spettrometria di massa e di risonanza magnetica nucleare (NMR). Questo studi hanno confermato la diversità

chimica dei TLMs, dal punto di vista della sequenza aminoacidica, sebbene sono risultate essere conservate alcune caratteristiche peculiari della thioviridamide, quali la presenza di un macrociclo, una carica elettrica positiva conferita da un residuo di dimetil-istidinio e la presenza di legami tioammidici nello scheletro peptidico. Inoltre, dai risultati ottenuti è emerso che i TLMs sono caratterizzati dalla presenza all'estremità N-terminale di un gruppo piruvile o lattile, e il gruppo 2-idrossi-2-metil-4-oxopentanoile, caratterizzante l'estremità N-terminale della thioviridamide, è risultato essere un artefatto, generato da una reazione di condensazione aldolica tra il gruppo piruvile della molecola naturale e l'acetone utilizzato come solvente nel processo di purificazione.

La thioalbamide, il prodotto naturale purificato in maggiore quantità, è stato quindi oggetto di indagini biologiche al fine di valutarne l'attività antiproliferativa e il potenziale antitumorale. I risultati ottenuti hanno evidenziato un'intensa attività antiproliferativa nei confronti di una vasta gamma di linee cellulari tumorali. Questi effetti sono risultati essere altamente selettivi per le cellule tumorali, in quanto il composto ha mostrato scarsa attività in un modello cellulare non tumorale.

La seconda parte di questo lavoro di tesi ha avuto l'obbiettivo di investigare a fondo sui meccanismi molecolari alla base dell'attività antitumorale della thioalbamide in diversi modelli *in vitro* di carcinoma mammario, il tumore maggiormente diagnosticato tra le donne nel mondo.

In questa parte del lavoro è stato utilizzato un approccio biochimico-metabolico, per valutare per la prima volta, gli effetti cellulari indotti dalla thioalbamide in linee cellulari tumorali che riflettono la diversità biologica dei diversi sottotipi di carcinoma mammario. Nei diversi modelli utilizzati, la molecola non ha mostrato significative differenze di attività antiproliferativa, dimostrando che il suo potenziale antitumorale è indipendente dal profilo recettoriale tumorale. In particolare, la thioalbamide ha dimostrato possedere abilità di indurre cambiamenti morfologici nelle cellule trattate, blocco del ciclo cellulare a livello del checkpoint G1/S e morte cellulare mediata da meccanismi apoptotici.

L'apoptosi è stata confermata con diversi approcci sperimentali atti a monitorare diversi eventi chiave del processo di morte programmata, quali la frammentazione del DNA, la perdita del potenziale di membrana mitocondriale e l'esposizione della fosfatidilserina sul foglietto esterno della membrana cellulare. In aggiunta, gli eventi di morte cellulare sono risultati essere il frutto dell'innesco dei pathway apoptotici estrinseco ed intrinseco, mediati rispettivamente dal attivazione proteolitica delle caspasi 8 e 9.

Lo studio delle alterazioni biochimiche indotte dalla thioalbamide è proseguito, facendo emergere la capacità del composto di derterminare nella cellula un aumento nella produzione di specie reattive dell'ossigeno (ROS), che si sono rivelate il fenomeno scatenante la morte apoptotica indotta dalla thioalbamide. L'eccessivo aumento dei livelli intracellulari di ROS indotto dal trattamento, è risultato interessare particolarmente il compartimento mitocondriale della cellula. Questa evidenza è emersa dal momento che la cellula tumorale risponde allo stress ossidativo, indotto dal composto, con un aumento selettivo dell'isoforma mitocondriale della superossido dismutasi (SOD2), enzima deputato alla neutralizzazione dell'anione superossido, principale subprodotto della respirazione cellulare.

Essendo i ROS generati dal metabolismo cellulare, il loro accumulo e il conseguente stress ossidativo sono spesso associati ad alterazioni dei pathway metabolici. La riprogrammazione metabolica è una delle caratteristiche del cancro, e i tumori richiedono cataboliti per produrre ATP, mantenere un equilibrio redox e generare biomassa. A seconda della disponibilità di nutrienti, alcune cellule all'interno del tumore sono prevalentemente glicolitiche, mentre altre hanno un fenotipo dipendente dalla fosforilazione ossidativa. Pertanto, in questo lavoro, è stato valutato anche il profilo energetico delle cellule trattate con thioalbamide, e i risultati ottenuti hanno evidenziato la capacità di questo prodotto naturale di inibire la glicolisi e la fosforilazione ossidativa, i due principali pathway energetici cellulari.

Il metabolismo della cellula tumorale rappresenta un potenziale target per la terapia oncologica. Infatti, è noto che le cancer stem cells (CSCs), la sottopopolazione di cellule tumorali responsabile dell'insorgenza di fenomeni di recidiva e metastatizzazione, sono caratterizzate da una elevata flessibilità metabolica. La thioalbamide, spegnendo il metabolismo energetico tumorale, si è rivelata in grado di inibire la crescita e propagazione delle CSCs, riducendo l'efficienza di formazione di mammospheres (MFE).

Nel complesso, questo lavoro di dottorato ha portato alla luce nuove conoscenze sui metaboliti secondari microbici, identificando nuovi membri della classe dei RiPPs che da oggi costituiscono la famiglia delle thioviridamide-like molecules (TLMs). Inoltre, per la prima volta, sono stati studiati i meccanismi molecolari indotti da questi nuovi prodotti naturali e, dai risultati ottenuti, è emerso che l'elevato potenziale antitumorale della thioalbamide è dovuto alla sua capacità di spegnere il metabolismo energetico della cellula maligna.

ABSTRACT
(ENGLISH VERSION)

Since the discovery of penicillin by Alexander Fleming in 1928, microbial natural products have been an essential resource for the development of new pharmacological agents. Within the wide variability of microorganisms populating terrestrial and marine ecosystems, bacteria belonging to the phylum *Actinobacteria* are the main source of natural bioactive molecules. Indeed, the secondary metabolism of these mircroorganisms is complex and very variable, and is responsible for the production of very different molecules from chemical, biosynthetic and biological activity points of view.

Ribosomally synthesized and post-translationally modified peptides (RiPPs) are a relatively recent but rapidly expanding class of secondary metabolites. These peptidic natural products are endowed with various biological activities and a huge pharmacological potential, with a spectrum of activities ranging, among others, from antibacterial to anti-tumor, and from hypolipidemic to immunomodulatory. Evidence of the biological potential of these molecules has, therefore, focused interest among biotechnological and pharmaceutical researchers on this class of secondary metabolites. The focus is, in particular, on the identification of new bacterial strains producing bioactive RiPPs and on the characterization of their biosynthetic pathways, in order to better understand the biochemical aspects underlying their biosynthesis.

This scenario includes thioviridamide, a RiPP biosynthesized by *Streptomyces olivoviridis* NA005001 and characterized by a powerful antiproliferative and pro-apoptotic activity against several tumor cell lines. This unique peptidic compound has a 2-hydroxy-2-methyl-4-oxopentanoyl group at the N-terminal end, a residue of β-hydroxy-N_1,N_3-dimethylistidinium (hdmHis), a residue of S-(2-aminovinyl)-cysteine (AviCys) which is part of a macro-cycle, as well as five thioamide groups that replace the amide groups in the peptide backbone. Recently, the gene cluster responsible for thioviridamide biosynthesis has been identified, demonstrating the ribosomal origin of this molecule, but the biosynthetic processes underlying its production are not yet fully known. The promising antitumor activity of thioviridamide, as well as its peculiar chemical structure and the interesting biosynthetic pathway, make this compound extremely interesting for research purposes.

The first part of this thesis work has aimed to identify, through a genomics-based approach, new natural products, thioviridamide analogues, biosynthesized by *Actinobacteria*, and to carry out their chemical-functional characterization, in order to evaluate their antitumor potential.

Bioinformatics studies, based on the use of tools for sequence homology analysis, have allowed to identify microorganisms whose genome contains gene clusters similar to those responsible for thioviridamide biosynthesis, from within the vast panorama of bacteria with a sequenced genome. The gene clusters identified in these microorganisms were found to be slightly different from those present in *S. olivoviridis*, with differences both at the level of the precursor peptide and at the level of the enzymatic maturation systems that convert it into a mature RiPP. These microorganisms, therefore, appear to be potential producers of molecules structurally similar to thioviridamide, with chemical and biological characteristics unknown to the scientific community.

Three of the different bacterial strains identified proved to produce, under specific experimental conditions, molecules similar to thioviridamide:

- Thiostreptamide S4, produced by *Streptomyces* sp. NRRL S-4

- Thiostreptamide S87, produced by *Streptomyces* sp. NRRL S-87

- Thioalbamide, produced by *Amycolatopsis Alba* DSM 44262

The correlation between the gene clusters and the new identified natural products was confirmed by two different molecular biology approaches:

- the deletion of the gene cluster in the producer bacterial strain, which led to the generation of mutants unable to produce the identified compounds.

- the heterologous expression of the gene cluster, which led to the production in a host microorganism, *Streptomyces coelicolor* M1146, of previously identified compounds.

The results obtained led us to establish that thioviridamide is not a unique molecule of its kind, but is part of a family of compounds, identified in this study, which we named thioviridamide-like molecules (TLMs).

A scale-up of the fermentation processes allowed us to purify the three new natural products in sufficient amounts for their chemical characterization, carried out by mass spectrometry and nuclear magnetic resonance (NMR). This study confirmed the chemical diversity of TLMs, from the point of view of their amino acid sequences, although some peculiar characteristics of thioviridamide have been preserved, such as the presence of a macrocycle, a positive electrical charge conferred by a dimethyl-histidine residue and the presence of thioamide bonds in the peptide backbone. In these studies, moreover, it was found that TLMs are characterized by the presence of a pyruvyl or lactyl group at the N-terminal end, and the 2-hydroxy-2-methyl-4-

oxopentanoyl group characterizing the N-terminus of thioviridamide is turned out to be an artifact, generated by an aldol condensation reaction between the pyruvyl group of the natural molecule and the acetone used as a solvent in the purification process.

Thioalbamide, the natural product purified in the greatest amounts, was therefore the subject of biological investigations in order to evaluate its antiproliferative activity and antitumor potential. The results obtained highlighted an intense antiproliferative activity against a wide range of tumor cell lines. These effects were found to be highly selective for cancer cells, as the compound showed more limited effects in a non-tumor cell model.

The second part of this thesis work aimed at investigating the molecular mechanisms underlying thioalbamide antitumor activity in several *in vitro* models of breast cancer, the most diagnosed tumor among women in the world.

In this part of the work, a biochemical-metabolic approach was used to evaluate, for the first time, the cellular effects induced by thioalbamide in tumor cell lines that reflect the biological diversity of the different subtypes of breast cancer. In the different models used, the molecule showed no significant differences in antiproliferative activity, demonstrating that its antitumor potential is independent of tumor receptor profile.

In particular, thioalbamide displayed the ability to induce morphological changes in treated cells, cell-cycle arrest at the G1/S checkpoint and cell death mediated by apoptotic mechanisms.

Apoptosis was confirmed as a result of experimental approaches aimed at monitoring several key events of the programmed death process, such as DNA fragmentation, loss of mitochondrial membrane potential and exposure of phosphatidylserine on the outer leaflet of cell membrane. Cell death events were found to be, in addition, the result of triggering the extrinsic and intrinsic apoptotic pathways, respectively mediated by the proteolytic activation of caspases -8 and -9.

The study of the biochemical alterations induced by thioalbamide continued, highlighting that the compound can lead to an increase in the production in the cell of reactive oxygen species (ROS), which proved to be the phenomenon triggering apoptotic death. Excessive increases in intracellular ROS levels induced by the treatment greatly affect the mitochondrial compartment of the cell. This emerged since the tumor cell responds to the oxidative stress induced by the compound, with a selective increase in the mitochondrial isoform of superoxide dismutase (SOD2), an enzyme responsible for neutralizing superoxide anion, the main subproduct of cellular respiration.

Since ROSs are generated by cellular metabolism, their accumulation and the consequent oxidative stress are often associated with alterations to cell metabolic pathways. Metabolic reprogramming is one of the characteristics of cancer, and tumors require catabolites to produce ATP, maintain a redox balance and generate biomass. Depending on the availability of nutrients, some cells within the tumor are predominantly glycolytic, while others have a phenotype dependent on oxidative phosphorylation. Therefore, in this work, the energy profile of cells treated with thioalbamide was also evaluated, and the results highlight the ability of this natural product to inhibit the two main cellular energy pathways, glycolysis and oxidative phosphorylation.

Tumor cell metabolism is a potential target for cancer therapy. It is known, indeed, that cancer stem cells (CSCs), the subpopulation of tumor cells responsible for the onset of recurrence and metastasis, are characterized by high metabolic flexibility. By extinguishing the tumor energy metabolism, thioalbamide proved to be able to inhibit the growth and propagation of CSCs, thus reducing the efficiency of mammospheres formation (MFE).

Overall, this doctoral work has brought to light new knowledge about microbial secondary metabolites, identifying new members of the class of RiPPs that now form the family of thioviridamide-like molecules (TLMs). Furthermore, for the first time, the molecular mechanisms induced by these new natural products have been studied, highlighting that the high antitumor potential of thioalbamide is due to its ability to shut down the energy metabolism of malignant cells.

PART 1

A genomics-based approach identifies a thioviridamide-like compound with selective anticancer activity

CHAPTER 1

INTRODUCTION

1.1 *Actinobacteria*

The phylum *Actinobacteria* includes Gram-positive (Gram +ve) bacteria genetically characterized by a high GC content in their DNA. Very abundant are the bacteria belonging to this phylum that, according to the current taxonomic classification based on 16S rRNA, is subdivided into 6 classes: *Actinobacteria*, *Acidimicrobiia*, *Coriobacteriia*, *Nitriliruptoria*, *Rubrobacteria* and *Thermoleophilia*. Each of these classes includes several orders, families and genera and, as a whole, this is one of the largest phyla within the bacterial kingdom. (https://www.ncbi.nlm.nih.gov/taxonomy)

In recent decades, the explosion of genomic sequencing has allowed an in depth study of these microorganisms to be carried out. Their genomic DNA is organized in a very large circular or linear chromosome, which can reach 12 Mb, characterized by a very high GC content that can exceed 74%.[1]

The enormous genetic diversity of the bacteria belonging to this phylum is reflected in a profound heterogeneity from the morphological, physiological and metabolic points of view.

The life cycle of these microorganisms is one of the most complex among prokaryotes and is very reminiscent of filamentous fungi development. Indeed, most of them grow by forming a vegetative mycelium that branches off into the ground which, at a certain point in its life cycle, gives rise to an aerial mycelium formation, which emerges from the surface. The hyphae that constitute the aerial mycelium can form unicellular spores, distributed singly or grouped in chains, needed for reproduction and diffusion in the surrounding environment. Every single spore, in favourable environmental conditions, can produce hyphae that show monopodial or dichotomous branching giving rise to a new mycelium, thus closing the cycle (Fig. 1).

However, not all *Actinobacteria* follow this life cycle. Many bacteria belonging to this phylum, in fact, are not able to produce an aerial mycelium or, in some cases, their aerial mycelium does not produce spores, so they generally reproduce through mycelium fragmentation. Several *Actinobacteria*, moreover, do not form a real mycelium and can be characterized by different morphologies, including coccoid (*Micrococcus*) and rod-coccoid (*Arthrobacter*), as well as fragmenting hyphal forms (*Nocardia* spp.).[2]

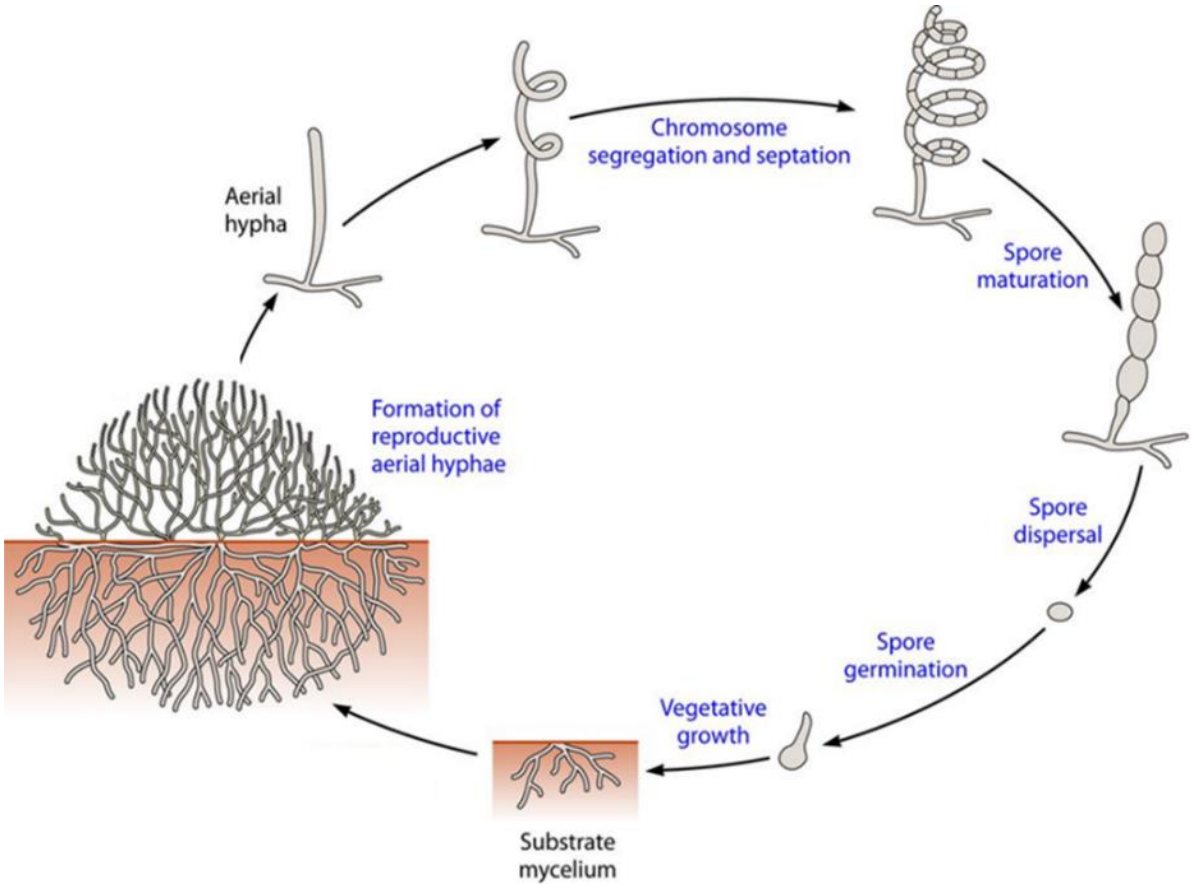

Fig. 1. Schematic life cycle of sporulating *Actinobacteria* (adapted from Barka, E. A. et al. "Taxonomy, physiology, and natural products of *Actinobacteria*." Microbiology and Molecular Biology Reviews 80.1 (2016): 1-43).

Actinobacteria are widely distributed both in terrestrial and aquatic ecosystems, although their main habitat is terrestrial soil, where they are the main microbial component. These bacteria grow both in depth and on the surface of soils rich in organic matter, which they use as a source of energy. Their density depends on the habitat they are in and the climatic conditions therein, and is usually around 10^6-10^9 cells per gram of soil.[2]

There are many factors influencing the growth of *Actinobacteria* and, among these, one of the most crucial is the temperature. Indeed, these organisms are mostly mesophilic and live at temperatures between 25 and 30 °C. There are, however, several thermophilic *Actinobacteria* that live in more extreme temperature conditions, with an optimal growth temperature of 50-60 °C.[2, 3]

Another factor having considerable impact on the development and growth of these microorganisms is the pH of the soil. Indeed, although some acidophilic species grow at pH values ranging from 3.5 to 6.5, the growth of most *Actinobacteria* occurs at neutral or slightly basic pH, with an optimum for growth of between 6 and 9 and a peak around neutrality.[2, 3]

In addition to living as free microorganisms in the environment, *Actinobacteria* can live inside organs and tissues of animals and plants as symbionts or pathogens.

A characteristic example of *Actinobacteria* in symbiosis with animals are the bacteria associated with leafcutter ants, able to produce secondary metabolites with antibacterial and antifungal activity that facilitate the survival of these insects.[4, 5]

As mentioned above, several *Actinobacteria* are, however, animal and plant pathogens. Pathogenic *Actinobacteria* for humans include *Mycobacterium tuberculosis*[6] and *Corynebacterium diphtheriae*[7], etiologic agents of tuberculosis and diphtheria, respectively. Examples of *Actinobacteria* that are pathogenic for plants are *Streptomyces scabies*, which causes holes and lesions in potatoes, beets and carrots[8], and *Leifsonia xyli*, a microorganism that stunts the growth of sugar cane sprouts.[9]

1.2 Secondary metabolites

A peculiar characteristic of *Actinobacteria*, which places them at the heart of biotechnological and pharmaceutical research, is their intense and variegated secondary metabolism, responsible for the production of very different natural compounds in terms of chemical structure, biosynthesis and biological activity. Secondary metabolism, by definition, is the set of biochemical processes that generates non-essential molecules for the growth and development of the microorganism. Secondary metabolites, however, play an important role in the microorganism-environment relationship.

Primary and secondary metabolic processes are closely related to each other, as the products of primary metabolism are generally the starting points for the biosynthesis of secondary metabolites.

These molecules are synthesized by microorganisms to perform different functions, such as sex hormones, ionophores and competitive weapons against other bacteria, fungi, amoebae, insects and plants.[10, 11]

Microbial secondary metabolites play an important role in human health, as they are endowed with a wide range of biological activities that can be exploited in the pharmaceutical field. Indeed, several molecules have, over the years, found application in clinical practice as antibacterial, antifungal, antitumor, hypolipidemic and immunosuppressor agents, and many such compounds are currently in preclinical and clinical trials.

The classical approach used for the identification of new biologically active natural products is the activity-guided approach. This methodology is based on the use of biological activity assays

to which the extracts of microorganisms are subjected. The extracts with the desired biological potential are subjected to fractionation, and activity-guided fractionation of the extract make possible the identification of the natural product that gives rise to the activity initially observed in the extract. This strategy is widely used and, over the years, has helped to identify innumerable natural bioactive products, many of which have been used in clinical practice or as leads for designing new drugs. After reaching its peak in the 1960s, the discovery of natural bioactive products has suffered a decline. Indeed, the activity-guided approach has some important limitations. One is the sensitivity of the biological activity assays used, which are not always able to detect the activity of natural products present in low concentrations in the extract under examination. Over the years, scientific progress has sought to solve this problem by providing increasingly sensitive and reliable biological tests. However, the activity-guided discovery of new natural products has another important limitation: many bioactive compounds are synthesized exclusively under certain conditions and are not produced under common laboratory conditions. Many organisms are potential producers of biologically interesting molecules, but may go unnoticed if subjected to an activity-guided screening. This makes the classical method not perfect for characterizing the unexpressed potential of microorganisms.

The rapid development of genome sequencing methods has revolutionized almost every aspect of biology including natural product research. The explosion of available microbial genomic data, observed in the last decade, has allowed to study in depth the genetic potential of microorganisms, highlighting the fact that the activity-guided screening has revealed only a small proportion of the bioactive compounds potentially produced in nature. The genomics-based approach, unlike the classic approach, starts from the genome of the microorganism, going to look for the presence of genes coding for biosynthetic machineries. Despite the profound chemical diversity characterizing secondary metabolites, biosynthetic logic and biosynthetic machineries for many of these compounds are often extremely well conserved. For this reason, mining for genes encoding enzymes putatively involved in secondary metabolite biosynthesis is the most "classical" variant of genome mining[12], and is possible using sequence-based comparison tools, such as BLAST (https://blast.ncbi.nlm.nih.gov/Blast.cgi). In addition, other software tools help focus not only on single genes, but on partial or complete gene clusters. A bioinformatics tool widely used for this purpose is antiSMASH[13] /https://antismash.secondarymetabolites.org), which can compare the identified biosynthetic gene clusters (BGCs) in a microbial genome with a collection of BGCs from other microorganisms. MultiGeneBlast algorithm[14], moreover, can be used to identify similar gene clusters for any given sequence, by searching in microbial genome databases.

In this way, bioinformatic tools enable identification of microbial biosynthetic gene clusters *in silico*, even revealing "cryptic" clusters, not expressed in common laboratory conditions. The identification of cryptic BGCs can therefore lead to the identification of new natural products through a combination of structure prediction, heterologous expression, or host manipulation.
It is important to underline that the genomics-based approach does not replace a classical one. Conversely, the interplay of classical discovery methods, with genomic data and genome mining strategies, has helped identify the gene clusters responsible for the biosynthesis of bioactive natural products discovered through an activity-based approach, giving a better understanding of the mechanisms that take part in their biosynthesis and helping to optimize their production.

The sections below will discuss the main classes of microbial secondary metabolites, with particular attention to their biosynthetic diversity and pharmacological potential.

1.2.1 Polyketides (PKs)

Polyketides (PKs) are secondary metabolites biosynthesized by condensation of carboxylic acid units, such as acetate, malonate and butyrate, thanks to the action of enzymatic complexes called polyketide synthases (PKSs). Polyketide biosynthesis provides a mechanism very similar to that of fatty acids and provides for the recurrence of decarboxylative condensation reactions of activated acyl-CoA units, each of which leads to the formation of a β-keto group on a growing carbon chain. Polyketide synthases can be classified as follows:

- type I PKSs are multifunctional enzymes that are organized into modules, each one containing a set of distinct, non-iteratively acting activities responsible for the catalysis of one cycle of polyketide chain elongation.
- type II PKSs are multienzyme complexes that carry a single set of iteratively acting activities.
- type III PKSs are homodimeric iteratively acting condensing enzymes.

Type I and II PKSs require acyl carrier protein (ACP) for the activation of acyl-CoA substrates, whereas type III PKSs, independent of ACP, act directly on acyl-CoA substrates. Despite structural and mechanistic differences, all types of PKSs biosynthesize polyketides by sequential decarboxylative condensation of the acyl-CoA precursors, catalysed by the ketoacyl synthase (KS) domain (for type I PKSs) or subunit (for type II and III PKSs).
The fundamental domains/subunits for the biosynthesis of the polyketides, which constitute the so-called minimal polyketide synthase, are a ketosynthase (KS) and chain length factor (CLF), an acyl carrier protein (ACP), and an acyltransferase (AT). The KS-CLF combination catalyzes

chain elongation through decarboxylative condensation of acyl building blocks, ACP delivers acyl building blocks to the KS-CLF, and AT supplies acyl groups to PKS.[15]

A series of additional domains/subunits can support the minimum configuration of the polyketide synthase, catalysing additional reactions that modify the growing carbon chain in growth leading to the formation of the mature polyketide. Among these, the keto-reductase (KR) domain reduces the β-keto group to a β-hydroxy group, the dehydratase (DH) domain catalyse dehydration reactions generating α-β-unsaturated alkene, while the enoyl-reductase (ER) domain reduces the α-β-double bond to generate a completely saturated bond (Fig. 2).[16]

This class of secondary metabolites includes molecules that differ greatly from a chemical and a pharmacological potential point of view. The polyketides that have been applied in clinic practice over the years include antibiotics, such as the macrolide azithromycin and the tetracycline doxycycline, antimycotics, such as nystatin, and hypocholesterolemic agents, such as lovastatin (Fig. 3).

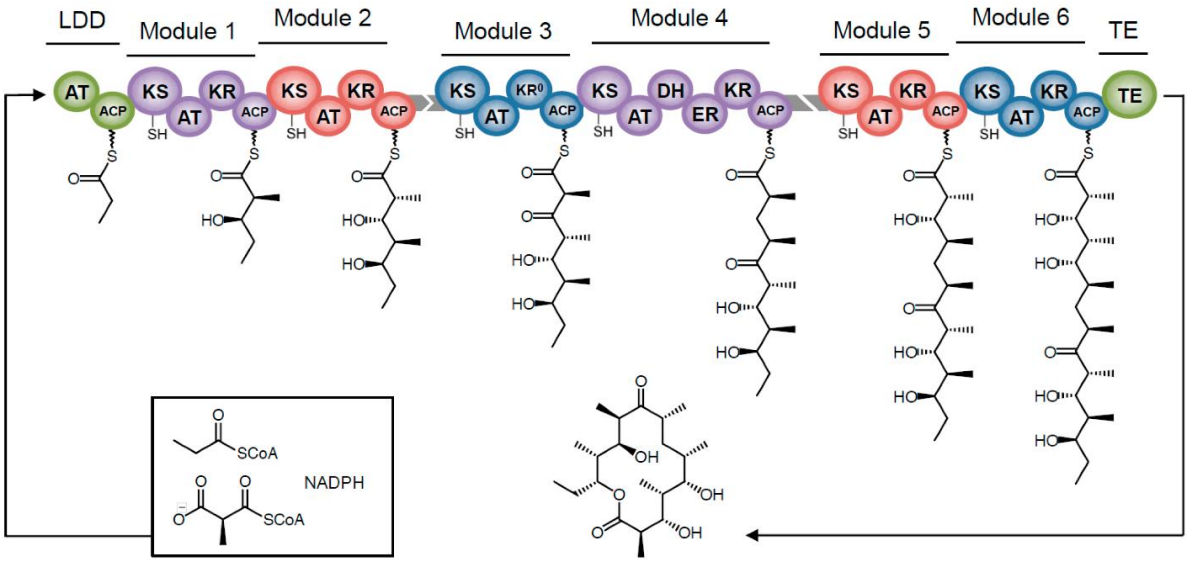

Fig. 2. An example of PKS architecture (From Bayly, C. L., & Yadav, V. G. (2017). Towards precision engineering of canonical polyketide synthase domains: recent advances and future prospects. *Molecules*, *22*(2), 235).

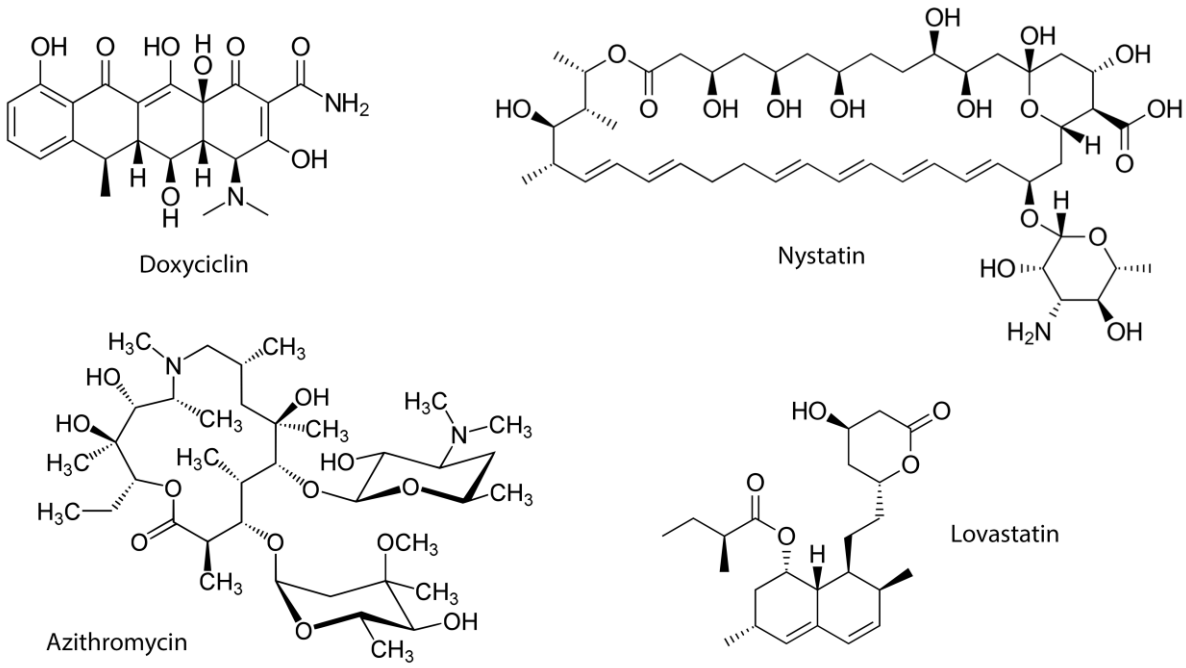

Fig. 3. Examples of clinical polyketide drugs. (Doxyciclin, Azithromycin, Nystatin and Lovastatin)

1.2.2 Non-Ribosomal Peptides (NRPs)

Non-ribosomal peptides (NRPs) are secondary metabolites of peptide nature, not synthesized at ribosomal level, but by multimodular enzymes called Non-Ribosomal Peptide synthetases. NRPs are therefore peptides not genetically coded and are totally independent of messenger RNA, and their structure is characterized by the massive presence of non-proteinogenic amino acids. Further reactions at the end of peptide synthesis can lead to the introduction of modifications such as glycosylations, acylations, halogenations and hydroxylations.

NRP synthetases are enzymatic complexes made up of different modules, each appointed to incorporate a specific amino acid into the growing peptide. Each module, in turn, can be divided into different domains, each of which is responsible for the catalysis of a different reaction. The three essential domains in a peptide elongation module are: the adenylation domain (A), the peptidyl carrier protein (PCP), also called thiolation domain (T), and the condensation domain (C). The elongation process involves the adenylation and activation of the amino acid to be incorporated, at the level of the A domain, the formation of the aminoacyl thioester by reaction with the phosphopantetheinyl arm, at the level of the T domain, and the formation of a peptide bond between the aminoacyl thioesters of two adjacent modules, catalyzed by the C domain (Fig. 4).[17, 18]

The first module of NRP synthetases lacks the C domain, while the last module includes domains responsible for the release of the final peptide, such as a thioesterase (Te) or reductase (R) domain, through hydrolysis, cyclization or oligomerization reactions. NRP synthetases modules can include several types of additional domains which co-synthetically modify the non-ribosomal peptide. These include catalytic domains responsible for formylation, epimerization, N-methylation, cyclization, reduction and oxidation reactions.

This class of secondary metabolites includes several pharmacologically active substances with wide activity spectra including antibiotic, such as Actinomycin and Vancomycin, cytostatic, such as Epothilone and Bleomycin, and immunosuppressive, including cyclosporine (Fig. 5).

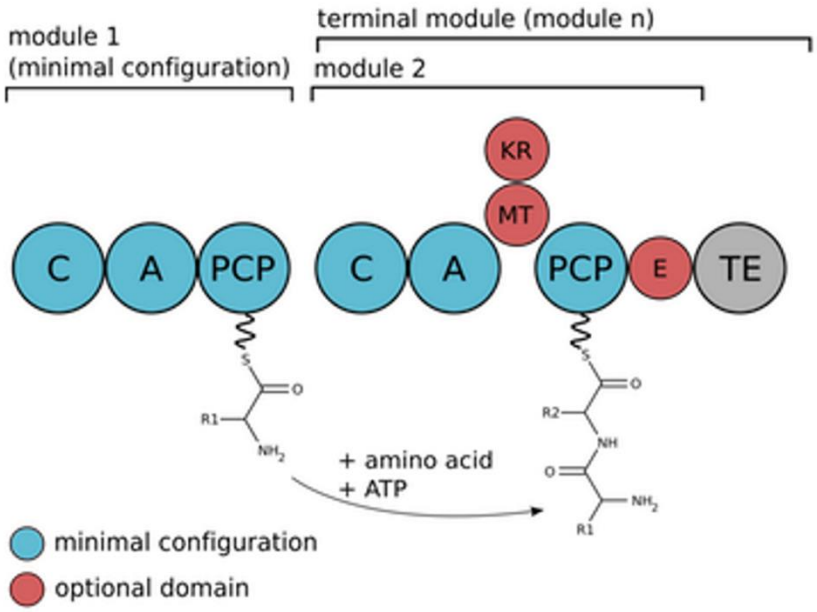

Fig. 4. NRP synthetase architecture. (Adapted from https://www.uni-potsdam.de/en/ibb-mikrobiologie/microbiology-research/ribosomal-and-non-ribosomal-peptides.html)

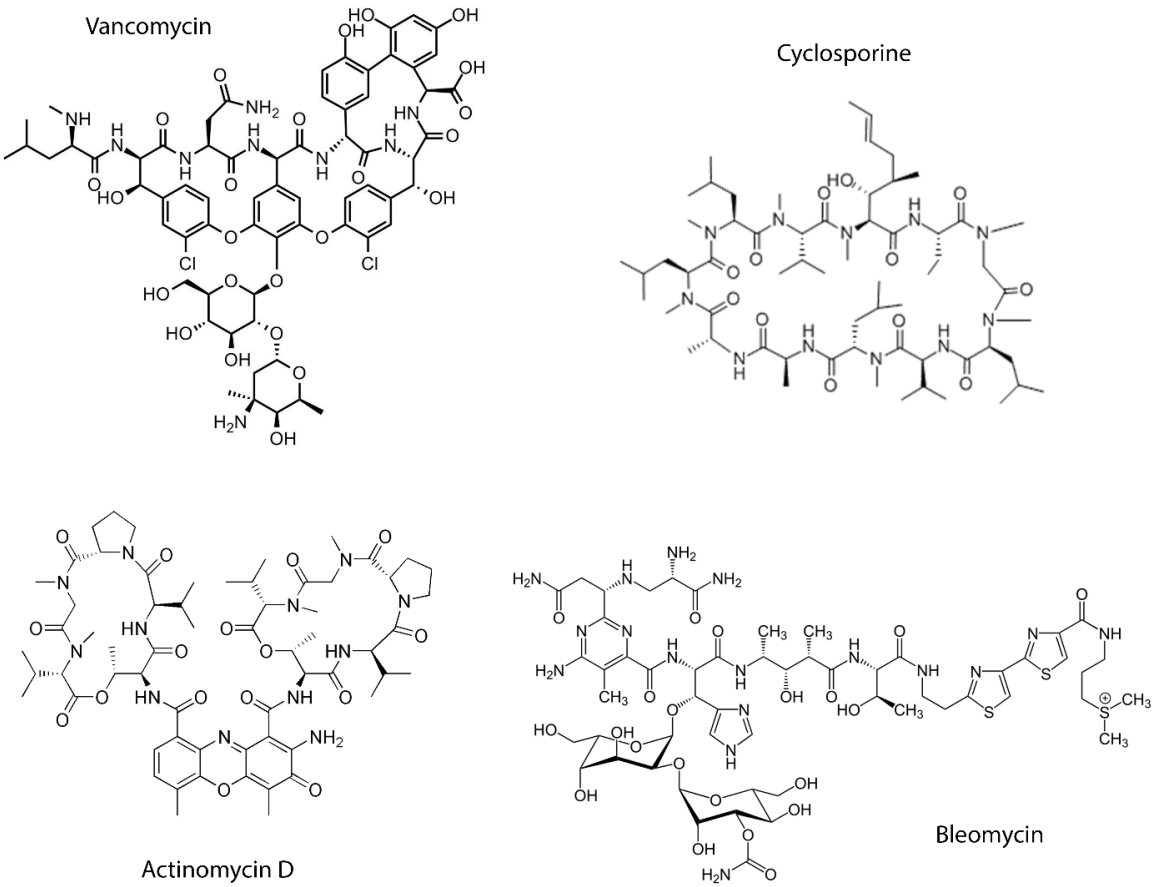

Fig. 5. Examples of bioactive NRPs. (Vancomycin, Actinomycin D, Cyclosporin and Bleomycin)

1.2.3 Ribosomally synthesized and post-translationally modified peptides (RiPPs)

An interesting class of biologically active secondary metabolites, relatively recent but rapidly expanding, are ribosomally synthesized and post-translationally modified peptides (RiPPs).

Unlike non-ribosomal peptides, whose structure originates from the incorporation of proteinogenic and non-proteinogenic aminoacids through the action of multimodular enzymatic complexes, RiPPs are the product of the ribosomal synthesis of a genetically encoded precursor peptide, and its modifications at post-translational level. The genes responsible for the biosynthesis of RiPPs are organized into clusters. A typical gene cluster involved in their biosynthesis is characterized by genes coding for a precursor peptide, a series of enzymes involved in the process of modification/maturation of the peptide compound (tailoring enzymes) and transport systems necessary for the transport of the RiPP at extracellular level, where, in mature form, it can carry out its biological activity.

Typically, the precursor peptide, genetically encoded and synthesized at ribosomal level, has a length ranging from 20 to 110 amino acid residues and can be divided into different regions, each with a different meaning from a biosynthetic point of view. The "core peptide" is the peptide segment which will subsequently undergo post-translational modifications by tailoring enzymes and represents the basic structure of the RiPP (Fig. 6).

Fused to the core peptide, at the N-terminal end, there is generally a "leader peptide", the amino acid sequence that enables the precursor peptide to be recognized by the tailoring enzymes and the systems dedicated to its exportation. In some cases, the peptide leader is not at the N-terminal end but at the C-terminal, and in this case it is called "follower peptide".

There may be further signal sequences at the N- or C-terminal end for the purpose of conveying the precursor peptide, in eukaryotic organisms, to the cellular compartment where post-translational modifications will occur. Once the precursor peptide has been modified by the tailoring enzyme, it undergoes a proteolytic process by specific proteases, which separate the modified core peptide from the leader/follower peptide, releasing the mature RiPP.[19]

The wide range of tailoring enzymes present in RiPPs gene clusters and the consequent variety of post-translational modifications which precursor peptides can undergo, are responsible for a profound chemical diversity among the members of this class of secondary metabolites (Fig. 7). The chemical complexity that RiPPs can reach gives them a wide range of biological activities, such as antibacterial, antimycotic, cytotoxic, antitumor and immunosuppressive actions. The peculiar chemical features, the logical and genetically engineered biosynthetic pathways and the high pharmacological potential characterizing RiPPs have, in recent decades,

made, this family of secondary metabolites into a focus of biotechnological and pharmaceutical research.

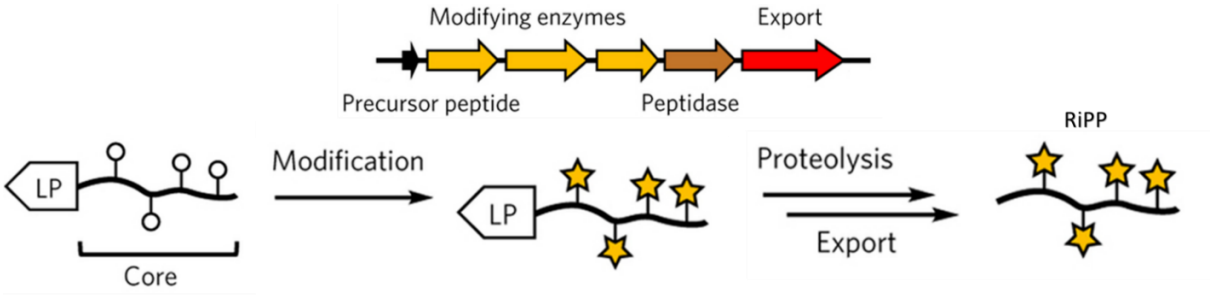

Fig. 6. Schematic synthesis of RiPPs. (Adapted from Burkhart, B. J., Hudson, G. A., Dunbar, K. L., & Mitchell, D. A. (2015). A prevalent peptide-binding domain guides ribosomal natural product biosynthesis. *Nature chemical biology*, *11*(8), 564).

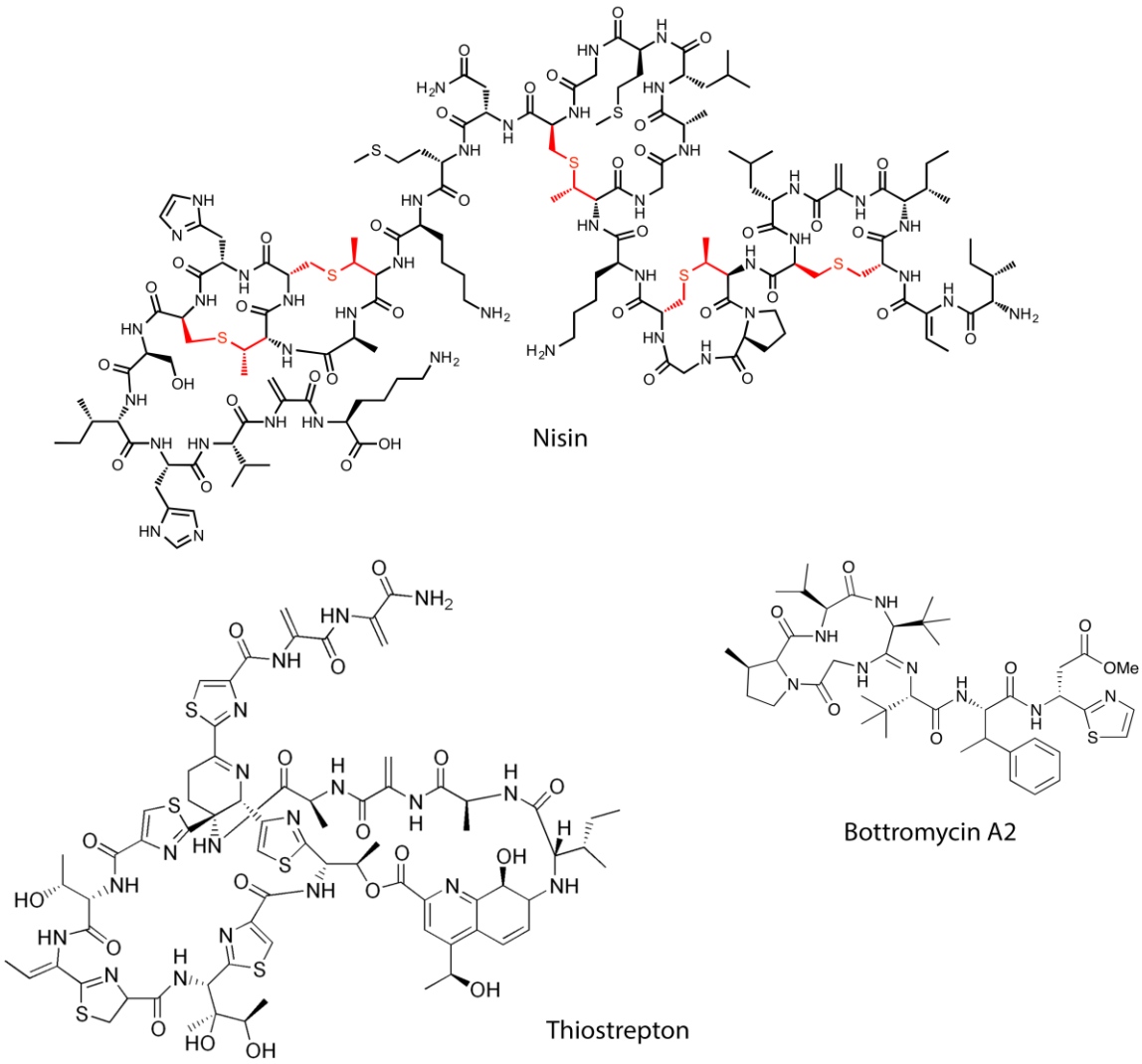

Fig. 7. Examples of bioactive RiPPs. (Nisin, Thiostrepton and Bottromycin A2)

1.3 Thioviridamide

Thioviridamide (Fig. 8) is a ribosomally synthesized and post-translationally modified peptide biosynthesized by *Streptomyces olivoviridis* NA00500. It was identified and isolated by Hayakawa et al in the course of a screening for antitumor antibiotics using 3Y1 rat fibroblasts transformed with adenovirus oncogenes.[20, 21] This new peptide compound has a prominent selective antiproliferative and proapoptotic activity against tumor cells and is characterized, from a chemical point of view, by the presence of a 2-hydroxy-2-methyl-4-oxopentanoyl group at the N-terminus, a β-hydroxy-N^1,N^3-dimethylhistidinium residue (hdmHis), and a S-(2-aminovinyl)cysteine residue (AviCys) forming part of a macrocycle. The peculiar characteristic of thioviridamide lies in its five thioamide groups that replace the amide groups in the peptide backbone. The presence of thioamide bonds is a very rare feature among natural products[22] and the presence of five contiguous thioamides in thioviridamide peptide backbone is unique among RiPPs.

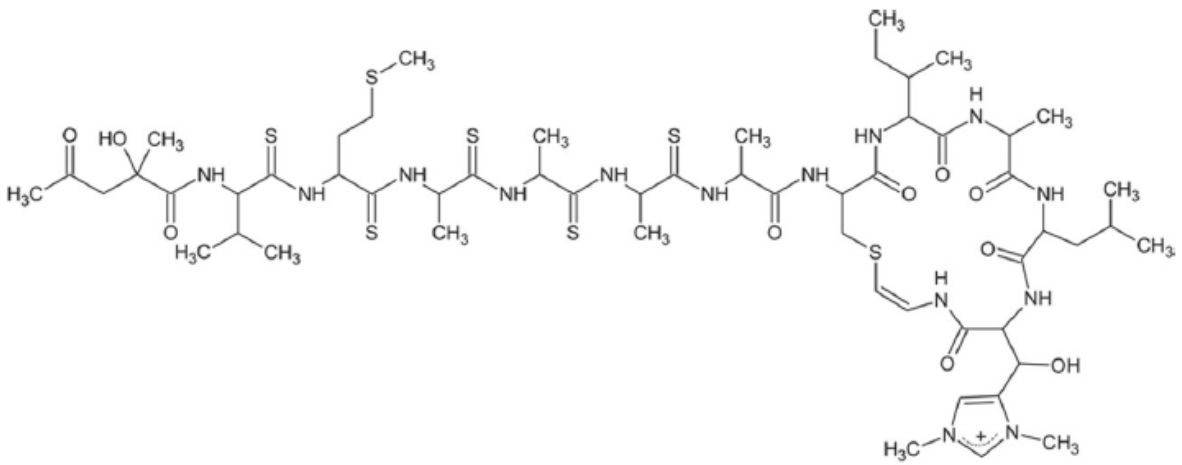

Fig. 8. Structure of thioviridamide.

Recently, the gene cluster responsible for thioviridamide biosynthesis has been identified and confirmed by heterologous expression experiments.[23] These studies have demonstrated the ribosomal origin of this molecule, which derives from a 13 amino acid core peptide at the C-terminus of the TvaA precursor peptide, modified at post-translational level thanks to the action of 11 proteins encoded by genes present in the gene cluster (TvaB−TvaL). Although little is known so far about the specific maturation steps which the precursor peptide undergoes, sequence homology studies make it possible to hypothesize the function of some of the genes that are part of the cluster (Table 1).

Table 1. Thioviridamide gene cluster

Protein	Size (aa)	Homologous protein (origin)	Identity/ similarity (%)	Deduced function
TvaA	75	ABC transporter (*Penicillium griseofulvum*)	46/62	Precursor peptide
TvaB	275	SARP family regulator (*S. lavendulae*)	35/55	Regulator
TvaC	377	Phosphotransferase family protein (*Nostoc* sp.)	29/45	Unknown
TvaD	328	Hypothetical protein (*Calothrix* sp.)	25/41	Unknown
TvaE	308	Aminoglycoside phosphotransferase (*Frankia* sp.)	48/65	Unknown
TvaF	197	Phosphopantothenoylcysteine decarboxylase (*Exiguobacterium* sp.)	39/60	Oxidative decarboxylase
TvaG	407	Type 12 methyltransferase (*Cyanothece* sp.)	43/61	Methyltransferase
TvaH	452	Methanogenesis marker protein 1 (*Methanolinea tarda*)	36/53	Unknown
TvaI	218	TfuA-like core domain-containing protein (*M. tarda*)	44/63	Regulator
TvaJ	280	Phytanoyl-CoA dioxygenase (*Roseobacter litoralis*)	29/44	Oxygenase
TvaK	220	Papain family cysteine protease (*Tannerella forsythia*)	27/39	Protease
TvaL	282	Integral membrane protein (*S. pristinaespiralis*)	31/49	Unknown
TvaM	160	Histidine kinase (*S. somaliensis*)	55/66	Regulator
TvaN	1003	Large transcriptional regulator (*S. pristinaespiralis*)	67/75	Regulator
TvaO	94	Hypothetical protein (*S. viridochromogenes*)	54/68	Unknown

The oxygenase encoded by the tvaJ gene and the methyl-transferase encoded by the tvaG gene, could be responsible for converting the histidine residue into β-hydroxy-N^1,N^3-dimethylhistidinium. In addition, tvaK gene encodes for a protease that could be responsible for proteolysis of the precursor peptide and release of the modified thioviridamide core peptide, while tvaB, tvaM and TvaN genes appear to codify for regulators and could be important in the modulation of thioviridamide production.

As mentioned above, thioviridamide contains an S-(2-aminovinyl)cysteine (AviCys) residue, which has been found in the linaridin family of RiPPs.[19] Epidermin[24], microbisporicin[25], and cypemycin[26] are known to be AviCys-containing linaridins. In these natural products, AviCys is formed by cyclization between a serine/cysteine-derived dehydroalanine and a C-terminal cysteine via oxidative decarboxylation. A cysteine oxidative decarboxylase appears to be encoded by the tvaF gene present in the thioviridamide cluster, but the absence of a gene coding

for a serine dehydratase, makes this modification different from those known in scientific literature.

The identification of the gene cluster responsible for thioviridamide biosynthesis did not, however, explain the biosynthetic origin of the 2-hydroxy-2-methyl-4-oxopentanoyl group at the N-terminal end, which remains, to date, unknown.

1.4 Aims of the study

The complex secondary metabolism of *Actinobacteria* has always been an important source of molecules with pharmacological activities and, over the years, different approaches have been used for their identification. The promising antitumor activity of thioviridamide, as described in this chapter, as well as its peculiar chemical structure and interesting biosynthetic pathway, make this compound highly interesting for research purposes. This first part of this PhD thesis aims to identify new natural products, thioviridamide analogues, biosynthetically produced by *Actinobacteria*, and to perform their chemical-functional characterization, in order to assess their anticancer potential. The main tasks of this part of the project were:

- To identify bacterial strains that might potentially produce thioviridamide-like compounds. For this purpose, a genomics-based approach was employed in order to identify bacterial strains containing in their genome gene clusters similar to the one responsible for thioviridamide biosynthesis.
- To confirm the correlation between gene clusters and their putative natural products. Two molecular biology approaches were applied: the deletion of the gene cluster in the producer strain and the expression of the cluster in a host microorganism.
- To highlight the biological potential of the newly discovered natural products. In particular, the antitumor and the antimicrobial properties of compounds were investigated on a wide panel of tumour cell lines and pathogenic microorganisms, respectively.

CHAPTER 2

MATERIALS AND METHODS

2.1 General chemical methods

All chemicals were supplied by Sigma-Aldrich or Fisher Scientific. The solvents were of HPLC grade or equivalent. NMR spectra were recorded on a Bruker Avance III 400 MHz NMR spectrometer equipped with 5 mm BBFO Plus probe. Chemical shifts were reported in ppm using the signals of the residual solvents as internal references (δH 3.31 and δC 49.0 for CD_3OD; δH 2.50 and δC 39.52 for DMSO-d_6).

2.2 General microbiological and molecular biology methods

Isolation of genomic DNA from *Actinobacteria* was performed by using a salting out procedure as described previously.[27] Isolation of plasmid DNA, DNA purification from agarose gels and DNA restriction/ligation were performed following manufacturers' protocols (Qiagen, Promega, NEB and Thermo-Scientific). PCR reactions were carried out in a Veriti thermal cycler (Applied Biosystems) using Herculase II Fusion DNA Polymerase (Agilent) for cloning purposes, and GoTaq G2 Flexi DNA Polymerase (Promega) to verify positive clones and mutants. Oligonucleotide primers are listed in Table 2.

Table 2. Oligonucleotides

Oligonucleotide name	Sequence (5'-3')
S4TAR1	TTGACGCCTCCCATGGTATAAATAGTGGCTCGAGCGGGGCGGTCGCAAGCCG CGTCGCTGACGGGCGGACGGTGGGCCGTGCGGGTTTAAACTGAACGTCAGA
S4TAR2	AGCAGCACGTTCCTTATATGTAGCTTTCGACATATGCCCCTGGACCCTTCGTA CGCCCTCGTCCGGACAGGTGGATCTGACGTTCAGTTTAAACCCGCACGGCCC
S4YCAOTRU-Fw	GATACAGAATTCCCTGCGGAGGGTGGGTGTCAC
S4YCAOTRU-Rv	GATACAGGATCCCGGGGACCGATCTTGTTGCGG
CHECKTAR-Fw	TTCGGGGCTCCCCTTCC
CHECKTAR-Rv	TACGAACATCCAATGAAGCACAC
pKC1132-ext	CACAGATGCGTAAGGAGAAAATACCGC

2.3 Identification of thioviridamide-like gene clusters

Proteins with at least 50% identity with TvaH (BAN83923.1) were identified used the NCBI Basic Local Alignment Search Tool (BLAST) server (https://blast.ncbi.nlm.nih.gov/Blast.cgi). Genomic regions of approximately 20 kb either side of these proteins were then used to construct a MultiGeneBlast database that was subjected to a homology search using the thioviridamide gene cluster, with a minimal % identity of 25% and a maximal distance between genes in locus of 20 kb. Proteins without a homologue encoded in the thioviridamide gene cluster were manually analyzed using NCBI CD-search and Pfam 30.0 for conserved domains.

2.4 Strains and fermentation conditions

Streptomyces sp. NRRL S-4, *Streptomyces sp.* NRRL S-15 and *Streptomyces sp.* NRRL S-87 were obtained from the ARS culture collection (NRRL; Peoria, Illinois, USA), and *Amycolatopsis alba* DSM 44262 and *Nocardiopsis potens* DSM 45324 were purchased from the DSMZ culture collection (Braunschweig, Germany). These were maintained on soya flour mannitol agar (SFM) at 28 °C and the strains were stored as spore suspensions in 20% glycerol at -20 °C. DNA manipulation was carried out in *Escherichia coli* DH5α, and the non-methylating *E. coli* strains ET12567/pUZ8002 and ET12567/pR9406 were used to introduce DNA into Streptomyces strains by intergeneric conjugation, as described previously.[27, 28] *E. coli* strains were grown on LB liquid or solid medium containing the appropriate antibiotic for selection. *Saccharomyces cerevisiae* VL6−48N[29] was used for TAR cloning experiments. Yeast cells were grown in liquid YPD medium (2% D-glucose, 1% yeast extract, and 2% peptone) supplemented with 100 mg/L adenine. *Staphylococcus aureus* (ATCC 25923), E. coli (ATCC 25922), *Klebsiella pneumonia* (ATCC 13883) and *Pseudomonas aeuruginosa* (ATCC 27853) were purchased from Thermo Scientific Remel. These pathogenic bacteria were grown in Mueller Hinton Broth (MHB, Difco) containing 2 g/L beef infusion solids, 17.5 g/L casein hydrolysate, 1.5 g/L starch, pH 7.4. *Candida albicans* (ATCC 10231) was purchased from Thermo Scientific Remel and was grown in Sabouraud dextrose broth (10 g/L peptone, 40 g/L dextrose, final pH adjusted to 5.6).

2.5 Small scale production of thioviridamide-like molecules (TLMs)

Each strain was grown on a solid version of bottromycin production medium[30] (BPM; 1% glucose, 1.5% soluble starch, 0.5% yeast extract, 1% soya flour, 0.5% NaCl, 0.3% $CaCO_3$, 2.2% agar) at 28 °C for 7 days. Plates were extracted with one volume of either ethyl acetate or

methanol for 30 min with shaking, and 1 mL samples were centrifuged at 20,000 x g prior to LC-MS analysis.

2.6 Liquid chromatography-mass spectrometry (LC-MS) analysis

LC-MS screening was carried out using a Shimadzu Nexera X2 UHPLC coupled to a Shimadzu ion-trap time-of-flight (IT-TOF) mass spectrometer. Samples (5 µL) were injected onto a Phenomenex Kinetex 2.6 u C18 column (50 x 2.1 mm, 100 Å), eluting with a linear gradient of 5 to 95% acetonitrile in water + 0.1% formic acid (FA) over 6 minutes with a flowrate of 0.6 mL min-1 at 40 °C. Positive mode mass spectrometry data was collected between m/z 200 and 1600 with an ion accumulation time of 20 ms featuring an automatic sensitivity control of 70% of the base peak. The curved desolvation line (CDL) temperature was 300 °C and the heat block temperature was 250 °C. MS^2 data was collected in a data-dependent manner using collision-induced dissociation energy of 50% and a precursor ion width of 3 Da. The instrument was calibrated using sodium trifluoroacetate cluster ions prior to every run. Additional high-resolution mass spectra were acquired on a Synapt G2-Si mass spectrometer (Waters) operated in positive mode with a scan time of 0.5 s in the mass range of m/z 50 to 1600. Samples (3 µL) were injected onto an Acquity UPLC BEH C18 column (1.7 µm, 1x100 mm, Waters) and eluted the following gradient of water + 0.1% formic acid (A) and acetonitrile + 0.1% formic acid (B) with a flow rate of 0.08 mL/min at 45 °C:

0 min: 95.0 A%, 5.0 B%

1 min: 95.0 A%, 5.0 B%

15 min: 5.0 A%, 95.0 B%

16 min: 5.0 A%, 95.0 B%

16.1 min: 95.0 A%, 5.0 B%

20 min: 95.0 A%, 5.0 B%

Synapt G2-Si MS data were collected with the following parameters: capillary voltage = 3.0 kV; cone voltage = 40 V; source temperature = 120 °C; desolvation temperature = 350 °C. For MS2 fragmentation, the masses of interest were put on an inclusion list, and fragmented using data directed analysis (DDA) with the following parameters: top3 precursor selection (inclusion list only); intensity threshold = 10,000; scan time = 1 s; isolation window = 0.5 Da; CE ramp = 30-40 eV at low mass (m/z 50) to 70-120 eV at high mass (m/z 1600). Leuenkephalin peptide was used to generate a dual lock-mass calibration with m/z = 278.1135 and m/z = 556.2766 measured every 20 s during the run.

2.7 Construction of *Streptomyces* sp. NRRL S-4 mutant by insertional mutagenesis

A 1.2 kb region of tsaH (ADK82_11830) was amplified from *Streptomyces* sp. NRRL S-4 genomic DNA by PCR, using primers S4YCAOTRU-Fw and S4YCAOTRU-Rv to introduce EcoRI and BamHI restriction sites at the 5′ and 3′ ends, respectively. This digested DNA fragment was ligated into pKC1132 vector[31] digested with EcoRI and BamHI, and transformed into *E. coli* DH5α. Colony PCR (using primers S4YCAOTRU-Fw and S4YCAOTRU-Rv) and plasmid sequencing were used to confirm positive clones. The plasmid was introduced into *E. coli* ET12567/pUZ8002 by electroporation and then into *Streptomyces sp*. NRRL S-4 by intergeneric conjugation. Apramycin-resistant *Streptomyces sp. NRRL S-4* exconjugants were screened by PCR (primers: S4YCAOTRU-Fw and pKC1132-ext) to confirm mutant generation.

2.8 *Streptomyces* sp. NRRL S-4 gene cluster TAR cloning and heterologous expression

A vector to capture the thiostreptamide S4 gene cluster from *Streptomyces sp.* NRRL S-4 genomic DNA was constructed by the use of a modified (ligase-free) Gibson assembly[32] procedure between a linearized pCAP03 vector[33] and two single-strand oligonucleotides (S4TAR1 and S4TAR2), each one containing 30 nucleotide homology sequence with pCAP03 and a 50 nucleotide homology sequence with upstream and downstream regions of the gene cluster. pCAP03 was digested with XhoI and NdeI enzymes, and the linearized plasmid and ss-oligos (1:10 ratio) were used in a ligase-free Gibson assembly reaction (100mM Tris-HCl pH 7.5, 10 mM MgCl2, 0.2 mM each dNTPs, 10 mM DTT, 1 mM NAD, 5% PEG-8000, 0.1125 units T5 exonuclease, 0.375 units Phusion polymerase, 20 µL total reaction volume), which was incubated at 50 °C for 2 hours. The Gibson assembly mixture was introduced into *E. coli* DH5α using electroporation, the colonies containing the correct capture vector were identified by PCR (primers: CHECKTAR-Fw and CHECKTAR-Rv) and then confirmed by plasmid sequencing. Genomic DNA from *Streptomyces sp*. NRRL S-4 was digested with AclI and the pCAP03-derived capture vector was linearized between capture arms with PmeI. These were both then introduced into *S. cerevisiae* VL6-48N by spheroplast transformation.[34] Successful gene cluster capture by pCAP03 was confirmed by colony PCR (primers: S4YCAOTRU-Fw and S4YCAOTRU-Rv), using a freeze-thaw microwave oven colony pre-treatment method[35] and then by restriction analysis of the extracted construct (pTARS4). *E. coli* ET12567/pR9604 was transformed with pTARS4 by electroporation, and transformants were then used to transfer pTARS4 into *S. coelicolor* M1146 by intergeneric conjugation. Apramycin-resistant *S. coelicolor* M1146 exconjugants containing integrated pTARS4 were verified by PCR.

2.9 Large scale extraction and isolation of TLMs

***Amycolatopsis alba* DSM 44262.** Production cultures grown on 3.2 L of solid BPM were extracted with 3.2 L of ethyl acetate and then with the same volume of methanol. After removing the solvents under reduced pressure, 1.7 g of ethyl acetate extract (A-EtOAc) and 20.25 g of methanol extract (A-MeOH) were obtained. These extracts were analyzed by LCMS (as described previously) to confirm the isolation of the target TLM compound. A-MeOH (20.25 g) was fractionated by vacuum liquid chromatography (VLC) on C18-reverse phase using mixtures of H_2O/MeOH (0-100% MeOH) as eluent to afford five fractions A1-A5. Fraction A5 (0.35 g) contained the TLM and it was separated on a Sephadex LH-20 column using a mixture of MeOH/DMSO (98:2) as the mobile phase, affording five final fractions A5A-A5E. The TLM was detected in fractions A5C (0.05 g) and A5D (0.10 g). These were further purified on a preparative HPLC column (Phenomenex Luna C18, 30 x 250 mm, 5 μm; 30 mL/min, UV detection at 270 nm) using CH_3CN/H_2O + 0.1% of trifluoroacetic acid (TFA) as a mobile phase, with a linear gradient of 40% to 70% CH_3CN over 45 min yielding pure thioalbamide (2, 6.4 mg, tR 37 min).

***Streptomyces* sp. NRRL S-4**. Production cultures grown on 3.2 L of solid BPM were extracted with 3.2 L of ethyl acetate and then with the same volume of methanol. After removing the solvents under reduced pressure, 0.95 g of ethyl acetate extract (S4-EtOAc) and 10.50 g of methanol extract (S4-MeOH) were obtained. S4-MeOH (10.50 g) was fractionated by vacuum liquid chromatography (VLC) on C18-reverse phase using mixtures of H_2O/MeOH (0-100% MeOH) as eluent to afford six fractions S4A-S4F. Fraction S4F (0.16 g) contained the TLM and was fractionated on a Sephadex LH-20 column using a mixture of MeOH/DMSO (98:2) as the mobile phase. Combined positive fractions were further purified on a preparative HPLC column (Phenomenex Luna C18, 30 x 250 mm, 5 μm; 30 mL/min, UV detection at 270 nm) using CH_3CN/H2O + 0.1% TFA as a mobile phase, with a linear gradient of 40% to 65% CH_3CN over 50 min yielding pure yielding thiostreptamide S4 (3, 1.2 mg, tR 26 min).

***Streptomyces sp.* NRRL S-87**. Production cultures grown on 3.2 L of solid media were extracted with 3.2 L of ethyl acetate and then with the same volume of methanol. After removing the solvents under reduced pressure, 0.55 g of ethyl acetate extract (S87-EtOAc) and 8.83 g of methanol extract (S87-MeOH) were obtained. These extracts were analyzed by LC-MS (as described previously) and the target TLM was only detected in the methanol extract. S87-MeOH (8.83 g) was fractionated by vacuum liquid chromatography (VLC) on C18-reverse phase using mixtures of H_2O/MeOH (0-100% of MeOH) as eluent to afford five fractions S87A-S87E. Fraction S87E (0.11 g) contained the TLM and was fractionated on a Sephadex

LH-20 column using a mixture of MeOH/DMSO (98:2) as the mobile phase. Combined positive fractions were further purified on a preparative HPLC column (Phenomenex Luna C18, 30 x 250 mm, 5 μm; 30 mL/min, UV detection at 270 nm) using CH_3CN/H2O + 0.1% TFA as a mobile phase, with a linear gradient of 40% to 70% CH3CN over 50 min yielding pure thiostreptamide S87 (4, 0.3 mg, tR 32 min).

2.10 Cell cultures

All the cell lines used in this work (MCF7, MDA-MB-231, A549, HeLa, PA-TU-8988T and MCF10A) were purchased from the American Culture Collection (ATCC, Manassas, VA). For maintenance purposes, cells were cultured in DMEM/F12 (Sigma) supplemented with 10% fetal bovine serum (FBS, Sigma), 2 mM L-glutamine (Gibco, Life Technologies) and 1% penicillin/streptomycin (Gibco, Life Technologies), except for the MCF 10A cell line, which was cultured in DMEM/F12 supplemented with 5% horse serum (HS, Sigma), 10 mg/mL insulin (Sigma), 0.5 mg/mL hydrocortisone (Sigma), 20 ng/mL human epidermal growth factor (hEGF, Sigma), 0.1 mg/mL cholera toxin (Sigma), 2 mM L-glutamine and 1% penicillin/streptomycin. Treatments were performed in the above-mentioned media containing a lower amount of supplemented serum (2%). All cell lines were cultured at 37 °C in 5% CO_2 in a humidified atmosphere.

2.11 Cell viability assay

Cell viability was determined by using 3-(4,5-Dimethyl-2-thiazolyl)-2,5-diphenyl-2H-tetrazolium bromide (MTT) assay. Cells were seeded in 48-well plates with a density of $2x10^4$ cells/well, cultured in complete medium overnight and then treated with different concentrations of compounds for 72 hours; DMSO was used as a vehicle control. At the end of the treatment period, MTT solution was added to each well (to a final concentration of 0.5 mg/mL) and plates were incubated at 37 °C for 2 h until the formation of formazan crystals. DMSO-solubilized formazan in each well was quantified by absorbance at 570 nm using a microplate reader. Non-linear regression analysis (GraphPad Prism 7) was used to generate sigmoidal dose-response curves to calculate IC50 values for each cell line.

2.12 Determination of MIC and MBC/MFC values

The minimum inhibitory concentration (MIC) of tested compounds was determined by the broth dilution method, according to CLSI standard guidelines. Briefly, overnight cultures of *S. aureus* ATCC 25923, *E. coli* ATCC 25922, *K. pneumonia* ATCC 13883, *P. aeuruginosa* ATCC

27853 and *C. albicans* ATCC 10231 were added to tubes (10^6 CFU/mL) containing serial dilutions of compound in MHB. Microorganism growth was determined visually after overnight incubation at 37 °C (bacteria) or 30 °C (yeast). The lowest concentration at which there was no visible growth turbidity was considered as the MIC value. In order to determine minimum bactericidal concentration (MBC) and minimum fungicidal concentration (MFC), cultures representing the MIC value and at least three higher concentrations were subcultured on Mueller Hinton agar (MHA) and plates were incubated overnight at 37 or 30 °C. MBC and MFC values were determined as the lowest concentration of compounds that causes at least a 99.9% decrease in CFU/mL compared to the control.

CHAPTER 3

RESULTS AND DISCUSSION

3.1 Genome mining to identify Thioviridamide-like pathways.

Bioinformatics studies have been carried out in order to identify organisms that are genetically capable of producing thioviridamide-like molecules, within the vast panorama of microorganisms with a sequenced genome. Initial analysis, carried out using BLAST, allowed to search for proteins similar to YcaO domain protein TvaH, present in the gene cluster responsible for thioviridamide biosynthesis. The result was the identification of 22 proteins with a sequence identity greater than 50% compared to TvaH. The genomic regions surrounding the different genes identified were then analyzed by MultiGeneBlast, using the gene cluster responsible for thioviridamide synthesis as a query. The results of this second analysis identified 14 microorganisms, all belonging to the phylum *Actinobacteria* except for the cyanobacterium *Mastigocladus laminosus*, containing in their genomes clusters similar to that of thioviridamide. Indeed, the gene clusters identified have putative precursor peptides with a high sequence homology compared to that of thioviridamide (TvaA), a conserved set of tailoring enzymes and a very similar organization of genes in different clusters (Fig. 9). In this research project it was therefore decided to select 5 publicly available strains that we predicted would collectively provide much of the diversity in this family of compounds: *Amycolatopsis alba* DSM 44262, *Streptomyces* sp. NRRL S-87, *Streptomyces* sp. NRRL S-4, *Streptomyces* sp. NRRL S-15 and *Nocardiopsis potens* DSM 45234.

Among the microorganisms selected as a result of this bioinformatic study, there are two bacterial strains, *Streptomyces* sp. NRRL S-4 and *Streptomyces* sp. NRRL S-15, characterized by the presence in their genome of identical thioviridamide-like gene clusters, suggesting that the two different microorganisms are able to produce the exact same compound.

Table 3 shows a comparison between the genes present in the thioviridamide cluster and their homologues present in the gene clusters in *Amycolatopsis alba* DSM 44262, *Streptomyces* sp. NRRL S-87 and *Streptomyces* sp. NRRL S-4. These data highlight the presence in *Streptomyces* sp. NRRL S-4 and *Streptomyces* sp. NRRL S-87 of homologues for all tailoring enzymes responsible for thioviridamide synthesis (TvaB-L). In contrast, *Amycolatopsis alba* DSM 44262 lacks the gene coding for TvaJ-like Oxygenase.

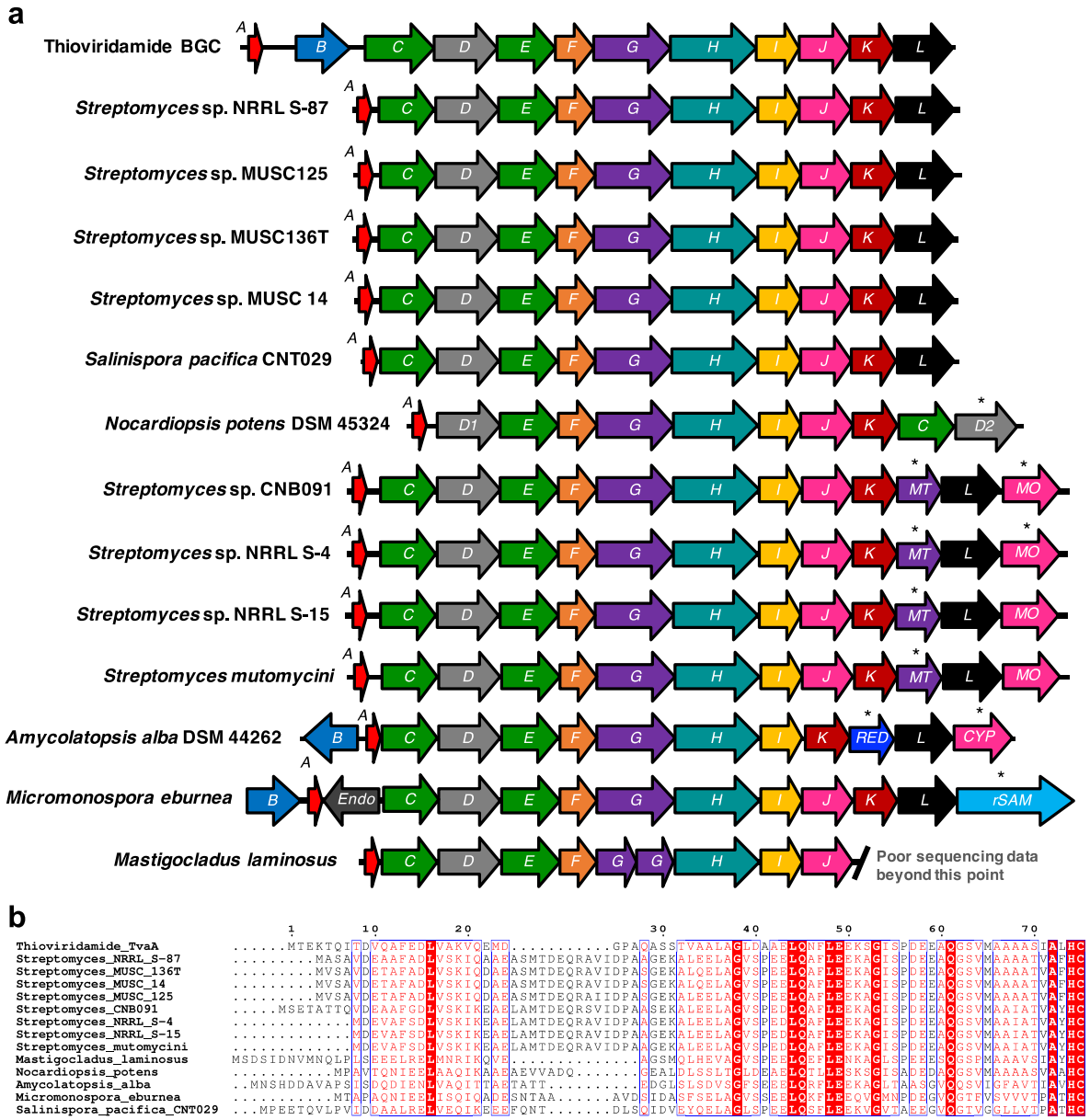

Fig. 9. Comparison of all TLM biosynthetic gene clusters. (a) All gene clusters with color coding to indicate predicted protein function: red = precursor peptide; blue = transcriptional regulator; green = phosphotransferase; grey = unknown; orange = oxidative decarboxylase; purple = methyltransferase; teal = YcaO domain; yellow = TfuA domain; pink = oxygenase; maroon = protease; black = putative membrane protein; light blue = radical SAM protein. (b) Multiple alignment of all precursor peptides. MUSCLE used for alignment, which is visualized using ESPript 3.0.[36] Identical residues are shown in white with a red background, while similar residues (Risler matrix set with global score of 0.7) are colored red and are boxed.

Table 3. Comparison of thioviridamide (*tva*) biosynthetic gene cluster (BGC) with the BGCs from *Streptomyces* sp. NRRL S-4, *Streptomyces* sp. NRRL S-87 and *A. alba* DSM 44262. Percentage identities to *tva* proteins are in brackets.

***tva* protein**	**Predicted function**	***Streptomyces sp.* NRRL S-4**	***Streptomyces sp.* NRRL S-87**	***A. alba* DSM 44262**
TvaA	Precursor peptide	ADK82_11860 **TsaA** (50%)	IF43_RS0103510 **TsdA** (52%)	AMYAL_RS0126030 **TaaA** (35%)
TvaB	Regulator	-	-	AMYAL_RS0126035 **TaaB** (28%)
TvaC	Phosphotransferase	ADK82_11855 **TsaC** (36%)	IF43_RS0103505 **TsdC** (30%)	AMYAL_RS0126025 **TaaC** (29%)
TvaD	Unknown	ADK82_11850 **TsaD** (30%)	IF43_RS0103500 **TsdD** (28%)	AMYAL_RS0126020 **TaaD** (29%)
TvaE	Phosphotransferase	ADK82_11845 **TsaE** (27%)	IF43_RS0103495 **TsdE** (29%)	AMYAL_RS0126015 **TaaE** (30%)
TvaF	Flavin-dependent oxidative decarboxylase	ADK82_11840 **TsaF** (41%)	IF43_RS0103490 **TsdF** (41%)	AMYAL_RS47825 **TaaF** (38%)
TvaG	*N*-methyltransferase	ADK82_11835 **TsaG** (50%)	IF43_RS0103485 **TsdG** (49%)	AMYAL_RS0126005 **TaaG** (45%)
TvaH	YcaO domain	ADK82_11830 **TsaH** (54%)	IF43_RS0103480 **TsdH** (54%)	AMYAL_RS0126000 **TaaH** (48%)
TvaI	TfuA-like domain	ADK82_11825 **TsaI** (55%)	IF43_RS0103475 **TsdI** (53%)	AMYAL_RS0125995 **TaaI** (48%)
TvaJ	Oxygenase	ADK82_11820 **TsaJ** (39%)	IF43_RS0103470 **TsdJ** (42%)	-
TvaK	Protease	ADK82_11815 **TsaK** (32%)	IF43_RS0103465 **TsdK** (26%)	AMYAL_RS47820 **TaaK** (29%)
TvaL	Membrane protein	ADK82_11805 **TsaL** (30%)	IF43_RS0103460 **TsdL** (33%)	AMYAL_RS0125980 **TaaL** (31%)
TvaM	Regulator	-	-	-
TvaN	Regulator	-	-	-
TvaO	Unknown	-	-	-

Tables 4, 5 and 6 show the putative thioviridamide-like gene clusters identified in *A. alba* DSM 44262, *Streptomyces sp.* NRRL S-4 and *Streptomyces sp*. NRRL S-87, respectively. The interesting data that emerges from these studies is the presence in the cluster of *A. alba* DSM 44262 and *Streptomyces sp.* NRRL S-4 of genes encoding tailoring enzymes not present in the BGC of thioviridamide, such as NAD(P)H-dependent reductase (taaRED) and a Cytochrome P450 (taaCYP), in *A. alba* DSM 44262, and O-methyltransferase (tsaMT) and monooxygenase (tsaMO) in *Streptomyces sp.* NRRL S-4. The presence of additional tailoring enzymes suggest the possibility for the precursor peptides to undergo additional post-translational modifications, and the ability of these microorganisms to synthesize thioviridamide-like compounds with peculiar chemical characteristics.

Table 4. Thioalbamide (taa) biosynthetic gene cluster. Genes coloured red do not have homologues in the thioviridamide BGC.

***tsd* gene name**	**Original locus tag**	**Protein size**	**Predicted function**	**Conserved domain**
taaB	AMYAL_RS0126035	252	Transcriptional regulator	pfam03704
taaA	AMYAL_RS0126030	80	Precursor peptide	-
taaC	AMYAL_RS0126025	367	Phosphotransferase	pfam01636
taaD	AMYAL_RS0126020	329	Unknown	-
taaE	AMYAL_RS0126015	290	Phosphotransferase	pfam01636
taaF	AMYAL_RS47825	199	Flavin-dependent oxidative decarboxylase	PRK05579
taaG	AMYAL_RS0126005	408	*N*-methyltransferase	pfam06325
taaH	AMYAL_RS0126000	451	YcaO domain	pfam02624
taaI	AMYAL_RS0125995	219	TfuA-like domain	pfam07812
taaK	AMYAL_RS47820	248	Protease	pfam00112
taaRED	AMYAL_RS0125985	281	NAD(P)H-dependent reductase	pfam00106
taaL	AMYAL_RS0125980	310	Membrane protein	-
taaCYP	AMYAL_RS46165	401	Cytochrome P450	pfam00067

Table 5. Thiostreptamide S4 (*tsa*) biosynthetic gene cluster. Genes coloured red do not have homologues in the thioviridamide BGC.

***tsa* gene name**	**Original locus tag**	**Protein size**	**Predicted function**	**Conserved domain**
tsaA	ADK82_11860	79	Precursor peptide	-
tsaC	ADK82_11855	287	Phosphotransferase	pfam01636
tsaD	ADK82_11850	302	Unknown	pfam09118
tsaE	ADK82_11845	330	Phosphotransferase	pfam01636
tsaF	ADK82_11840[a]	203	Flavin-dependent oxidative decarboxylase	PRK05579
tsaG	ADK82_11835	372	*N*-methyltransferase	pfam06325
tsaH	ADK82_11830	455	YcaO domain	pfam02624
tsaI	ADK82_11825	240	TfuA-like domain	pfam07812
tvaJ	ADK82_11820[a]	280	2-oxoglutarate and Fe(II)-dependent oxygenase	pfam05721
tsaK	ADK82_11815	271	Protease	pfam00112
tsaMT	ADK82_11810[a]	234	*O*-methyltransferase	pfam13649
tsaL	ADK82_11805	259	Membrane protein	-
tsaMO	ADK82_11800	336	Monooxygenase[b]	pfam00296

a. Annotated as pseudogenes in the originally deposited genome sequence, but there appear to be no problems with the revised open reading frames.
b. The structure of thiostreptamide S4 indicates that this protein does not function in the pathway, although a role cannot be ruled out.

Table 6. Thiostreptamide S87 (*tsd*) biosynthetic gene cluster.

***tsd* gene name**	**Original locus tag**	**Protein size**	**Predicted function**	**Conserved domain**
tsdA	IF43_RS0103510	83	Precursor peptide	-
tsdC	IF43_RS0103505	332	Phosphotransferase	pfam01636
tsdD	IF43_RS0103500	335	Unknown	-
tsdE	IF43_RS0103495	265	Phosphotransferase	pfam01636
tsdF	IF43_RS0103490	201	Flavin-dependent oxidative decarboxylase	PRK05579
tsdG	IF43_RS0103485	372	*N*-methyltransferase	pfam06325
tsdH	IF43_RS0103480	450	YcaO domain	pfam02624
tsdI	IF43_RS0103475	229	TfuA-like domain	pfam07812
tvdJ	IF43_RS0103470	292	2-oxoglutarate and Fe(II)-dependent oxygenase	pfam05721
tsdK	IF43_RS0103465	237	Protease	pfam00112
tsdL	IF43_RS0103460	280	Membrane protein	-

3.2 Production of thioviridamide-like molecules.

Each of the bacterial strains selected for this study was subjected to the same fermentation conditions reported for the production of thioviridamide.[20] Contrary to expectations, this strategy did not allow any thioviridamide-like compound to be identified. For this reason, the microorganisms were subjected to fermentation in different culture media and growth conditions and microbial extracts were subjected to LC-MS analysis, looking for fermentation products compatible with those predicted by the study of gene clusters. A solid version of bottromycin production medium (BPM)[30] was found to be the most suitable growth condition for TLMs production, since it allowed different microorganisms to produce different compounds with masses compatible with the TLMs predicted by the analysis of the respective precursor peptides, except for *N. potens* DSM 45234, which did not lead to the production of the expected compound.

Fig. 10a shows extracted ion chromatograms from *A. alba* DSM 44262, *Streptomyces* sp. NRRL S-4, and *Streptomyces* sp. NRRL S-87 showing relative levels of production of the newly identified compounds.

A. alba DSM 44262 produced a compound (thioalbamide, Fig. 10b) with m/z 1329.6349, corresponding to the molecular formula $C_{61}H_{97}N_{14}O_{11}S_4^+$ (calculated M^+: 1329.6339). High resolution (HR) MS^2 analysis of this molecule (Fig. 11) provided a fragmentation pattern that supported a thioviridamide-like structure, including the presence of thioamides (and associated losses of H2S, −33.99 Da), fragmentation consistent with the predicted linear portion of the molecule, and an MS^2 fragment (m/z 607.3376, Fig. 10 and Fig. 11) that correlated with a (2-aminovinyl)-3-methyl-cysteine (AviMeCys) containing macrocycle (predicted m/z 607.3385).

As predicted by the study of gene clusters, the identical gene clusters present in *Streptomyces sp.* NRRL S-4 and *Streptomyces sp.* NRRL S-15, led to production in each of the two strains of a compound (thiostreptamide S4, Fig. 10b and Fig. 13) with m/z 1377.5479 that eluted at an identical retention time (Fig. 12), corresponding to the molecular formula $C_{60}H_{93}N_{14}O_{11}S_6^+$ (calculated M^+ = 1377.5467). As with thioalbamide, $HRMS^2$ analysis of this molecule provided a fragmentation pattern that supported a thioviridamide-like structure, including multiple thioamides and a putative AviMeCys-containing macrocycle fragment (observed m/z 687.3260, predicted m/z 687.3283, Fig. 2b and Fig. 13). This preliminary analysis indicated that *Streptomyces sp.* NRRL S-4 and S-15 pathways produce identical compounds, although differences in stereochemistry cannot be ruled out.

Streptomyces sp. NRRL S-87 produced a compound (thiostreptamide S87, Fig. 10b) with m/z 1305.4871, corresponding to the molecular formula $C_{56}H_{85}N_{14}O_{10}S_6^+$ (calculated M^+: 1305.4892). As before, $HRMS^2$ analysis (Fig. 14) provided thioviridamide-like fragments that were consistent with the predicted precursor peptide.

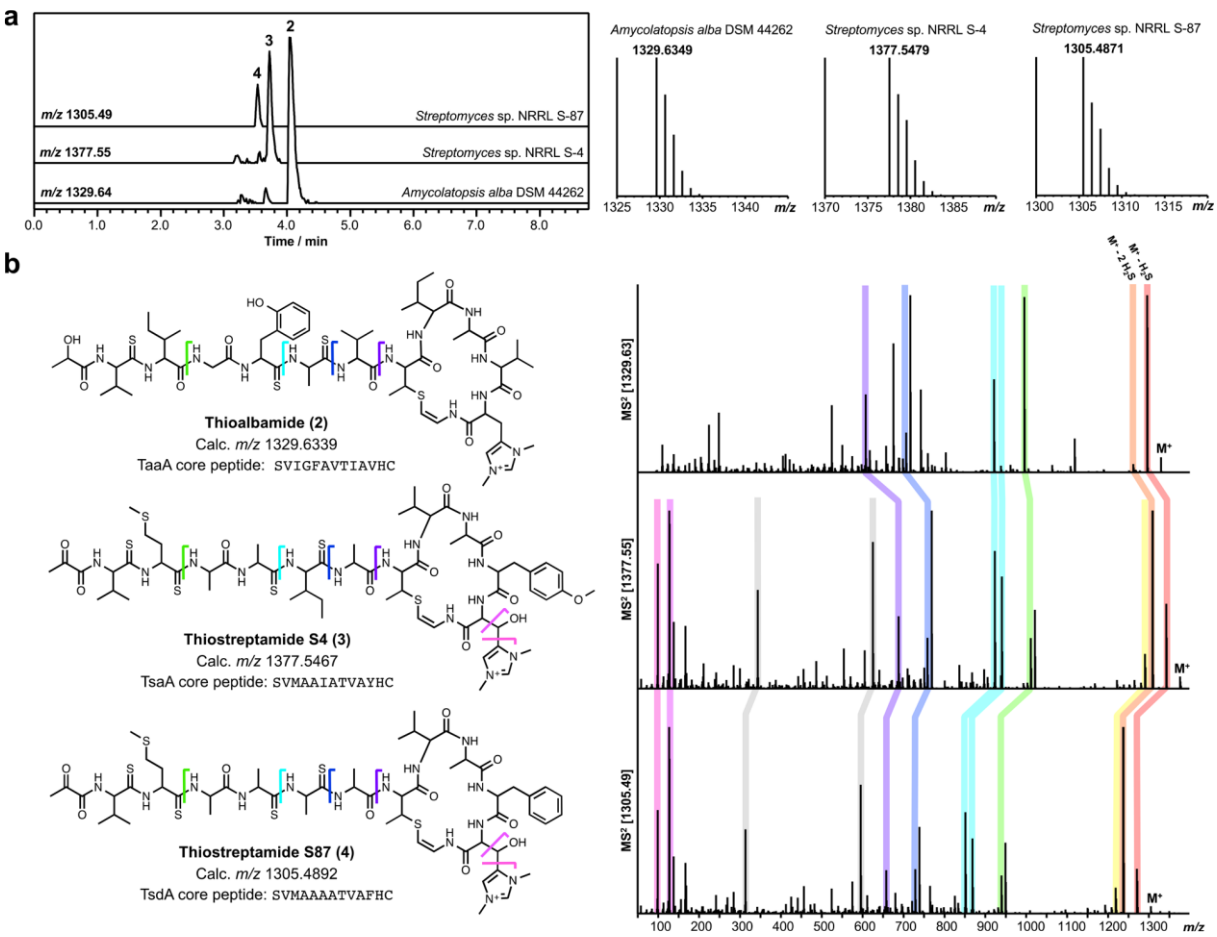

Fig. 10. Identification of novel TLMs. (a) Extracted ion chromatograms from *A. alba* DSM 44262, *Streptomyces sp.* NRRL S-4, and *Streptomyces sp.* NRRL S-87 showing relative levels of production and exact masses for each compound. (b) Structures of each compound alongside MS^2 data indicating analogous fragments from each compound (grey shading indicates abundant common fragments that could not be annotated). The core peptide sequences for each compound are also shown. The structures of thioalbamide and thiostreptamide S-4 were confirmed by NMR, while the structure of thiostreptamide S-87 is a proposal that correlates with MS^2 data, the core peptide sequence, and predicted post-translational modifications.

An important difference between thioviridamide and the compounds identified at this stage of the work is the number and position of thioamide groups in the various molecules. The most striking structural feature of thioviridamide is a contiguous sequence of five thioamide-containing residues. Conversely, exact mass and MS^2 data, obtained up to this point, suggest the presence of three noncontiguous thioamide linkages in thioalbamide, and four in thiostreptamide S4 and thiostreptamide S87. UV absorption spectra of each compound provided maxima of 270−272 nm (Fig. 15), which is characteristic of thioamides. [37] A second difference is the absence of the 2-hydroxy-2-methyl-4-oxopentanoyl group at the N-terminus, replaced by a lactyl group, in thioalbamide, and by a pyruvyl group in thiostreptamide S-4 and thiostreptamide S-87.

Analysis of the fermentation samples of *Streptomyces* sp. NRRL S-4 and *Streptomyces* sp. NRRL S-87 allowed to identify two additional thioviridamide-like compounds with m/z 1393.5427 and m/z 1321.4813, respectively. These masses indicated the addition of one oxygen (calculated. m/z 1393.5416 and m/z 1321.4841) to thiostrepamide S4 and thiostreptamide S87, respectively and the $HRMS^2$ analysis confirmed that these molecules are the oxidation products of the two previously identified compounds at the level of the sulfur atom on the side chain of the methionine residue (Fig. 16 and Fig. 17). Indeed, the MS^2 analysis performed on the two compounds showed the loss of methanesulfenic acid (CH_3SOH, 64.00Da) from the parent ion, which is characteristic of oxidized methionine.[38, 39] However, the small and not constant production of these products and the absence in their respective gene clusters of genes coding for enzymes suitable for carrying out this modification, implied that these derivatives are the result of a spontaneous oxidation reaction during the process of extraction and isolation of the molecules. The absence of collateral products in the fermentation samples of *A.alba* DSM 44262 is due to the absence of methionine residues in the core peptide, replaced by an isoleucine residue.

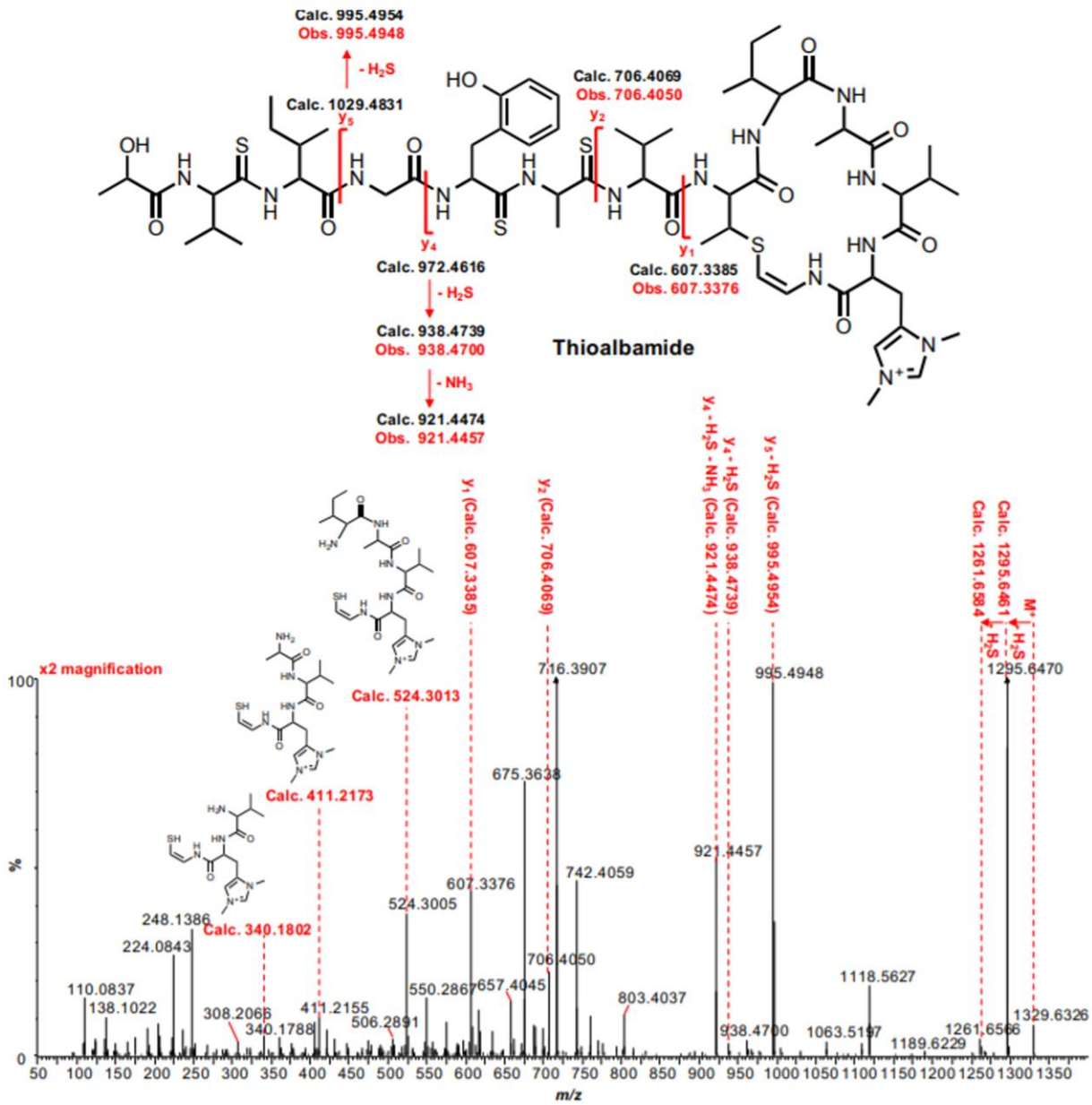

Fig. 11. MS^2 analysis of thioalbamide. y fragment numbering is limited to the linear portion of the peptide. Data acquired on Synapt G2-Si mass spectrometer

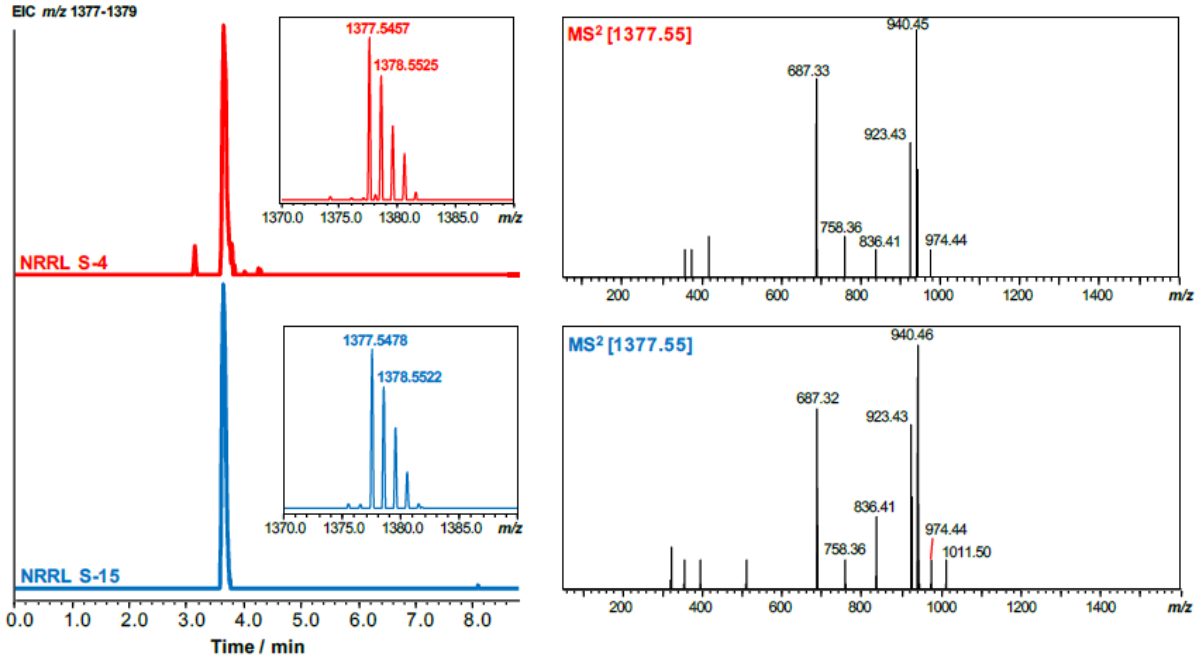

Fig. 12. Production of thiostreptamide S4 by *Streptomyces* sp. NRRL S-4 and *Streptomyces* sp. NRRL S-15. Data acquired on a Shimadzu IT-TOF mass spectrometer.

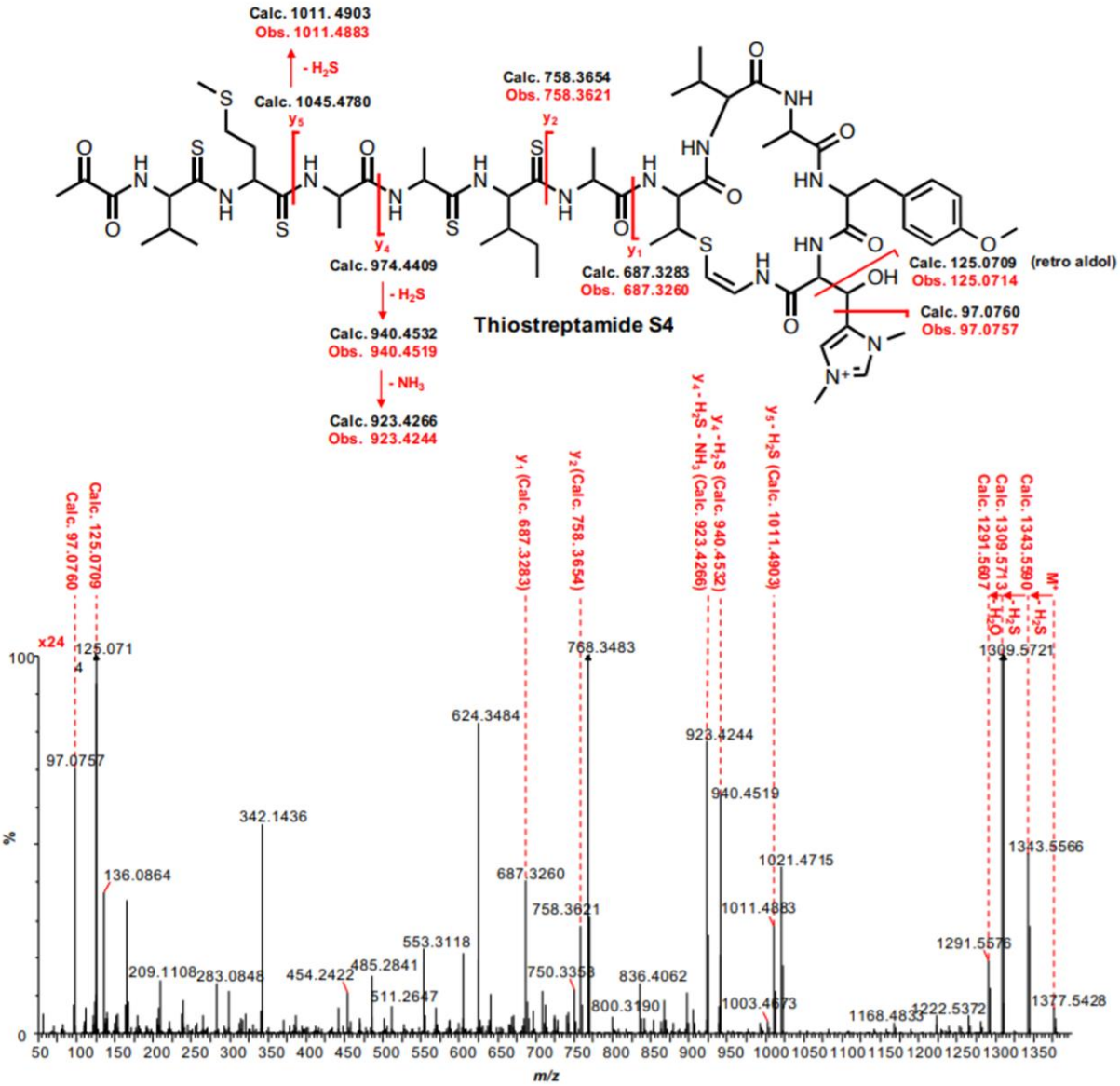

Fig. 13. MS^2 analysis of thiostreptamide S4. Data acquired on a Synapt G2-Si mass spectrometer.

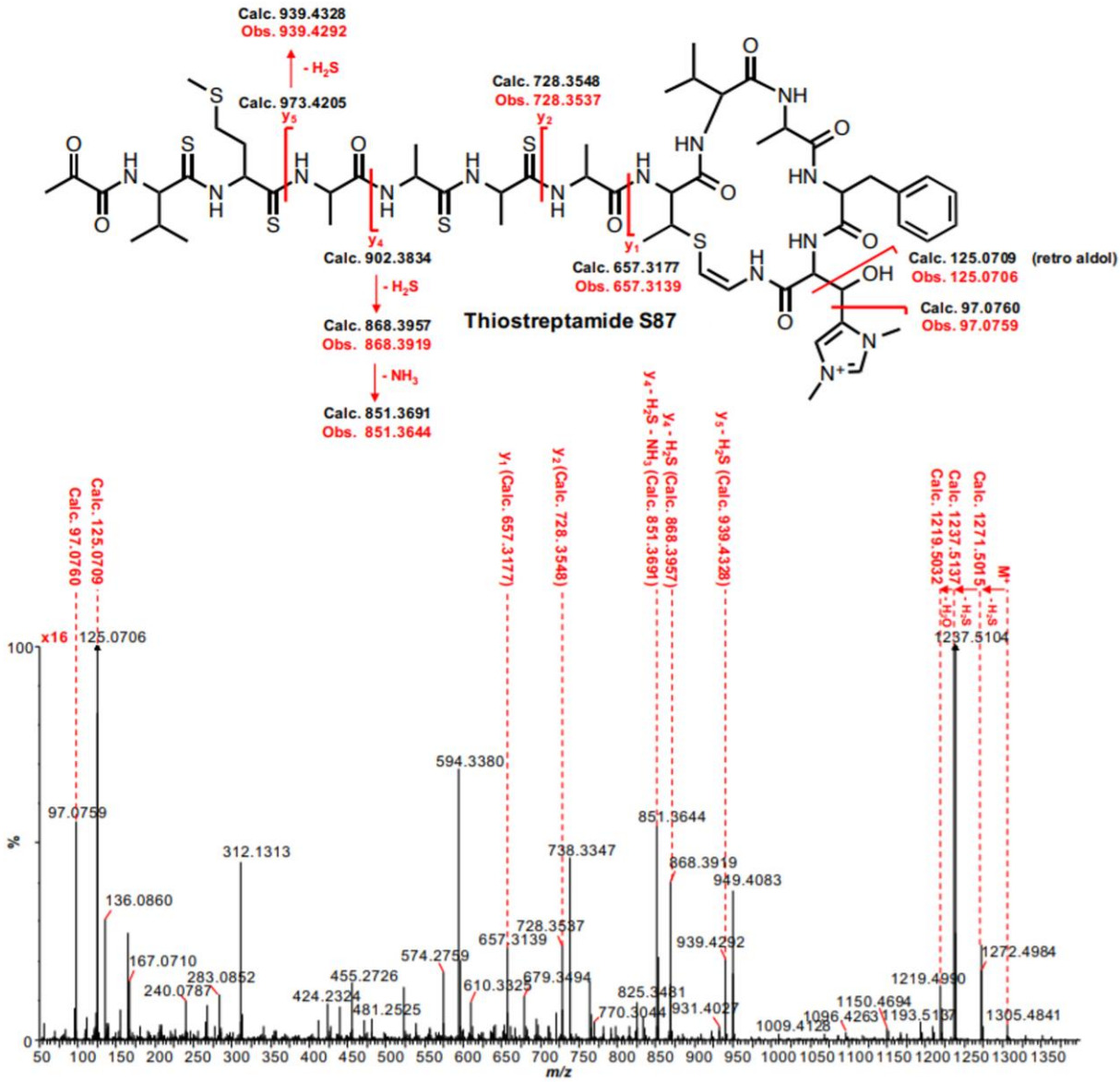

Fig. 14. MS^2 analysis of thiostreptamide S87. Data acquired on a Synapt G2-Si mass spectrometer.

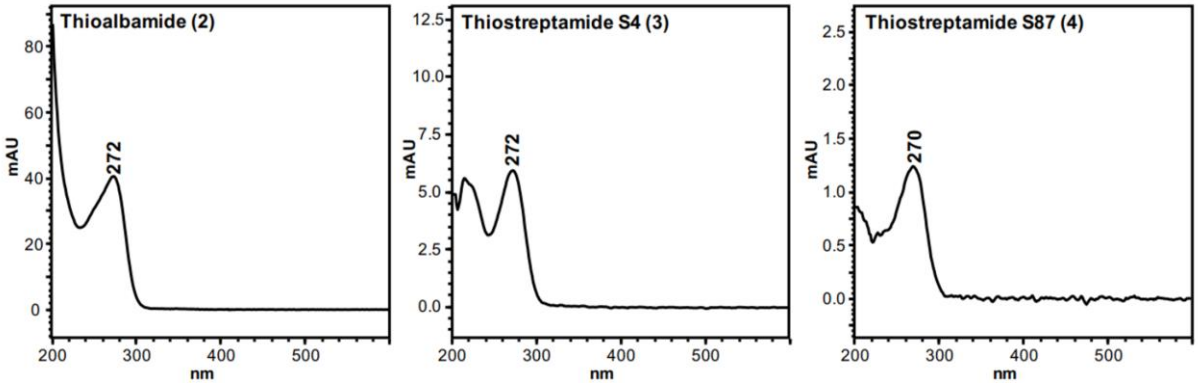

Fig. 15. UV absorption spectra for thioalbamide, thiostreptamide S4 and Thiostreptamide S87 showing maxima of 270-272 nm that are characteristic of thioamide groups. Spectra were obtained on a Shimadzu Nexera X2 UHPLC during LC-MS analysis.

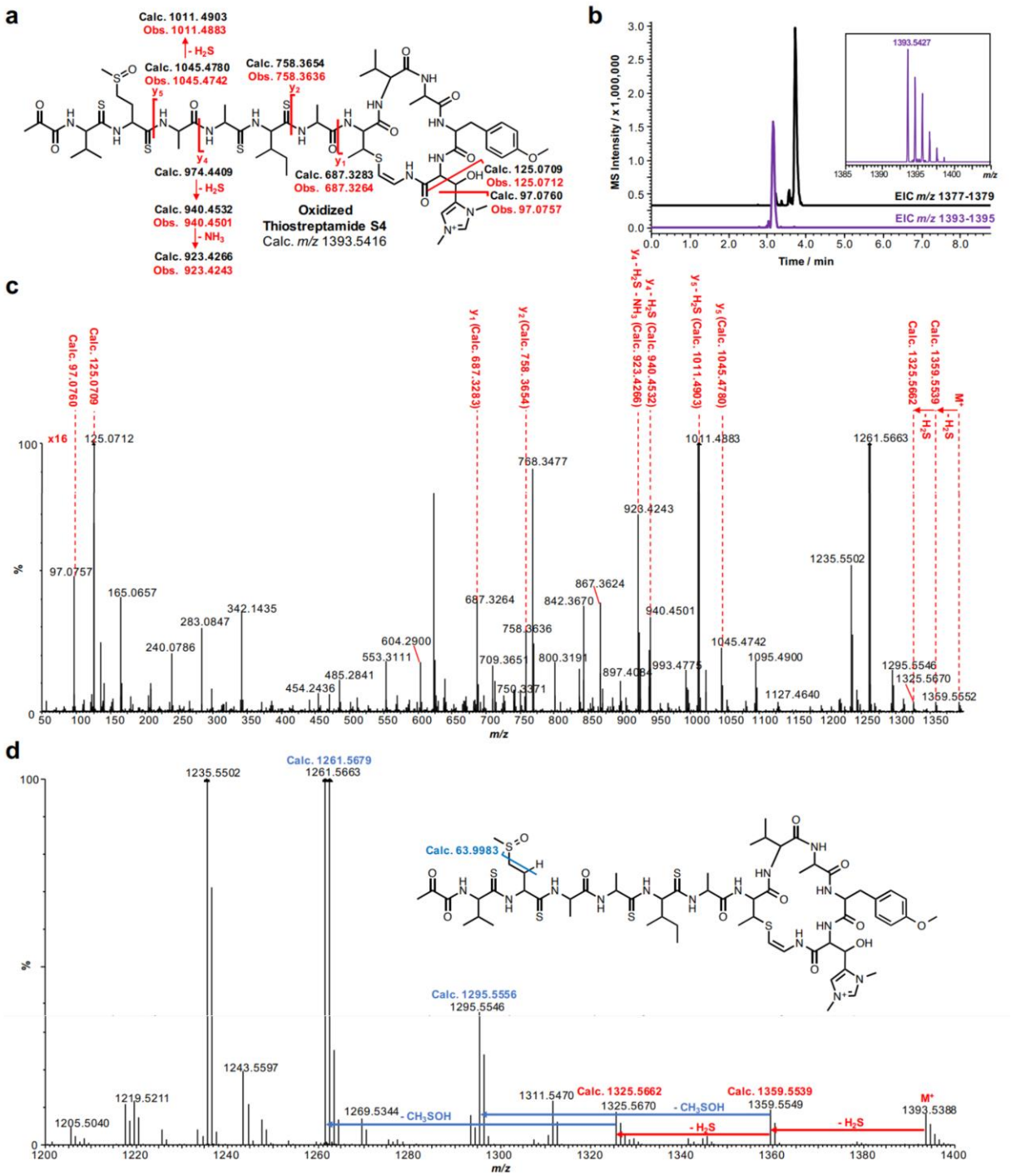

Fig. 16. LC-MS^2 analysis of oxidized thiostreptamide S4 produced by *Streptomyces sp.* NRRL S-4. (a) Structure and MS^2 fragmentation of oxidized thiostreptamide S4. (b) LC-MS profile of oxidized and non oxidized thiostreptamide S4. (c) MS^2 fragmentation of oxidized thiostreptamide S4. (d) Zoomed section of MS^2 spectrum showing losses of H_2S and methanesulfenic acid. Data are acquired on a Synapt G2-Si mass spectrometer.

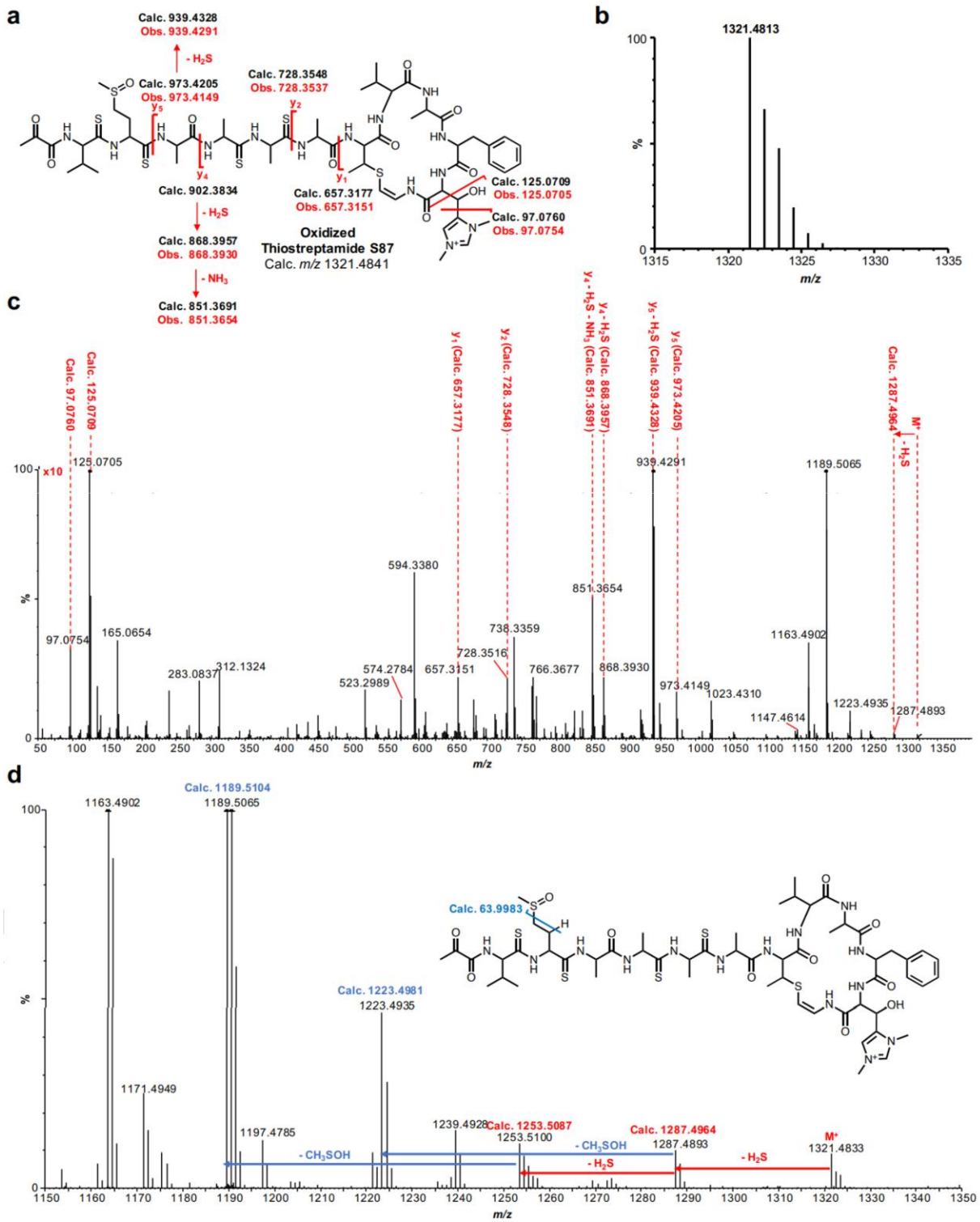

Fig. 17. LC-MS^2 analysis of oxidized thiostreptamide S87 produced by *Streptomyces sp.* NRRL S-87. (a) Structure and MS^2 fragmentation of oxidized thiostreptamide S87. (b) MS spectrum of oxidized thiostreptamide S4. (c) MS^2 fragmentation of oxidized thiostreptamide S4. (d) Zoomed section of MS^2 spectrum showing losses of H_2S and methanesulgenic acid. Data are acquired on a Synapt G2-Si mass spectrometer.

3.3 Gene cluster disruption in native strain and gene cluster heterologous expression.

To confirm that these molecules were indeed produced by thioviridamide-like pathways, we employed two different genetic approaches: gene disruption in a native producer strain and heterologous expression of a gene cluster.

The different bacterial strains were initially subjected to experiments to identify the microorganism most suitable for genetic manipulation. Through intergeneric conjugation, several integrative plasmids were introduced into each: pIB139 (containing the integration site ΦC31) and pIJ10257 (containing the integration site ΦBT1). These experiments highlighted the possibility to easily manipulate the genome of *Streptomyces sp.* NRRL S-4, which was then chosen as a model microorganism for gene cluster disruption experiments.

Gene cluster disruption was achieved by single crossover recombination between the tsaH gene (encoding a YcaO domain protein) and its truncated sequence cloned in pKC1132 to generate *Streptomyces sp.* NRRL S-4 ΔtsaH. The mutant strain obtained was cultured, at the growth conditions optimized in the previous phase of the project, and the extract obtained was analysed by LC/MS and compared with that from a culture of the wild-type strain. Production of thiostreptamide S4 was completely abolished in this mutant strain (Fig. 19), indicating that the gene cluster does indeed make this thioviridamide-like molecule.

To support this result, it was decided to clone the entire gene cluster responsible for thiostreptamide S4 biosynthesis and to express it in a host microorganism.

The molecular cloning of large regions of DNA, such as whole gene clusters, involves the use of molecular biology techniques different from those used for common cloning. The technique chosen for this purpose was cloning through yeast-mediated recombination (TARcloning). This technique is based on double crossing-over recombination, in yeast, between the regions adjacent to the gene cluster to be cloned and homologous regions (capture arms) present on a specific vector, called "capture vector".

A 19 kbp sequence from *Streptomyces sp.* NRRL S-4 containing the putative thiostreptamide S4 gene cluster, as well as flanking regions up- and downstream, was cloned into the ΦC31 integrative vector pCAP03[33] using TARcloning in *Saccharomyces cerevisiae* VL6-48N.[29] A successful clone (TARS4) was verified by PCR and restriction analysis (Fig. 18), in order to evaluate the real presence of the entire gene cluster and to avoid collateral recombination events with consequent partial cloning of the gene cluster. Verified TARS4 was introduced into *Streptomyces coelicolor* M1146[40] by intergeneric conjugation. *S. coelicolor* M1146-TARS4

was cultured under previously standardized conditions, and its LC-MS fermentation profile was compared with a control strain containing an empty pCAP03 vector and wild-type *Streptomyces* sp. NRRL S-4 as a positive control (Fig. 19). *S. coelicolor* M1146-TARS4 produced a compound with m/z 1377.55 that had an identical retention time and MS^2 spectrum to those of thiostreptamide S4 (Fig. 19 and Fig. 20), thereby proving that the cloned region is sufficient for thiostreptamide S4 biosynthesis.

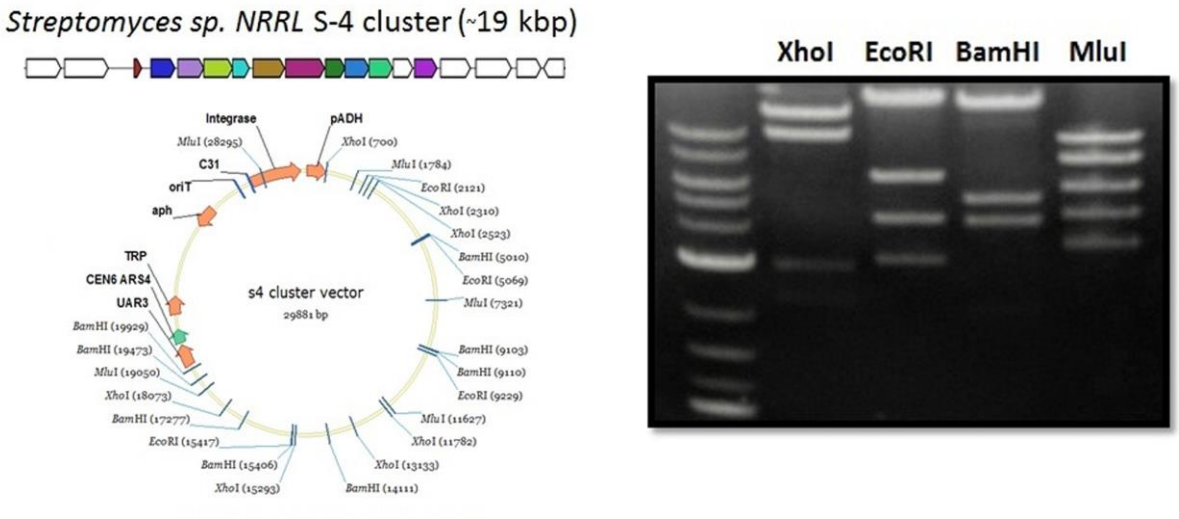

Fig. 18. Restriction analysis of TARS4, by using XhoI, EcorI, BamHI and MluI restriction enzymes.

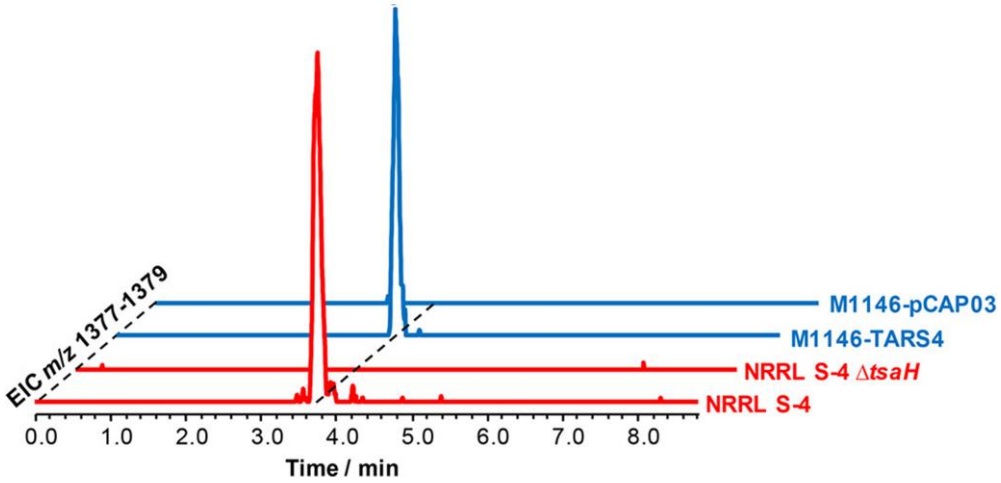

Fig. 19. Production of thiostreptamide S4 in *Streptomyces sp.* NRRL S-4 and in *S. coelicolor* M1146-TARS4. Control strains unable to produce the compound are also shown.

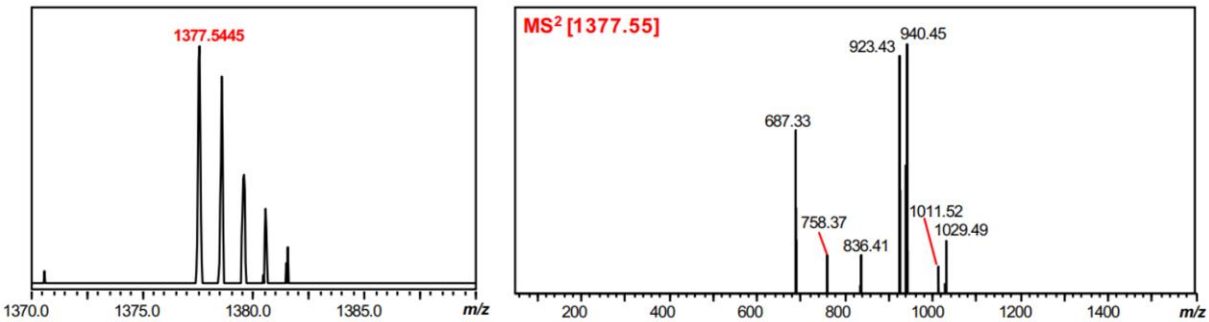

Fig. 20. MS and MS^2 analysis of thiostreptamide S4 produced by *S. coelicolor* M1146-TARS4. Data acquired on a Shimadzu IT-TOF mass spectrometer.

3.4 Detailed structural analysis reveals the diversity within the thioviridamide family.

To confirm the MS^2 data and to pinpoint the location of additional post-translational modifications, fermentation cultures of the native producer strains were scaled up, and each compound was purified for structural elucidation by NMR. Thioalbamide and thiostreptamide S4 were obtained in yields of 2 and 0.38 mg per liter of solid culture from their respective native producers, and 1D and 2D NMR experiments (^{1}H, ^{13}C, COSY, HSQC, HMBC, Figures 21-29, Table 7) allowed us to establish their chemical structures.

The ^{13}C NMR spectrum for thioalbamide showed three downfield signals at δC 206.7, 207.0, and 207.5 corresponding to nonprotonated carbons and indicating the presence of thioamide groups. These signals and their associated HMBC data correlate with the MS^2 data for this compound, proving that the molecule has three thioamide linkages in the linear portion of the molecule. HMBC and COSY correlations also confirmed that the molecule has an AviMeCys-containing macrocycle, consistent with a Thr8 residue in the core peptide of TaaA instead of the Ser8 residue of the core peptide of thioviridamide. NMR analysis of the N1,N3-dimethylhistidinium residue showed that its β-carbon is a CH_2 group (δC 22.6) and therefore lacks the β-hydroxy group present in thioviridamide. This is in agreement with the lack of a TvaJ-like 2- oxoglutarate/Fe(II)-dependent hydroxylase in the thioalbamide pathway. Moreover, MS^2 data indicated that Phe5 is hydroxylated in thioalbamide, but the precise location of this modification could not be determined by MS^2. The ^{1}H NMR spectrum of thioalbamide showed the presence of four nonequivalent aromatic protons at δH 6.83 (^{1}H, ddd, 8.1, 8.0, 1.6), 6.87 (^{1}H, dd, 8.0, 1.6), 7.12 (^{1}H, ddd, 8.1, 8.0, 1.6), and 7.19 (^{1}H, dd, 8.0, 1.6), corresponding to protons on the 1, 2, 3, and 4 positions of the phenyl group, and indicating that it is hydroxylated at the 5-position of the ring. Alongside the absence of a β-hydroxy group on histidine, this suggests that a cytochrome P450 (TaaCYP) encoded in the taa cluster does not functionally replace the hydroxylase absent from this pathway and instead catalyzes aromatic hydroxylation, thereby generating additional structural diversity within the TLM family. The

predicted N-terminal lactate moiety of thioalbamide was also confirmed based on the HMBC correlations between the methyl group at δH 1.38 (3H, d, 6.8) with carbon signals at δC 69.2 and 177.6. Interestingly, this is analogous to the N-terminus of JBIR-140, which is produced when the thioviridamide BGC is expressed in *Streptomyces avermitilis* SUKA17.[41] We propose that a NAD(P)H-dependent reductase (TaaRED) catalyzes this reduction in the thioalbamide pathway, whereas it is likely that the reduction to generate JBIR-140 is catalyzed by a promiscuous reductase from *S. avermitilis*.

We were also able to pinpoint the post-translational modifications of thiostreptamide S4 by analysis of the MS^2 and NMR data. While it was not possible to establish full 2D NMR correlations throughout this compound, four thioamide linkages were identified by HMBC data (δC 200.6, 201.2, 202.2, and 204.6). HMBC correlations between a methyl group at δH 2.35 (3H, s) with carbon signals at δC 160.4 and 197.0, along with HMBC correlations between an amide proton at δH 8.22 with carbon signals at δC 160.4 and 63.1, allowed us to confirm the N-terminal pyruvyl group attached to Val′ (Fig. 30). The MS^2 fragment predicted to be the AviMeCys-containing macrocycle (m/z 687.33) matches a mass calculated from the core peptide and expected post-translational modifications if the macrocycle features a methyl group in addition to a hdmHis residue. Accordingly, the ^{1}H NMR spectrum displayed a singlet at δH 3.71 and two equivalent aromatic protons at δH 6.79 (2H, d, 8.7) and 7.03 (2H, d, 8.7) that were consistent with O-methylation of Tyr11, presumably catalyzed by the additional methyltransferase (TsaMT, pfam08242) encoded in the tsa gene cluster. The lack of any further oxidative modifications indicated that the flavin-dependent monooxygenase at the end of the gene cluster (TsaMO) is not involved in thiostreptamide S4 biosynthesis. Along with characteristic NMR signals, the presence of a hdmHis residue was supported by an MS^2 fragment of m/z 125.07 for thiostreptamide S4 that concurs with retro-aldol fragmentation of the hdmHis residue (Fig. 13) and was not present in the MS^2 spectrum of thioalbamide.

We were unable to obtain a sufficient amount of thiostreptamide S87 for detailed NMR characterization, but its exact mass and MS^2 spectrum (Fig. 14) were fully consistent with the structure reported in Fig. 10. This is in agreement with a lack of any additional tailoring enzymes encoded in the S-87 tsd gene cluster compared to the tva gene cluster (Fig. 9a). MS^2 data for thiostreptamide S87 provided a macrocycle mass (m/z 657.31) that fits with the core peptide sequence assuming AviMeCys formation and the presence of the hdmHis residue. This is supported by MS^2 fragmentation to generate m/z 125.07, which was also seen for thiostreptamide S4 and is indicative of the hdmHis residue. Notably, the y fragments of thiostreptamide S87 signified an N-terminal pyruvyl group.

Table 7. NMR assignments for thioalbamide in CD_3OD

Residue[a]	δ_C, mult.	δ_H, mult. (*J*, in Hz)	Residue[a]	δ_C, mult.	δ_H, mult. (*J*, in Hz)
LA			**avMCys**		
1	177.6, C		1	173.2, C	
2	69.2, CH	4.17 (q, 6.8)	2	57.3, CH	3.44 (dd, 10.7, 6.5)
3	21.3, CH_3	1.38 (d, 6.8)	3	44.5, CH	3.44 (dd, 10.7, 6.5)
Val'			4	20.2, CH_3	1.19 (d, 6.5)
1	206.7, C		5	99.3, CH	5.47 (d, 7.0)
2	65.0, CH	4.57 (d, 7.9)	6	136.4, CH	7.29 (d, 7.0)
3	35.2, CH	2.22 (dd, 7.9, 6.9)	NH		8.05 (d, 6.5)
4[b]	20.2, CH_3	0.91 (d, 6.9)	**Ile 2**		
5[b]	18.6, CH_3	0.96 (d, 6.9)	1	175.0, C	
NH		ND[c]	2	64.4, CH	3.84 (dd, 7.5, 4.5)
Ile 1			3	37.1, CH	2.07, m
1	175.5, C		4	15.7, CH_3	0.98 (d, 6.7)
2	65.6, CH	4.82, m	5	28.4, CH_2	1.31, m; 1.83, m
3	36.8, CH	2.13, m	6	11.2, CH_3	0.95 (t, 6.7)
4	16.5, CH_3	1.02 (d, 7.2)	NH		7.21 (d, 4.5)
5	26.6, CH_2	1.35, m; 1.64, m	**Ala**		
6	11.0, CH_3	0.95 (t, 7.2)	1	177.0, C	
NH		ND[c]	2	54.3, CH	4.08 (dd, 7.3, 4.5)
Gly			3	17.5, CH_3	1.59 (d, 7.3)
1	173.6, C		NH		7.39 (d, 4.6)
2	46.3, CH_2	3.65 (d, 16.0);	**Val 2**		
		3.91 (d, 16.0)	1	173.6, C	
NH		ND[c]	2	58.4, CH	4.44 (dd, 9.5, 4.3)
PheOH'			3	30.2, CH	2.43, m
1	207.0, C		4[b]	19.3, CH_3	0.86 (d, 7.0)
2	67.0, CH	4.91 (dd, 9.8, 4.0)	5[b]	17.1, CH_3	0.78 (d, 7.0)
3	35.1, CH_2	3.15 (d, 13.7);	NH		7.64 (d, 9.5)
		3.31 (d, 13.7)	**dmHis**		
4	124.4, C		CO	169.3, C	
5	156.1, C		α	54.1, CH	4.32 (dd, 10.4, 5.3)
6	116.4, CH	6.87 (dd, 8.0, 1.6)	β	22.6, CH_2	3.20 (ddd, 16.1, 10.4, 5.3)
7	129.8, CH	7.12 (ddd, 8.1, 8.0, 1.6)			3.73 (dd, 16.1, 10.4)
8	121.3, CH	6.83 (ddd, 8.1, 8.0, 1.6)	2	137.8, CH	8.75, br s
9	132.2, CH	7.19 (dd, 8.0, 1.6)	4	133.7, C	
NH		ND[c]	5	123.5, CH	7.51, br s
Ala'			N^{τ}-Me	36.4, CH_3	3.91, s
1	207.5, C		N^{π}-Me	34.0, CH_3	3.86, s
2	65.0, CH	5.45 (q, 7.2)	NH		10.6 (d, 10.4)
3	19.2, CH_3	1.75 (d, 7.2)			
NH		ND[c]			
Val 1					
1	173.2, C				
2	69.6, CH	4.28 (d, 10.6)			
3	30.9, CH	2.36, m			
4[b]	21.5, CH_3	1.04 (d, 6.7)			
5[b]	20.4, CH_3	1.03 (d, 6.7)			
NH		ND[c]			

a. Residue naming and numbering is shown in Figure S12.
b. For each valine, these signals may be interchanged.
c. As the spectra were acquired in CD_3OD, some of the NH protons were not visible due to deuterium exchange, although all of the NH protons from the macrocycle are visible due to their unusual stability towards D exchange.

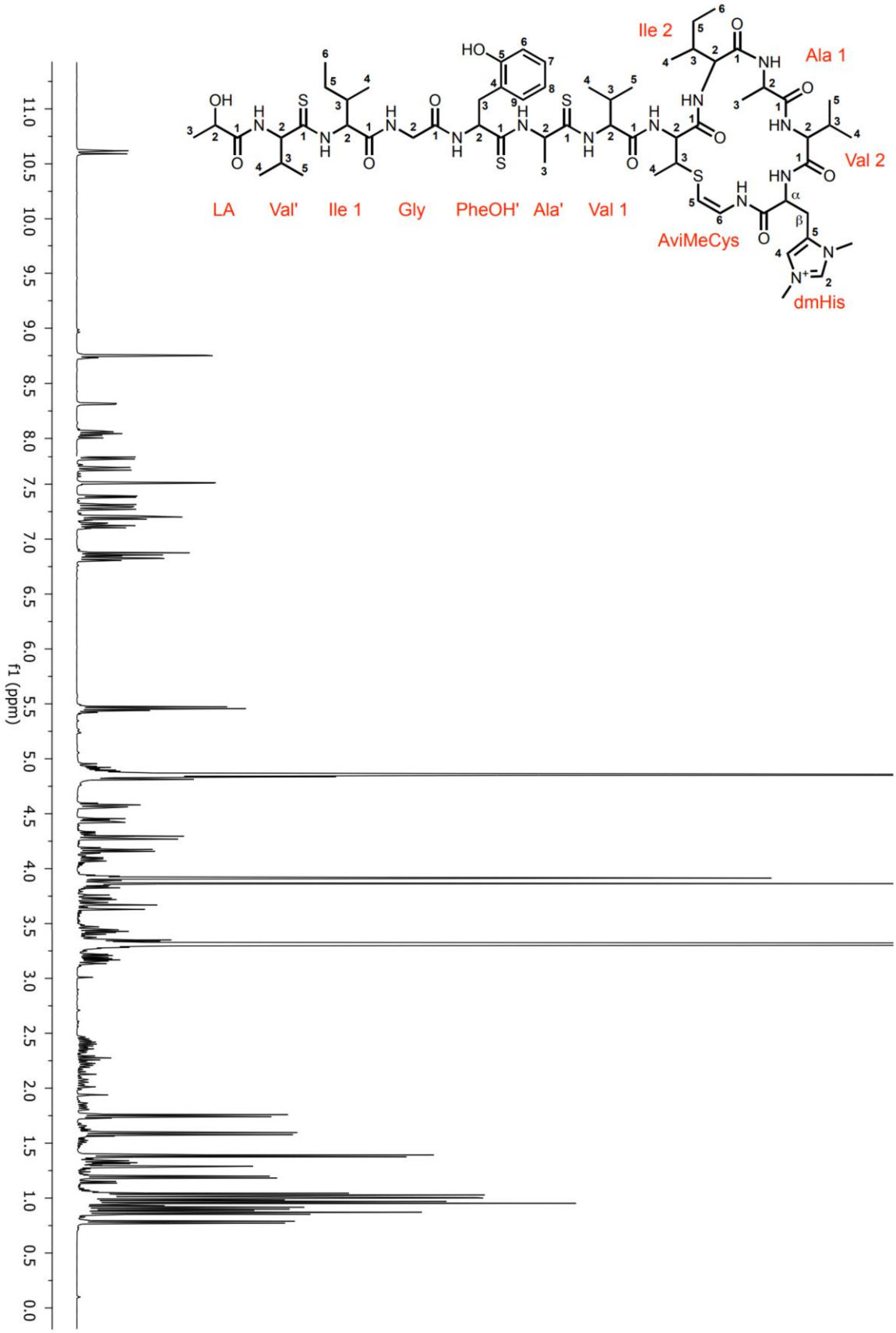

Fig. 21. ^{1}H NMR spectrum of thioalbamide in CD_3OD with residue naming and numbering scheme.

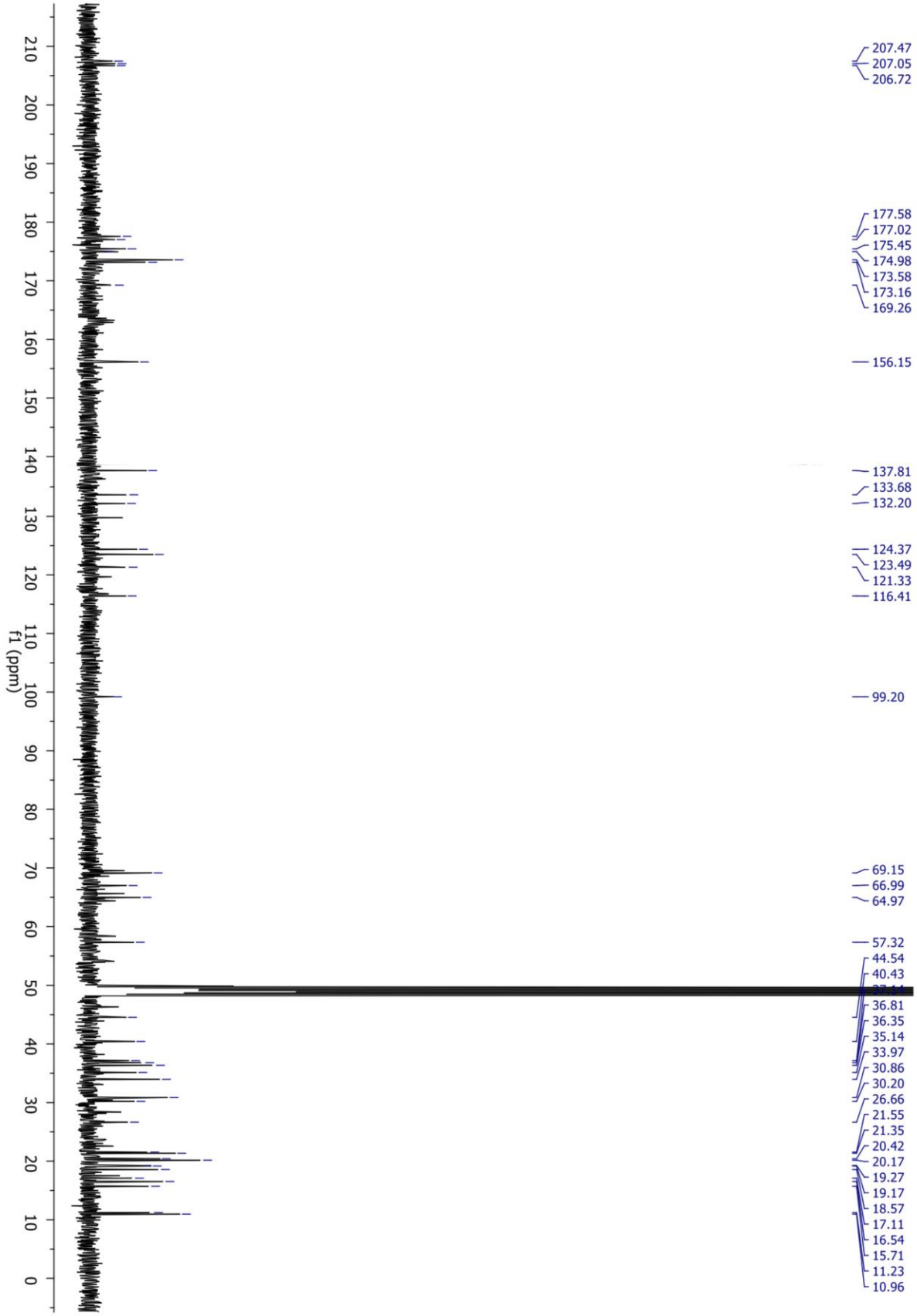

Fig. 22. ^{13}C NMR spectrum of thioalbamide in CD_3OD.

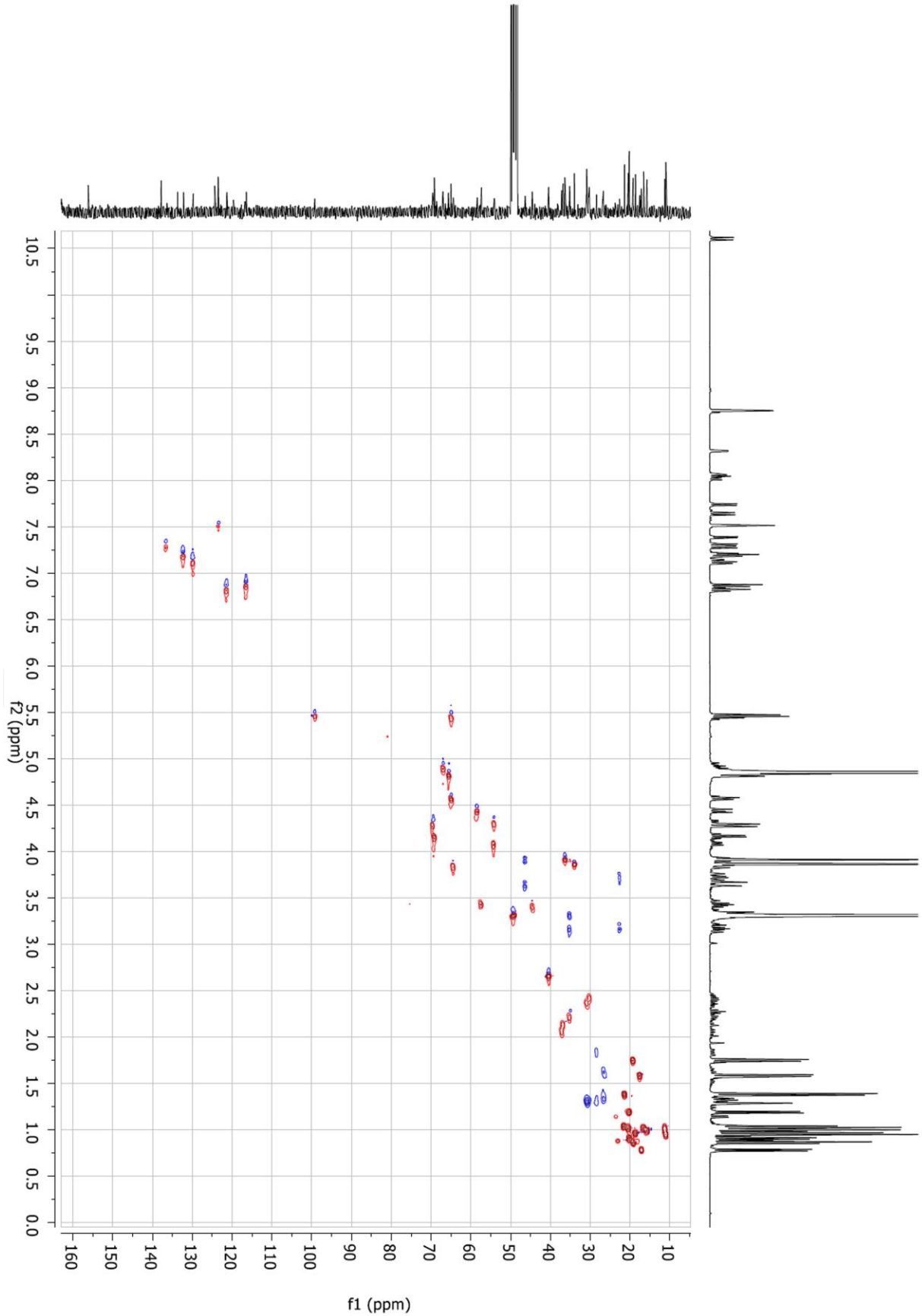

Fig. 23. HSQC spectrum of thioalbamide in CD_3OD

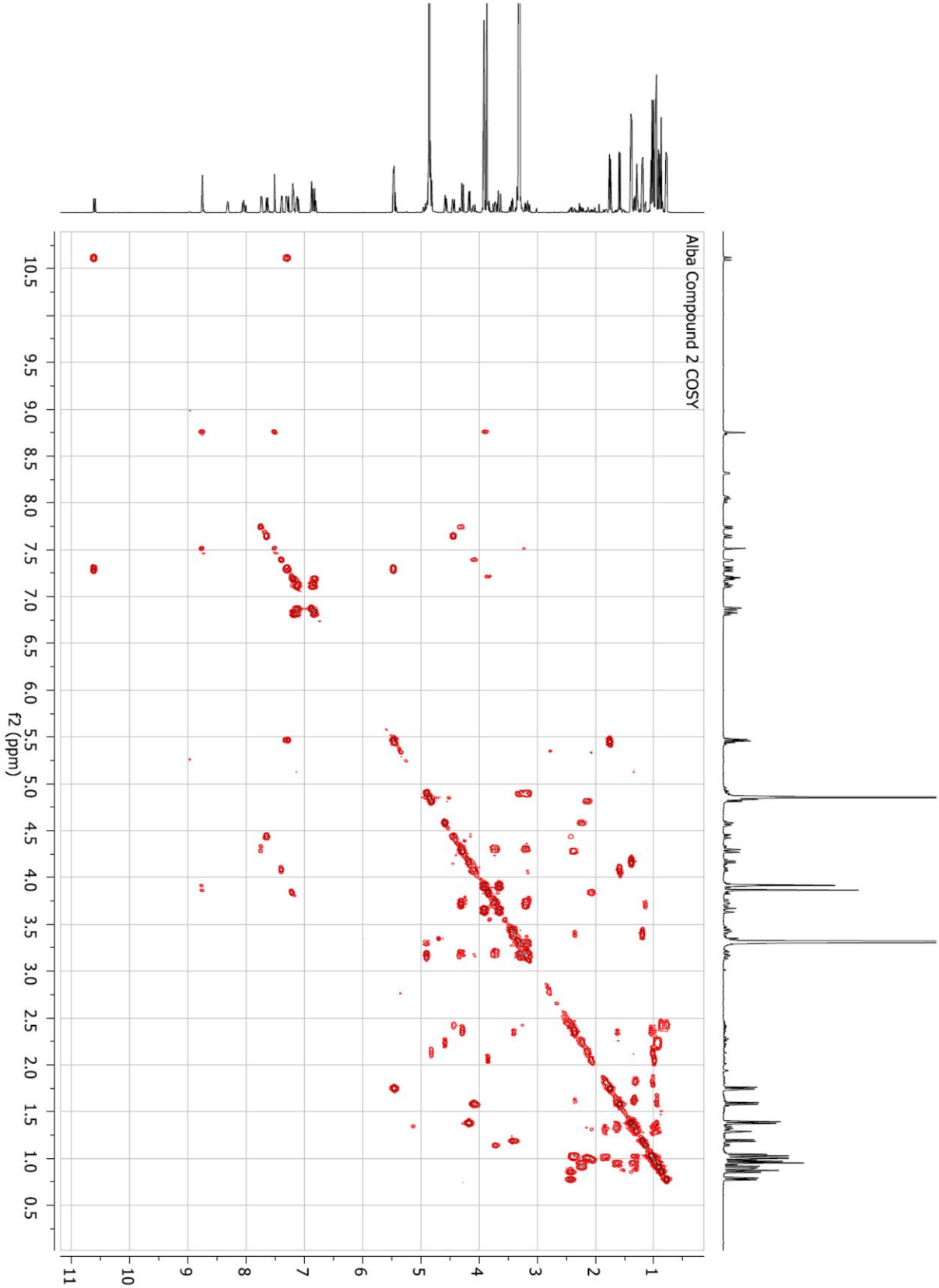

Fig. 24. COSY spectrum of thioalbamide in CD_3OD

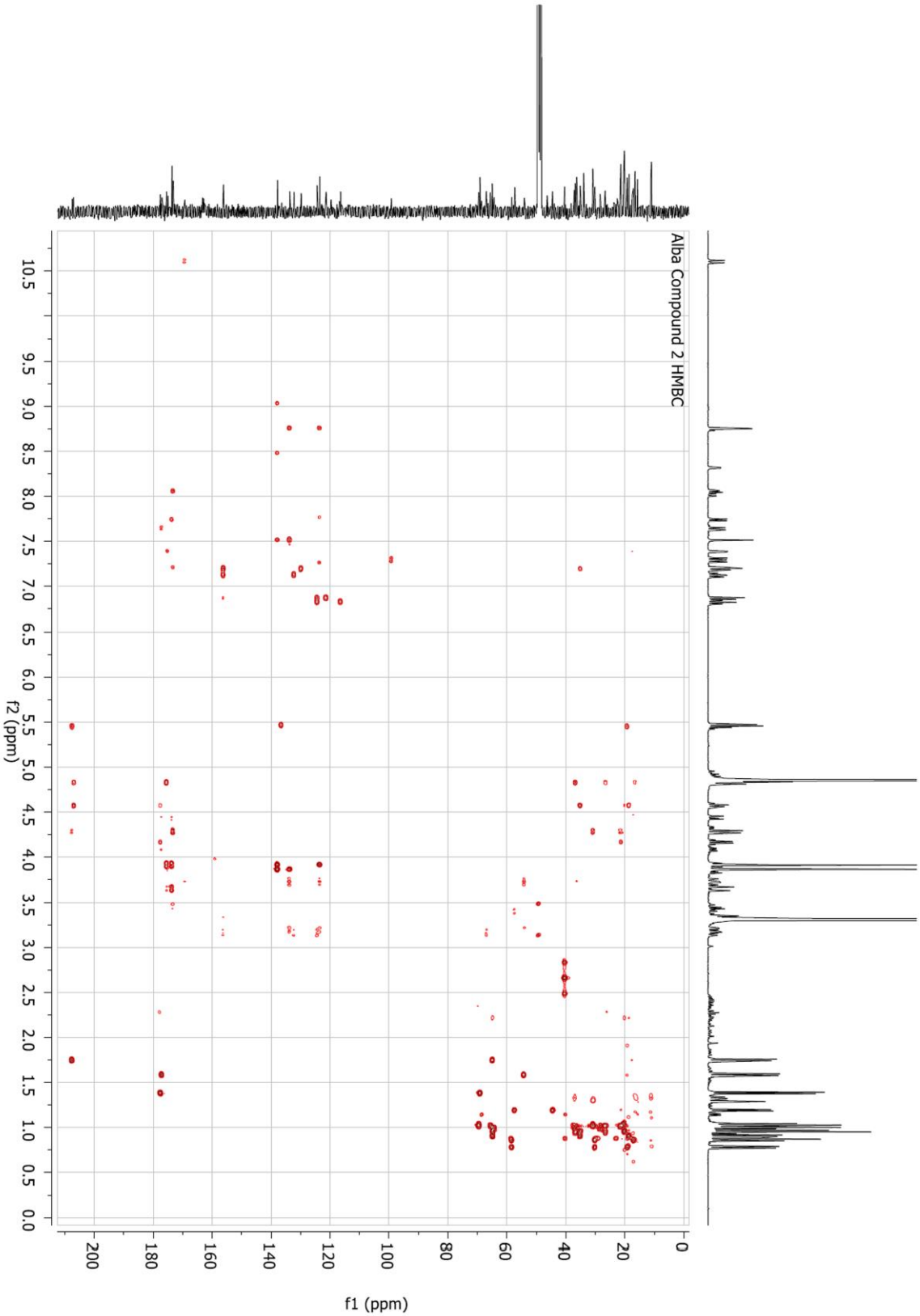

Fig. 25. HMBC spectrum of thioalbamide in CD_3OD

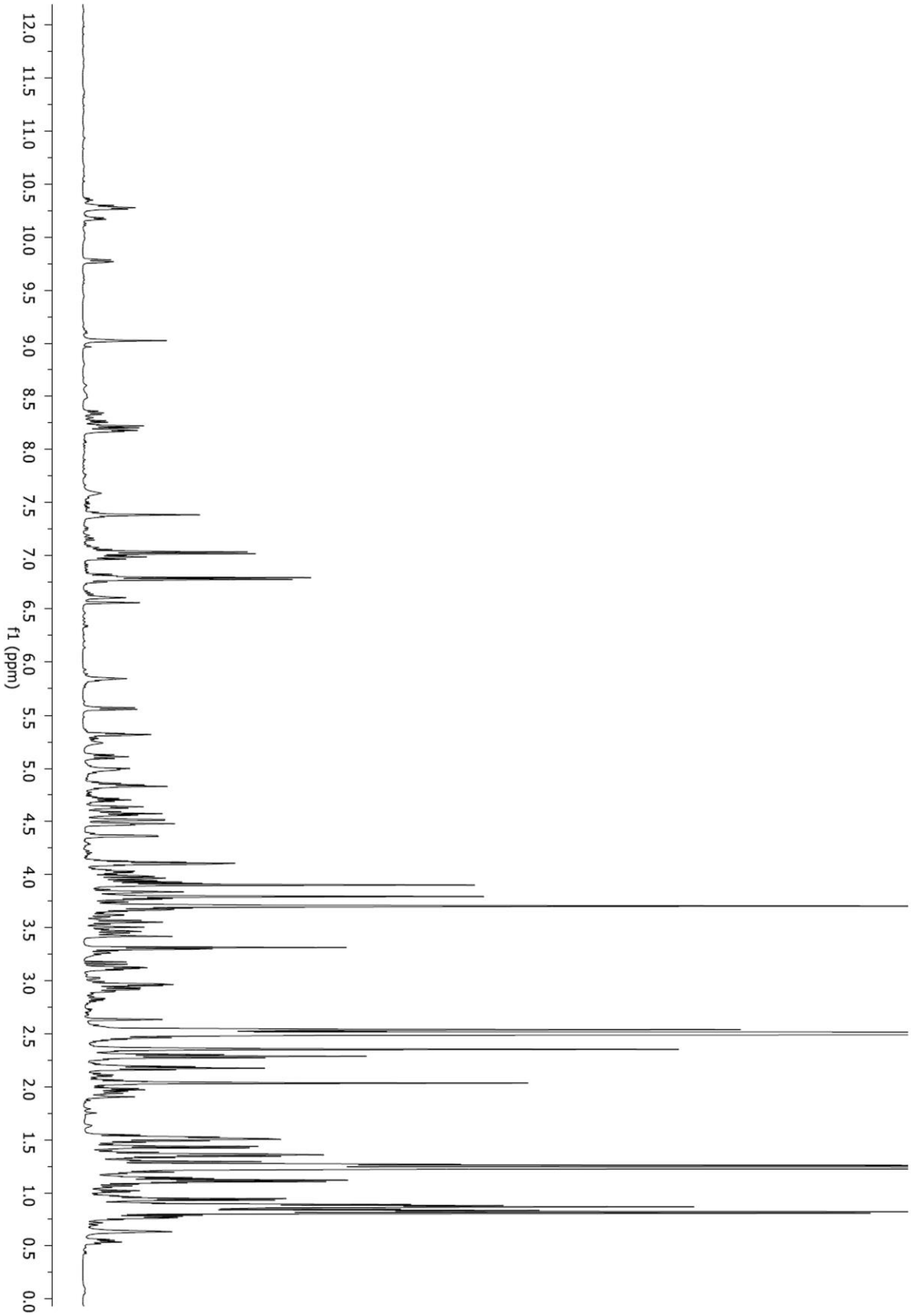

Fig. 26. ^{1}H NMR spectrum of thiostreptamide S4 in DMSO-d_6.

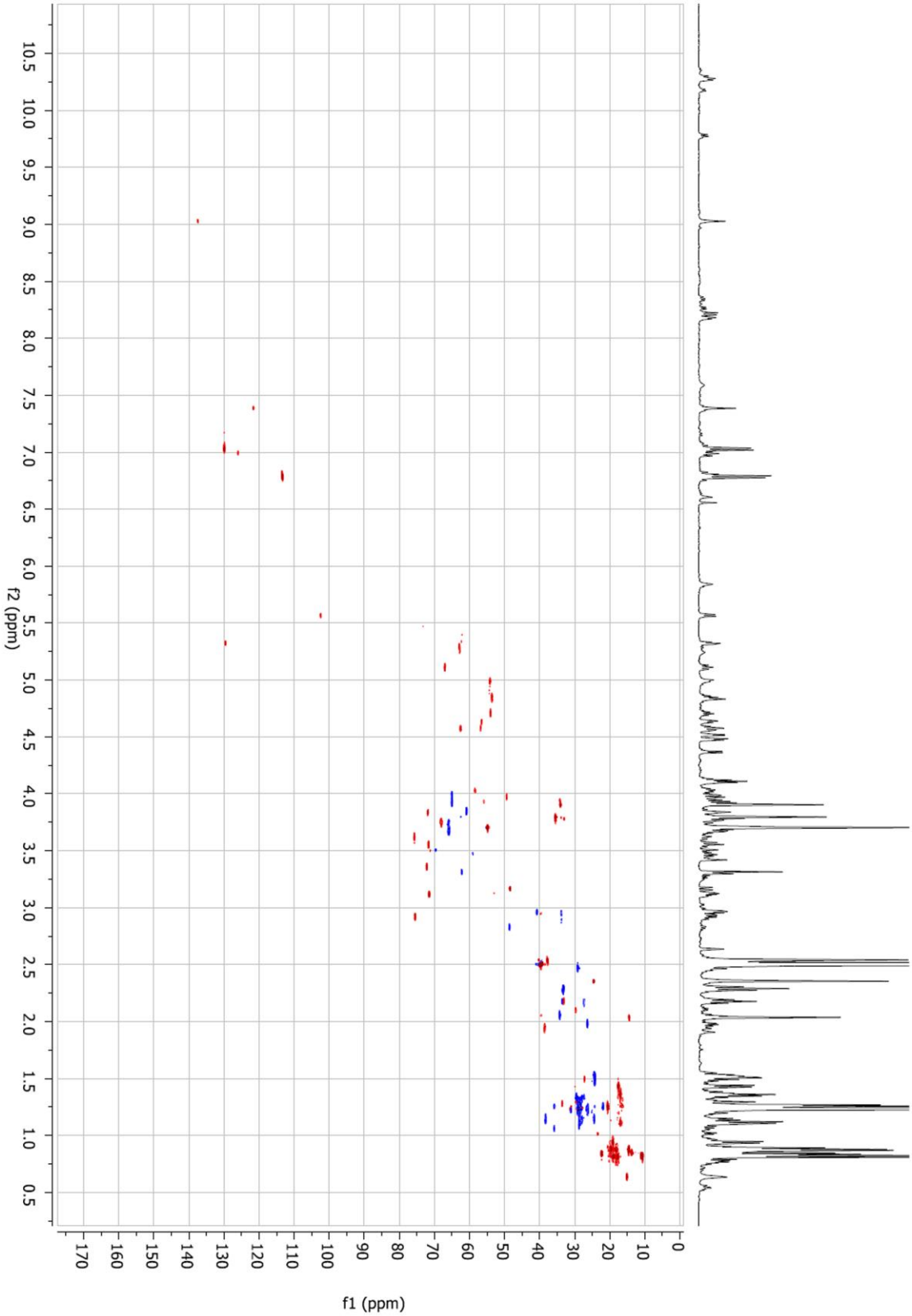

Fig. 27. HSQC spectrum of thiostreptamide S4 in DMSO-d_6.

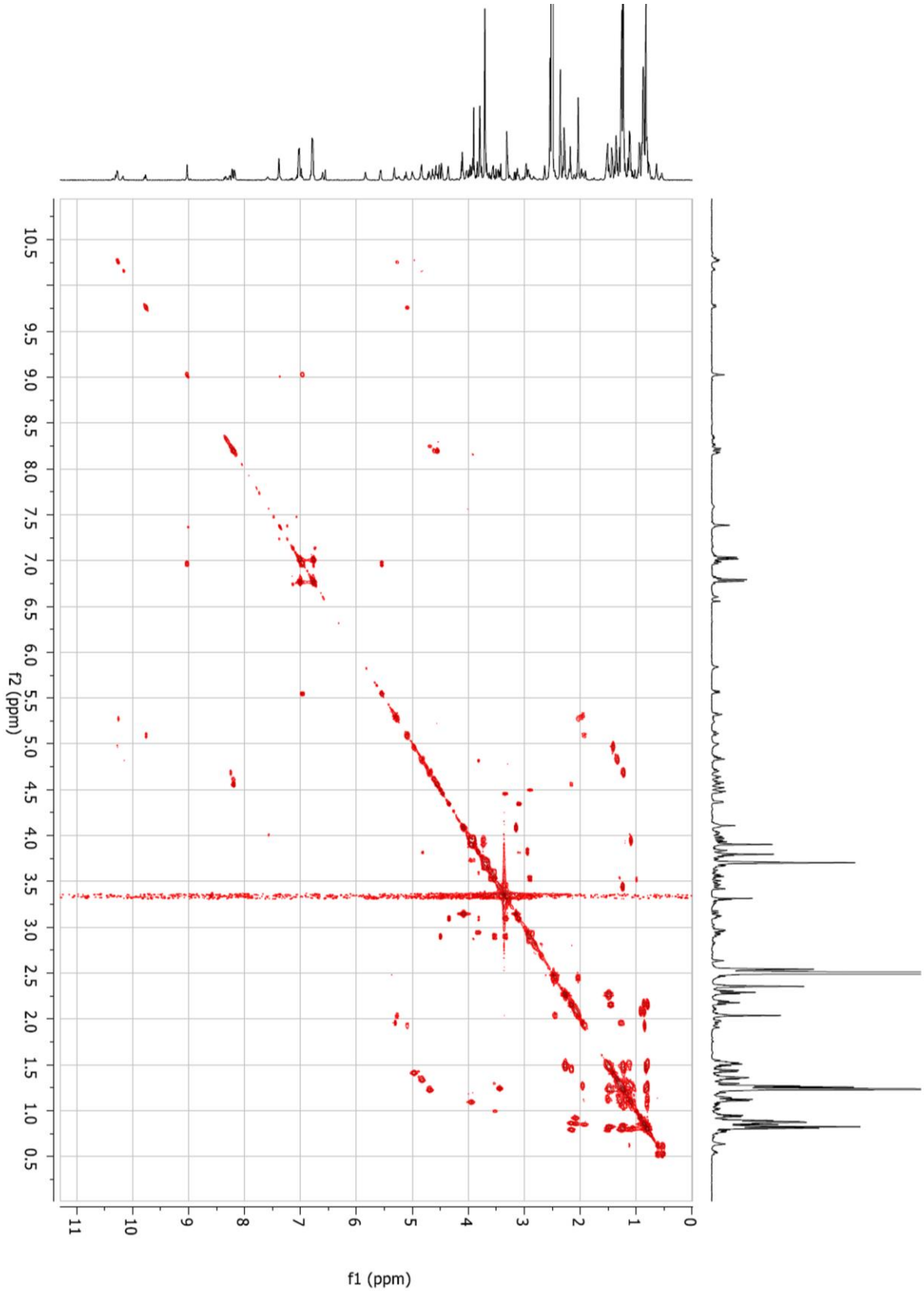

Fig. 28. COSY spectrum of thiostreptamide S4 in DMSO-d_6.

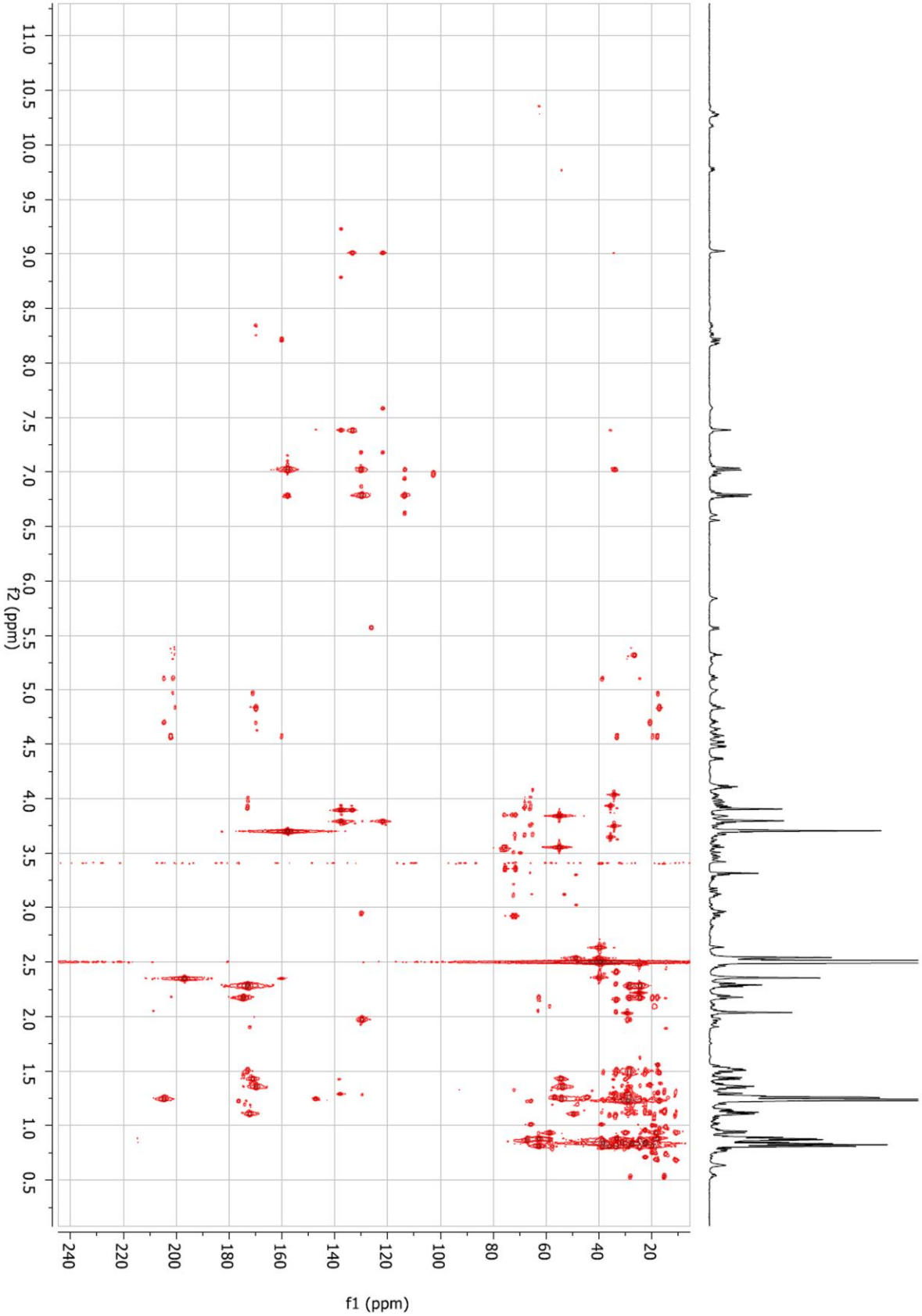

Fig. 29. HMBC spectrum of thiostreptamide S4 in DMSO-d_6.

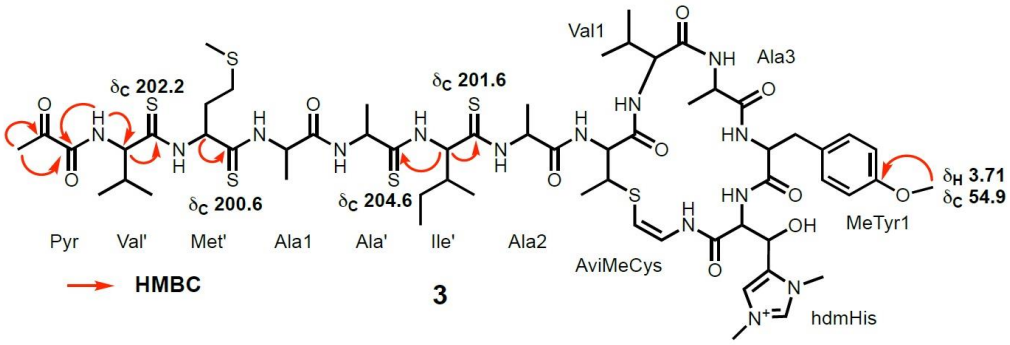

Fig. 30. Selected HMBC correlations observed in the NMR spectra of thiostreptamide S4.

3.5 A nonenzymatic origin of the unusual N-terminus of Thioviridamide.

An interesting aspect highlighted by the identification and characterization of these new TLMs is the peculiar variability of the N-terminal end. Indeed, thioviridamide has in its structure a 2-hydroxy-2-methyl-4-oxopentanoyl group, differentiating it from thioalbamide, which has a lactyl group, and from thiostreptamide S4 and thiostreptamide S87, both characterized by the presence of a pyruvyl group. However, the tva gene cluster does not appear to encode any additional biosynthetic enzymes in comparison to the clusters reported here and, in addition, no one has ever succeeded in explaining or hypothesizing, the biosynthetic origin of this peculiar feature of thioviridamide.

The TLMs in this study were isolated from the cultures of the different microorganisms, following extraction with methanol or ethyl acetate, unlike the thioviridamide isolation protocol[20], in which acetone was used as solvent for the extraction. In the course of our study, we were able to observe that the use of acetone for the extraction of solid cultures of both *Streptomyces* sp. NRRL S-4 and *S. coelicolor* M1146-TARS4, resulted in the production of a mixture of thiostreptamide S4 (m/z 1377.55) and a comparable amount of a compound with m/z 1435.58 (Fig. 31a) that was not found when other solvents were used for extraction. MS^2 data for this new compound (Fig. 32) are consistent with an N-terminal 2-hydroxy-2-methyl-4-oxopentanoyl group, the same N-terminal group as thioviridamide. This observation led us to speculate that the unusual N-terminus of thioviridamide could feasibly be generated from an aldol reaction between a pyruvyl group and the acetone used as solvent for its extraction, which implies that the true product of the thioviridamide pathway has an N-terminal pyruvyl group (Fig. 31b). Our hypothesis was fully confirmed in a study published later, in which it was shown that the real product of the thioviridamide gene cluster is characterized by the presence of a pyruvyl group.[42]

The pyruvyl group at the N-terminal end of the TLMs, can be easily explained from a biosynthetic point of view, not as a post-translational modification but as the product of a

dehydration reaction of a serine residue, which then spontaneously tautomerizes and exchanges with water following removal of the leader peptide (Fig. 31c). This result is consistent with a conserved serine residue at this position in almost all TLM precursor peptides (Fig. 9b), and a homologous reaction has been proposed to be involved in the generation of the unusual N-terminus of polytheonamide from threonine[43], the N-terminal 2-oxobutanoyl group of lacticin 3147 A2[44], and a pyruvyl group in a thiostrepton derivative generated by mutagenesis.[45] Serine dehydration in TLM biosynthesis could feasibly be catalyzed by the same dehydratase that introduces the 2,3-didehydrobutyrine residue required for forming the AviMeCys macrocycle. Also the precursor peptide from which thioalbamide originates is characterized by the presence of a serine residue but, unlike what is observed for the other TLMs, this does not result in the formation of a pyruvyl group but of a lactyl one instead. The presence of the lactyl group in thioalbamide can be easily explained, from a biosynthetic point of view, as the product of a reduction reaction of the pyruvyl group, probably catalyzed by the additional oxidoreductase (TaaRED) present exclusively in the gene cluster of *A. alba* DSM 44262, as mentioned above.

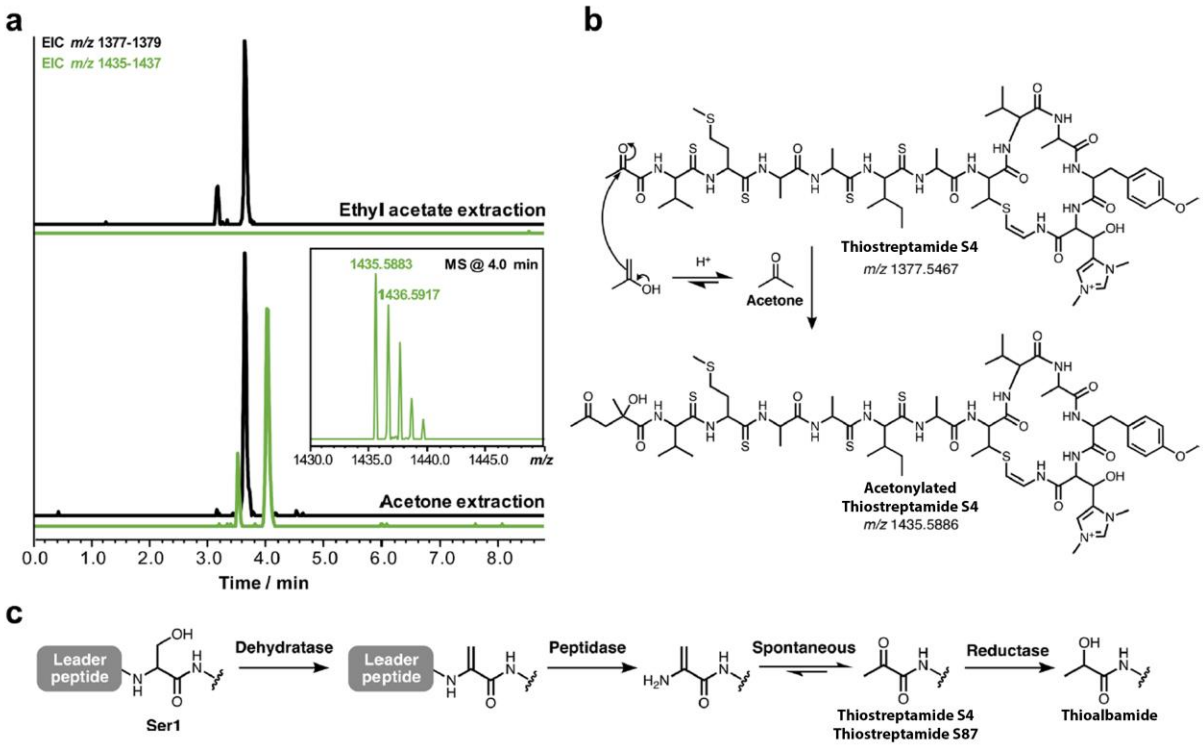

Fig. 31. N-terminal modification of TLMs. (a) LC-MS extracted ion chromatograms of *S. coelicolor* M1146-TARS4 extracted with either ethyl acetate (top) or acetone (bottom). (b) Generation of the N-terminal 2-hydroxy-2-methyl-4-oxopentanoyl group via reaction with acetone. (c) Biosynthetic proposal for the generation of the N-terminal pyruvyl and lactyl moieties.

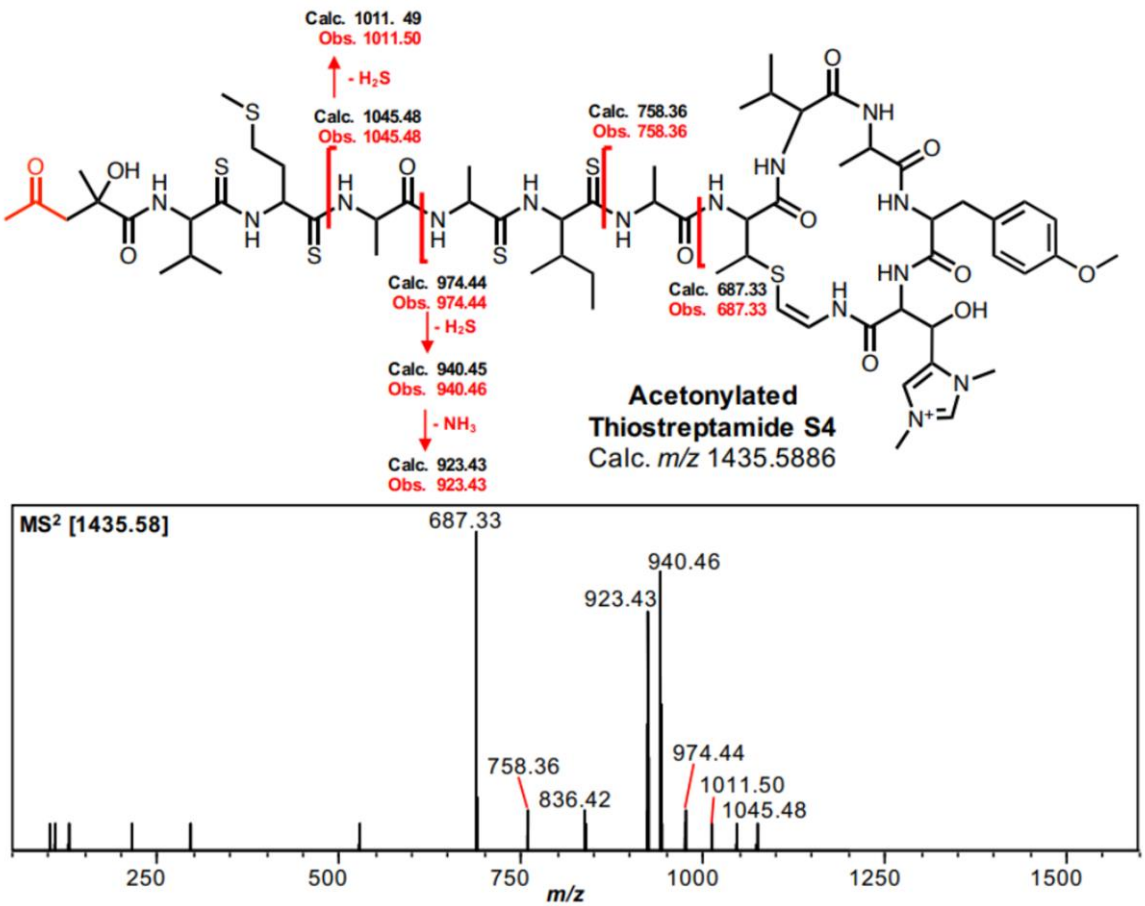

Fig. 32. MS^2 analysis of acetonylated thiostreptamide S4 obtained by acetone extraction of *S. coelicolor* M1146-TARS4. Data acquired on a Shimadzu IT-TOF mass spectrometer.

3.6 Thioalbamide is a potent anticancer compound with selective activity.

Thioviridamide has been reported to possess a potent antiproliferative effect against cancer cell lines.[20] We were therefore interested in determining whether any of our newly discovered compounds exhibited comparable bioactivity. Thioalbamide, the compound purified in greater amounts, was therefore subjected to a series of activity assays on various model organisms, including both prokaryotic and eukaryotic systems. A wide panel of cancer cell lines were tested, including alveolar (A549), uterine cervical (HeLa), pancreatic (PA-TU-8988T), and luminal and basal breast (MCF7 and MDA-MB-231) adenocarcinoma cell lines (Fig. 33). Thioalbamide showed intense antiproliferative activity on all tumor lines tested, with IC_{50} values ranging from 48 to 72 nM (Table 8). Remarkably, the cytotoxic activity of this compound was found to be highly specific to tumor cells, as IC_{50} values on a nontumor breast epithelial cell line (MCF 10A) were 6 times higher than those found in cancer cells. This selectivity means that thioalbamide activity toward tumor lines is superior (>10× lower IC_{50}) to the clinically used doxorubicin but exhibits a comparable IC_{50} to doxorubicin toward the one

healthy cell line we tested. In order to further investigate the specificity of the cytotoxic activity of thioalbamide, it was tested against Gram-positive (*Staphylococcus aureus*) and Gram-negative (*Escherichia coli*, *Klebsiella pneumoniae*, and *Pseudomonas aeruginosa*) bacteria strains, and against the fungus *Candida albicans*. In each case, it did not inhibit the growth of the microorganisms, except for *S. aureus*, which was sensitive to high concentrations of the compound, with a minimum inhibitory concentration (MIC) of 24 μM (Table 9). At this concentration, however, activity was purely bacteriostatic and not bactericidal, as the minimum bactericidal concentration was over 48 μM.

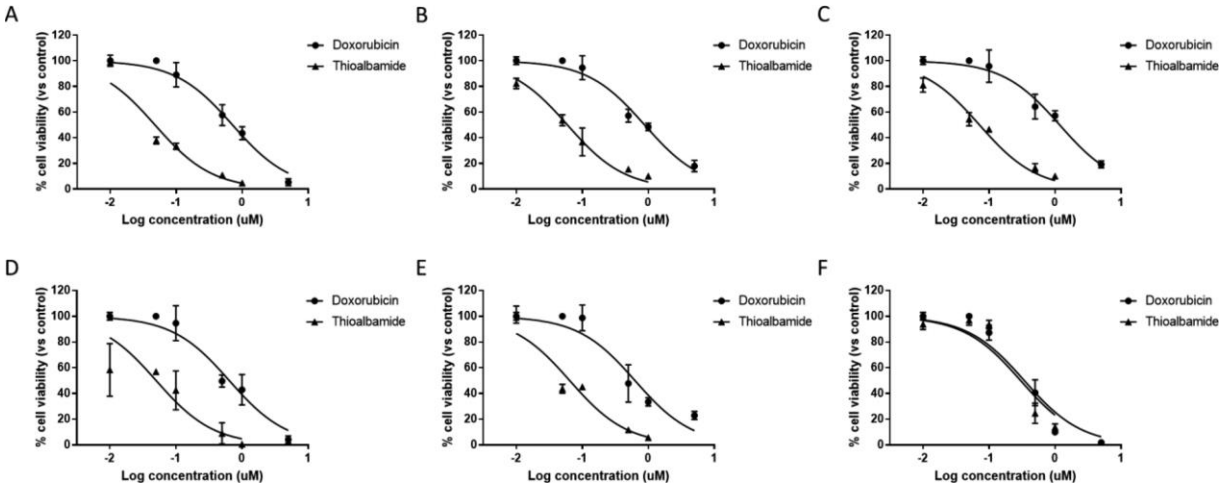

Fig. 33. **Effect of thioalbamide on cell growth**. Cellular growth assessment after treatment of A549 (A), MCF7 (B), MDA-MB-231 (C), HeLa (D), PA-TU-8988T (E), and MCF-10A (F) cell lines with different concentrations (0.01 to 1 μM) of thioalbamide for 72 h. Results, quantified by the MTT assay, are expressed as a percentage of growth versus control cells treated with DMSO. Values represent mean ± SD of three independent experiments, each one performed with triplicate samples.

Table 8. Cytotoxic activity of Thioalbamide in comparison to Doxorubicin[a]

Cell line		Doxorubicin	Thioalbamide
A549	**IC_{50}**	**0.712**	**0.048**
	95% confident interval	0,582 to 0,872	0,035 to 0,064
MCF7	**IC_{50}**	**0.878**	**0.059**
	95% confident interval	0,723 to 1,071	0,049 to 0,072
MDA-MB-231	**IC_{50}**	**1.174**	**0.072**
	95% confident interval	0,938 to 1,477	0,058 to 0,088
HeLa	**IC_{50}**	**0.644**	**0.050**
	95% confident interval	0,487 to 0,852	0,027 to 0,090
PA-TU-8988T	**IC_{50}**	**0.630**	**0.065**
	95% confident interval	0,451 to 0,888	0,047 to 0,089
MCF 10A	**IC_{50}**	**0.343**	**0.302**
	95% confident interval	0,253 to 0,464	0,206 to 0,444

[a]Data are presented as IC_{50} values (μM) and 95% confidence intervals obtained by nonlinear regression analysis of three independent experiments.

Table 9. Antimicrobial activity of tested compounds. Data are presented as MIC and MBC/MFC values (μM). Ciprofloxacin and miconazole were used as positive controls for bacteria and fungi, respectively.

Compound	*S. aureus* ATCC 25923		*E. coli* ATCC 25922		*K. pneumoniae* ATCC 13883		*P. aeuruginosa* ATCC 27853		*C. albicans* ATCC 10231	
	MIC	MBC	MIC	MBC	MIC	MBC	MIC	MBC	MIC	MFC
Miconazole	-	-	-	-	-	-	-	-	4.8	9.6
Ciprofloxacin	0.75	3	0.09	0.18	0.18	0.38	0.38	0.75	-	-
Thioalbamide	24	>48	>48	>48	>48	>48	>48	>48	>48	>48

The promising antiproliferative activity demonstrated by thioalbamide during these preliminary studies has led us to investigate further the antitumor potential of this new natural product. In the second part of this thesis, in particular, the study of the molecular mechanisms induced by thioalbamide, in different *in vitro* models of breast carcinoma, will be treated with a biochemical-metabolic approach. This cancer is the most diagnosed malignant neoplasm in women and, given its biological complexity responsible for the occurrence of pharmacological resistance and recurrence phenomena, it is still one of the leading causes of oncologic death worldwide, and one of the main challenges for cancer research.

PART 2

Elucidating thioalbamide activity in breast cancer cells: new insights into TLMs anticancer mechanism

CHAPTER 4

INTRODUCTION

4.1 Breast cancer

Breast cancer is a malignant neoplasm characterized by the uncontrolled proliferation of epithelial cells of the mammary glandular tissue, and is the most common malignancy in women around the world.[46, 47] Breast cancer is highly heterogeneous in terms of its etiology and its onset is associated with various risk factors:

- Age.
- Previous thoracic radiotherapy.
- Previous mammary pathologies (dysplasias or neoplasms of breast tissue).
- Early menarche and late menopause.
- Nulliparity or first term pregnancy in old age (> 30 years).
- Failure to breastfeed.
- Incorrect lifestyle (obesity, low physical activity, high consumption of alcohol, carbohydrates and saturated fats).
- Using HRT (Hormone Replacement Therapy)
- Familiarity and genetic factors: mutations of BRCA-1 and BRCA-2 genes, p53 (LiFraumeni syndrome), PTEN (Cowden's disease) and ATM (ataxia-telangiectasia).

Mutations in BRCA-1 genes (BReast CAncer susceptibility gene 1), on chromosome 17, and BRCA-2 (BReast CAncer susceptibility gene 2), on chromosome 13, are responsible for two-thirds of hereditary breast carcinomas. The products of the BRCA1 and BRCA2 genes are two proteins that participate in the cellular repair response following DNA damage. Mutations in these genes may result in altered expression of these proteins or in expression of proteins with impaired function, predisposing the individual to the onset of neoplasia. Familiar breast cancer, linked to mutations in BRCA-1 and BRCA-2 genes, tends to occur at a younger age compared to sporadic cases, although the increased risk associated with the presence of these mutations persists throughout life.[48, 49]

4.2 Histological classification

Mammary carcinoma develops from the epithelial cells of the glandular tree and may originate different histotypes, among which the most frequent are ductal carcinoma and lobular

carcinoma. The two terms were introduced considering that the first form derives from the ducts and the second from the lobules. However, most of the carcinomas of the breast occur at the level of the terminal ductal-lobular units (TDLU) (Fig. 34) giving rise to different tumors from both the morphological and the biological behaviour points of view.

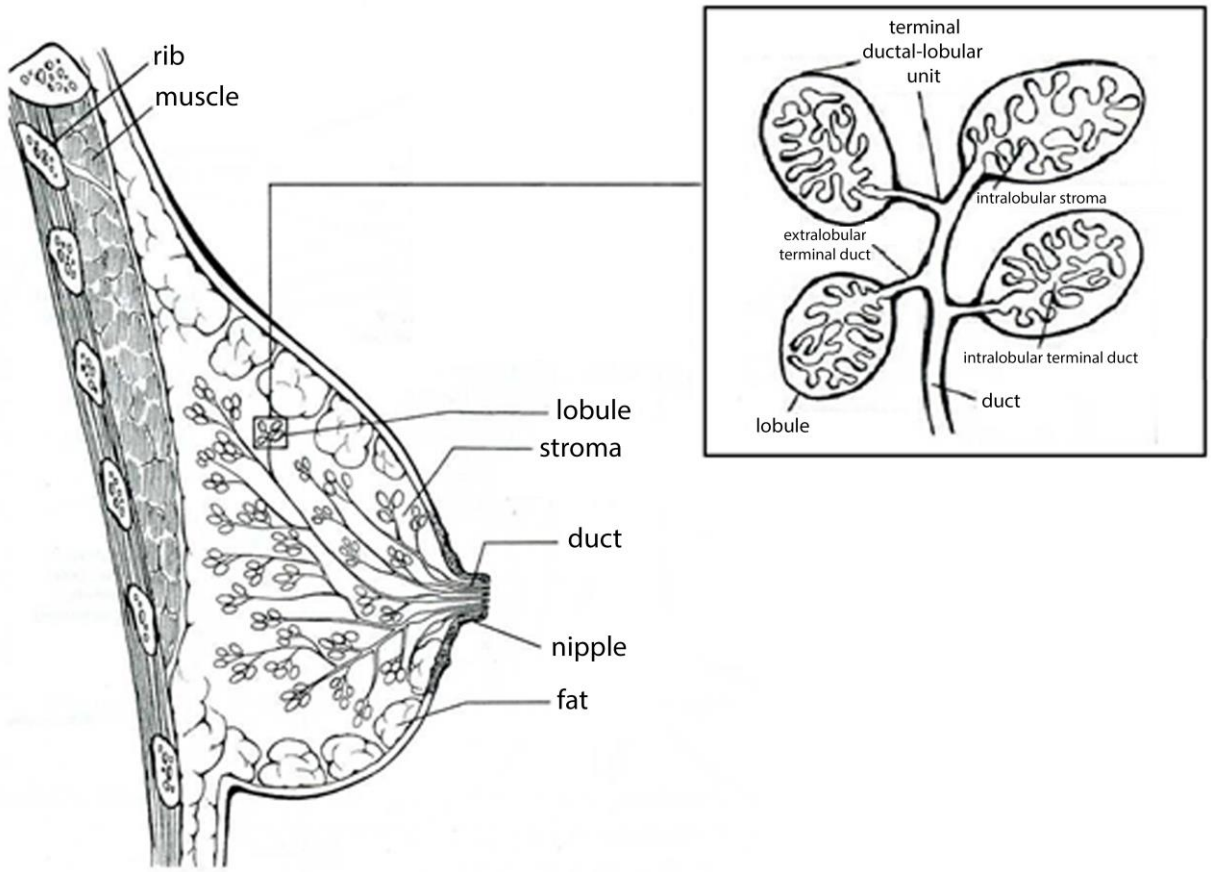

Fig. 34. Anatomic structure of the mammary gland.

Breast carcinomas can be divided into two large subtypes: an *in situ* form and an *infiltrating* form. The *in situ* carcinoma subtype refers to a proliferation of epithelial cells that do not possess infiltrating capacity, i.e. the ability to invade tissues located beyond the basal membrane. Infiltrating carcinomas, by contrast, are characterized by a reduced ability to express the protein cadherin-E, guarantor of the intercellular junction, which is missing, favouring a disintegration of the neoplastic mass; such cells can, individually or in small clusters, infiltrate the surrounding tissues. The World Health Organization (WHO) histological classification of invasive breast carcinoma is reported in Table 10.

The most common histological types of breast cancer are invasive carcinomas of no special type (NST), representing 40%–75% of all breast cancers and including all invasive ductal carcinomas that fail to exhibit sufficient characteristics to achieve classification as a specific

histological type, and invasive lobular carcinomas, representing 5-15% of total breast cancers. The other histological subtypes of breast carcinoma individually represent 0-4% of breast malignancies and generally have a favorable prognosis.[50]

Table 10. World Health Organization (WHO) histological classification of invasive breast carcinoma.

Type	Classification
Invasive carcinoma of no special type (NST)	8500/3
Pleomorphic carcinoma	8522/3
Carcinoma with osteoclast-like stromal giant cells	8035/3
Carcinoma with choriocarcinomatous features	
Carcinoma with melanotic features	
Invasive lobular carcinoma	8520/3
Classic lobular carcinoma	
Solid lobular carcinoma	
Alveolar lobular carcinoma	
Pleomorphic lobular carcinoma	
Tubulolobular carcinoma	
Mixed lobular carcinoma	
Tubular carcinoma	8211/3
Cribriform carcinoma	8201/3
Mucinous carcinoma	8480/3
Carcinoma with medullary features	
Medullary carcinoma	8510/3
Atypical medullary carcinoma	8513/3
Invasive carcinoma NST with medullary features	8500/3
Carcinoma with apocrine differentiation	
Carcinoma with signet-ring-cell differentiation	
Invasive micropapillary carcinoma	8507/3
Metaplastic carcinoma of no special type	8575/3
Low-grade adenosquamous carcinoma	8570/3
Fibromatosis-like metaplastic carcinoma	8572/3
Squamous cell carcinoma	8070/3
Spindle cell carcinoma	8032/3
Metaplastic carcinoma with mesenchymal differentiation	
Chondroid differentiation	8571/3
Osseous differentiation	8571/3
Other types of mesenchymal differentiation	8575/3
Mixed metaplastic carcinoma	8575/3
Myoepithelial carcinoma	8982/3
Epithelial-myoepithelial tumors	
Adenomyoepithelioma with carcinoma	8983/3
Adenoid cystic carcinoma	8200/3
Rare types	
Carcinoma with neuroendocrine features	
Neuroendocrine tumor, well-differentiated	8246/3
Neuroendocrine carcinoma poorly differentiated (small cell carcinoma)	8041/3
Carcinoma with neuroendocrine differentiation	8574/3
Secretory carcinoma	8502/3
Invasive papillary carcinoma	8503/3
Acinic cell carcinoma	8550/3
Mucoepidermoid carcinoma	8430/3
Polymorphous carcinoma	8525/3
Oncocytic carcinoma	8290/3

4.3 Tumor Nodes Metastases (TNM) classification

The Tumor Nodes Metastases (TNM) system is the international classification system for the evolution of malignant tumors, which considers three parameters: dimensions of the primary tumor (T), involvement of regional lymph nodes adjacent to the tumor (N) and the presence of distant metastases (M).[51]

According to the size of the primary tumor we have the following classification:

- T0: No evidence of primary tumor
- T1: Tumor ≤ 20 mm in greatest dimension
- T1mi: Tumor ≤ 1 mm in greatest dimension
- T2: Tumor > 20 mm but ≤ 50 mm in greatest dimension
- T3: Tumor > 50 mm in greatest dimension
- T4: Tumor of any size with direct extension to the chest wall and/or to the skin

With regard to the lymph nodes, N0 is defined as a condition in which the regional lymph nodes are not affected, and with a rising code from N1 to N3 the progressive involvement of a greater number of lymph node stations:

- N0: No regional lymph node metastases
- N1: Metastases to movable ipsilateral level I, II axillary lymph node(s)
- N2: Metastases in ipsilateral level I, II axillary lymph nodes that are clinically fixed or matted; or in clinically detected ipsilateral internal mammary nodes in the absence of clinically evident axillary lymph node metastases
- N3: Metastases in ipsilateral infraclavicular (level III axillary) lymph node(s) with or without level I, II axillary lymph node involvement; or in clinically detected ipsilateral internal mammary lymph node(s) with clinically evident level I, II axillary lymph node metastases; or metastases in ipsilateral supraclavicular lymph node(s) with or without axillary or internal mammary lymph node involvement

The presence of distant metastases is characterized by the indication M1, while M0 indicates their absence. Overall, this classification allows to attribute the staging of breast cancer, as reported in Table 11.

Table 11. Anatomic stage/prognostic groups

Stage 0	Tis	N0	M0
Stage IA	T1	N0	M0
Stage IB	T0	N1mi	M0
	T1	N1mi	M0
Stage IIA	T0	N1	M0
	T1	N1	M0
	T2	N0	M0
Stage IIB	T2	N1	M0
	T3	N0	M0
Stage IIIA	T0	N2	M0
	T1	N2	M0
	T2	N2	M0
	T3	N1	M0
	T3	N2	M0
Stage IIIB	T4	N0	M0
	T4	N1	M0
	T4	N2	M0
Stage IIIC	Any T	N3	M0
Stage IV	Any T	Any N	M1

4.4 Molecular classification

The biological and molecular characterization of breast carcinoma has, in recent years, offered innovative elements regarding the prognostic and therapeutic aspects of this pathology (Fig. 35). The application of molecular biology methods has allowed breast cancers to be classified into six different subtypes, depending on the expression of specific receptors/proteins:

- Luminal A: characterized by the expression of estrogen (ER) and progesterone (PR) receptors, absence of HER2/neu receptor overexpression and low proliferative index (low expression of Ki67 antigen).
- Luminal B (HER2-negative): characterized by hormone receptor expression, absence of HER2/neu receptor overexpression and high proliferative index (high expression of Ki67 antigen).

- Luminal B (HER2-positive): characterized by hormone receptor expression and HER2/neu receptor overexpression.
- Non-luminal HER2-positive: not expressing hormone receptors and overexpressing the HER2/neu receptor.
- Basal-like: characterized by absence of both hormone receptors expression and HER2/neu receptor overexpression.
- Claudin-low: characterized by a triple-negative receptor profile and lacking cell–cell junction proteins.

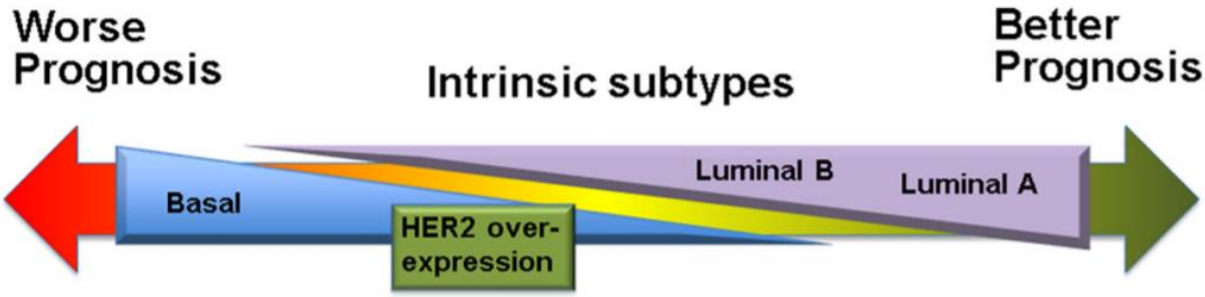

Fig. 35. Adapted from Dai, X., Li, T., Bai, Z., Yang, Y., Liu, X., Zhan, J., & Shi, B. (2015). Breast cancer intrinsic subtype classification, clinical use and future trends. *American journal of cancer research*, *5*(10), 2929.

Luminal tumors are the most common subtype of breast cancer, and subtype A is more frequent than subtype B (50-60% vs 15-20% of all breast cancer).[52] These tumors are characterized by a more favorable prognosis than the other subtypes, even though luminal subtype B has a significantly less favorable prognosis than luminal A subtype.[53] The therapeutic strategy also differs between the two subtypes. Luminal A tumors are generally treated with endocrine therapy, using selective estrogen receptor modulators (SERM), such as Tamoxifen, and/or aromatase inhibitors, such as Anastrozole. On the other hand, luminal B tumors, which are more proliferative, may benefit from the combined therapeutic strategy of chemotherapy, endocrine therapy and other targeted approaches, such as anti-angiogenic strategies.[54]

HER2-positive carcinomas represent 15-20% of all breast cancers.[52] The overexpression of this receptor makes the tumor more aggressive and gives it a worse prognosis than luminal subtypes.[53] The therapy for this tumor subtype, generally resistant to endocrine therapy, involves the use of anti-HER2 monoclonal antibodies, such as trastuzumab. Furthermore, it has been observed that these tumors are more sensitive than the other subtypes to the antitumor antibiotic Doxorubicin. Doxorubicin sensitivity among HER2-positive breast cancer cells is possibly due to co-amplification of the topoisomerase-2 gene, the drug's target, which is close the HER2 locus on chromosome 17.[55]

Basal-like tumors represent 8-37% of all breast cancers, are highly proliferative and characterized by aggressive clinical behaviour and a high rate of metastasis to visceral organs, brain and lung.[52] This subtype is associated with the least favorable prognosis among breast cancer and a greater risk of tumor recurrence. These tumors, characterized by a triple-negative receptor profile, cannot be treated with target specific therapeutic strategies, such as endocrine therapy and immunotherapy, and the only practicable strategy is classical chemotherapy.[54]

The most recently identified breast cancer group is represented by the claudin-low tumors, a triple negative subtype characterized by low expression of genes involved in tight junctions and cell-cell adhesions including claudins 3, 4 and 7, occludin and E cadherin, showing high expression of epithelial to mesenchymal transition genes. The induction of a mesenchymal state in a mammary epithelial cell is associated with the acquisition of undifferentiated mammary stem cell-like features[52, 56, 57], at the basis of the resistance, metastasization and recurrence processes which breast cancers can undergo.

4.5 Cancer stem cells (CSCs)

Despite advances in anticancer therapies, many cancer patients, who initially respond well to the treatment, experience recurrence, resistance and metastasis at regional or distant sites. These phenomena are due to the presence in the tumor of a sub-population of cells with staminal properties, called cancer stem cells (CSCs). The tumor stem cell possesses peculiar properties such as self-renewal and high proliferation rate, which make it the cellular type responsible for driving tumor propagation and pathogenesis. Cancer stem cells, moreover, possess Epithelial to Mesenchymal Transition (EMT) ability, a characteristic that facilitates cell migration and promotes metastatic events.[58-60]

There are several theories concerning the origin of breast cancer stem cells (BCSCs), in which stem cells, progenitor cells or differentiated cells act as the starting cell type in BCSCs formation (Fig. 36). To support the hypothesis that BCSCs originate from mammary stem cells or progenitor cells, there is evidence that BCSCs share characteristics very similar with such cells, such as $CD44^+/CD24^-$ cell surface markers profile, as well as the ability to undergo self-renewal and differentiation. Other hypotheses, meanwhile, posit that BCSCs arise from differentiated mammary cells, following a de-differentiation process caused by environmental factors. These factors also include chemotherapy and radiotherapy, which can induce de-differentiation of non-stem cancer cells leading to enrichment of BCSCs in the tumor.[59]

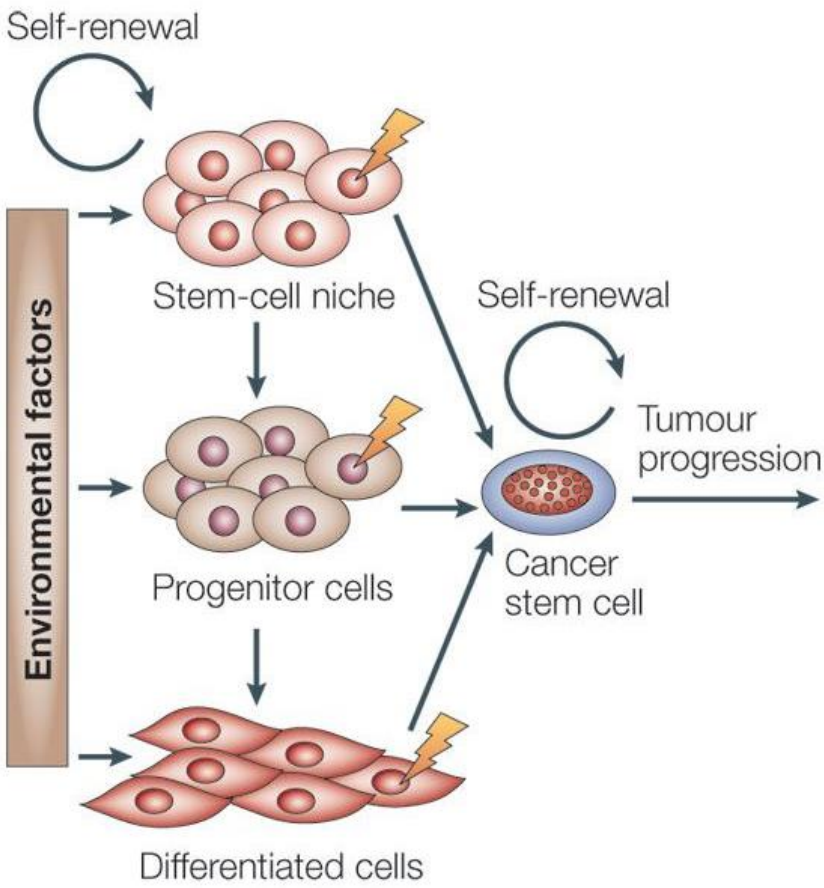

Fig. 36. Theories concerning the origin of cancer stem cells (from Bjerkvig, R., Tysnes, B. B., Aboody, K. S., Najbauer, J., & Terzis, A. J. A. (2005). The origin of the cancer stem cell: current controversies and new insights. *Nature Reviews Cancer*, *5*(11), 899.).

Current therapeutic strategies are characterized by a low efficacy in targeting cancer stem cells, acting exclusively on non-stem malignant cells. The resistance of cancer stem cells to conventional chemotherapeutic regimens is associated with phenomena of tumor recurrence and oncological mortality. Given the recent advances in the knowledge of cancer stem cell biology, pharmaceutical research is focusing on the identification of new molecules and therapeutic approaches that can affect BCSCs and facilitate breast cancer eradication (Fig. 37). One of the innovative therapeutic strategies for eradicating cancer stem cells is represented by the use of agents able to interfere with stemness pathways.[58] Indeed, one of the main differences between the normal and cancer stem cell is the deregulation of these pathways. Currently, several molecules are undergoing preclinical and clinical studies as CSC specific drugs, as they are able to interfere with different stemness pathways, such as WNT, JAK/STAT, Hedgehog and NOTCH signalling pathways.

Another innovative approach, representing a focus of cancer stem cells research, could be the use of drugs that can affect their energy metabolism. Cancer stem cells possess a metabolic phenotype that differs both from that of normal stem cells, which mainly use oxidative

phosphorylation (OXPHOS) for the production of energy, and from common cancer cells, which mainly use the glycolytic pathway. Indeed, CSCs are characterized by a high metabolic flexibility that allows them to switch between the two metabolic pathways in order to maintain cancer homeostasis and to promote tumor growth.[61-63] The use of drugs able to inhibit CSC metabolic flexibility is therefore a potential therapeutic strategy for tumor eradication.

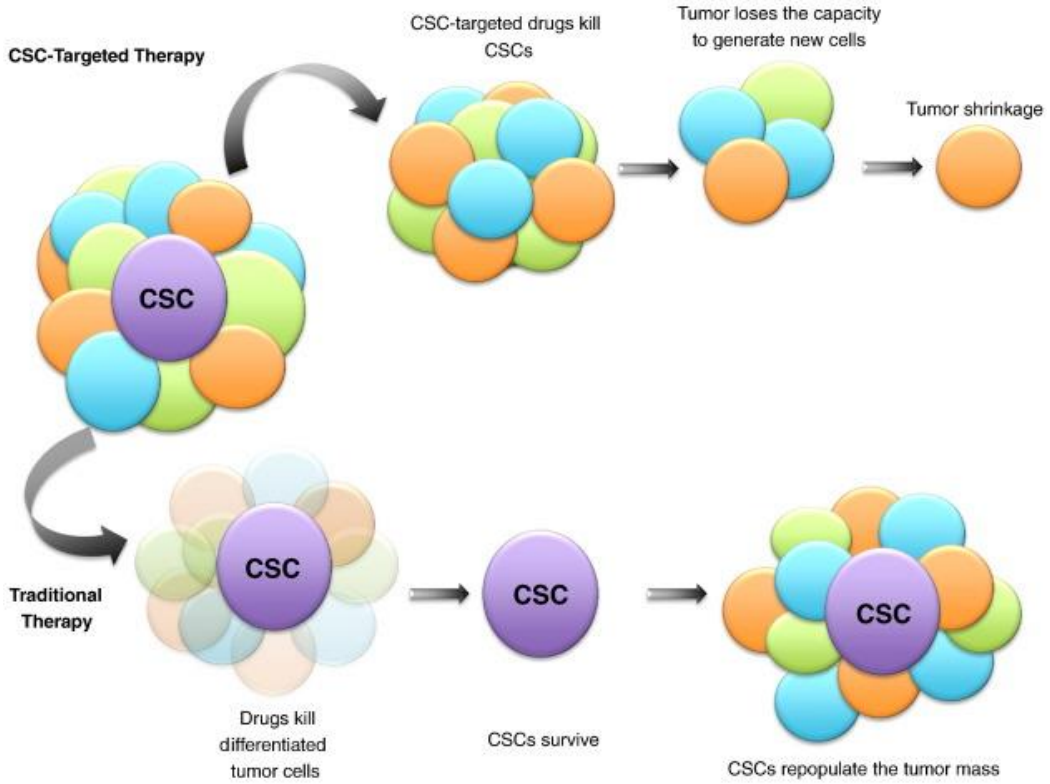

Fig. 37. Cancer stem cell specific therapy versus conventional cancer therapy (From Leon, G., MacDonagh, L., Finn, S. P., Cuffe, S., & Barr, M. P. (2016). Cancer stem cells in drug resistant lung cancer: Targeting cell surface markers and signaling pathways. Pharmacology & therapeutics, 158, 71-90.)

4.6 Aims of the study.

Thioalbamide, the microbial natural product on which this PhD work focuses, has shown to possess a powerful antiproliferative activity in several tumor cell lines.[64] The aims of the second part of this project were:

- To evaluate the effects of this promising compound on a wide range of breast cancer cell lines. The selected cell lines (MCF7, T47D, SKBR3, MDA-MB-231 and MDA-MB-468) represent valid *in vitro* models for studying of the different breast cancer subtypes.
- To investigate on thioalbamide mode of action. For the first time, through the use of a biochemical-metabolic approach, the cellular events triggered by thioalbamide were examined, in order to identify the molecular targets responsible for its antitumor activity.

CHAPTER 5

MATERIALS AND METHODS

5.1 Cell cultures

All the cell lines used in this work (MCF7, T47D, SKBR3, MDA-MB-231, MDA-MB-468 and MCF10A) were purchased from the American Culture Collection (ATCC, Manassas, VA). For maintaining purpose cells were cultured as follow:

- MCF7 and MDA-MB-231 cells were cultured in DMEM/F12 (Sigma) supplemented with 10% fetal bovine serum (FBS, Sigma), 2 mM L-glutamine (Gibco, Life Technologies) and 1% penicillin/streptomycin (Gibco, Life Technologies).
- MDA-MB-468 cells were cultured in DMEM (High Glucose) (Sigma) supplemented with 10% fetal bovine serum, 2 mM L-glutamine and 1% penicillin/streptomycin.
- SKBR3 cells were cultured in RPMI supplemented with 10% fetal bovine serum, 2 mM L-glutamine and 1% penicillin/streptomycin.
- T47D cells were cultured in RPMI supplemented with 0.2 U/ml insulin (Gibco, Life Technologies) 10% fetal bovine serum, 2 mM L-glutamine and 1% penicillin/streptomycin.
- MCF10A cells were cultured in DMEM/F12 supplemented with 5% horse serum (HS, Sigma), 10 mg/mL insulin (Sigma), 0.5 mg/mL hydrocortisone (Sigma), 20 ng/mL human epidermal growth factor (hEGF, Sigma), 0.1 mg/mL cholera toxin (Sigma), 2 mM L-glutamine and 1% penicillin/streptomycin.

Treatments were performed in the above-mentioned media containing a lower amount of supplemented serum (2%). All cell lines were cultured at 37 °C in 5% CO_2 in a humidified atmosphere.

5.2 Cell viability assay

Cell viability was determined by using 3-(4,5-Dimethyl-2-thiazolyl)-2,5-diphenyl-2H-tetrazolium bromide (MTT) assay. Cells were seeded in 48-well plates with a density of $2x10^4$ cells/well and cultured in complete medium overnight. Cells were then treated with different concentrations of compounds for 72 hours, and DMSO was used as a vehicle control. At the end of the treatment period, MTT solution was added to each well (to a final concentration of 0.5 mg/mL) and plates were incubated at 37 °C for 2 h until the formation of formazan crystals. DMSO-solubilized formazan in each well was quantified by absorbance at 570 nm using a

microplate reader. Non-linear regression analysis (GraphPad Prism 7) was used to generate sigmoidal dose-response curves to calculate IC50 values for each cell line.

5.3 Cell morphology analysis

MCF7 cells were seeded into 6-well plate with a density of 1×10^5 cells/well and cultured overnight in complete medium. Then, cells were treated with 50nM thioalbamide for 72 h or DMSO (control cells)and subjected to fixed and stained with May Grünwald-Giemsa (Bio-Optica), as previously described. Images, at different magnifications, were taken on Olympus BX41 microscope with CSV1.14 software, using a CAMXC-30 for image acquisition.

5.4 Cell Cycle analysis

Cell-cycle analysis was performed on MCF7 cells, seeded in 6-well plate with a density of 1×10^5 cells/well, treated with DMSO or 50nM thioalbamide for 72 hours. After treatment, cells were collected by trypsinization, washed twice with chilled PBS and spun at 1500rpm for 5 minutes. Cells were fixed by re-suspending pellet in 70% Ethanol for 30 minutes at 4°C. Cells were washed twice with PBS and stained in 3.8mM sodium citrate, 50 µg/ml propidium iodide (PI), 100 µg/ml RNAse and 0,1% Igepal in PBS for 1 hour at 37°C. Samples were subjected to cytofluorimetric analysis by using BD FACSJazz™ Cell Sorter (Becton, Dickinson and Co).

5.5 Immunoblot analysis

For immunoblot analysis of the different proteins assessed in this study, cells were grown to 70-80% confluence and treated with 50nM thioalbamide or DMSO for 24/72 hours.

For total lysates preparation, cells were harvested and lysed in 200 µL of 50 mM Tris–HCl, 150 mM NaCl, 1% NP-40, 0.5% sodium deoxycholate, 2 mM sodium fluoride, 2 mM EDTA, 0.1% SDS, containing a mixture of protease inhibitors (aprotinin, phenylmethylsulfonyl fluoride, and sodium orthovanadate; SigmaAldrich).

For cytosolic fraction isolation, cells were mechanically-lysed in IBC buffer (10mM Tris/MOPS, 1mM EDTA/Tris, 200mM sucrose, pH 7.4**)** using glass potter homogenizer and lysates were centrifuged at 12000 rpm for 20 minutes. Supernatants and pellets were collected as cytosolic and mitochondrial fractions, respectively.

Same amounts of proteins, from total lysate or cytosolic fraction, were resolved on SDS-polyacrylamide gel, transferred to a nitrocellulose membrane and probed with appropriate primary antibody (Santa Cruz, Biotechnology, CA, USA and Merck KGaA, DA, DE). To confirm equal loading and transfer, membranes were stripped and incubated with anti-GAPDH

antibody (Santa Cruz, Biotechnology, CA, USA). The antigen-antibody complex was detected by incubation of the membranes with peroxidase-coupled goat anti-mouse or goat anti-rabbit antibodies and revealed using the ECL System (Bio-Rad Laboratories, CA, USA). The blots were then exposed to film, and the bands of interest were quantified by using ImageJ software.

5.6 TUNEL assay

Fragmentation of DNA, late event of apoptosis, was determined by using enzymatic labelling of DNA strand breaks using terminal deoxynucleotidyl transferase-mediated deoxyuridine triphosphate nick end-labeling (TUNEL). TUNEL labelling was conducted using TUNEL assay Kit (Promega) on cells treated for 72h with DMSO or 50 μM thioalbamide, fixed in freshly prepared 4% methanol-free paraformaldehyde solution in PBS (pH 7.4) for 25 minutes at 4°C. After fixation, cells were permeabilized in 0.2% Triton® X-100 solution in PBS for 5 min. Then washing twice with washing buffer for 5 min, the cells were covered with equilibration buffer at room temperature for 10 minutes. The labeling reaction was performed using fluorescin-dUTP mix and rTdT enzyme for each sample and incubated for 1 hour at 37°C where rTdT enzyme catalyses the binding of fluorescein-dUTP to free 3'OH ends in the nicked DNA. After rinsing, cells were washed with SSC solution buffer and subsequently incubated with 0,2 mg/ml 4',6- diamidino-2-phenylindole (DAPI; Sigma) to stain nuclei, protected from light, analyzed and photographed by using a fluorescent microscope (Olympus BX4 with CSV1.14 software, using a CAMXC-30 for image acquisition).

5.7 AnnexinV-PI assay

Phospatidilserine externalization on outer leafleat of cell membrane was detected by AnnexinV-PI assay, according to manufacterer's procedure (Annexin V, Alexa Fluor™ 488 conjugate kit, Thermo Fisher Scientific). Briefly, $1x10^5$ MCF7 cells were seeded in 6-well plates and treated with 50 μM thioalbamide for 24 hours. After treatment, cells were collected, rinsed with PBS and incubated with FITC-AnnexinV and 100 μg/ml propidium iodide in 1X AnnexinV buffer for 15 minutes at room temperature. After staining, samples were subjected to cytofluorimetric analysis by using BD FACSJazz™ Cell Sorter (Becton, Dickinson and Co).

5.8 Mitochondrial membrane potential analysis

To measure mitochondrial membrane potential, cells were stained with MioTracker Orange probe (ThermoFisher), whose accumulation in mitochondria is dependent upon membrane potential, according manufacturer's procedure. Briefly, $1x10^5$ cells/well were seeded in 6-well

plates and treated with 50nM thioalbamide or DMSO for 72 hours**.** After treatment, cells were harvested, rinsed and incubated in 10 nM MitoTracker Orange solution in PBS for 30 minutes at 37°C. After staining cells were fixed with 3.7% formaldehyde in complete growth medium at 37°C for 15 minutes, rinsed and resuspended in PBS. Samples were then subjected to cytofluorimetric analysis by using BD FACSJazz™ Cell Sorter (Becton, Dickinson and Co).

5.9 Reactive oxygen species (ROS) assessment

$1x10^5$ MCF7 cells/well were seeded in 6-well plates and treated with 50nM thioalbamide or DMSO for 24/72 hours. After treatment, cells were washed with PBS, collected, resuspended in 5µM CM-H_2DCFDA (ThermoFisher Scientific) in PBS and incubated 45 minutes at 37°C. Stained cells were collected by centrifuge and resuspended in fresh pre-chilled medium. Finally, fluorescence of samples was quantified with a fluorimeter, and fluorescence intensity normalized on cell number.

5.10 ROS-scavenging assay

To evaluate if thioalbamide cytotoxicity was mediated by oxidative stress phenomena, cells were treated with 50µM thioalbamide in presence or absence of 1mM Vitamin E for 72 hours. After treatment cell viability was assessed as previously described (cell viability assay section).

5.11 Superoxide dismutase activity assay

Superoxide dismutase activity was assessed on total cell lysates (50 µg of proteins), prepared as previously reported, by using a colorimetric SOD assay kit (Sigma Aldrich) and following manufacturer's procedure. This is an indirect assay method based on xanthine oxidase mediated production of superoxide anion that is able to reduce 2-(4-Iodophenyl)-3-(4-nitrophenyl)-5-(2,4-disulfophenyl)-2H-tetrazolium monosodium salt (WST-1) in a water-soluble formazan dye. SOD activity, neutralizing superoxide anions, inhibits WST-1 reduction and dye formation.

5.12 Seahorse XFe96 metabolic profile analysis

Real-time oxygen consumption rates (OCR), extracellular acidification rates (ECAR) rates for MCF7 cells treated with thioalbamide were determined using the Seahorse Extracellular Flux (XFe96) analyzer (Seahorse Bioscience, USA), in order to assess mitochondrial function and glycolytic stress, respectively. Briefly, 1 x 10^4 cells per well were seeded into XFe96 well cell culture plates, and incubated overnight to allow cell attachment. Then, cells were treated with thioalbamide (50nM and 100nM) for 48 hours. Vehicle alone (DMSO) control cells were

processed in parallel. After 48 hours of incubation, cells were washed in pre-warmed XF assay media (or for OCR measurement, XF assay media supplemented with 10mM glucose, 1mM Pyruvate, 2mM L-glutamine and adjusted at 7.4 pH). Cells were then maintained in 175 µL/well of XF assay media at 37°C, in a non-CO_2 incubator for 1 hour. During the incubation time, we loaded 25 µL of 80mM glucose, 9µM oligomycin, and 1M 2-deoxyglucose (for ECAR measurement) or 10µM oligomycin, 9µM FCCP, 10µM rotenone, 10µM antimycin A (for OCR measurement), in XF assay media into the injection ports in the XFe96 sensor cartridge.

5.13 Mammospheres formation assay

A single cell suspension was prepared using enzymatic (1x Trypsin-EDTA, Sigma Aldrich), and manual disaggregation (25 gauge needle), to create a single cell suspension. Cells were seeded at a density of 5000 cells/well in mammosphere medium (DMEM-F12 + B27 supplement + 20 ng/ml EGF + Penicillin/Streptomycin) under non-adherent conditions, in 6-well plates pre-coated with (2-hydroxyethylmethacrylate) (poly-HEMA, Sigma,). Then, cells were treated with thioalbamide at concentrations ranging from 25 nM to 100 nM. Vehicle alone (DMSO) treated cells were processed in parallel as a control. Cells were grown for 5 days and maintained in a humidified incubator at 37°C. After 5 days of culture, 3D-spheres >50 µm were counted using an eye piece ("graticule"), and the percentage of cells plated which formed spheres was calculated and is referred to as percent mammosphere formation, and was normalized to one (1 = 100% MSF).

5.14 Statistical analysis

Data are presented as mean values ± standard deviation, taken over ≥3 independent experiments, with ≥3 replicates per experiment, unless otherwise stated. Statistical significance was measured by using analysis of variance (ANOVA) test. P value ≤ 0.05 was considered statistical significant. Non-linear regression analysis (GraphPad Prism 7) was used to generate sigmoidal dose-response curves to calculate IC_{50} values.

CHAPTER 6

RESULTS AND DISCUSSIONS

6.1 Thioalbamide affects cell viability of several breast cancer cellular lines.

The antiproliferative effects of thioalbamide were evaluated over a wide range of breast cancer cellular lines characterized by differences in the status of the three main receptors conventionally used for breast cancer subtyping: estrogen receptor (ER), progesterone receptor (PR), and human epithelial receptor 2 (HER2).[54] In particular, we evaluated the cellular effects of thioalbamide in luminal lines MCF7 and T47D, in HER2 positive line SKBR3 and in triple-negative lines MDA-MB-231 and MDA-MB-468. Thioalbamide showed an intense antiproliferative activity on all the lines tested (Fig. 38), and the IC_{50} values, calculated for each experimental model, were very similar, in a range between 54 and 75 nM (Table 12). The effects on cell viability observed, significantly higher than the clinically used Doxorubicin, were therefore independent of the receptor profile of mammary tumor cells.

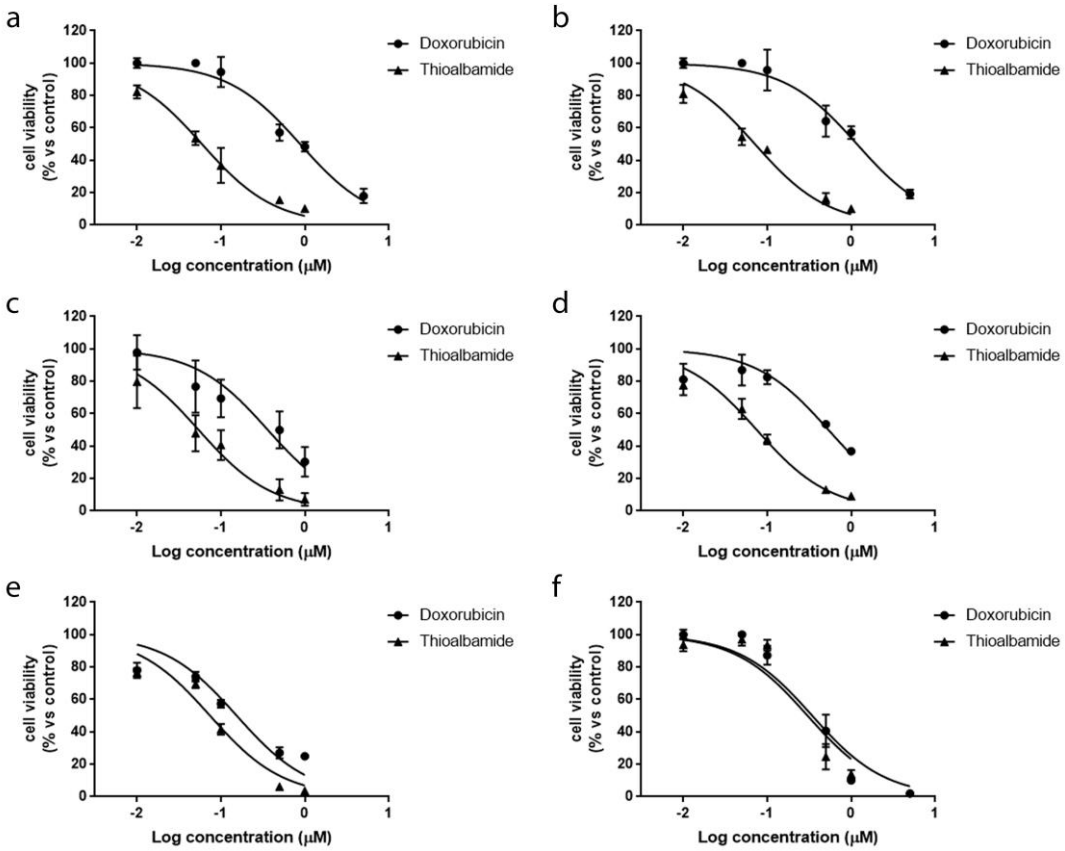

Fig. 38. Effect of thioalbamide on breast cancer cell lines growth. Cellular growth assessment after treatment of MCF7 (a), MDA-MB-231 (b), MDA-MB-468 (c), T47D (d), SKBR3 (e), and MCF-10A (f) cell lines with different concentrations (0.01 to 1 μM) of thioalbamide for 72 h. Results, quantified by the MTT assay, are expressed as percentage of growth vs control cells treated with DMSO. Values represent mean ± SD of three independent experiments, each performed with triplicate samples.

Table 12. Cytotoxic activity of Thioalbamide in comparison to Doxorubicin[a]

Cell line		Doxorubicin	Thioalbamide
MCF7	**IC_{50} (µM)**	**0.878**	**0.059**
	95% confidence interval	0.723 to 1.071	0.049 to 0.072
MDA-MB-231	**IC_{50} (µM)**	**1.174**	**0.072**
	95% confidence interval	0.938 to 1.477	0.058 to 0.088
MDA-MB-468	**IC_{50} (µM)**	**0.362**	**0.054**
	95% confidence interval	0.259 to 0.504	0.043 to 0.069
T47D	**IC_{50} (µM)**	**0.536**	**0.075**
	95% confidence interval	0.380 to 0.756	0.061 to 0.092
SKBR3	**IC_{50} (µM)**	**0.154**	**0.074**
	95% confidence interval	0.108 to 0.221	0.056 to 0.097
MCF 10A	**IC_{50} (µM)**	**0.343**	**0.302**
	95% confidence interval	0.253 to 0.464	0.206 to 0.444

[a]Data are presented as IC_{50} values (µM) and 95% confidence intervals obtained by nonlinear regression analysis of three independent experiments.

As reported in Table 12, the IC_{50} value calculated for the non-malignant mammary epithelial cell line MCF10A was up to 6-fold higher than those calculated for the tumor lines, remarking thioalbamide's specificity for the malignant phenotype.

Since thioalbamide has shown to possess antiproliferative activity at very similar concentrations in all tumor cell lines tested, independently of their tumor subtype of belonging, it was decided to continue the mechanistic studies on a single experimental model, the luminal breast carcinoma cell line MCF7.

6.2 Thioalbamide induces cellular morphology changes.

First of all, the ability of thioalbamide to induce morphological changes in the treated cells was evaluated, and the cellular model chosen to investigate thioalbamide effects was the luminal mammary adenocarcinoma cell line, MCF-7. After 72 hours of treatment, cell morphology, highlighted by May-Grunwald and Giemsa staining, turned out to be drastically altered, and the cells, observed under the microscope, appeared more heterogeneous in terms of shape and size. As shown in Fig. 39, the untreated control cells grew well, appeared healthy and exhibited epithelial-like features, forming a monolayer on the surface of the culture plate. Conversely, the growth of MCF7 treated with thioalbamide for 72 hours was reduced, colony formation ability was affected, and cell fusion, shrinkage, nuclear condensation and apoptotic bodies appeared.

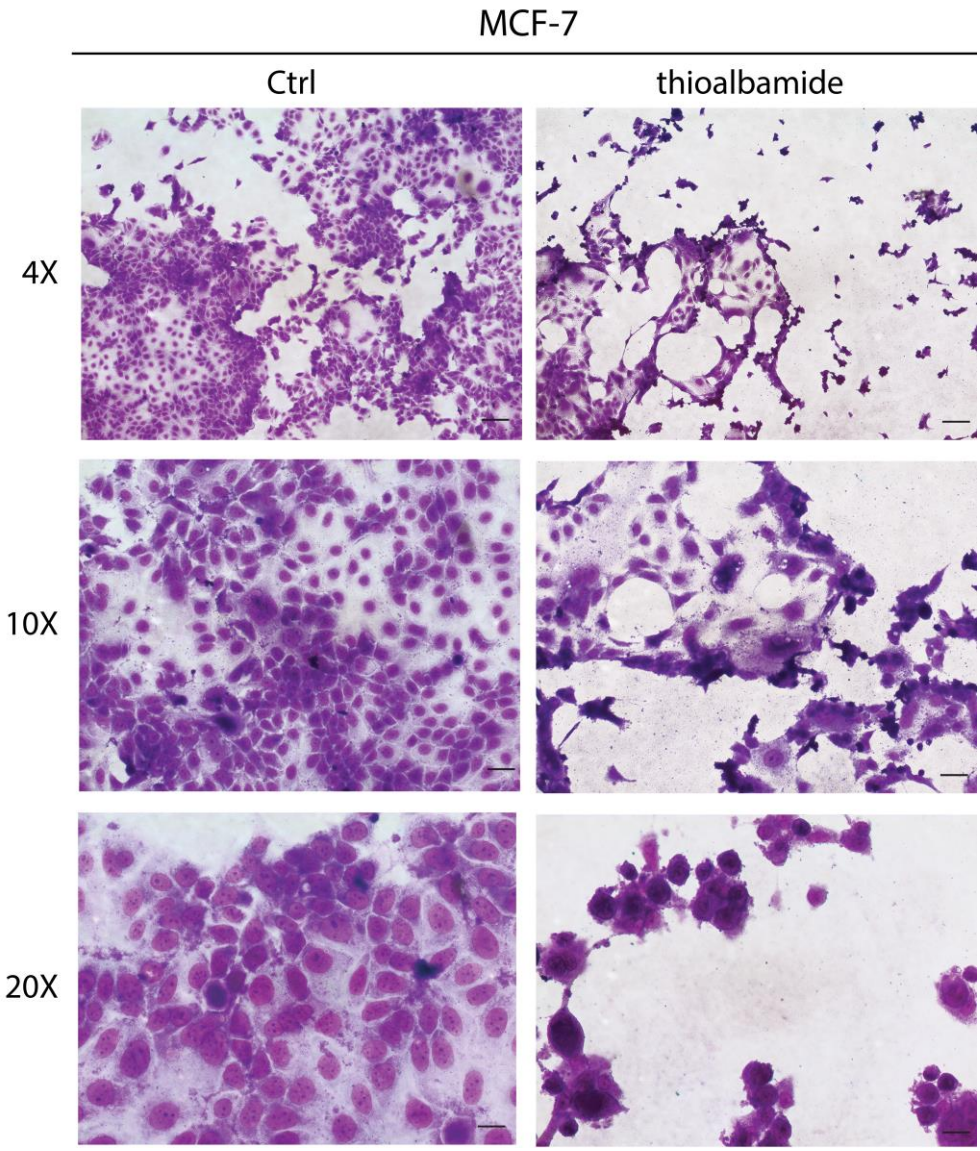

Fig. 39. Thioalbamide affects cellular morphology. MCF-7 cells were treated with DMSO (Ctrl) or 50nM thioalbamide and subjected to May-Grunwald Giemsa staining. Images, at different magnifications, were taken on Olympus BX41 microscope with CSV1.14 software, using a CAMXC-30 for image acquisition. Scale bars: 4X (125 µm), 10X (50 µm), 20X (25 µm).

6.3 Thioalbamide induces arrest of cell cycle in G1 phase.

The effects of thioalbamide on cell growth were, therefore, more investigated. In particular, the ability of thioalbamide to alter the distribution of the treated cells in the different phases of the cell cycle was evaluated. As shown in Fig. 40a-b, the cytofluorimetric analysis of the cell cycle showed a substantial loss of cells in S phase and in G2 and M phases of the cell cycle, and the appearance of a significant hypodiploid population (sub-G1). The peak of hypodiploid cells is generally associated with cells characterized by an apoptotic process in place ([65, 66]), in which genomic DNA appears drastically fragmented. These outcomes seem to suggest that, in cells, thioalbamide can block the transition from the G1 phase to the subsequent phases of the cell

cycle, and cells accumulate in this phase before going to cell death. This result was confirmed by the immunoblotting analysis of several proteins involved in the G1-S transition (Fig. 40c-d). It is known that the G1-S checkpoint is regulated by cyclin-dependent kinase 2 and 4 (CDK2 and CDK4), whose activity is linked to the expression of cyclins E and D1, respectively, which are able to form complexes with CDKs.[67, 68] Our findings evidenced a drastic reduction in both CDKs and their respective cyclins, in MCF7 cell line, after 72 hours of treatment. Cell cycle arrest in G1 phase induced by thioalbamide was also confirmed by the dephosphorylation and activation of Retinoblastoma protein (Rb), an oncosuppressor able to bind to E2F transcription factors family[69, 70], inhibiting their function and DNA replication.

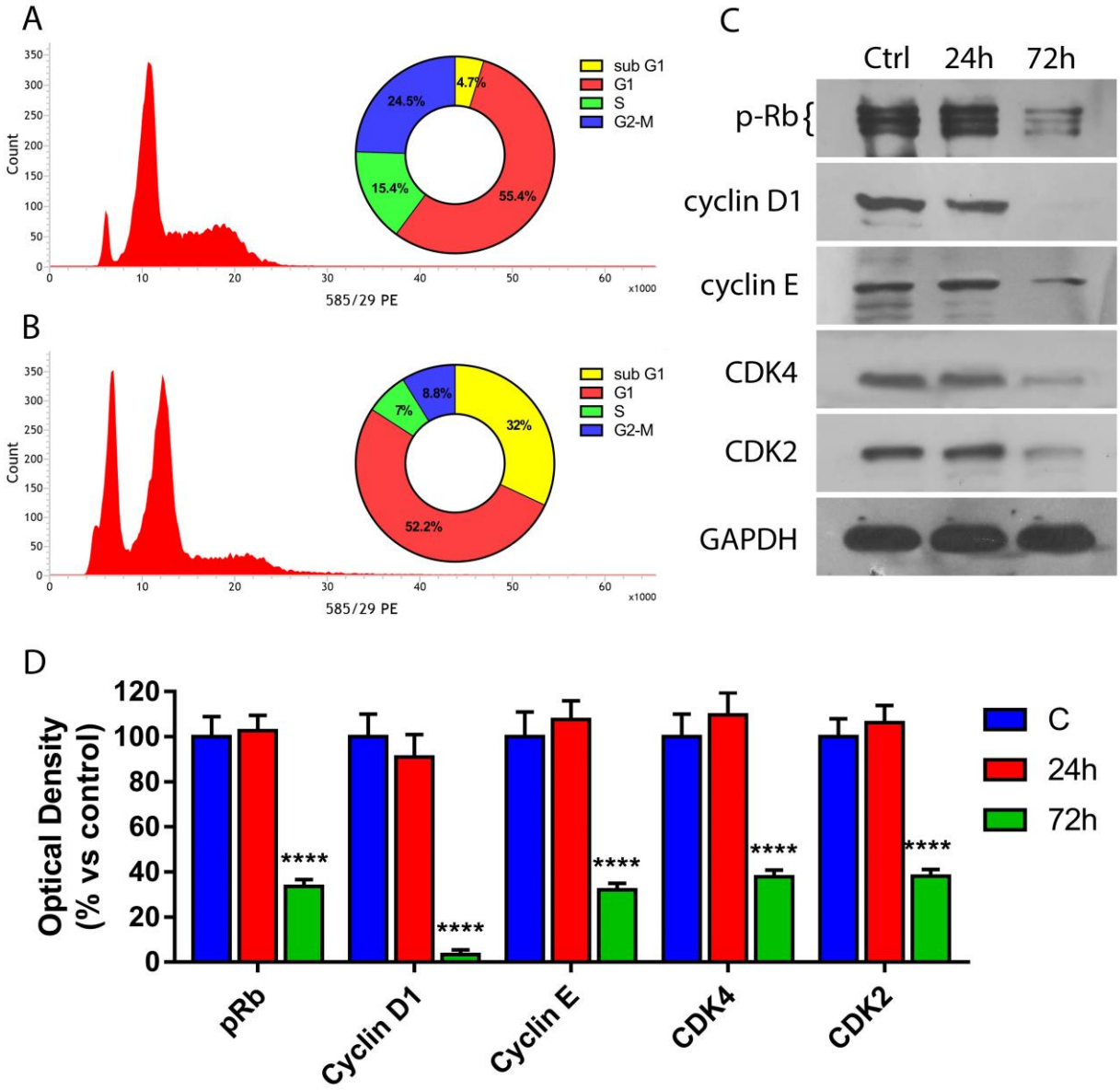

Fig. 40. Thioalbamide affects cell cycle progression. Cytofluorimetric analysis of MCF7 treated for 72h with DMSO (control, a) and thioalbamide at IC_{50} (b) and stained with PI. (c) Immunoblot analysis of the main regulators of G1/S phase transition and (d) quantification of their expression levels by densitometry. Values represent mean ± SD of three independent experiments. ****P value <0,001

6.4 Thioalbamide induces cell death by activation of both extrinsic and intrinsic apoptotic pathways.

Thioviridamide, the first identified molecule belonging to TLMs family is known to induce cellular death through apoptotic processes.[20] This knowledge, together with the evidence that thioalbamide treatment is able to enrich the hypodiploid cell population, has led us to investigate whether the induction of apoptotic mechanisms is a common feature of thioviridamide-like molecules. For this reason, MCF7 cells were treated with Thioalbamide and then subjected to different assays, each one specific for a different event characterizing apoptotic pathway. TUNEL assay was performed to highlight the ability of thioalbamide to induce DNA fragmentation, a late event in apoptosis. As shown in Fig. 41, after 72 hours of treatment the percentage of positive cells turned out to be really high, according to the population of hypodiploid cells observed in previous cytofluorimetric cell-cycle analysis.

Subsequently, Annexin V assay was performed to monitor the externalization of phosphatidylserine on the outer leaflet of the cell membrane. This event characterizes the early stage of apoptosis and, in physiological conditions, facilitates apoptotic cells recognition from macrophages and destruction of apoptotic bodies.[71, 72] Our experiments established that 24 hours of treatment were sufficient for 80% of the treated cells to enter an early stage of apoptosis (Fig. 46a-b-c).

In order to definitively confirm the induction of the apoptotic process, the ability of thioalbamide to determine a loss of mitochondrial membrane potential and the release of cytochrome C into the cytosol were evaluated. The loss of mitochondrial membrane potential represents the “point of no-return” in the apoptotic process. Indeed, this event is responsible for a change in mitochondrial membrane permeability and leads to the translocation into the cytoplasm of cytochrome C, normally confined within the intermembrane space. This heme-protein, reacting with other cytosolic proteins, leads to the formation of a complex called apoptosome, which triggers the apoptotic cascade of caspases.[73] After treatment, MCF7 cells showed a significant reduction in mitochondrial membrane potential with respect to untreated cells; moreover, immunoblotting analysis of cytochrome C levels in the cytosolic fraction confirmed thioalbamide-induced cytochrome C release (Fig. 46d-e-f). At this point, it was decided to evaluate the cleavage and activation of procaspases -8 and -9, initiator caspases involved in extrinsic and intrinsic apoptosis pathways respectively.[74] Immunoblot analysis revealed in treated MCF7 the activation of both pathways (Fig. 47).

In order to understand if the apoptotic mechanisms induced by thioalbamide, observed on MCF7 line, were also at the basis of the antiproliferative and cytotoxic effects observed on the

other mammary tumor lines, TUNEL assay was performed to highlight thioalbamide's ability to determine apoptotic DNA fragmentation in MDA-MB-231, MDA-MB-468, T47D and SKBR3 lines. Our results demonstrate that thioalbamide-induced apoptosis death is an occurrence common to all the tested breast cancer cell lines (Figures 42 to 45).

These results show how the pro-apoptotic activity, previously reported for thioviridamide, is a common feature of thioviridamide-like molecules. This behaviour emphasizes that, despite the variability of the amino acid residues that make up these metabolites, the peculiar common chemical characteristics of these natural products lie at the basis of their enormous antitumor potential.

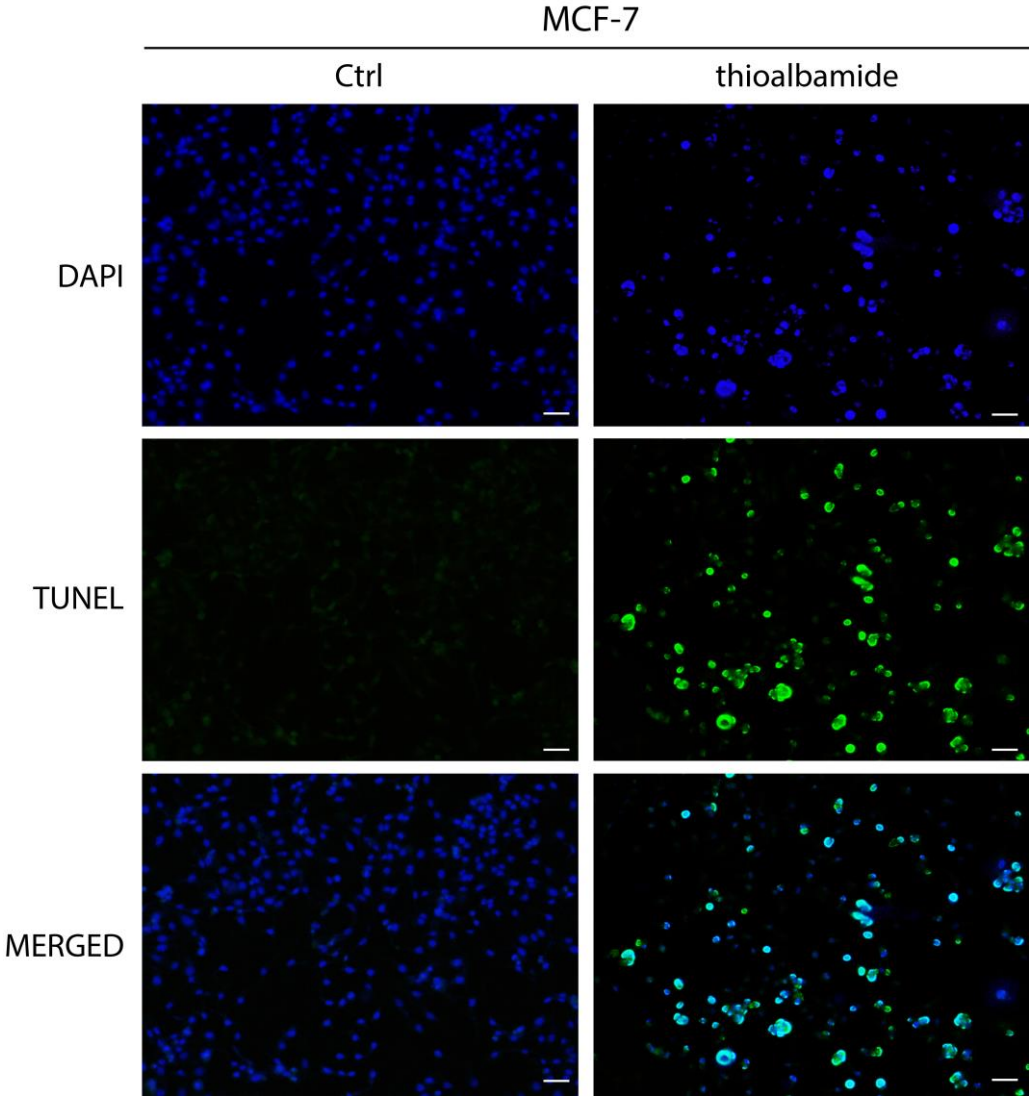

Fig. 41. Thioalbamide-induced DNA fragmentation in MCF7 cells confirms its ability to trigger apoptosis. TdT-mediated dUTP nick-end-labeling (TUNEL) assay in MCF7 cells treated for 72h with vehicle (Ctrl) or thioalbamide at IC50. DAPI has been used for DNA staining. Images, at 10X magnification, were taken on Olympus BX41 microscope with CSV1.14 software, using a CAMXC-30 for image acquisition (scale bar: 50µm).

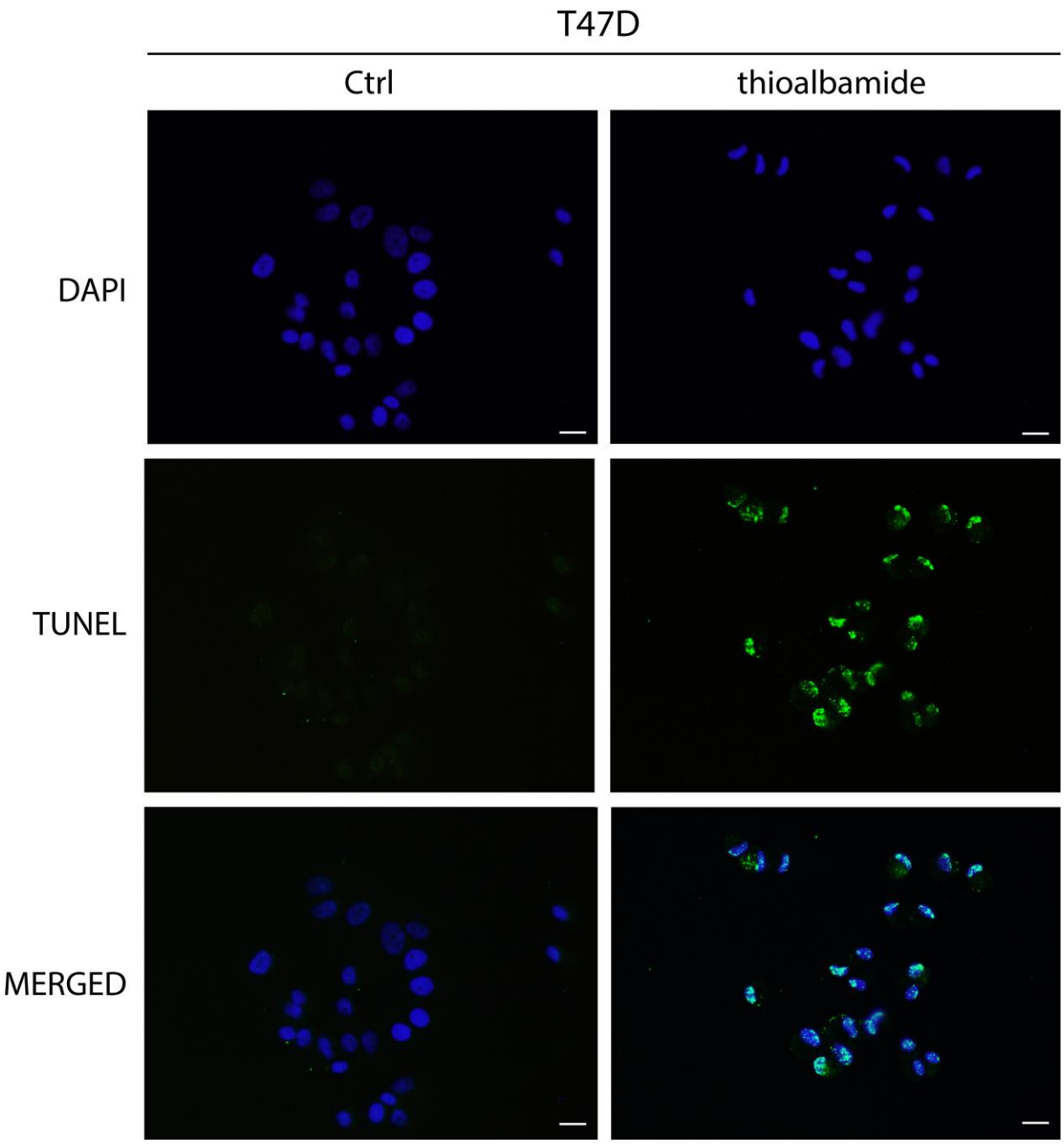

Fig. 42. Thioalbamide-induced DNA fragmentation in T47D cells. TdT-mediated dUTP nick-end-labeling (TUNEL) assay in T47D cells treated for 72h with vehicle (Ctrl) or thioalbamide at IC50. DAPI has been used for DNA staining. Images, at 20X magnification, were taken on Olympus BX41 microscope with CSV1.14 software, using a CAMXC-30 for image acquisition (scale bar: 25μm).

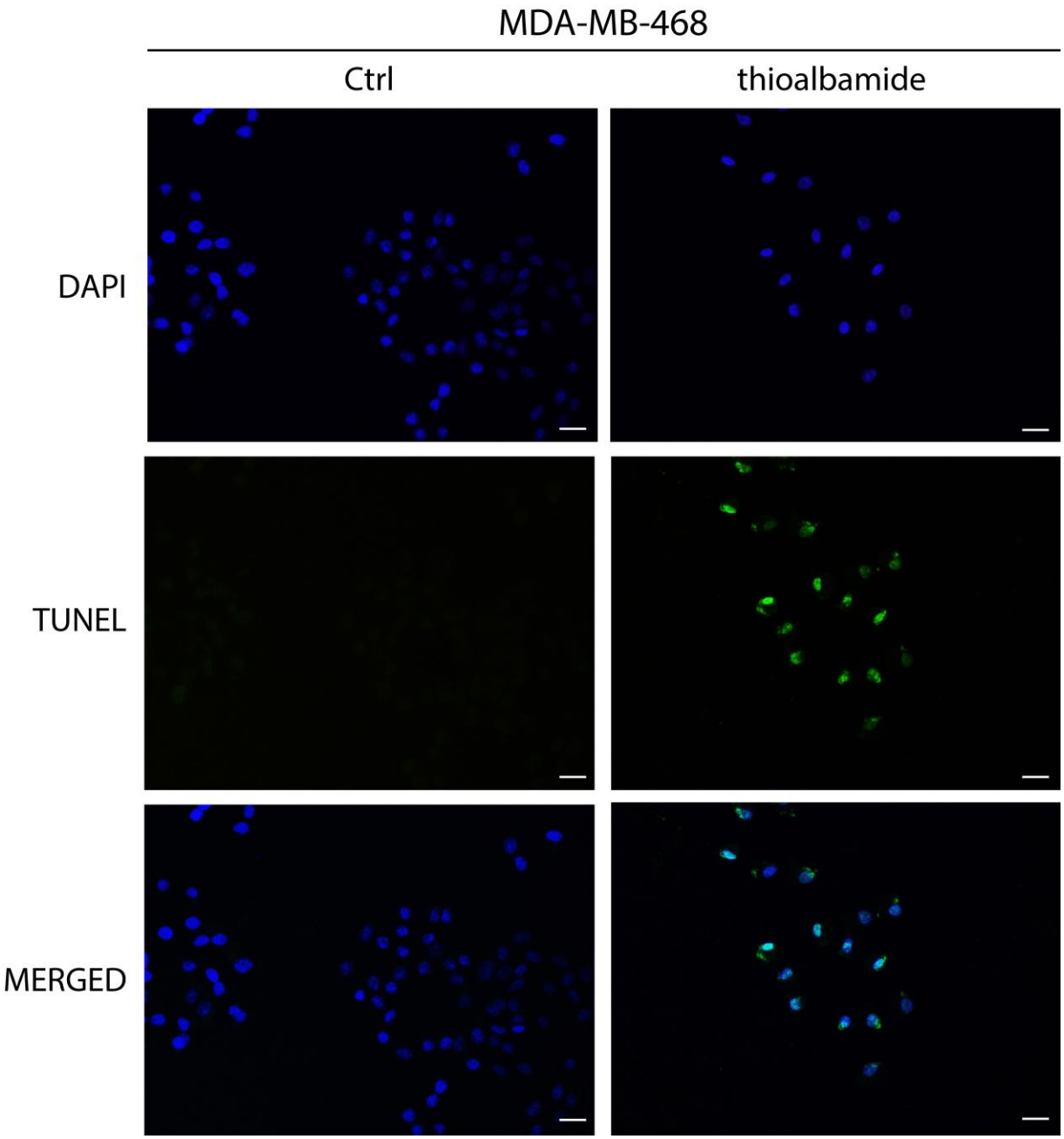

Fig. 43. Thioalbamide-induced DNA fragmentation in MDA-MB-468 cells. TdT-mediated dUTP nick-end-labeling (TUNEL) assay in MDA-MB-468 cells treated for 72h with vehicle (Ctrl) or thioalbamide at IC50. DAPI has been used for DNA staining. Images, at 20X magnification, were taken on Olympus BX41 microscope with CSV1.14 software, using a CAMXC-30 for image acquisition (scale bar: 25μm).

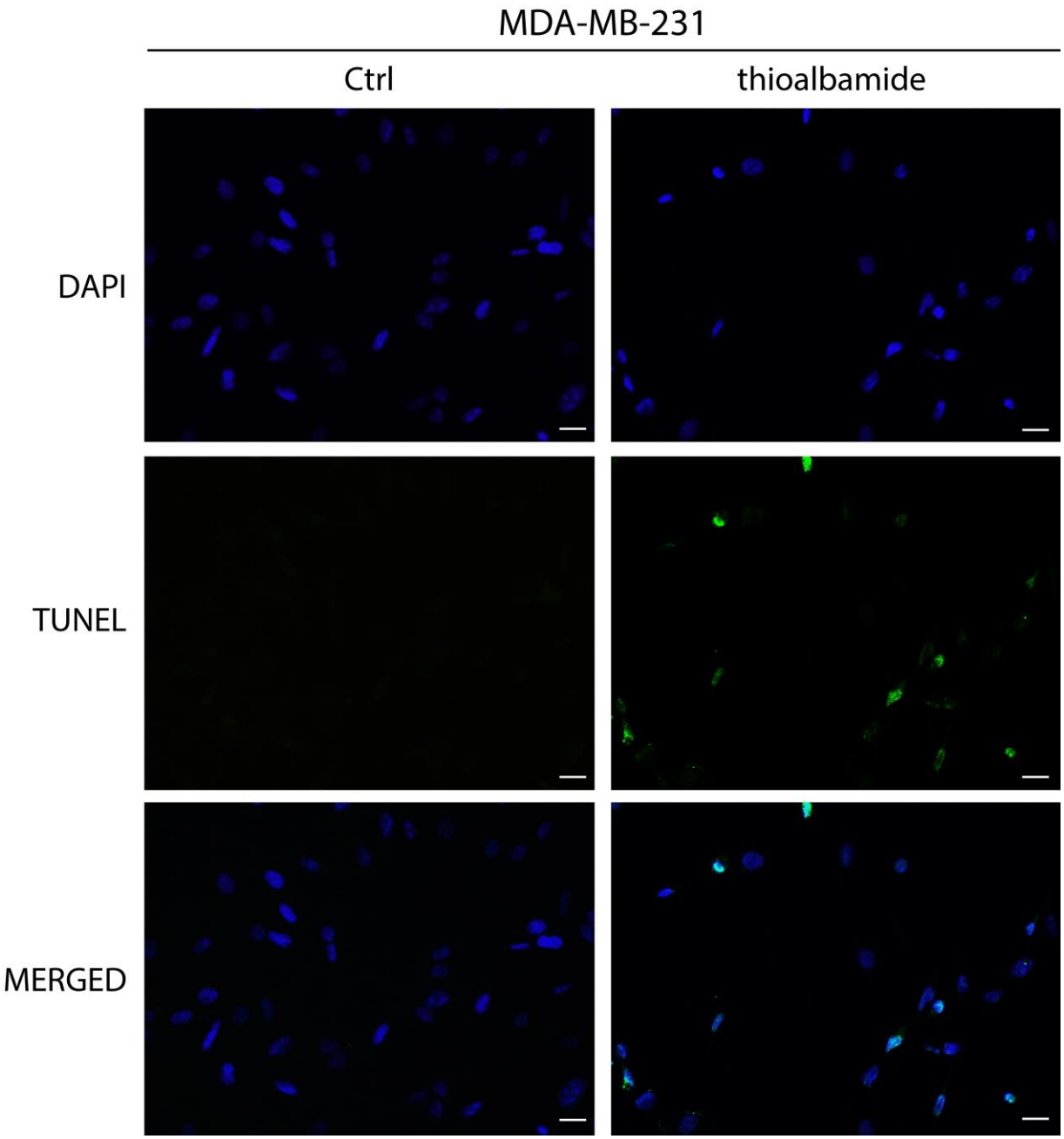

Fig. 44. Thioalbamide-induced DNA fragmentation in MDA-MB-231 cells. TdT-mediated dUTP nick-end-labeling (TUNEL) assay in MDA-MB-231 cells treated for 72h with vehicle (Ctrl) or thioalbamide at IC50. DAPI has been used for DNA staining. Images, at 20X magnification, were taken on Olympus BX41 microscope with CSV1.14 software, using a CAMXC-30 for image acquisition (scale bar: 25μm).

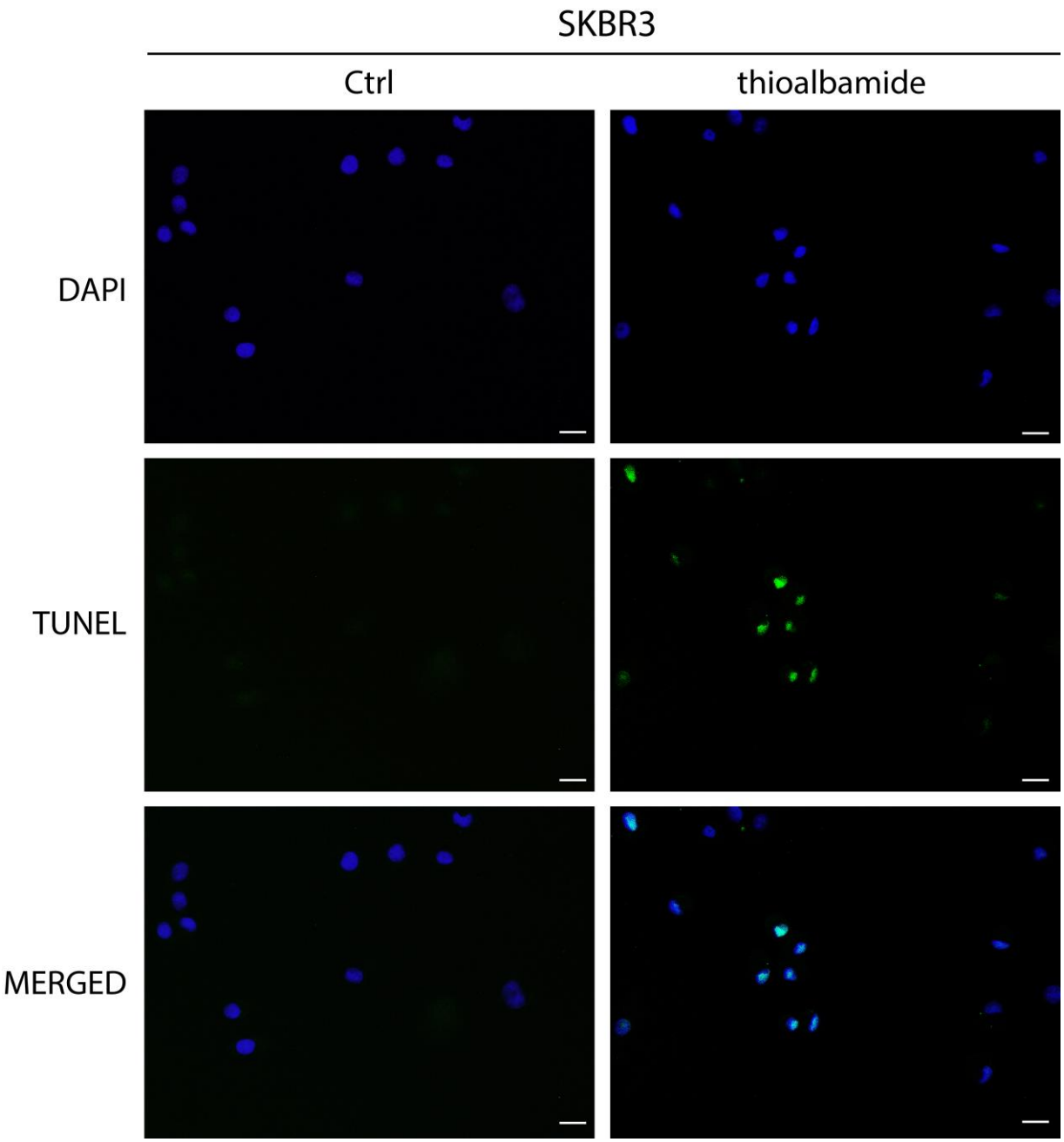

Fig. 45. Thioalbamide-induced DNA fragmentation in SKBR3 cells. TdT-mediated dUTP nick-end-labeling (TUNEL) assay in SKBR3 cells treated for 72h with vehicle (Ctrl) or thioalbamide at IC50. DAPI has been used for DNA staining. Images, at 20X magnification, were taken on Olympus BX41 microscope with CSV1.14 software, using a CAMXC-30 for image acquisition (scale bar: 25μm).

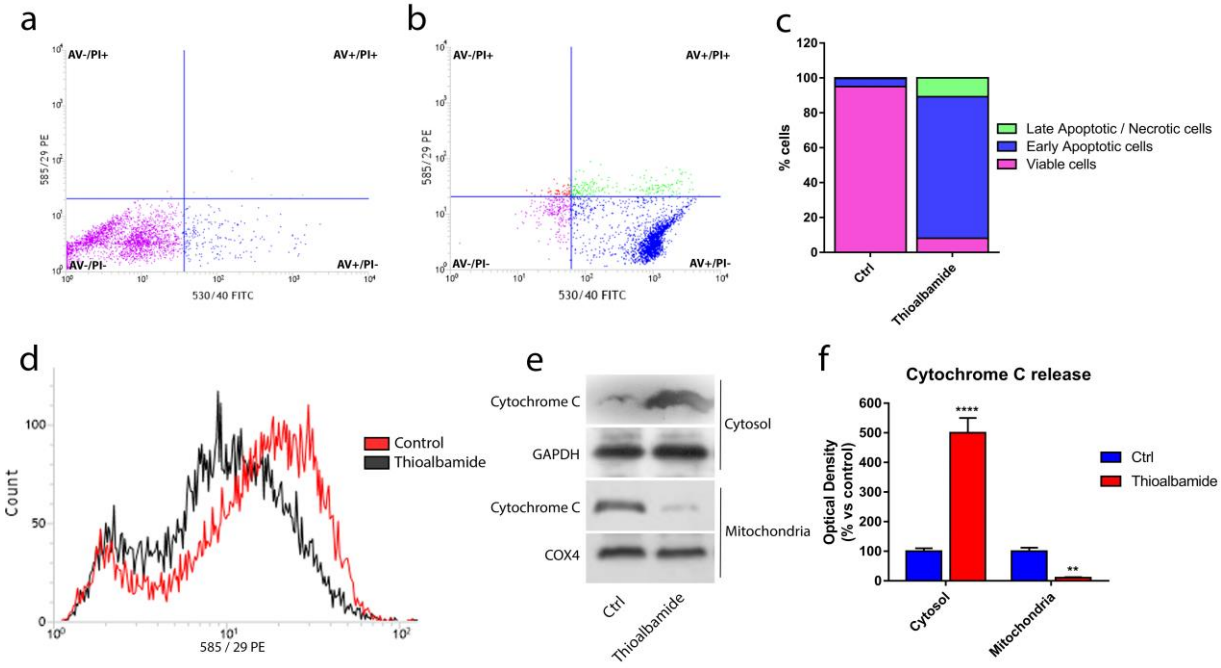

Fig. 46. Thioalbamide triggers apoptotic mechanisms. Externalization of phosphatidylserine onto the outer leaflet of cell membrane by performing AnnexinV-PI assay (a, DMSO-treated cells) (b, cells treated with thioalbamide at IC_{50} for 24h) (c, histograms representing the percentage of cell populations after treatment). (d) Loss of mitochondrial membrane potential after 72h of treatment with thioalbamide, assessed by using MitoTracker Orange CMTMRos probe. (e) Release of Cytochrome C into the cytosolic fraction of cells treated for 72h with thioalbamide, assessed by immunoblot analysis. GAPDH and COX4 have been used as loading control of cytosolic and mitochondrial fractions, respectively. (f) Quantification of Cytochrome C levels in the cytosolic and mitochondrial fractions by densitometry. Values represent mean ± SD of three independent experiments.
P value <0,01;**P value <0,001

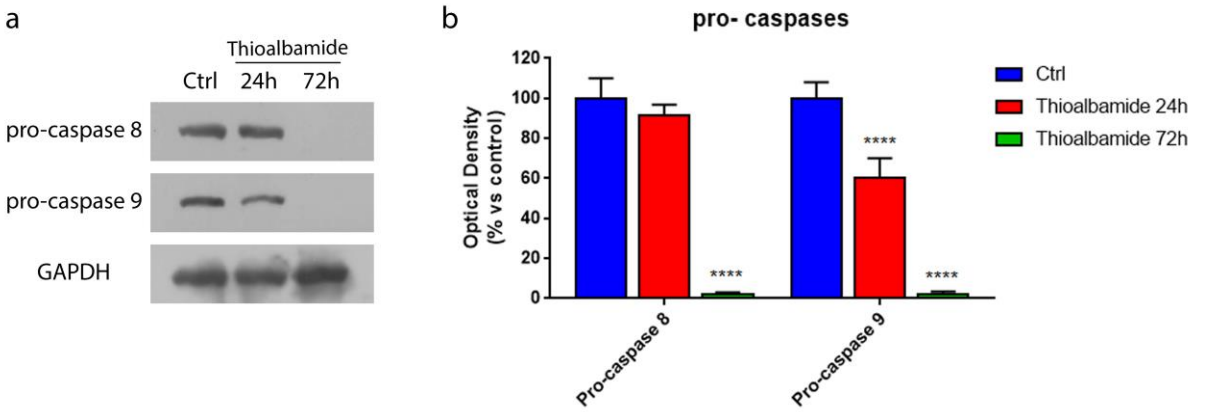

Fig. 47. Thioalbamide triggers both extrinsic and intrinsic apoptotic pathways. (a) Immunoblot analysis of pro-caspases 8 and 9 after 24 and 72h of treatment with thioalbamide. GAPDH has been used as loading control. (b) Quantification of procaspases expression levels by densitometry. Values represent mean ± SD of three independent experiments. ****P value <0,001

6.5 Oxidative stress underlies the cytotoxic effects of thioalbamide.

In order to better understand the mechanisms underlying thioalbamide-induced apoptosis, reactive oxygen species (ROS) produced by untreated and treated MCF7 cells were compared. ROS are, in fact, well known biochemical mediators of apoptosis, as they are strongly reactive towards several biological macromolecules and in particular towards proteins involved in the electro-chemical equilibrium straddling the mitochondrial membrane.[75] We found a significant increase in ROS accumulation after just 24 hours, and after 72 hours a 4-fold increase in ROS was detected (Fig. 48a). In order to confirm that oxidative stress is really responsible for thioalbamide-induced cytotoxicity, a viability assay was performed on MCF7 treated with thioalbamide alone and in the presence of a ROS scavenger such as Vitamin E. After 72 hours of treatment no cytotoxicity was detected in Thioalbamide-Vitamin E co-treated cells (Fig. 48b), confirming that oxidative stress is the event responsible for apoptosis induction and cytotoxicity. The same result was obtained in all the other tumor lines tested, demonstrating that the oxidative phenomena induced by thioalbamide are responsible for the apoptotic processes observed in all the different mammary tumor lines used in this study (Fig. 49).

In order to understand whether thioalbamide-induced ROS accumulation is due to an effective increase in ROS production or to a deficiency of the enzymatic neutralization systems, the activity of SuperOxide Dismutases (SODs), one of the main enzymatic families involved in ROS neutralization, was evaluated in MCF7. This family of enzymes are specifically responsible for the neutralization of superoxide anion ($\cdot O_2^-$), one of the main sub-products of cellular metabolism that originates from an incomplete reduction of molecular oxygen in the mitochondrial respiratory chain.[76] Total SODs activity in cells treated for 24 hours resulted to be duplicated, as a physiological cell response to the increase in ROS production (Fig. 48c). Interestingly, the increase in SODs activity appeared to be limited and not enough to balance the time-dependent ROS accumulation induced by thioalbamide treatment.

Since there are several isoforms of SOD, each of which is characteristic of a specific cell compartment[77], immunoblotting analysis of the different SODs isoforms was performed, in order to understand whether the increase in SODs activity observed is specific to a cellular compartment. The results obtained showed an increase in the expression of SOD2, the mitochondrial isoform, while the levels of SOD1, the cytoplasmic isoform, were found to be unaltered (Fig. 48d-e). These results could reflect an increase in ROS production at mitochondrial level[78] and suggest an important involvement of mitochondria in thioalbamide's mode of action.

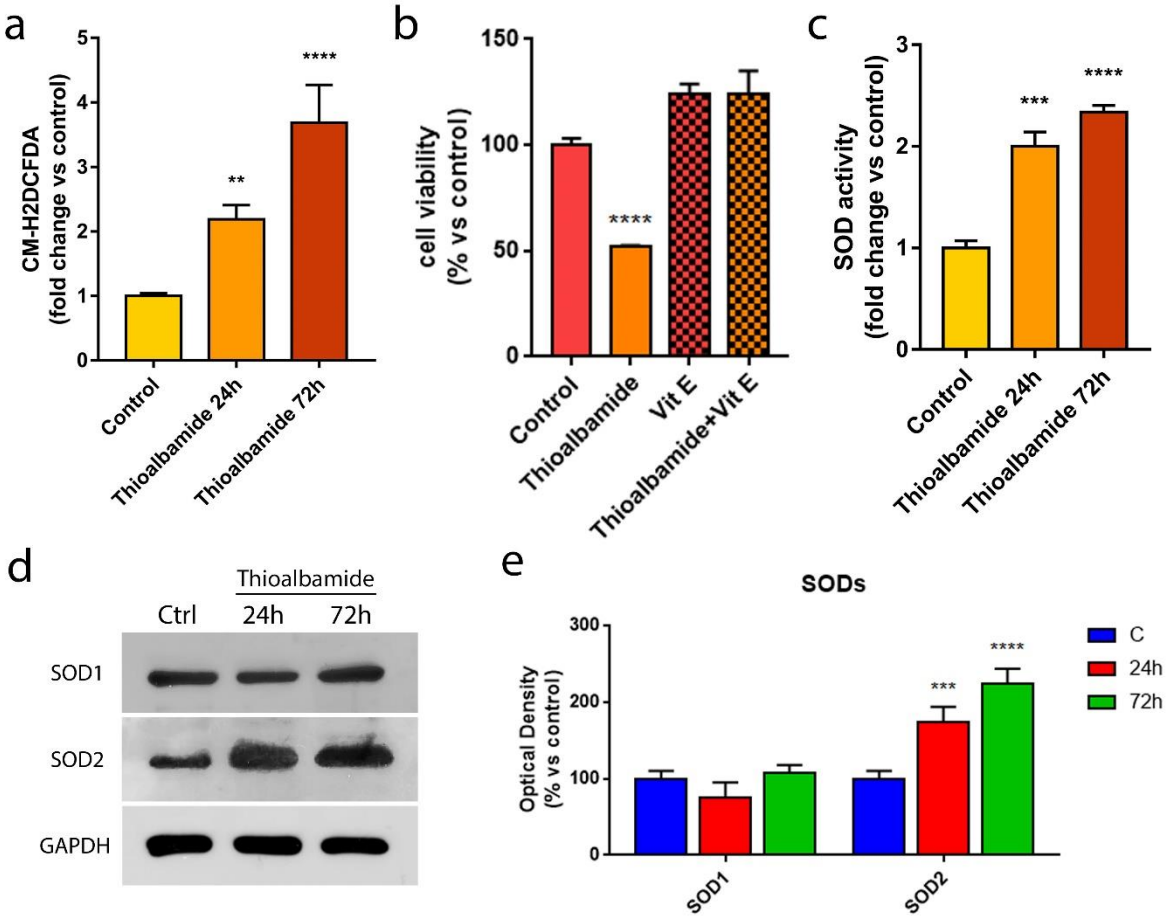

Fig. 48. Thioalbamide triggers oxidative stress phenomena in MCF7. (a) Reactive Oxygen Species (ROS) intracellular levels after treatment of MCF7 for 24 and 72h with thioalbamide. (b) MCF7 cells viability assessment after treatment for 72h with thioalbamide alone or in association with Vitamin E (Vit E). (c) Total SODs activity assay performed on MCF7 treated for 24 and 72h with thioalbamide. (d) Immunoblot analysis of SOD1 and SOD2 expression levels in MCF7 cells treated with thioalbamide for 24 and 72h. GAPDH has been used as loading control. (e) Quantification of SODs expression levels by densitometry. Values represent mean ± SD of three independent experiments. *P value<0,05; **P value <0,01; ***P value <0,005; ****P value <0,001

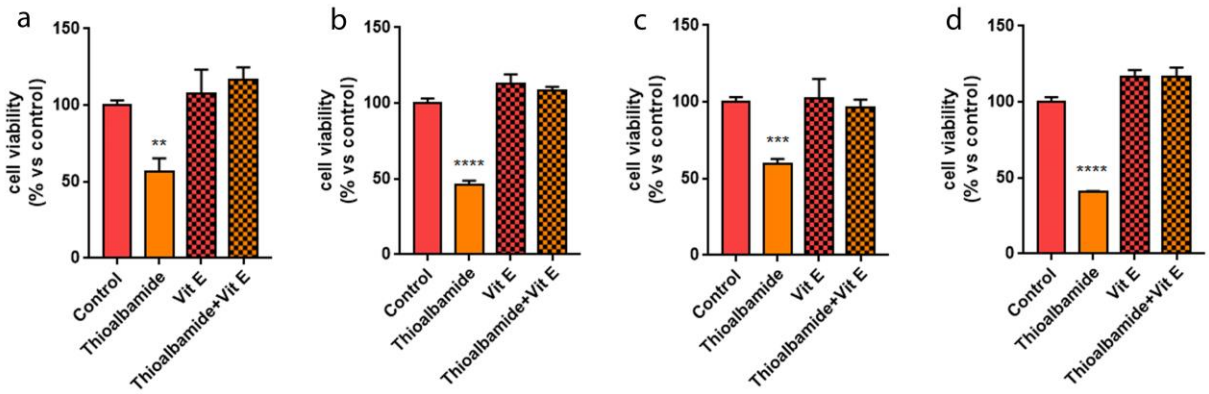

Fig. 49. Oxidative stress underlies the cytotoxic effects of thioalbamide in all tested breast cancer cell lines. Viability assessment of MDA-MB231 (a), MDA-MB-468 (b), T47D (c) and SKBR3 (d) after treatment for 72h with thioalbamide at IC_{50} values, alone or in association with Vitamin E (Vit E), as indicated. Values represent mean ± SD of three independent experiments. **P value <0,01; ***P value <0,005; ****P value <0,001.

6.6 Thioalbamide treatment affects glycolysis and mitochondrial respiration.

The tumor cell is characterized by a metabolic reprogramming that accelerates the energy metabolism to support the high proliferation rate of malignant neoplasms.[79] For this reason, metabolic processes represent an important pharmacological target for the treatment of oncological diseases. The production of reactive oxygen species is closely related to cellular energy metabolism, and this knowledge led us to investigate whether the accumulation of ROS, induced by thioalbamide, was the consequence of an alteration of the cellular metabolic profile. The ability of thioalbamide treatment to affect the metabolic profile of breast cancer cells was evaluated by employing mitochondrial respiration and glycolytic function analysis, using a Seahorse XFe96 analyzer.

Mitochondrial function was assessed by monitoring oxygen consumption rate (OCR), and sequentially injections of Oligomycin, FCCP and Antimycin/Rotenone mix, allowed us to evaluate mitochondrial function parameters (Fig. 50a), such as:

- Basal respiration, which reflects the energetic demand of the cell under baseline conditions.
- ATP production, which reflects ATP produced by the mitochondria that contributes to meeting the energetic needs of the cell.
- Proton leak, which reflects mechanisms that regulate the mitochondrial ATP production.
- Maximal respiration, which reflects the maximum rate of respiration that the cell can reach.
- Spare capacity, which reflects the energetic flexibility and cells ability to respond to energetic demand.

The result of mitochondrial stress test performed on MCF7 cells, after 48h of treatment with thioalbamide, proved the ability of this natural compound to significantly affect all the different mitochondrial respiration parameters (Fig. 50b-c).

Glycolytic function was assessed by monitoring extracellular acidification rate (ECAR), and sequentially injections of glucose, Oligomycin and 2-Deoxy-D-glucose (2-DG), allowed us to evaluate glycolytic function parameters (Fig. 50d), such as:

- Glycolysis, which reflects the glycolytic rate at saturating glucose concentration.
- Glycolytic capacity, which reflects the maximum glycolytic rate that cells can achieve when oxidative phosphorylation is inhibited.
- Glycolytic reserve, which reflects the capability of cells to respond to an energetic demand.

Results of glycolytic stress test performed on MCF7 cells, after 48h of treatment with 50nM thioalbamide, highlighted the ability of this molecule to significantly reduce glycolysis and glycolytic capacity, while the glycolytic reserve resulted to be affected at higher concentrations

(Fig. 50e-f). Similar effects on cell metabolism were also observed in other breast cancer lines (Fig. 51), emphasizing once again that the effects induced by the molecule are the same in all breast cancer subtypes, despite the biological heterogeneity.

Overall, our results highlight the ability of thioalbamide to "switch off" the energy metabolism of cancer cells, affecting the two main energy pathways of cell metabolism, glycolysis and oxidative phosphorylation. This effect results in a significant change in the metabolic phenotype of cancer cells from a highly energy status to a quiescent one.

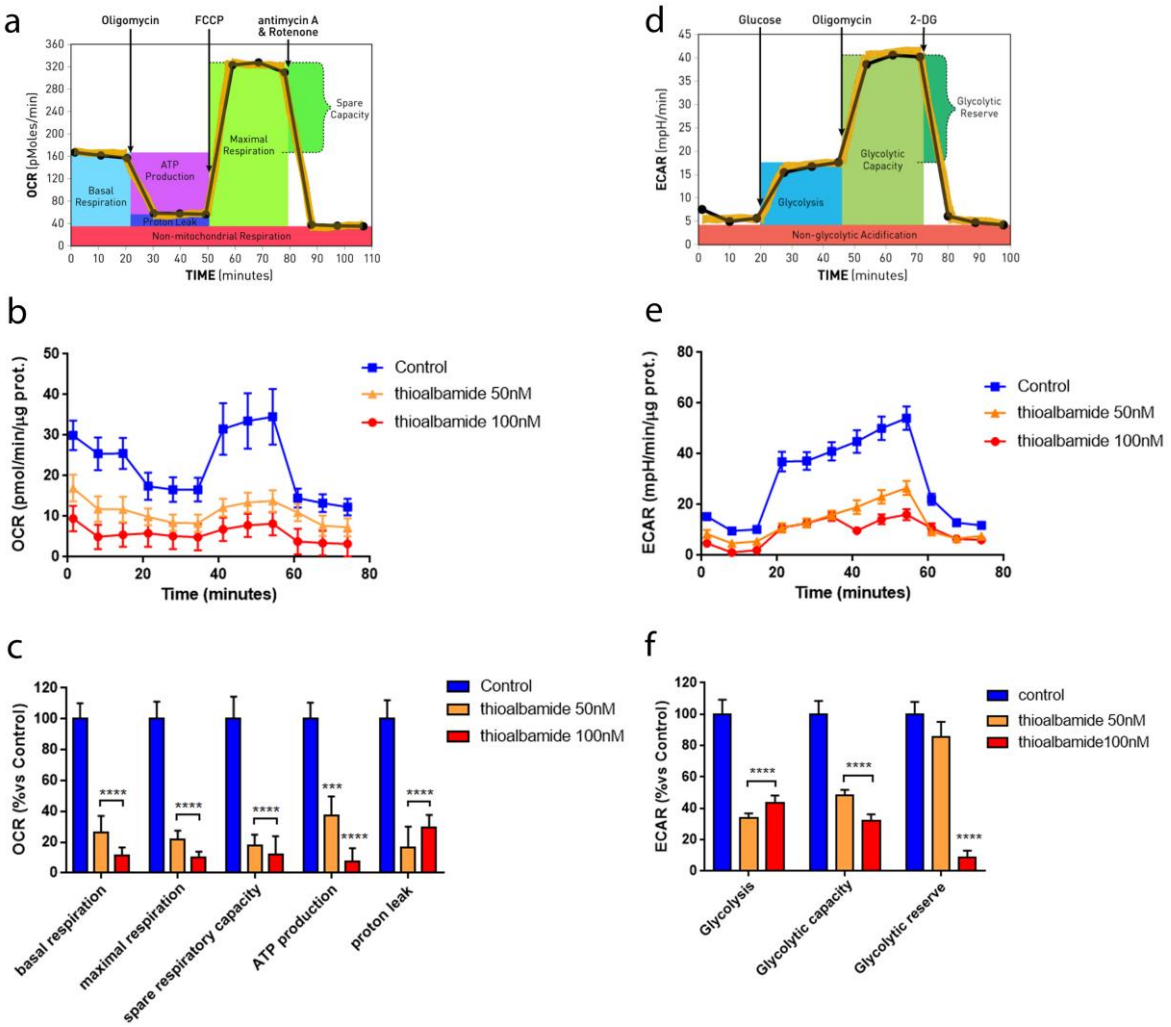

Fig. 50. Metabolic profile of MCF7 cells treated with thioalbamide. Seahorse XFe96 analyser has been employed to analyze mitochondrial respiration and glycolytic function in MCF7 treated with thioalbamide for 48h, by monitoring oxygen consumption rate (OCR) and extracellular acidification rate (ECAR), respectively. (a) Schematic representation of mitochondrial respiration analysis. (b) OCR of MCF7 cells treated for 48h with DMSO (control) and 50/100 nM thioalbamide. (c) Histograms of mitochondrial respiration parameters. (d) Schematic representation of glycolytic function analysis. (e) ECAR of MCF7 cells treated for 48h with DMSO (control) and 50/100 nM thioalbamide. (f) Histograms of glycolytic function parameters. Values represent mean ± SEM of >7 independent experiments. ***P value <0,005; ****P value <0,001

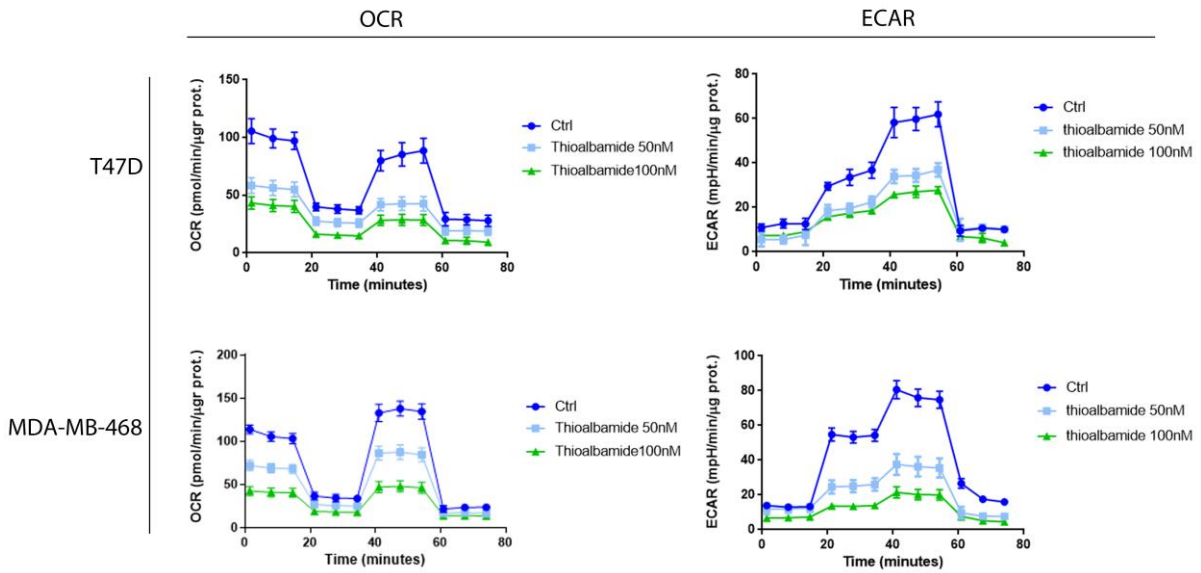

Fig. 51. Metabolic profile of T47D and MDA-MB-468 cells treated with thioalbamide. Seahorse XFe96 analyser has been employed to analyze mitochondrial respiration and glycolytic function in T47D and MDA-MB-468 cells treated with thioalbamide for 48h, by monitoring oxygen consumption rate (OCR) and extracellular acidification rate (ECAR), respectively. Values represent mean ± SEM of >5 independent experiments.

6.7 Thioalbamide affects breast cancer stem cells propagation.

As reported in the introductory chapter, cancer research in recent years is focusing on the identification of molecules able to affect cancer stem cells, the sub-population of tumor cells responsible for the occurrence of chemotherapy resistance and tumor recurrence phenomena. One of the strategies to eradicate cancer stem cells is to hit their energy metabolism in order to reduce the metabolic flexibility responsible for their tumorogenicity.[61-63]

Since mitochondrial function is required for anchorage-independent survival and propagation of cancer stem-like cells[80], and considering the evidence that thioalbamide strongly affects breast cancer cells metabolism, we decided to investigate thioalbamide ability to reduce mammosphere formation efficiency (MFE).

The results obtained, shown in Fig. 52, indicate that thioalbamide is able to reduce, in a dose-dependent manner, mammosphere formation efficiency in all the cell lines tested, a result that reflects an inhibition of mammary tumor cell staminality. This result, in addition to confirming the effects on metabolism induced by thioalbamide, opens new scenarios regarding the use of this natural product in the oncologic field.

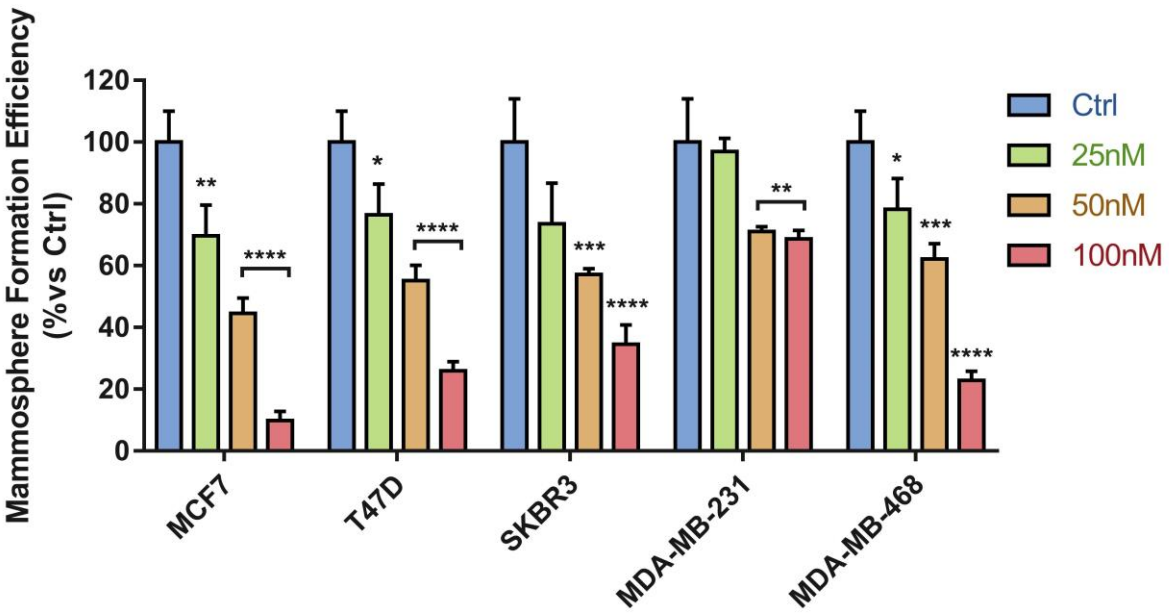

Fig. 52. Thioalbamide affects mammosphere formation. Cells were treated with DMSO (ctrl) or with 25/50/100 nM, as indicated, in anchorage-independent conditions. Histograms show the percentage of plated cells forming spheres (mean ± SD), normalized on untreated control. *P value <0,05; **P value <0,01; ***P value <0,005; ****P value <0,001.

CHAPTER 7

CONCLUSIONS

The results obtained in this PhD thesis work highlight new aspects of the pharmacological potential of microbial secondary metabolites. By the end of this study, thioviridamide, an antiproliferative and proapoptotic agent known in the literature, was found to be no longer a molecule unique of its kind, but part of a family of natural products that today takes the name of Thioviridamide-like molecules (TLMs).

This result was achieved by using a genomics-based approach that allowed us to identify thioviridamide analogues, based exclusively on the information contained in the microorganisms' DNA. This made it possible to discover the innate genetic potential of different bacteria, which has remained hidden so far, because of the use of classical strategies for the identification of bioactive natural products, such as the activity-guided approach.

The chosen methodology, based on seeking microorganisms with the genetic equipment for biosynthetic machinery similar to that of thioviridamide, proved to be perfect for achieving the set objectives. Searching for molecules analogous to thioviridamide led to the discovery of a whole family of peptidic compounds, slightly different in their amino acid sequences, but with highly conserved peculiar characteristics, such as the presence of thioamide bonds in the peptide backbone, a rare characteristic among microbial natural products.

The approach used is the result of the application and integration of bioinformatic, chemical and molecular biology methodologies, which enabled us, respectively, to select potential bacterial strains producing thioviridamide-like molecules, to identify three new natural products and, finally, to correlate them to the respective gene clusters and classify them as TLMs.

A biochemical-metabolic approach was subsequently used to investigate the mechanisms underlying the antitumor activity of thioalbamide, the natural product purified in the greatest amounts by microorganisms. The results obtained, first on a wide range of tumor cell lines and subsequently focusing on breast cancer, showed the powerful antiproliferative/cytotoxic activity of thioalbamide, which was found to be highly selective towards the tumor lines, showing limited effects on the non-tumor mammary gland epithelium cell line MCF10A.

The antiproliferative action of the compound was more thoroughly studied, and a cell-cycle arrest at the G1-S checkpoint was shown to underlie these effects.

Cytotoxic effects were also the object of the study, and our experiments showed that at the basis of thioalbamide-induced cell death is the triggering of extrinsic and intrinsic apoptotic pathways. This result is consistent with what has been observed for thioviridamide, the progenitor of the TLMs family, and our results, on the whole, show that pro-apoptotic action is a common feature of this new class of natural products.

In addition, for the first time, the biochemical effects underlying the proapototic activity of TLMs were studied. In particular, our findings have shown that at the basis of the thioalbamide-induced cell death is an intense oxidative stress, in turn triggered by a strong alteration of cellular metabolic pathways. In detail, this natural product has shown to be able to strongly inhibit the glycolytic pathway and oxidative phosphorylation, the two main energy sources for the malignant cell. The effects on the metabolism observed make thioalbamide, and TLMs in general, pharmacological agents potentially suitable for eradicating cancer stem cells, the cellular subpopulation responsible for the phenomena of recurrence and tumor metastasis.

However, to better understand thioalbamide's mechanism of action, in order to identify its exact molecular target, it will be necessary to examine the effects on several well-established signalling pathways, which have been shown to promote proliferation, inflammation and stemness, by using a proteomic approach. Moreover, further preclinical studies will allow us to evaluate thioalbamide *in vivo* efficacy. Experiments on tumor xenograft and experimental metastasis models in mice are, indeed, in progress, in order to facilitate the transfer of knowledge into clinical studies.

The results obtained have shown once again how nature is, through microorganisms, an invaluable source of biologically active compounds of immense pharmacological potential. Nature makes an unexpressed potential available to scientific research, and our task is simply to identify it, understand it and unlock it, in order to apply it to resolving the evils that afflict human health.

References

1. Ranjani, A., Dharumadurai, D. & P M, G. *An Introduction to Actinobacteria*. (2016).
2. Barka, E.A. *et al.* Taxonomy, Physiology, and Natural Products of Actinobacteria. *Microbiology and molecular biology reviews : MMBR* **80**, 1-43 (2016).
3. Gao, B. & Gupta, R.S. Phylogenetic framework and molecular signatures for the main clades of the phylum Actinobacteria. *Microbiology and molecular biology reviews : MMBR* **76**, 66-112 (2012).
4. Dangelo, R.A., de Souza, D.J., Mendes, T.D., Couceiro Jda, C. & Lucia, T.M. Actinomycetes inhibit filamentous fungi from the cuticle of Acromyrmex leafcutter ants. *Journal of basic microbiology* **56**, 229-237 (2016).
5. Qin, Z. *et al.* Formicamycins, antibacterial polyketides produced by Streptomyces formicae isolated from African Tetraponera plant-ants. *Chemical science* **8**, 3218-3227 (2017).
6. Le Chevalier, F., Cascioferro, A., Majlessi, L., Herrmann, J.L. & Brosch, R. Mycobacterium tuberculosis evolutionary pathogenesis and its putative impact on drug development. *Future microbiology* **9**, 969-985 (2014).
7. Sangal, V. & Hoskisson, P.A. Evolution, epidemiology and diversity of Corynebacterium diphtheriae: New perspectives on an old foe. *Infection, genetics and evolution : journal of molecular epidemiology and evolutionary genetics in infectious diseases* **43**, 364-370 (2016).
8. Lerat, S., Simao-Beaunoir, A.M. & Beaulieu, C. Genetic and physiological determinants of Streptomyces scabies pathogenicity. *Molecular plant pathology* **10**, 579-585 (2009).
9. Setubal, J.C., Moreira, L.M. & da Silva, A.C. Bacterial phytopathogens and genome science. *Current opinion in microbiology* **8**, 595-600 (2005).
10. Demain, A.L. & Fang, A. The natural functions of secondary metabolites. *Advances in biochemical engineering/biotechnology* **69**, 1-39 (2000).
11. Sharma, A.K., N.; Menghani, E. BIOACTIVE SECONDARY METABOLITES: AN OVERVIEW. *International Journal of Scientific & Engineering Research* **5**, 13 (2014).
12. Ziemert, N., Alanjary, M. & Weber, T. The evolution of genome mining in microbes - a review. *Natural product reports* **33**, 988-1005 (2016).
13. Blin, K. *et al.* antiSMASH 4.0-improvements in chemistry prediction and gene cluster boundary identification. *Nucleic acids research* **45**, W36-W41 (2017).
14. Medema, M.H., Takano, E. & Breitling, R. Detecting sequence homology at the gene cluster level with MultiGeneBlast. *Molecular biology and evolution* **30**, 1218-1223 (2013).
15. Shen, B. Polyketide biosynthesis beyond the type I, II and III polyketide synthase paradigms. *Current opinion in chemical biology* **7**, 285-295 (2003).
16. Bayly, C.L. & Yadav, V.G. Towards Precision Engineering of Canonical Polyketide Synthase Domains: Recent Advances and Future Prospects. *Molecules* **22** (2017).
17. Bloudoff, K. & Schmeing, T.M. Structural and functional aspects of the nonribosomal peptide synthetase condensation domain superfamily: discovery, dissection and diversity. *Biochimica et biophysica acta. Proteins and proteomics* **1865**, 1587-1604 (2017).
18. Weber, T. & Marahiel, M.A. Exploring the domain structure of modular nonribosomal peptide synthetases. *Structure* **9**, R3-9 (2001).
19. Arnison, P.G. *et al.* Ribosomally synthesized and post-translationally modified peptide natural products: overview and recommendations for a universal nomenclature. *Natural product reports* **30**, 108-160 (2013).
20. Hayakawa, Y. *et al.* Thioviridamide, a novel apoptosis inducer in transformed cells from Streptomyces olivoviridis. *The Journal of antibiotics* **59**, 1-5 (2006).
21. Hayakawa, Y., Sasaki, K., Nagai, K., Shin-ya, K. & Furihata, K. Structure of thioviridamide, a novel apoptosis inducer from Streptomyces olivoviridis. *The Journal of antibiotics* **59**, 6-10 (2006).

22. Banala, S. & Sussmuth, R.D. Thioamides in nature: in search of secondary metabolites in anaerobic microorganisms. *Chembiochem : a European journal of chemical biology* **11**, 1335-1337 (2010).
23. Izawa, M., Kawasaki, T. & Hayakawa, Y. Cloning and heterologous expression of the thioviridamide biosynthesis gene cluster from Streptomyces olivoviridis. *Applied and environmental microbiology* **79**, 7110-7113 (2013).
24. Bierbaum, G. *et al.* The biosynthesis of the lantibiotics epidermin, gallidermin, Pep5 and epilancin K7. *Antonie van Leeuwenhoek* **69**, 119-127 (1996).
25. Foulston, L.C. & Bibb, M.J. Microbisporicin gene cluster reveals unusual features of lantibiotic biosynthesis in actinomycetes. *Proceedings of the National Academy of Sciences of the United States of America* **107**, 13461-13466 (2010).
26. Claesen, J. & Bibb, M. Genome mining and genetic analysis of cypemycin biosynthesis reveal an unusual class of posttranslationally modified peptides. *Proceedings of the National Academy of Sciences of the United States of America* **107**, 16297-16302 (2010).
27. Kieser, T.B., M.J.; Buttner, M.J.; Chater, K.F.; Hopwood D.A. *Practical Streptomyces Genetics*. (John Innes Foundation, ISBN 0-7084-0623-8).
28. Jones, A.C. *et al.* Phage p1-derived artificial chromosomes facilitate heterologous expression of the FK506 gene cluster. *PloS one* **8**, e69319 (2013).
29. Noskov, V. *et al.* A genetic system for direct selection of gene-positive clones during recombinational cloning in yeast. *Nucleic acids research* **30**, E8 (2002).
30. Crone, W.J.K. *et al.* Dissecting Bottromycin Biosynthesis Using Comparative Untargeted Metabolomics. *Angewandte Chemie International Edition* **55**, 9639-9643 (2016).
31. Bierman, M. *et al.* Plasmid cloning vectors for the conjugal transfer of DNA from Escherichia coli to Streptomyces spp. *Gene* **116**, 43-49 (1992).
32. Gibson, D.G. *et al.* Enzymatic assembly of DNA molecules up to several hundred kilobases. *Nature methods* **6**, 343-345 (2009).
33. Tang, X. *et al.* Identification of Thiotetronic Acid Antibiotic Biosynthetic Pathways by Target-directed Genome Mining. *ACS chemical biology* **10**, 2841-2849 (2015).
34. Kouprina, N. & Larionov, V. Selective isolation of genomic loci from complex genomes by transformation-associated recombination cloning in the yeast Saccharomyces cerevisiae. *Nature protocols* **3**, 371-377 (2008).
35. De Maeseneire, S.S., W.; and De Mey, M. in Applied Synthetic Biology in Europe, 1st Symposium, Vol. Abstract 62 (2012).
36. Robert, X. & Gouet, P. Deciphering key features in protein structures with the new ENDscript server. *Nucleic acids research* **42**, W320-324 (2014).
37. Huang, Y. *et al.* Electronic interactions of i, i + 1 dithioamides: increased fluorescence quenching and evidence for n-to-pi* interactions. *Chemical communications* **52**, 7798-7801 (2016).
38. Guan, Z., Yates, N.A. & Bakhtiar, R. Detection and characterization of methionine oxidation in peptides by collision-induced dissociation and electron capture dissociation. *Journal of the American Society for Mass Spectrometry* **14**, 605-613 (2003).
39. Miles, C.O., Melanson, J.E. & Ballot, A. Sulfide oxidations for LC-MS analysis of methionine-containing microcystins in Dolichospermum flos-aquae NIVA-CYA 656. *Environmental science & technology* **48**, 13307-13315 (2014).
40. Gomez-Escribano, J.P. & Bibb, M.J. Engineering Streptomyces coelicolor for heterologous expression of secondary metabolite gene clusters. *Microbial biotechnology* **4**, 207-215 (2011).
41. Izumikawa, M. *et al.* Novel thioviridamide derivative--JBIR-140: heterologous expression of the gene cluster for thioviridamide biosynthesis. *The Journal of antibiotics* **68**, 533-536 (2015).
42. Izawa, M., Nagamine, S., Aoki, H. & Hayakawa, Y. Identification of essential biosynthetic genes and a true biosynthetic product for thioviridamide. *The Journal of general and applied microbiology* **64**, 50-53 (2018).

43. Freeman, M.F. *et al.* Metagenome mining reveals polytheonamides as posttranslationally modified ribosomal peptides. *Science* **338**, 387-390 (2012).
44. Cotter, P.D. *et al.* Complete alanine scanning of the two-component lantibiotic lacticin 3147: generating a blueprint for rational drug design. *Molecular microbiology* **62**, 735-747 (2006).
45. Li, C., Zhang, F. & Kelly, W.L. Mutagenesis of the thiostrepton precursor peptide at Thr7 impacts both biosynthesis and function. *Chemical communications* **48**, 558-560 (2012).
46. Becker, S. A historic and scientific review of breast cancer: The next global healthcare challenge. *International journal of gynaecology and obstetrics: the official organ of the International Federation of Gynaecology and Obstetrics* **131 Suppl 1**, S36-39 (2015).
47. Ataollahi, M.R., Sharifi, J., Paknahad, M.R. & Paknahad, A. Breast cancer and associated factors: a review. *Journal of medicine and life* **8**, 6-11 (2015).
48. Mehrgou, A. & Akouchekian, M. The importance of BRCA1 and BRCA2 genes mutations in breast cancer development. *Medical journal of the Islamic Republic of Iran* **30**, 369 (2016).
49. Roy, R., Chun, J. & Powell, S.N. BRCA1 and BRCA2: different roles in a common pathway of genome protection. *Nature reviews. Cancer* **12**, 68-78 (2011).
50. Sinn, H.P. & Kreipe, H. A Brief Overview of the WHO Classification of Breast Tumors, 4th Edition, Focusing on Issues and Updates from the 3rd Edition. *Breast care* **8**, 149-154 (2013).
51. Singletary, S.E. *et al.* Revision of the American Joint Committee on Cancer staging system for breast cancer. *Journal of clinical oncology : official journal of the American Society of Clinical Oncology* **20**, 3628-3636 (2002).
52. Yersal, O. & Barutca, S. Biological subtypes of breast cancer: Prognostic and therapeutic implications. *World journal of clinical oncology* **5**, 412-424 (2014).
53. Haque, R. *et al.* Impact of breast cancer subtypes and treatment on survival: an analysis spanning two decades. *Cancer epidemiology, biomarkers & prevention : a publication of the American Association for Cancer Research, cosponsored by the American Society of Preventive Oncology* **21**, 1848-1855 (2012).
54. Dai, X. *et al.* Breast cancer intrinsic subtype classification, clinical use and future trends. *American journal of cancer research* **5**, 2929-2943 (2015).
55. Ishikawa, T. *et al.* The Pathological Response to Anthracycline is Associated with Topoisomerase IIalpha Gene Amplification in the HER2 Breast Cancer Subset. *Journal of surgery and science* **2**, 10-12 (2014).
56. Perou, C.M. Molecular stratification of triple-negative breast cancers. *The oncologist* **15 Suppl 5**, 39-48 (2010).
57. Prat, A. & Perou, C.M. Deconstructing the molecular portraits of breast cancer. *Molecular oncology* **5**, 5-23 (2011).
58. Ajani, J.A., Song, S., Hochster, H.S. & Steinberg, I.B. Cancer stem cells: the promise and the potential. *Seminars in oncology* **42 Suppl 1**, S3-17 (2015).
59. Sin, W.C. & Lim, C.L. Breast cancer stem cells-from origins to targeted therapy. *Stem cell investigation* **4**, 96 (2017).
60. Bozorgi, A., Khazaei, M. & Khazaei, M.R. New Findings on Breast Cancer Stem Cells: A Review. *Journal of breast cancer* **18**, 303-312 (2015).
61. Chae, Y.C. & Kim, J.H. Cancer stem cell metabolism: target for cancer therapy. *BMB reports* **51**, 319-326 (2018).
62. Snyder, V., Reed-Newman, T.C., Arnold, L., Thomas, S.M. & Anant, S. Cancer Stem Cell Metabolism and Potential Therapeutic Targets. *Frontiers in oncology* **8**, 203 (2018).
63. Vlashi, E. & Pajonk, F. The metabolic state of cancer stem cells-a valid target for cancer therapy? *Free radical biology & medicine* **79**, 264-268 (2015).
64. Frattaruolo, L., Lacret, R., Cappello, A.R. & Truman, A.W. A Genomics-Based Approach Identifies a Thioviridamide-Like Compound with Selective Anticancer Activity. *ACS chemical biology* **12**, 2815-2822 (2017).

65. Nicoletti, I., Migliorati, G., Pagliacci, M.C., Grignani, F. & Riccardi, C. A rapid and simple method for measuring thymocyte apoptosis by propidium iodide staining and flow cytometry. *Journal of immunological methods* **139**, 271-279 (1991).
66. Prieto, A. *et al.* Apoptotic rate: a new indicator for the quantification of the incidence of apoptosis in cell cultures. *Cytometry* **48**, 185-193 (2002).
67. Schafer, K.A. The cell cycle: a review. *Veterinary pathology* **35**, 461-478 (1998).
68. Cai, Z. & Liu, Q. Cell Cycle Regulation in Treatment of Breast Cancer. *Advances in experimental medicine and biology* **1026**, 251-270 (2017).
69. Giacinti, C. & Giordano, A. RB and cell cycle progression. *Oncogene* **25**, 5220-5227 (2006).
70. Seville, L.L., Shah, N., Westwell, A.D. & Chan, W.C. Modulation of pRB/E2F functions in the regulation of cell cycle and in cancer. *Current cancer drug targets* **5**, 159-170 (2005).
71. Nagata, S., Suzuki, J., Segawa, K. & Fujii, T. Exposure of phosphatidylserine on the cell surface. *Cell death and differentiation* **23**, 952-961 (2016).
72. Segawa, K. & Nagata, S. An Apoptotic 'Eat Me' Signal: Phosphatidylserine Exposure. *Trends in cell biology* **25**, 639-650 (2015).
73. Kroemer, G. Mitochondrial control of apoptosis: an overview. *Biochemical Society symposium* **66**, 1-15 (1999).
74. Fulda, S. & Debatin, K.M. Extrinsic versus intrinsic apoptosis pathways in anticancer chemotherapy. *Oncogene* **25**, 4798-4811 (2006).
75. Armentano, M.F. *et al.* Antioxidant and proapoptotic activities of Sclerocarya birrea [(A. Rich.) Hochst.] methanolic root extract on the hepatocellular carcinoma cell line HepG2. *BioMed research international* **2015**, 561589 (2015).
76. Quijano, C., Trujillo, M., Castro, L. & Trostchansky, A. Interplay between oxidant species and energy metabolism. *Redox biology* **8**, 28-42 (2016).
77. Johnson, F. & Giulivi, C. Superoxide dismutases and their impact upon human health. *Molecular Aspects of Medicine* **26**, 340-352 (2005).
78. Kim, Y.S., Gupta Vallur, P., Phaeton, R., Mythreye, K. & Hempel, N. Insights into the Dichotomous Regulation of SOD2 in Cancer. *Antioxidants* **6** (2017).
79. Phan, L.M., Yeung, S.C. & Lee, M.H. Cancer metabolic reprogramming: importance, main features, and potentials for precise targeted anti-cancer therapies. *Cancer biology & medicine* **11**, 1-19 (2014).
80. De Luca, A. *et al.* Mitochondrial biogenesis is required for the anchorage-independent survival and propagation of stem-like cancer cells. *Oncotarget* **6**, 14777-14795 (2015).

28-Feb-2019
NAR-03974-Z-2018.R1
Uncovering the unexplored diversity of thioamidated ribosomal peptides in Actinobacteria using the RiPPER genome mining tool
Santos-Aberturas, Javier; Chandra, Govind; Frattaruolo, Luca; Lacret, Rodney; Pham, Thu; Vior, Natalia; Eyles, Tom; Truman, Andrew W
Dear Dr Truman,
We are pleased to tell you that your manuscript has been accepted for publication in NAR and will now be processed by our Production office at OUP. You should receive a welcome email from the Production office within one week. If you have questions or concerns during the production process, you should contact the Production office directly (jnls.author.support@oup.com) and they will be pleased to assist you.
Please do take a moment to check that all names, affiliations, as well as acknowledgements and sources of funding are accurate. We will not be able to make corrections once the final typeset article has been published.
As well, we request that you now remove any 'holds' that may be in place on data that is intended to be made available to the public via a webserver or repository.
If your electronic figures are of production quality, you should receive page proofs of your article within 6 working days. The Journal's goal is to have a definitive, Medline-indexed version of your manuscript available online in approximately 10 working days. To meet this schedule, you must take the following actions:
◦ LICENCE TO PUBLISH. In order to publish your article, Oxford University Press requires that you complete a licence agreement online. A link to the online licensing system, and instructions on how to select and complete a licence, will be provided to you by the Production Editor at Oxford University Press in due course.
◦ OPEN ACCESS FORM. OUP provides free access to your article to readers worldwide and automatically deposits your paper in a public repository. Open access charges make this possible. For 2019 the all-inclusive publication charge is £746 / $1454 / €1118 per article for NAR member institutions; £1491 / $2909 / €2237 for non-members. You will be able to use our online system to pay your open access fee with a credit card, or request an invoice. Further instructions will be provided by the Production office in due course.
◦ Note that to claim your member institution discount, you will need to be connected to the Internet via an institutional Internet Protocol (IP) address, and you may need to empty your browser cache or delete browser cookies. There are discounts for authors in developing countries and for authors publishing two papers in NAR within a 12-month period, and there is a surcharge for over-length papers. Further information, including how an institution may purchase membership, are available at:
https://academic.oup.com/nar/pages/Open_Access_Initiative

◦ PAGE PROOFS. Rapid publication requires that you return page proofs promptly upon receipt. Proofs will be sent to you as an email attachment. If you anticipate being away from the Internet during the period when proofs become available, please send an email in advance to Production (jnls.author.support@oup.com) with contact details for someone who can correct proofs in your place.

◦ NIH PUBLISHING AGREEMENT. Applicable to NIH employees only. NAR complies with the NIH public access policy. As long as the NIH or one of its subsidiaries is listed in the funding section of your article, it will be publicly available in PubMed Central no later than 12 months after issue publication without author involvement.

Prof. Janusz Bujnicki

Executive Editor
Nucleic Acids Research

PRODUCTION OFFICE CONTACT DETAILS:
Nucleic Acids Research
Oxford Journals
Oxford University Press
Great Clarendon Street
OXFORD, OX2 6DP, UK
Tel: +44 (0)1865 353254
Fax: +44 (0)1865 355847
Email: jnls.author.support@oup.com

Uncovering the unexplored diversity of thioamidated ribosomal peptides in Actinobacteria using the RiPPER genome mining tool

Javier Santos-Aberturas[1], Govind Chandra[1], Luca Frattaruolo[1], Rodney Lacret[1], Thu H. Pham[1], Natalia M. Vior[1], Tom H. Eyles[1] and Andrew W. Truman[1,*]

[1] Department of Molecular Microbiology, John Innes Centre, Norwich, Norfolk, NR4 7UH, UK

* To whom correspondence should be addressed. Tel: +44(0)1603 450750; Email: andrew.truman@jic.ac.uk

ABSTRACT

The rational discovery of new specialized metabolites by genome mining represents a very promising strategy in the quest for new bioactive molecules. Ribosomally synthesized and post-translationally modified peptides (RiPPs) are a major class of natural product that derive from genetically encoded precursor peptides. However, RiPP gene clusters are particularly refractory to reliable bioinformatic predictions due to the absence of a common biosynthetic feature across all pathways. Here, we describe RiPPER, a new tool for the family-independent identification of RiPP precursor peptides and apply this methodology to search for novel thioamidated RiPPs in Actinobacteria. Until now, thioamidation was believed to be a rare post-translational modification, which is catalyzed by a pair of proteins (YcaO and TfuA) in Archaea. In Actinobacteria, the thioviridamide-like molecules are a family of cytotoxic RiPPs that feature multiple thioamides, which are proposed to be introduced by YcaO-TfuA proteins. Using RiPPER, we show that previously undescribed RiPP gene clusters encoding YcaO and TfuA proteins are widespread in Actinobacteria and encode a highly diverse landscape of precursor peptides that are predicted to make thioamidated RiPPs. To illustrate this strategy, we describe the first rational discovery of a new structural class of thioamidated natural products, the thiovarsolins from *Streptomyces varsoviensis*.

INTRODUCTION

Microorganisms have provided humankind with a vast plethora of specialized metabolites with invaluable applications in medicine and agriculture (1). The advent of widespread genome sequencing has shown that the metabolic potential of bacteria had been substantially underestimated, as their genomes contain many more biosynthetic gene clusters (BGCs) than known compounds (2,3). Much of this enormous potential is either unexplored or undetectable under laboratory culture conditions, and is likely to include structurally novel bioactive specialized metabolites. Among the main classes of specialized metabolites produced by microorganisms, the ribosomally synthesized and post-translationally modified peptides (RiPPs) (4) may harbor the largest amount of unexplored structural diversity. This is due to the inherent difficulties related to the *in silico* prediction of their BGCs, as RiPP

biosynthetic pathways lack any kind of universally shared feature apart from the existence of a pathway-specific precursor peptide.

RiPP BGCs can be identified by the co-occurrence of specific RiPP tailoring enzymes (RTEs) alongside a precursor peptide that contains sequence motifs that are characteristic of a given RiPP family. This makes it relatively simple to identify further examples of known RiPP families (5,6), but the identification of currently undiscovered RiPP families remains a significant unsolved problem. Unlike specialized metabolites such as polyketides, non-ribosomal peptides and terpenes, there are no genetic features that are common to all RiPP BGCs to aid in their identification. Furthermore, genes encoding precursor peptides are often missed during genome annotation due to their small size, yet the reliable prediction of precursor peptides constitutes a crucial task, as this starting scaffold is essential for RiPP structural prediction. Numerous analyses of specific RiPP classes signal the existence of a wide array of uncharacterized RiPP families (7-9), but currently available prediction tools still rely on precursor peptide features or generic RTEs that are associated with known RiPP families (10-14).

YcaO domain proteins are a widespread superfamily of enzymes with an intriguing catalytic potential in RiPP biosynthesis (15). These were originally shown to be responsible for the introduction of oxazoline and thiazoline heterocycles in the precursor peptide backbone of microcins (16), and were very recently demonstrated to catalyze the formation of the macroamidine ring of bottromycin (17-19). YcaO proteins act as cyclodehydratases, activating the amide bond substrate by nucleophilic attack, which is followed by ATP-driven O-phosphorylation of the hemiorthoamide intermediate and subsequent elimination of phosphate. In most azoline-containing RiPPs, this catalytic activity requires a partner protein (E1-like or Ocin-ThiF-like proteins that are clustered with or fused to the YcaO domain), which acts as a docking element to bring the precursor peptide to the active site of the cyclodehydratase (15). YcaO proteins can also act as standalone proteins, as in bottromycin biosynthesis (18,19), and many YcaO proteins are encoded in genomes without E1-like or Ocin-ThiF-like partner proteins (9,15), including in the BGCs of thioviridamide-like molecules (6, 20-24).

Thioviridamide and related compounds are cytotoxic RiPPs that contain multiple thioamide groups (Figure 1), but no azole or macroamidine rings. Thioamides are rare in nature (25-31) and it has been hypothesized that YcaO proteins could be responsible for this rare amide bond modification in thioviridamide biosynthesis, potentially in cooperation with TfuA domain proteins (15) (Figure 1). This protein pair has been identified elsewhere in nature, including in archaea, where they are involved in the ATP-dependent thioamidation of a glycine residue of methyl-coenzyme M reductase (32,33). We therefore hypothesized that the identification of *tfuA*-like genes could be employed as a rational criterion for the identification of BGCs responsible for the production of novel thioamidated RiPPs in bacteria.

An exploration of the diversity of *tfuA*-containing BGCs required methodology to identify precursor peptides that have no homology to known precursor peptides. Here, we report RiPPER (RiPP Precursor Peptide Enhanced Recognition), a method for the identification of precursor peptides that requires no information about RiPP structural class (available at https://github.com/streptomyces/ripper). This evaluates regions surrounding any putative RTE for short open reading frames (ORFs) based on the likelihood that these are truly peptide-coding genes. Peptide similarity networking is then used to identify

putative RiPP families. We apply this methodology to identify RiPP BGCs encoding TfuA proteins in Actinobacteria, which reveals a highly diverse landscape of BGC families that are predicted to make thioamidated RiPPs. This analysis informed the discovery of the thioamidated thiovarsolins from *Streptomyces varsoviensis*, which are predicted to belong to a wider family of related thioamidated RiPPs and represents the first rational discovery of a new family of thioamidated compounds from nature.

MATERIALS AND METHODS

Chemicals

Unless otherwise specified, chemicals were purchased from Sigma-Aldrich, and enzymes from New England Biolabs. Molecular biology kits were purchased from Promega and GE Healthcare.

Strains and culture conditions

Streptomyces varsoviensis DSM 40346 was acquired from the German Collection of Microorganisms and Cell Cultures (DSMZ, Germany) and used as genetic source for the thiovarsolin gene cluster. *Streptomyces coelicolor* M1146, *S. coelicolor* M1152 (34) and *Streptomyces lividans* TK21 were used as heterologous expression hosts. All culture media and primers used in this work are described in full in the Supplementary Methods. Unless otherwise specified, all *Streptom*yces strain were grown in SFM (solid) and TSB (liquid) media at 28 °C. Spores and mycelium stocks were kept at -20 °C and -80 °C in 20% glycerol. *Saccharomyces cerevisiae* VL6-48N (35) was used for transformation-associated recombination (TAR) cloning and was grown at 30 °C with shaking at 250 rpm in YPDA medium. Recombinant yeast selection was performed using selective media SD+CSM-Trp complemented with 5-fluoorotic acid (Fluorochem, 1 mg mL^{-1}). Yeast cell stocks were kept at -80 °C in 20% glycerol. *Escherichia coli* DH5α was used for standard DNA manipulations. *E. coli* DH5α BT340 was used for Flp-*FRT* recombination. *E. coli* BW25113/pIJ790 was used for Lambda-Red mediated recombination. *E. coli* ET12567/pR9604 and *E. coli* ET12567/pUZ8002 were used to transfer DNA to *Streptomyces* by intergeneric conjugation. All *E. coli* strains were grown in LB medium at 37 °C unless specified by particular protocols (pIJ790-carrying strains were grown at 30 °C for plasmid replication, and Flp-*FRT* recombination was performed at 42 °C). *E. coli* hygromycin selection was performed in DNAm (solid) and DNB (liquid) media. *E. coli* cell stocks were kept at -20 °C and -80 °C in 20% glycerol.

RiPPER details

RiPPER consists of a series of Perl script that require the RODEO2 Python script (13,14), BioPerl (36), a locally installed Pfam database (37,38) and a modified build of Prodigal (39) (which we name Prodigal-short) to operate. Analysis parameters for RiPPER are defined in an associated configuration file (local.conf), which can be modified to optimize the genome mining process. EGN (Evolutionary Gene and genome Network) (40) was used to construct protein similarity networks, which were visualized using Cytoscape 2.8.3 (41). Further information is provided in the documentation provided with the RiPPER scripts at https://github.com/streptomyces/ripper. For ease of use, a Docker container is

provided that contains all features required for using RiPPER. This is available at https://hub.docker.com/r/streptomyces/ripdock/ along with instructions on installation and usage. A workflow for using RiPPER is described below.

Workflow for RiPPER

Below is a summary of the RiPPER workflow, which has been developed for gene cluster visualization in Artemis (42) (Figure S1). Where relevant, default analysis parameters are listed. These are all customizable from the local.conf configuration file associated with a given RiPPER analysis.

Using RODEO (13,14), accession numbers for a set of putative RiPP tailoring enzymes (RTEs) are used to obtain nucleotide regions (as GenBank files) centered on the tailoring enzyme, which is highlighted as a green gene for clarity in Artemis. 25 kb regions were obtained for the TfuA analysis (flankLen = 12.5 kb), and 35 kb regions were obtained for the known RiPP families (flankLen = 17.5 kb, default).

1. Every retrieved genomic region is subjected to RODEO analysis to obtain a RODEO output for each input accession, as well as Pfam domain data across the gene cluster.
2. GenBank files are then analyzed using a specially built version of Prodigal (39), which we call Prodigal-short. This is configured to find genes as short as 60 nucleotides instead of the usual size cut-off of 90 nucleotides.
3. For all the genes found by Prodigal-short the following is done:
    a. The Prodigal score is enhanced if the gene is on the same strand as the tailoring enzyme (sameStrandReward, default = 5).
    b. Genes are only retained for analysis if they overlap with existing annotated genes by 20 nucleotides or less.
    c. RiPPER uses Prodigal-short to only identify putative ORFs within a likely size window for precursor peptide genes. Therefore, genes are only retained for analysis if the length of the encoded peptide is between minPPlen and maxPPlen. A window of 20 – 120 AA (default) was used in all analyses in this study.
    d. If a gene is not filtered out in the above steps, it is annotated in the GenBank file and its distance from the tailoring enzyme is determined.
    e. All putative genes identified are provided in the resulting GenBank file and are color-coded from pale red (low score) to bright pink (high score) (Figure S1). Scoring criteria are viewable in Artemis as notes for each putative gene.
    f. RiPPER also retrieves and scores genes that were already annotated if they encode peptides below the maxPPlen (default = 120 AA). This means that annotated precursor peptides are also retrieved for downstream analysis.
4. The resulting annotated GenBank files can be viewed in Artemis at this stage for manual identification of RiPP precursor peptides.
5. If the gene is within a specified distance (maxDistFromTE) from the RTE, it is included in the output list and also saved in a Sqlite3 table. A distance of ± 8 kb is used as default.

6. Within this region, the top scoring short peptides (no lower score threshold) are retrieved. The number retrieved is defined by fastaOutputLimit (default = 3) In addition, any further peptides with Prodigal scores over a threshold (prodigalScoreThresh) within this region are retrieved. A score threshold of 15 was used in the TfuA analysis and a score threshold of 7.5 (default) was used in the analysis of known RiPP families.
7. All retrieved peptides are analyzed for Pfam domains, and all information is tabulated alongside various associated data (tailoring enzyme accession, strain, peptide sequence, distance from tailoring enzyme, coding strand in relation to tailoring gene, Prodigal score) in a tab-separated out.txt file. All data are collated in a single file if multiple genomic regions are analyzed in parallel.
8. All peptides identified by RiPPER across the entire Genbank file that were not retrieved in step 6 (no distance or score threshold) are searched for characterized precursor peptide domains (38). Data for these peptides is then tabulated in a tab-separated distant.txt file.
9. Optional follow-on analysis: protein similarity networking and BGC comparative analysis. Protein similarity networking does not form part of the automated RiPPER workflow, but this does assist with the identification of authentic precursor peptides. The RiPPER output includes fasta files (out.faa and distant.faa) for all retrieved peptides that are compatible for analysis with EGN (40). The following settings were used for all analyses: E-value threshold = 10, hit identity threshold = 40%, hit covers at least 35% of the shortest sequence, minimum hit length = 15 AA. The resulting networks were visualized using Cytoscape 2.8.3 (41), where data obtained from RiPPER were imported as node attributes. The similarity between BGCs associated with the same network was assessed using MultiGeneBlast (43). Peptides from each network were aligned using MUSCLE (44) and alignments were visualized using ESPript 3.0 (45).

Identification of precursors to lasso peptides, microviridins and thiopeptides

Studies by Tietz *et al*. (13), Ahmed *et al*. (46), and Schwalen *et al*. (14) had previously used RTE accessions to mine for precursors to lasso peptides, microviridins and thiopeptides, respectively. The same accession codes were used to mine for precursor peptides using RiPPER (Supplementary Datasets 1-3), although not all accessions could be retrieved as some records no longer exist on NCBI. RiPPER was run using analysis parameters as described above and the results are described in Table 1. Peptide similarity networking was carried out using EGN (as described above), which provided large networks for each dataset (Network 1, Figures S2-S4, Supplementary Datasets 1-3). To determine the ability of RiPPER to retrieve authentic precursor peptide sequences, a bespoke script was used to compare the RiPPER outputs with the prior studies.

TfuA-like protein retrieval and phylogenetic analysis

The NCBI Conserved Domain Architecture Retrieval Tool (CDART) (47) was used to retrieve all TfuA domain protein sequences from the phylum Actinobacteria in the NCBI non-redundant protein sequence

database. These 325 proteins were manually assessed by Pfam analysis for TfuA domains, which resulted in the removal of five proteins from this dataset. To limit the overrepresentation of highly similar proteins in an analysis of phylogeny and gene cluster diversity, ElimDupes (https://www.hiv.lanl.gov/content/sequence/ELIMDUPES/elimdupes.html) was used to remove proteins with at least 99% identity to each other from the dataset to leave one representative protein. This provided a dataset of 229 TfuA domain proteins. Three proteins that contained fused YcaO and TfuA domains were removed for phylogenetic analysis, along with one (KZS83678.1) that is truncated. The standalone TfuA domain protein dataset (225 proteins) was aligned using MUSCLE 3.8.31 (44) with default settings. The resulting alignment was used to construct a maximum likelihood tree using RAxML-HPC2 on XSEDE (with 100 bootstrap replications) on the CIPRES Science Gateway (https://www.phylo.org/). The tree was visualized using the interactive Tree Of Life (iTOL) (48) (Supplementary Dataset 5). The statistical analysis of the lengths of predicted precursor peptides is described in the Supplementary Methods.

TAR cloning and heterologous expression of the thiovarsolin gene cluster

A vector to capture the thiovarsolin gene cluster from *S. varsoviensis* genomic DNA (gDNA) was constructed using yeast assembly between a linearized pCAP03 vector (49) and two single-strand oligonucleotides (TARvar-1 and TARvar-2). Oligonucleotides had 35 nucleotide homology sequences with pCAP03 and were designed to generate a vector with 50 nucleotide homology sequences with upstream and downstream regions of the gene cluster either side of a PmeI restriction site. pCAP03 was digested with XhoI and NdeI, and the linearized plasmid and ss-oligos (1:10 ratio) were transformed into *S. cerevisiae* VL6-48N by lithium acetate/polyethylene glycol 3350 mediated transformation. For yeast-colony PCR, each colony was resuspended in 50 µL 1 M sorbitol (Fisher) and 2 µL of zymolyase (5 U μL^{-1}) added to each cell suspension and incubated at 30 °C for 1 hour. Cell suspensions were then boiled for 10 minutes, centrifuged (15 s, 1,000 x *g*) and 1 µL of the supernatant was analyzed by PCR.

To transfer the plasmids from yeast into *E. coli*, colonies of yeast were grown in 10 mL of liquid SD+CSM-Trp for 18 h at 250 rpm, 30 °C. Cells were harvested by centrifugation (5 min, 1,789 x *g*), and resuspended in 200 µL 1 M sorbitol plus 2 µL of zymolyase (5 U μL^{-1}). Cell suspensions were incubated at 30 °C for 1 hour to produce spheroplasts, which were then pelleted (10 min, 600 x *g*). The supernatant was aspirated, and plasmid DNA extracted from the pellet using a standard Wizard miniprep protocol (Promega). 1 µL plasmid DNA was then transformed into *E. coli* DH5α by electroporation and selected with kanamycin (50 µg mL^{-1}) Colonies containing the correct capture vector were identified by PCR (primers: CAP03_check-fw and CAP03_check-rv), and the plasmid was isolated and confirmed by sequencing.

gDNA from *S. varsoviensis* was digested with EcoRV and ScaI, and the pCAP03-derived capture vector was linearized between the capture arms with PmeI. These were both then introduced into *S. cerevisiae* VL6-48N by spheroplast polyethylene glycol 8000 transformation. Successful gene cluster capture by pCAP03 was confirmed by colony PCR (primers: TARcheck-fw and TARcheck-rv). The plasmids from three positive clones were recovered and transformed into electrocompetent *E. coli*

DH5α for amplification and further restriction analysis of the purified construct (pTARvar). *E. coli* ET12567/pR9604 was transformed with pTARvar by electroporation, and transformants were then used to transfer pTARvar into *S. coelicolor* (M1146 and M1152) and *S. lividans* TK21 by intergeneric conjugation. Nalidixic acid (25 µg mL^{-1}) and kanamycin-resistant (50 µg mL^{-1}) exconjugants containing integrated pTARvar (*S. coelicolor* M1146-var, *S. coelicolor* M1152-var and *S. lividans* TK21-var) were verified by PCR using GoTaq polymerase (Promega) (primers: TAR_check-fw and TAR_check-rv).

Fermentation conditions for metabolite screening

Seed cultures of *S. coelicolor* M1146-var, *S. coelicolor* M1152-var and *S. lividans* TK21-var were obtained by fermentation in a 250 mL flask containing 50 mL of TSB for 72 h. 250 µL seed culture was used to inoculate 5 mL of a variety of culture media (TSB, BPM, GYM, MI, TPM, E25; see Supplementary Methods) in 50 mL conical centrifuge tubes with caps replaced by foam bungs. Control strains carrying a genome-integrated empty pCAP03 vector were cultured in the same way for comparison. All fermentations were conducted in triplicate and incubated at 28 °C with shaking at 250 rpm. Culture samples (500 µL) were taken at 72 h and 168 h, mixed with one volume of methanol and agitated for 30 min at room temperature. These mixtures were then centrifuged (13,000 rpm, 30 min) and 600 µL of the resulting supernatant was transferred to glass vials for liquid chromatography-mass spectrometry (LC-MS) analysis. Details on the large-scale fermentation, isolation and structural elucidation of thiovarsolins A and B are described in the Supplementary Methods.

LC-MS analysis

Spectra were obtained using a Shimadzu Nexera X2 UHPLC coupled to a Shimadzu IT-TOF mass spectrometer. Samples (5 µL) were injected onto a Phenomenex Kinetex 2.6 µm XB-C18 column (50 mm x 2.1 mm, 100 Å) set at a temperature of 40 °C and eluting with a linear gradient of 5 to 95% acetonitrile in water + 0.1% formic acid over 6 minutes with a flow-rate of 0.6 mL min^{-1}. Positive mode mass spectrometry data was collected between *m/z* 200 and 2000, and MS^2 data was collected using collision-induced dissociation of the most abundant singly charged species in a scan, with an exclusion time of 0.8 seconds. Untargeted comparative metabolomics was carried out on triplicate data using Profiling Solution 1.1 (Shimadzu) with an ion *m/z* tolerance of 100 mDa, a retention time tolerance of 0.1 min and an ion intensity tolerance of 100,000 units.

For the accurate mass measurement of the thiovarsolins, high-resolution mass spectra were acquired by LC-MS on a Synapt G2-Si mass spectrometer equipped with an Acquity UPLC (Waters). Samples were injected onto an Acquity UPLC® BEH C18 column, 1.7 µm, 1x100 mm (Waters) and eluted with a gradient of (B) acetonitrile/0.1% formic acid in (A) water/0.1% formic acid with a flow rate of 0.08 mL min^{-1} at 45 °C. The concentration of B was kept at 1% for 2 min followed by a gradient up to 30% B in 4 min. MS data were collected with the following parameters: resolution mode, positive ion mode, scan time 0.5 s, mass range *m/z* 50-1200 (calibrated with sodium formate), capillary voltage = 3.0 kV; cone voltage = 40 V; source temperature = 120 °C; desolvation temperature = 350 °C. Leu-

enkephalin peptide was used to generate a lock-mass calibration with *m/z* = 556.2766 measured every 30 s during the run.

Deletion of genes in the thiovarsolin biosynthetic gene cluster

The mutational analysis of the thiovarsolin BGC was performed using an *E. coli*-based Lambda-Red-mediated PCR-targeting strategy (50), which allowed the substitution of genes or groups of genes in pTARvar by a PCR-generated cassette containing the apramycin resistance gene *aac(3)IV*. Given the presence of an *oriT* in the original pCAP03 vector, the upstream primer design was modified with respect to the original protocol in order to exclude a second *oriT* from the PCR-targeting resistance cassette and avoid undesired recombinations. Therefore, resistance cassettes were PCR amplified using pIJ773 as template (see primers in Table S3 and mutants in Table S4). In the case or *varA*, an additional in-frame deletion mutant affecting only the core precursor peptide was created employing a pIJ773-derived cassette lacking OriT (pIJ773 Δ*oriT*) but preserving both *FRT* recombination sites (primers RD1 and RD3), which allowed the elimination of the apramycin resistance cassette after Flp-*FRT* recombination in *E. coli* DH5α BT340 and the creation of a clean *varA* mutant (Δ*varA*_clean). The PCR-targeting mutant versions of pTARvar were transferred to *S. coelicolor* M1146 by *E. coli* ET12567/pUZ8002-mediated intergeneric conjugation and selected by resistance to nalidixic acid (25 μg mL^{-1}), kanamycin (50 μg mL^{-1}) and, when required, apramycin (50 μg mL^{-1}).

Constructs for the complementation of mutants showing differences in thiovarsolin production in comparison to *S. coelicolor* M1146-var (Δ*varA*, Δ*varY*, Δ*varT* and Δ*varO*) were obtained by high-fidelity PCR amplification (Herculase II, Agilent) of each of these genes (primers CP1 and CP2 for *varA*, CP3 and CP4 for *varA*p, CP5 and CP6 for *varY*, CP7 and CP8 for *varT*, and CP9 and CP10 for *varO*), digestion of the PCR product with NdeI and HindIII and cloning by ligation (T4 DNA ligase, Invitrogen) into NdeI – HindIII digested pIJ10257 (51). Ligation mixtures were transformed into chemically competent *E. coli* DH5α, plasmids were recovered by alkaline lysis and then sequenced. The resulting plasmids (pJ10257-*varA*, pIJ1027-*varA*p, pIJ10257-*varY*, pIJ10257-*varT* and pIJ10257-*varO*) were introduced into the corresponding *S. coelicolor* M1146-var mutants by *E. coli* ET12567/pUZ8002-mediated intergeneric conjugation. Exconjugants were selected by resistance to nalidixic acid (25 μg mL^{-1}), kanamycin (50 μg mL^{-1}), hygromycin (50 μg mL^{-1}) and, when required, apramycin (50 μg mL^{-1}). The construction of a minimal thiovarsolin gene cluster (pIJ10257-*varA*p*YT*) and the site-directed mutagenesis of *varA* are described in the Supplementary Methods.

RESULTS AND DISCUSSION

Development of a family-independent RiPP genome mining tool.

Within a given RiPP family, all BGCs usually encode at least one tailoring enzyme and one precursor peptide that each feature domains conserved across the RiPP family (4). This has led to the development of genome mining methodology that can identify these well-characterized RiPP families with high accuracy (10-13). However, there is a growing number of widespread RiPP BGCs with little or no homology to known RiPP BGCs (7,52). Theoretically, backbone modifications such as

thioamidation or epimerization (53) can occur on any residue. In addition, well-characterized RiPP tailoring enzymes can be associated with unusual precursor peptides that lack homology to known RiPP classes (9). We therefore sought to develop a method to identify likely precursor peptides that was independent of precursor peptide sequence and could be applicable for any RiPP family. The starting point for this method was to employ the functionality of RODEO (13,14) to identify genomic regions associated with a series of putative RTEs. RODEO uses a mixture of heuristic scoring and support vector machine classification to identify precursor peptides for lasso peptides (13) and thiopeptides (14), but does not accurately identify other precursor peptides, whose sequences are highly variable and are often not annotated in genomes.

To enable the sequence independent discovery of precursor peptides, we sought to identify short ORFs that possess similar genetic features as other genes in a given gene cluster, including ribosome binding sites, codon usage and GC content. Prodigal (PROkaryotic DYnamic programming Gene-finding ALgorithm) uses these criteria to identify bacterial ORFs (39). Therefore, following RODEO retrieval of nucleotide data, we implemented a modified form of this algorithm to specifically search for ORFs that encode for peptides of between 20 and 120 amino acids within apparently non-coding regions near to a predicted RTE (Figure 2A). Given the prevalence of characterized precursor peptides that are encoded on the same strand as a tailoring gene, a same strand score is added (custom parameter; default = 5). A modified GenBank file is generated by RiPPER that annotates these putative short ORFs within the putative BGC (Figure S1), and these are ranked alongside annotated short genes based on their Prodigal score. RiPPER then retrieves the top three scoring ORFs within ±8 kb of the RTE, plus any additional high scoring ORFs over a specified score threshold that represent probable genes. These are then assessed for Pfam domains (37) and data associated with each peptide is tabulated for further processing.

To validate this approach, we used RTE accession numbers that had previously been used to identify lasso peptide (13) (RODEO), microviridin (46) and thiopeptide (14) (RODEO) gene clusters. In each case, class-specific rules had been used to identify associated precursor peptides. These RiPP classes are well-suited to method validation as they have diverse gene cluster features and precursor peptide sequences, and span multiple bacterial taxa. In addition, the genes encoding these small peptides are often not annotated in genome sequences (13). We therefore used RiPPER with the same protein accessions as those previous studies to retrieve BGCs and associated precursor peptides. Comparison of the RiPPER outputs with these studies revealed that lasso peptide and microviridin precursor identification was highly reliable. 1056 out of 1122 (94.1%) and 279 out of 288 (96.7%) peptides identified by those prior mining studies were identified by RiPPER (Table 1, Supplementary Datasets 1-2). An analysis of Prodigal scores of these validated precursor peptides showed that this scoring approach is suited to the identification of RiPP precursor peptides (Figure S5), despite their small size and the possibility that horizontal gene transfer could influence codon usage bias.

In contrast, RiPPER only retrieved 438 of the 591 (74.1%) thiopeptide precursors previously identified (Table 1, Supplementary Dataset 3). This was possibly due to the comparatively large size of thiopeptide BGCs, which meant that the ±8 kb search window was not suited to a subset of these BGCs.

Widening the generic search reduced specificity of the retrieval, so an additional targeted search step was introduced. All short peptides across the entire gene cluster region (default = 35 kb) that were not retrieved by the first search were analyzed for precursor peptide domains using hidden Markov models (HMMs) recently built by Haft *et al.* (38). Any peptides containing a domain were therefore also retrieved. This provided a minor improvement to RiPPER retrieval of lasso precursor peptides but significantly improved thiopeptide precursor peptide retrieval to 549 out of 591 (92.9%) peptides identified by RODEO (14).

This data demonstrated that the RiPPER methodology was applicable to multiple diverse classes of RiPP, but the generic nature of retrieval meant that only between a half and a quarter (depending on RiPP class) of total retrieved peptides were likely to be precursor peptides (Table 1). We therefore generated peptide similarity networks (40) using peptides retrieved from each RiPPER analysis, where peptides with at least 40% identity were connected to each other. Despite the large sequence variance within each RiPP class, this was highly effective at filtering the peptides into networks of likely precursor peptides. For each RiPPER analysis, the largest network ("network 1") contained the majority of precursor peptides identified by previous studies (Table 1, Figures S2-S4). Unexpectedly, network 1 of the lasso peptide dataset also contained PqqD domain proteins, a conserved feature of lasso peptide pathways that function as RiPP precursor peptide recognition elements (54,55). These peptides were manually filtered by the Pfam domain results; alternatively, a higher identity cut-off for networking would have separated PqqD domains from network 1. In addition, network 2 comprises of 56 *Burkholderia* peptides that are precursors to capistruin lasso peptides (all identified by RODEO). Notably, for each RiPPER analysis, network 1 contained peptides with the expected precursor peptide domain that were not retrieved by either RODEO (13,14) or the bespoke microviridin analysis (46). In total, this provided over 200 new candidate precursor peptides (Table 1), as well as additional networked peptides with no known domains that could feasibly be authentic precursor peptides. The ability of RiPPER to correctly identify a comparable number of precursor peptides to prior targeted methods demonstrates that the combination of rational ORF identification and scoring, Pfam analysis, and peptide similarity networking can identify RiPP precursor peptides with a high degree of accuracy and coverage without any prior knowledge of the RiPP class.

Identification of thioamidated RiPP BGCs using RiPPER.

As a backbone modification, thioamidation potentially has no requirement for specific amino acid side chains, which means that there may be no conserved sequence motifs within precursor peptide substrates. To guide our identification of thioamidated RiPP BGCs, we identified a curated set of 229 TfuA-like proteins in Actinobacteria whose putative BGCs were retrieved using RiPPER, which showed that each TfuA protein was encoded alongside a YcaO protein but their associated gene clusters could be highly variable. RiPPER retrieved 743 peptides (Supplementary Dataset 4) and peptide similarity networking (40% identity cut-off) yielded 74 distinct networks of peptides, where 30 of these networks featured four or more peptides (Figure 2B, Figure S6, Table S1). MultiGeneBlast (43) was then employed to compare the BGCs corresponding to each network.

As an initial proof of concept, this correctly grouped all thioviridamide-like precursor peptides into a single network (Figure 3A). Surprisingly, these precursor peptides were connected with four additional peptides encoded in putative BGCs that are extremely different to thioviridamide-like BGCs; three of these peptides were not previously annotated as genes. These peptides feature extensive sequence similarities with the thioviridamide-like precursor peptides (Figure S7), but the BGCs themselves are extremely different, where the only common features with the thioviridamide-like BGCs are the YcaO, TfuA and precursor peptide genes (Figure 3B). More generally, peptide networking guided the identification of a wide variety of probable *tfuA*-containing RiPP BGCs (Figures S7-S20). For example, many mycobacteria encode a YcaO-TfuA protein pair, and the largest network of putative precursor peptides is associated with this mycobacterial BGC (Figure 2B, Network 1) where they are usually encoded near a Type III polyketide synthase (PKS) and a sulfotransferase (Figure S8). Network 2 consists of 25 related *Streptomyces* peptides that possess high Prodigal scores and are encoded at the start of a conserved biosynthetic operon (Figure S9). This is a strong candidate as an authentic RiPP BGC family, yet only 6 of these 25 short peptides were originally annotated.

Thioamidated RiPPs are a largely unexplored area of the natural products landscape.

To investigate whether BGC families correlate with the evolutionary relationships of the TfuA proteins, a maximum likelihood tree was constructed from standalone TfuA domain proteins and the peptide networks were mapped to this tree (Figure 4, Supplementary Dataset 5). This showed strong correlations between TfuA phylogeny and precursor peptide similarity. Despite the significant differences between their gene clusters, the thioviridamide-like and non-thioviridamide-like peptides of Network 5 are all associated with closely related TfuA proteins. Unsurprisingly, some TfuA domain proteins are associated with multiple peptide networks due to the abundance of small peptides that are unlikely to be precursor peptides, such as regulatory proteins and RiPP precursor peptide recognition elements (55). For example, almost all peptides from Networks 9, 11 and 18 are associated with the same set of TfuA domain proteins, but Pfam analysis indicates that Networks 11 and 18 consist of acyl carrier proteins and ThiS-like proteins (56), respectively. Therefore, the Network 9 peptides, which are encoded at the beginning of each BGC and feature no conserved domains, are likely precursor peptides for this BGC family (Figure 4).

Pfam analysis indicated that all precursor peptides in Network 7 feature nitrile hydratase domains, which is a common feature amongst precursor peptides across diverse RiPP families (8,57). In total, at least 15 distinct predicted RiPP families were predicted from the top 30 peptide networks (Supplementary Dataset 4, Table S1, Figures S7-S20), while many smaller networks and singletons are also likely to be authentic precursor peptides, based on their Prodigal scores and positions within BGCs. A comparative analysis with the source GenBank entries indicated that over half of the peptides encoded in these BGCs were not previously annotated (Supplementary Dataset 4). For peptides predicted to be authentic precursor peptides (Table S1), unannotated peptides identified by RiPPER were, on average, significantly shorter than annotated peptides (Figure S21).

Characterization of a novel family of TfuA-YcaO BGCs.

To determine whether the newly identified YcaO-TfuA BGCs actually produce thioamidated RiPPs, we focused on Network 22 (Figure 5A), a group of five orphan BGCs with multiple unusual features (Figure 5B). Most notably, the predicted precursor peptides feature a series of imperfect repeats that could reflect a repeating core peptide (Figure 5C), where the family varies from a non-repeating precursor peptide (*Asanoa ishikariensis*) to five repeats (*Streptomyces varsoviensis*). In addition, the *Nocardiopsis* and *Streptomyces* BGCs encode two additional conserved proteins, an amidinotransferase (AmT) and an ATP-grasp ligase, which are homologous to proteins in the pheganomycin pathway (58), and are adjacent to genes encoding non-ribosomal peptide synthetases or PKSs (Figure 5B). Efforts to genetically manipulate *S. varsoviensis* and *Nocardiopsis baichengensis* were unsuccessful and we were unsure of the gene cluster boundaries, so transformation-associated recombination (TAR) cloning (49,59) was employed to capture a 31.7 kb DNA fragment comprising 25 genes (Table S2) centered around the *ycaO-tfuA* core of the *S. varsoviensis* BGC. Two independent positive TAR clones were conjugated into three different host strains: *Streptomyces lividans* TK24 and *Streptomyces coelicolor* M1146 and M1152 (34) and the resulting TARvar exconjugants were fermented in a variety of media. Liquid chromatography-mass spectrometry (LC-MS) analysis revealed two major compounds (*m/z* 399.18 and *m/z* 401.20), and two minor compounds (*m/z* 385.16 and *m/z* 387.18) not present in the negative control strains (Figure 5D). Small amounts of these compounds could be detected when *S. varsoviensis* was fermented for 10 days (Figure 6, Figure S22).

To associate the production of these new compounds to the cloned DNA fragment, PCR-targeting mutagenesis (50) was employed to generate a series of deletion mutants on the putative BGC. A progressive trimming process determined that a cluster of seven genes that are mostly conserved across the *Nocardiopsis* and *Streptomyces* BGCs was sufficient for compound production: *varA* (encoding the predicted repeating precursor peptide), *varY* (the YcaO protein), *varT* (the TfuA protein), *varO* (a heme oxygenase-like protein (60)), *varL* (an ATP-grasp ligase), *varP* (a major facilitator superfamily transporter) and *varS* (an amidinotransferase). The deletion of *varA*, *varY* and *varT* completely abolished the production of the four new compounds, while the Δ*varO* mutant produced only *m/z* 401.20 and *m/z* 387.18, suggesting that VarO may function as a dehydrogenase (Figure 6). Deletion of *varL*, *varP* and *varS* did not affect production, despite their conservation in related BGCs (Figure 5B). Δ*varY*, Δ*varT* and Δ*varO* mutants were successfully complemented by expressing these genes under the control of the *ermE** promoter, whereas complementation of Δ*varA* required its native promoter. As expected, expression of a 3.7 kb DNA fragment including only *varA*, *varY* and *varT* in *S. coelicolor* M1146 led to the production of *m/z* 401.20 and *m/z* 387.18 (Figure 6, *varAYT*). Collectively, this data show that *varAYTO* are the only genes required for the biosynthesis of this new group of RiPPs, thiovarsolins A-D (observed *m/z* 399.1818, 401.1968, 385.1652 and 387.1808, respectively, Table S5).

The thiovarsolins are thioamidated peptides that derive from the repetitive core of the precursor peptide.

The structures of thiovarsolins A and B were determined by NMR (^{1}H, ^{13}C, COSY, HSQC and HMBC; Figures S23-S34, Table S6) following large scale fermentation and purification of each compound. This analysis showed that thiovarsolins A and B are *N*-acetylated APR tripeptides in which the amide bond between Pro and Arg is substituted by a thioamide (δ_C 200 ppm) (Figure 5D). This was supported by accurate mass data (Table S5) and an absorbance maximum at ~270 nm for both molecules, which is characteristic of a thioamide group (61). Additionally, a trans double bond is present between Cβ and Cγ of the arginine side chain in thiovarsolin A. This peptide backbone is fully compatible with an APR sequence within the repeats of VarA (Figure 5C). The name thiovarsolin corresponds to linear thioamidated peptides made by *S. varsoviensis*.

Tandem MS (MS^2) analysis of the thiovarsolins (Figure S35) revealed a clear structural relationship between thiovarsolins A (*m/z* 399.18) and C (*m/z* 385.16), as well as between thiovarsolins B (*m/z* 401.20) and D (*m/z* 387.18), which suggested that each 14 Da mass difference could be due to one methyl group. Interestingly, the first repetition of the putative modular core peptide features a GPR motif instead of APR, which could potentially explain this 14 Da mass difference, as well as their observed abundances in relation to thiovarsolins A and B. To test this hypothesis, a mutated version of *varA* was constructed (*varA**, Figure S36) in which the Ala residue in each repeat was substituted by Gly. This was expressed in M1146 TARvar Δ*varA* using a pGP9-based expression plasmid (62). The resulting strain was only able to produce thiovarsolins C and D (Figure 6, *varA**), confirming that these two minor compounds derive from a GPR core peptide. Such an extensively repeating precursor peptide is rare, but is comparable to the variable repeats found in precursor peptides for some cyanobactins (63) and the fungal RiPP phomopsin (64).

Our genetic and chemical analysis of the *var* BGC strongly suggests that the YcaO (VarY) and TfuA (VarT) proteins cooperate to introduce a thioamide bond. Given the absence of a specific protease in the gene cluster, it is plausible that endogenous peptidases are responsible for the liberation of the non-degradable thioamidated APR and GPR tripeptides, which later undergo an *N*-terminal acetylation catalyzed by an endogenous *N*-acetyltransferase, as previously reported for other metabolites containing primary amines (65,66). The timing of VarO-catalyzed dehydrogenation is unclear and could happen directly on the precursor peptide or after proteolysis. Small amounts of thiovarsolins A and B are produced by *S. varsoviensis*, but the lack of a function for *varS* and *varL* suggests that the described thiovarsolins might not be the final products of these pathways. However, no further thiovarsolin-related metabolites could be detected in either *S. varsoviensis* or *S. coelicolor* M1146 TARvar when analyzed by comparative metabolomics and by assessment of MS^2 data for losses of H_2S (*m/z* 33.99), which is a fragmentation profile that is characteristic of thioamides (6).

CONCLUSION

The discovery of the thiovarsolins supports the existence of an unexplored array of thioamidated RiPPs in Actinobacteria. The discovery that a minimal gene set of *varA* (precursor peptide), *varY* (YcaO protein) and *varT* (TfuA protein) is sufficient for the biosynthesis of thiovarsolin B (Figure 6) provides strong evidence that the YcaO-TfuA protein pair catalyze peptide thioamidation in bacteria, which is supported

by a parallel study by Mitchell and colleagues on thiopeptide thioamidation (14). It was previously determined that a distantly related pair of homologs catalyze thioamidation of methyl-coenzyme M reductase in archaea (32,33), and that a subset of archaeal YcaO proteins catalyze thioamidation in the absence of a TfuA protein (33). It is therefore possible that there are even more pathways making thioamidated RiPPs than the ones identified in our study, although the closest actinobacterial homologs of the thioamidating TfuA-independent YcaO protein from *Methanopyrus kandleri* (AAM01332.1) are encoded alongside TfuA proteins. Further experimental work is therefore required to determine the breadth of YcaO-domain catalysis and the role of the TfuA partner protein.

The relatively simple thiovarsolin pathway represents a promising system for future biochemical studies of this reaction in the context of RiPP biosynthesis. Unexpectedly, genes conserved across multiple homologous *var*-like pathways (*varS*, *varP* and *varL*, Figure 5B) were not required for thiovarsolin biosynthesis. Along with *N*-terminal acetylation, this suggests that the identified thiovarsolins may be shunt products, although the production of thiovarsolins by *S. varsoviensis* indicates that they are made naturally, so production is not simply a consequence of heterologous pathway expression. The introduction of a double bond in the arginine residue side chain of the thiovarsolins by VarO would represent new RiPP biochemistry, as heme oxygenases have never been associated with RiPP biosynthesis. This shows that the breadth and diversity of RiPP post-translational modifications is still expanding, which has also been highlighted by recent discoveries of radical SAM enzyme-catalyzed epimerization (57), cyclization (67,68) and β-amino acid formation (69) in RiPP pathways.

RiPPER is a flexible prediction tool that can be applied to any class of predicted RiPP tailoring enzyme to aid in the discovery of this metabolic dark matter. This more general approach complements existing genome-mining tools such as BAGEL (10), RODEO (13,14), PRISM (70) and antiSMASH (12), which all provide in-depth analyses and product predictions for established RiPP families. The underlying logic of RiPPER differs significantly to BAGEL4, antiSMASH 4.0 (which incorporates RODEO) and PRISM 3, which all identify gene clusters based on sets of conserved protein domains predicted to be involved in biosynthesis. With these tools, if established RiPP gene cluster families are identified, predicted precursor peptides and modifications are sometimes displayed. In contrast, the user dictates the gene clusters searched in RiPPER, which aids in the identification of precursor peptides, and this is most effective when multiple similar gene clusters are analyzed in parallel (e.g. Fig. 2B). This difference in operation and output makes it difficult to make meaningful comparisons between tools.

The *de novo* identification of precursors to lasso peptides, microviridins and thiopeptides highlights the scope of RiPPER, which was achieved without any specific rules for these RiPP families. The methodology proved to be highly adept at identifying previously overlooked precursor peptide genes, and the method parameters can be easily adapted based on prior knowledge of a given RiPP family (min/max gene length, max distance from RTE, same strand score and peptide score threshold, for example). In our TfuA analysis, peptide networking proved to be a highly effective method to prioritize related precursor peptides and their associated BGCs for further analysis, where it highlighted the

existence of likely RiPP families as opposed to the coincidental presence of a small ORF near a putative BGC. The diversity of TfuA-associated precursor peptides identified in Actinobacteria highlights the utility of a generic precursor peptide identification tool and provides the basis for investigating the breadth of this RiPP family. It will be fascinating to determine both the structure and function of these cryptic metabolites.

AVAILABILITY

RiPPER is available at:
https://github.com/streptomyces/ripper and https://hub.docker.com/r/streptomyces/ripdock/
Thiovarsolin gene cluster information is available at https://mibig.secondarymetabolites.org (accession number BGC0001849).

SUPPLEMENTARY DATA

Supplementary Data are available at NAR online.

FUNDING

This work was supported by a Royal Society University Research Fellowship to A.W.T., the Biotechnology and Biological Sciences Research Council (BBSRC) [BB/M003140/1 to A.W.T.], the Erasmus Programme (L.F.), and BBSRC Institute Strategic Programme Grants [BB/J004561/1 and BB/P012523/1] to the John Innes Centre.

CONFLICT OF INTEREST

The authors declare no conflict of interest.

ACKNOWLEDGEMENTS

We thank Bradley Moore (Scripps Institution of Oceanography, University of California San Diego, U.S.A.) for pCAP03, Vladimir Larionov (National Cancer Institute, NIH, U.S.A.) for *S. cerevisiae* VL6-48N, Mervyn Bibb (John Innes Centre, U.K.) for *S. coelicolor* strains, and Daniel Haft (NCBI/NIH, U.S.A.) for providing the precursor peptide HMMs. We thank Lionel Hill, Paul Brett and Gerhard Saalbach (John Innes Centre, Norwich, UK) for assistance with LC-MS, and Gwenaelle Le Gall and Ian Colquhoun (Quadrum Institute, Norwich, UK) for assistance with NMR.

REFERENCES

1. Baltz,R.H. (2017) Gifted microbes for genome mining and natural product discovery. *J. Ind. Microbiol. Biotechnol.*, **44**, 573–588.
2. Bentley,S.D., Chater,K.F., Cerdeño-Tárraga,A.-M., Challis,G.L., Thomson,N.R., James,K.D., Harris,D.E., Quail,M.A., Kieser,H., Harper,D., *et al.* (2002) Complete genome sequence of the model actinomycete *Streptomyces coelicolor* A3(2). *Nature*, **417**, 141–147.
3. Ikeda,H., Ishikawa,J., Hanamoto,A., Shinose,M., Kikuchi,H., Shiba,T., Sakaki,Y., Hattori,M. and Ōmura,S. (2003) Complete genome sequence and comparative analysis of the industrial microorganism *Streptomyces avermitilis*. *Nat. Biotechnol.*, **21**, 526–531.
4. Arnison,P.G., Bibb,M.J., Bierbaum,G., Bowers,A.A., Bugni,T.S., Bulaj,G., Camarero,J.A., Campopiano,D.J., Challis,G.L., Clardy,J., *et al.* (2013) Ribosomally synthesized and post-translationally modified peptide natural products: overview and recommendations for a universal nomenclature. *Nat. Prod. Rep.*, **30**, 108–160.
5. Goto,Y., Li,B., Claesen,J., Shi,Y., Bibb,M.J. and van der Donk,W.A. (2010) Discovery of unique lanthionine synthetases reveals new mechanistic and evolutionary insights. *PLOS Biol.*, **8**, e1000339.
6. Frattaruolo,L., Lacret,R., Cappello,A.R. and Truman,A.W. (2017) A Genomics-Based Approach Identifies a Thioviridamide-Like Compound with Selective Anticancer Activity. *ACS Chem. Biol.*, **12**, 2815–2822.
7. Haft,D.H. and Basu,M.K. (2011) Biological Systems Discovery In Silico: Radical S-Adenosylmethionine Protein Families and Their Target Peptides for Posttranslational Modification. *J. Bacteriol.*, **193**, 2745–2755.
8. Haft,D.H., Basu,M.K. and Mitchell,D.A. (2010) Expansion of ribosomally produced natural products: a nitrile hydratase- and Nif11-related precursor family. *BMC Biol.*, **8**, 70.
9. Cox,C.L., Doroghazi,J.R. and Mitchell,D.A. (2015) The genomic landscape of ribosomal peptides containing thiazole and oxazole heterocycles. *BMC Genomics*, **16**, 778.
10. van Heel,A.J., de Jong,A., Song,C., Viel,J.H., Kok,J. and Kuipers,O.P. (2018) BAGEL4: a user-friendly web server to thoroughly mine RiPPs and bacteriocins. *Nucleic Acids Res.*, **46**, W278–W281.
11. Skinnider,M.A., Johnston,C.W., Edgar,R.E., Dejong,C.A., Merwin,N.J., Rees,P.N. and Magarvey,N.A. (2016) Genomic charting of ribosomally synthesized natural product chemical space facilitates targeted mining. *Proc. Natl. Acad. Sci. U.S.A.*, **113**, E6343–E6351.
12. Blin,K., Wolf,T., Chevrette,M.G., Lu,X., Schwalen,C.J., Kautsar,S.A., Suarez Duran,H.G., de Los Santos,E.L.C., Kim,H.U., Nave,M., *et al.* (2017) antiSMASH 4.0-improvements in chemistry prediction and gene cluster boundary identification. *Nucleic Acids Res.*, **45**, W36–W41.
13. Tietz,J.I., Schwalen,C.J., Patel,P.S., Maxson,T., Blair,P.M., Tai,H.-C., Zakai,U.I. and Mitchell,D.A. (2017) A new genome-mining tool redefines the lasso peptide biosynthetic landscape. *Nat. Chem. Biol.*, **13**, 470–478.

14. Schwalen,C.J., Hudson,G.A., Kille,B. and Mitchell,D.A. (2018) Bioinformatic Expansion and Discovery of Thiopeptide Antibiotics. *J. Am. Chem. Soc.*, **140**, 9494–9501.
15. Burkhart,B.J., Schwalen,C.J., Mann,G., Naismith,J.H. and Mitchell,D.A. (2017) YcaO-Dependent Posttranslational Amide Activation: Biosynthesis, Structure, and Function. *Chem. Rev.*, **117**, 5389–5456.
16. Dunbar,K.L., Melby,J.O. and Mitchell,D.A. (2012) YcaO domains use ATP to activate amide backbones during peptide cyclodehydrations. *Nat. Chem. Biol.*, **8**, 569–575.
17. Crone,W.J.K., Vior,N.M., Santos-Aberturas,J., Schmitz,L.G., Leeper,F.J. and Truman,A.W. (2016) Dissecting Bottromycin Biosynthesis Using Comparative Untargeted Metabolomics. *Angew. Chem. Int. Ed.*, **55**, 9639–9643.
18. Franz,L., Adam,S., Santos-Aberturas,J., Truman,A.W. and Koehnke,J. (2017) Macroamidine Formation in Bottromycins Is Catalyzed by a Divergent YcaO Enzyme. *J. Am. Chem. Soc.*, **139**, 18158–18161.
19. Schwalen,C.J., Hudson,G.A., Kosol,S., Mahanta,N., Challis,G.L. and Mitchell,D.A. (2017) In Vitro Biosynthetic Studies of Bottromycin Expand the Enzymatic Capabilities of the YcaO Superfamily. *J. Am. Chem. Soc.*, **139**, 18154–18157.
20. Izawa,M., Kawasaki,T. and Hayakawa,Y. (2013) Cloning and heterologous expression of the thioviridamide biosynthesis gene cluster from *Streptomyces olivoviridis*. *Appl. Environ. Microbiol.*, **79**, 7110–7113.
21. Izawa,M., Nagamine,S., Aoki,H. and Hayakawa,Y. (2018) Identification of essential biosynthetic genes and a true biosynthetic product for thioviridamide. *J. Gen. Appl. Microbiol.*, **64**, 50–53.
22. Kawahara,T., Izumikawa,M., Kozone,I., Hashimoto,J., Kagaya,N., Koiwai,H., Komatsu,M., Fujie,M., Sato,N., Ikeda,H., *et al.* (2018) Neothioviridamide, a Polythioamide Compound Produced by Heterologous Expression of a *Streptomyces* sp. Cryptic RiPP Biosynthetic Gene Cluster. *J. Nat. Prod.*, **81**, 264–269.
23. Hayakawa,Y., Sasaki,K., Nagai,K., Shin-ya,K. and Furihata,K. (2006) Structure of thioviridamide, a novel apoptosis inducer from *Streptomyces olivoviridis*. *J. Antibiot.*, **59**, 6–10.
24. Kjaerulff,L., Sikandar,A., Zaburannyi,N., Adam,S., Herrmann,J., Koehnke,J. and Müller,R. (2017) Thioholgamides: Thioamide-Containing Cytotoxic RiPP Natural Products. *ACS Chem. Biol.*, **12**, 2837–2841.
25. Feistner,G. and Staub,C.M. (1986) 6-Thioguanine from *Erwinia amylovora*. *Curr. Microbiol.*, **13**, 95–101.
26. Kim,H.J., Graham,D.W., Dispirito,A.A., Alterman,M.A., Galeva,N., Larive,C.K., Asunskis,D. and Sherwood,P.M.A. (2004) Methanobactin, a copper-acquisition compound from methane-oxidizing bacteria. *Science*, **305**, 1612–1615.
27. Pan,M., Mabry,T.J., Beale,J.M. and Mamiya,B.M. (1997) Nonprotein amino acids from *Cycas revoluta*. *Phytochemistry*, **45**, 517–519.

28. Lincke,T., Behnken,S., Ishida,K., Roth,M. and Hertweck,C. (2010) Closthioamide: an unprecedented polythioamide antibiotic from the strictly anaerobic bacterium *Clostridium cellulolyticum*. *Angew. Chem. Int. Ed.*, **49**, 2011–2013.
29. Banala,S. and Süssmuth,R.D. (2010) Thioamides in nature: in search of secondary metabolites in anaerobic microorganisms. *ChemBioChem*, **11**, 1335–1337.
30. Dunbar,K.L., Scharf,D.H., Litomska,A. and Hertweck,C. (2017) Enzymatic Carbon-Sulfur Bond Formation in Natural Product Biosynthesis. *Chem. Rev.*, **117**, 5521–5577.
31. Litomska,A., Ishida,K., Dunbar,K.L., Boettger,M., Coyne,S. and Hertweck,C. (2018) Enzymatic Thioamide Formation in a Bacterial Antimetabolite Pathway. *Angew. Chem. Int. Ed.*, **57**, 11574–11578.
32. Nayak,D.D., Mahanta,N., Mitchell,D.A. and Metcalf,W.W. (2017) Post-translational thioamidation of methyl-coenzyme M reductase, a key enzyme in methanogenic and methanotrophic Archaea. *eLife*, **6**, e29218.
33. Mahanta,N., Liu,A., Dong,S., Nair,S.K. and Mitchell,D.A. (2018) Enzymatic reconstitution of ribosomal peptide backbone thioamidation. *Proc. Natl. Acad. Sci. U.S.A.*, **115**, 3030–3035.
34. Gomez-Escribano,J.P. and Bibb,M.J. (2011) Engineering *Streptomyces coelicolor* for heterologous expression of secondary metabolite gene clusters. *Microb. Biotechnol.*, **4**, 207–215.
35. Noskov,V., Kouprina,N., Leem,S.-H., Koriabine,M., Barrett,J.C. and Larionov,V. (2002) A genetic system for direct selection of gene-positive clones during recombinational cloning in yeast. *Nucleic Acids Res.*, **30**, E8.
36. Stajich,J.E., Block,D., Boulez,K., Brenner,S.E., Chervitz,S.A., Dagdigian,C., Fuellen,G., Gilbert,J.G.R., Korf,I., Lapp,H., *et al.* (2002) The Bioperl toolkit: Perl modules for the life sciences. *Genome Res.*, **12**, 1611–1618.
37. Finn,R.D., Coggill,P., Eberhardt,R.Y., Eddy,S.R., Mistry,J., Mitchell,A.L., Potter,S.C., Punta,M., Qureshi,M., Sangrador-Vegas,A., *et al.* (2016) The Pfam protein families database: towards a more sustainable future. *Nucleic Acids Res.*, **44**, D279–D285.
38. Haft,D.H., DiCuccio,M., Badretdin,A., Brover,V., Chetvernin,V., O'Neill,K., Li,W., Chitsaz,F., Derbyshire,M.K., Gonzales,N.R., *et al.* (2018) RefSeq: an update on prokaryotic genome annotation and curation. *Nucleic Acids Res.*, **46**, D851–D860.
39. Hyatt,D., Chen,G.-L., Locascio,P.F., Land,M.L., Larimer,F.W. and Hauser,L.J. (2010) Prodigal: prokaryotic gene recognition and translation initiation site identification. *BMC Bioinformatics*, **11**, 119.
40. Halary,S., McInerney,J.O., Lopez,P. and Bapteste,E. (2013) EGN: a wizard for construction of gene and genome similarity networks. *BMC Evol. Biol.*, **13**, 146.
41. Shannon,P., Markiel,A., Ozier,O., Baliga,N.S., Wang,J.T., Ramage,D., Amin,N., Schwikowski,B. and Ideker,T. (2003) Cytoscape: a software environment for integrated models of biomolecular interaction networks. *Genome Res.*, **13**, 2498–2504.

42. Carver,T., Harris,S.R., Berriman,M., Parkhill,J. and McQuillan,J.A. (2012) Artemis: an integrated platform for visualization and analysis of high-throughput sequence-based experimental data. *Bioinformatics*, **28**, 464–469.
43. Medema,M.H., Takano,E. and Breitling,R. (2013) Detecting sequence homology at the gene cluster level with MultiGeneBlast. *Mol. Biol. Evol.*, **30**, 1218–1223.
44. Edgar,R.C. (2004) MUSCLE: multiple sequence alignment with high accuracy and high throughput. *Nucleic Acids Res.*, **32**, 1792–1797.
45. Robert,X. and Gouet,P. (2014) Deciphering key features in protein structures with the new ENDscript server. *Nucleic Acids Res.*, **42**, W320–W324.
46. Ahmed,M.N., Reyna-González,E., Schmid,B., Wiebach,V., Süssmuth,R.D., Dittmann,E. and Fewer,D.P. (2017) Phylogenomic Analysis of the Microviridin Biosynthetic Pathway Coupled with Targeted Chemo-Enzymatic Synthesis Yields Potent Protease Inhibitors. *ACS Chem. Biol.*, **12**, 1538–1546.
47. Geer,L.Y., Domrachev,M., Lipman,D.J. and Bryant,S.H. (2002) CDART: protein homology by domain architecture. *Genome Res.*, **12**, 1619–1623.
48. Letunic,I. and Bork,P. (2016) Interactive tree of life (iTOL) v3: an online tool for the display and annotation of phylogenetic and other trees. *Nucleic Acids Res.*, **44**, W242–W245.
49. Tang,X., Li,J., Millán-Aguiñaga,N., Zhang,J.J., O'Neill,E.C., Ugalde,J.A., Jensen,P.R., Mantovani,S.M. and Moore,B.S. (2015) Identification of Thiotetronic Acid Antibiotic Biosynthetic Pathways by Target-directed Genome Mining. *ACS Chem. Biol.*, **10**, 2841–2849.
50. Gust,B., Challis,G.L., Fowler,K., Kieser,T. and Chater,K.F. (2003) PCR-targeted Streptomyces gene replacement identifies a protein domain needed for biosynthesis of the sesquiterpene soil odor geosmin. *Proc. Natl. Acad. Sci. U.S.A.*, **100**, 1541–1546.
51. Hong,H.-J., Hutchings,M.I., Hill,L.M. and Buttner,M.J. (2005) The role of the novel Fem protein VanK in vancomycin resistance in Streptomyces coelicolor. *J. Biol. Chem.*, **280**, 13055–13061.
52. Haft,D.H. (2011) Bioinformatic evidence for a widely distributed, ribosomally produced electron carrier precursor, its maturation proteins, and its nicotinoprotein redox partners. *BMC Genomics*, **12**, 21.
53. Morinaka,B.I., Verest,M., Freeman,M.F., Gugger,M. and Piel,J. (2017) An Orthogonal D_2O-Based Induction System that Provides Insights into D-Amino Acid Pattern Formation by Radical S-Adenosylmethionine Peptide Epimerases. *Angew. Chem. Int. Ed.*, **56**, 762–766.
54. Latham,J.A., Iavarone,A.T., Barr,I., Juthani,P.V. and Klinman,J.P. (2015) PqqD is a novel peptide chaperone that forms a ternary complex with the radical S-adenosylmethionine protein PqqE in the pyrroloquinoline quinone biosynthetic pathway. *J. Biol. Chem.*, **290**, 12908–12918.
55. Burkhart,B.J., Hudson,G.A., Dunbar,K.L. and Mitchell,D.A. (2015) A prevalent peptide-binding domain guides ribosomal natural product biosynthesis. *Nat. Chem. Biol.*, **11**, 564–570.
56. Dorrestein,P.C., Zhai,H., McLafferty,F.W. and Begley,T.P. (2004) The biosynthesis of the thiazole phosphate moiety of thiamin: the sulfur transfer mediated by the sulfur carrier protein ThiS. *Chem. Biol.*, **11**, 1373–1381.

57. Fuchs,S.W., Lackner,G., Morinaka,B.I., Morishita,Y., Asai,T., Riniker,S. and Piel,J. (2016) A Lanthipeptide-like N-Terminal Leader Region Guides Peptide Epimerization by Radical SAM Epimerases: Implications for RiPP Evolution. *Angew. Chem. Int. Ed.*, **55**, 12330–12333.
58. Noike,M., Matsui,T., Ooya,K., Sasaki,I., Ohtaki,S., Hamano,Y., Maruyama,C., Ishikawa,J., Satoh,Y., Ito,H., *et al.* (2015) A peptide ligase and the ribosome cooperate to synthesize the peptide pheganomycin. *Nat. Chem. Biol.*, **11**, 71–76.
59. Yamanaka,K., Reynolds,K.A., Kersten,R.D., Ryan,K.S., Gonzalez,D.J., Nizet,V., Dorrestein,P.C. and Moore,B.S. (2014) Direct cloning and refactoring of a silent lipopeptide biosynthetic gene cluster yields the antibiotic taromycin A. *Proc. Natl. Acad. Sci. U.S.A.*, **111**, 1957–1962.
60. Kikuchi,G., Yoshida,T. and Noguchi,M. (2005) Heme oxygenase and heme degradation. *Biochem. Biophys. Res. Commun.*, **338**, 558–567.
61. Judge,R.H., Moule,D.C. and Goddard,J.D. (1987) Thioamide spectroscopy: long path length absorption and quantum chemical studies of thioformamide vapour, $CHSNH_2$/$CHSND_2$. *Can. J. Chem.*, **65**, 2100–2105.
62. Kuščer,E., Coates,N., Challis,I., Gregory,M., Wilkinson,B., Sheridan,R. and Petkovic,H. (2007) Roles of *rapH* and *rapG* in positive regulation of rapamycin biosynthesis in *Streptomyces hygroscopicus*. *J. Bacteriol.*, **189**, 4756–4763.
63. McIntosh,J.A., Lin,Z., Tianero,M.D.B. and Schmidt,E.W. (2013) Aestuaramides, a natural library of cyanobactin cyclic peptides resulting from isoprene-derived Claisen rearrangements. *ACS Chem. Biol.*, **8**, 877–883.
64. Ding,W., Liu,W.-Q., Jia,Y., Li,Y., van der Donk,W.A. and Zhang,Q. (2016) Biosynthetic investigation of phomopsins reveals a widespread pathway for ribosomal natural products in Ascomycetes. *Proc. Natl. Acad. Sci. U.S.A.*, **113**, 3521–3526.
65. García,I., Vior,N.M., González-Sabin,J., Braña,A.F., Rohr,J., Moris,F., Méndez,C. and Salas,J.A. (2013) Engineering the biosynthesis of the polyketide-nonribosomal peptide collismycin A for generation of analogs with neuroprotective activity. *Chem. Biol.*, **20**, 1022–1032.
66. Ye,S., Molloy,B., Braña,A.F., Zabala,D., Olano,C., CortEs,J., Moris,F., Salas,J.A. and Méndez,C. (2017) Identification by Genome Mining of a Type I Polyketide Gene Cluster from Streptomyces argillaceus Involved in the Biosynthesis of Pyridine and Piperidine Alkaloids Argimycins P. *Front Microbiol*, **8**, 194.
67. Khaliullin,B., Ayikpoe,R., Tuttle,M. and Latham,J.A. (2017) Mechanistic elucidation of the mycofactocin-biosynthetic radicalS-adenosylmethionine protein, MftC. *J. Biol. Chem.*, **292**, 13022–13033.
68. Bushin,L.B., Clark,K.A., Pelczer,I. and Seyedsayamdost,M.R. (2018) Charting an Unexplored Streptococcal Biosynthetic Landscape Reveals a Unique Peptide Cyclization Motif. *J. Am. Chem. Soc.*, 10.1021/jacs.8b10266.
69. Morinaka,B.I., Lakis,E., Verest,M., Helf,M.J., Scalvenzi,T., Vagstad,A.L., Sims,J., Sunagawa,S., Gugger,M. and Piel,J. (2018) Natural noncanonical protein splicing yields products with diverse β-amino acid residues. *Science*, **359**, 779–782.

70. Skinnider,M.A., Merwin,N.J., Johnston,C.W. and Magarvey,N.A. (2017) PRISM 3: expanded prediction of natural product chemical structures from microbial genomes. *Nucleic Acids Res.*, **45**, W49–W54.

FIGURE AND TABLE CAPTIONS

Table 1. Comparison of RiPPER with prior studies on the identification of RiPP precursor peptides.

RiPP class[a]	No. of RTEs used in RiPPER search	Generic RiPPER search		RiPPER including HMM search		Network 1 data from RiPPER analysis		
		Total peptides retrieved	Match with prior data[b]	Total peptides retrieved	Match with prior data[b]	Total peptides in network	Match with prior data[b]	Additional HMM hits
Lasso peptides	1198	4503	1056/1122 (94.1%)	4558	1063/1122 (94.7%)	1211[c]	934/1122 (83.2%)	125
Microviridins	159	586	270/280 (96.4%)	596	270/280 (96.4%)	270	269/280 (96.1%)	1
Thiopeptides	486	1526	438/591 (74.1%)	1675	549/591 (92.9%)	690	543/591 (91.9%)	75

[a] Data obtained for lasso peptides from ref. 13, microviridins from ref. 46 and thiopeptides from ref. 14.

[b] These numbers are sometimes greater than the number of RTEs used in the RiPPER search due to the identification of multiple precursor peptides per BGC.

[c] Proteins with PqqD domains removed.

Figure 1. An example of a thioviridamide-like molecule, thioalbamide, and inset, a proposed biochemical route to thioamides. Thioamides are highlighted in blue and other post-translational modifications are colored red.

Figure 2. RiPPER identification of putative precursor peptides. (A) Schematic of RiPPER workflow where a cluster is identified based on a putative RiPP tailoring enzyme (RTE). (B) The 30 largest peptide similarity networks identified using RiPPER for peptides associated with *tfuA*-like genes in Actinobacteria. Red numbers indicate networks predicted to comprise of authentic precursor peptides (see Table S1 and Figures S7-S20) and triangular nodes indicate peptides encoded on the opposite strand to the RTE gene. Additional color-coding of nodes reflects domains with a probable association with a biosynthetic gene cluster and includes putative precursor peptides (nitrile hydratase-like (8) and type-A lantibiotic) and other small proteins (PqqD-like proteins (54,55), acyl carrier proteins and regulatory proteins).

Figure 3. Thioviridamide-like precursor peptides. (A) The precursor peptide network that includes both thioviridamide-like precursor peptides (red nodes) and a related but uncharacterized family of precursor peptides from BGCs that are highly different to thioviridamide-like BGCs (blue nodes). Characterized compounds are listed with their respective nodess. (B) Comparative analysis of thioviridamide-like and non- thioviridamide-like BGCs from this network where related genes share the same color. See Figure S7 for full BGC details.

Figure 4. Examples of putative RiPP BGCs and associated TfuA phylogeny. A maximum likelihood tree (branch lengths removed) of TfuA-like proteins is color-coded to indicate the relationship between TfuA-like proteins and the associated networks of putative precursor peptides. Representative BGCs are also shown, where grey genes indicate genetic features that are conserved across multiple BGCs within that family. Fully annotated BGCs are shown in Figures S7-S20.

Figure 5. Identification of the thiovarsolin family of RiPPs. (A) The associated precursor peptide network. (B) BGCs associated with each precursor peptide. The protein product of each *var* gene is listed at the top (HO = heme oxygenase; AmT = amidinotransferase; MFS = major facilitator superfamily) and genes common to multiple BGCs are color-coded by the predicted function of the protein product (see Figure S17 for full details). (C) Putative repeating precursor peptides identified by similarity networking. The predicted leader peptide is aligned, while the repeat regions are highlighted. Underlined text indicates the partially conserved core peptide that the thiovarsolins derive from, and bold text indicates equivalent residues in the other precursor peptides. (D) Analysis of thiovarsolin production by *S. coelicolor* M1146 TARvar, which contains a 31.7 kb DNA fragment centered on the *S. varsoviensis* BGC. Base peak chromatograms of crude extracts of *S. coelicolor* M1146 TARvar and an empty vector negative control (pCAP03) are shown, with peaks corresponding to thiovarsolins A-D indicated. Thioamidation and dehydrogenation post-translational modifications are highlighted on the thiovarsolin structures.

Figure 6. Mutational analysis of thiovarsolin biosynthesis. Extracted ion chromatograms (EICs) are shown for each thiovarsolin (A = *m/z* 399.18, B = *m/z* 401.20, C = *m/z* 385.16, D = *m/z* 387.18). M1146 pCAP03 indicates the empty plasmid control, while each Δ*var* mutation was made in the TARvar construct and expressed in *S. coelicolor* M1146. See text and Figure S36 for details of *varA**.

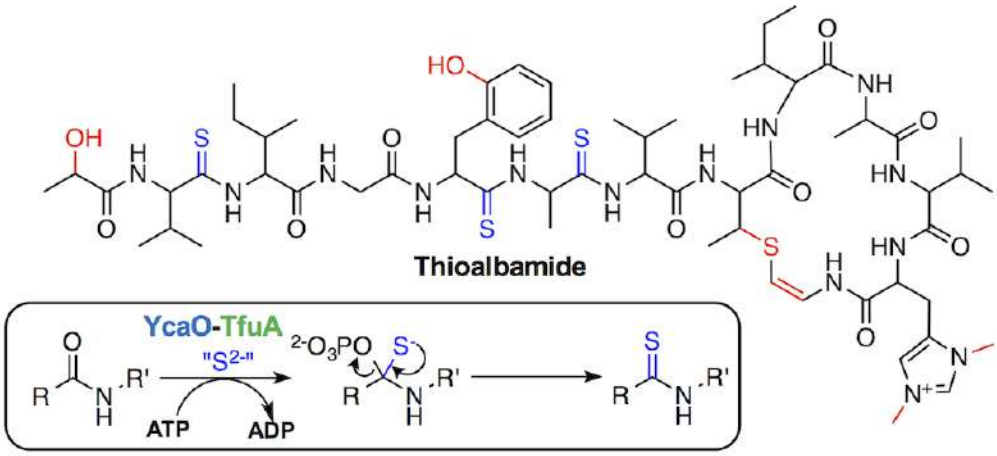

Figure 1

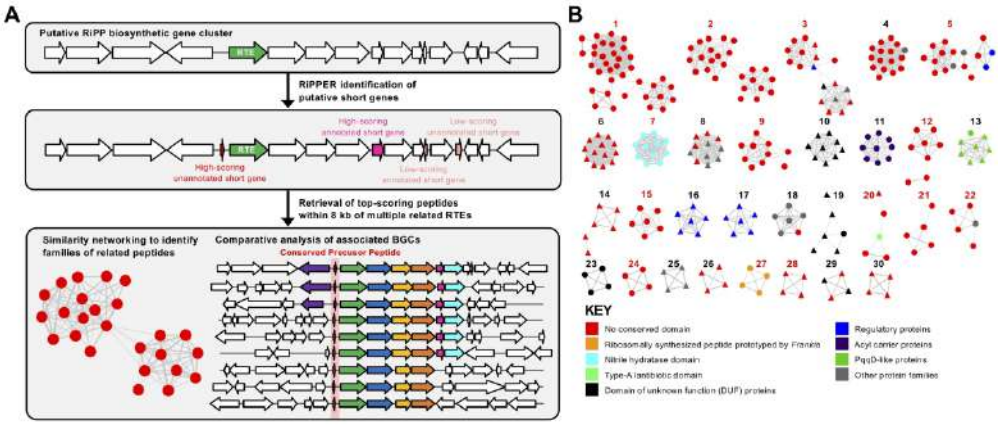
A
Putative RiPP biosynthetic gene cluster
RiPPER identification of putative short genes
High-scoring annotated short gene
Low-scoring unannotated short gene
High-scoring unannotated short gene
Low-scoring annotated short gene
Retrieval of top-scoring peptides within 8 kb of multiple related RTEs
Similarity networking to identify families of related peptides
Comparative analysis of associated BGCs
Conserved Precursor Peptide
B
KEY
No conserved domain
Ribosomally synthesized peptide prototyped by Franklin
Nitrile hydratase domain
Type-A lanthibiotic domain
Domain of unknown function (DUF) proteins
Regulatory proteins
Acyl carrier proteins
PqqD-like proteins
Other protein families

Figure 2

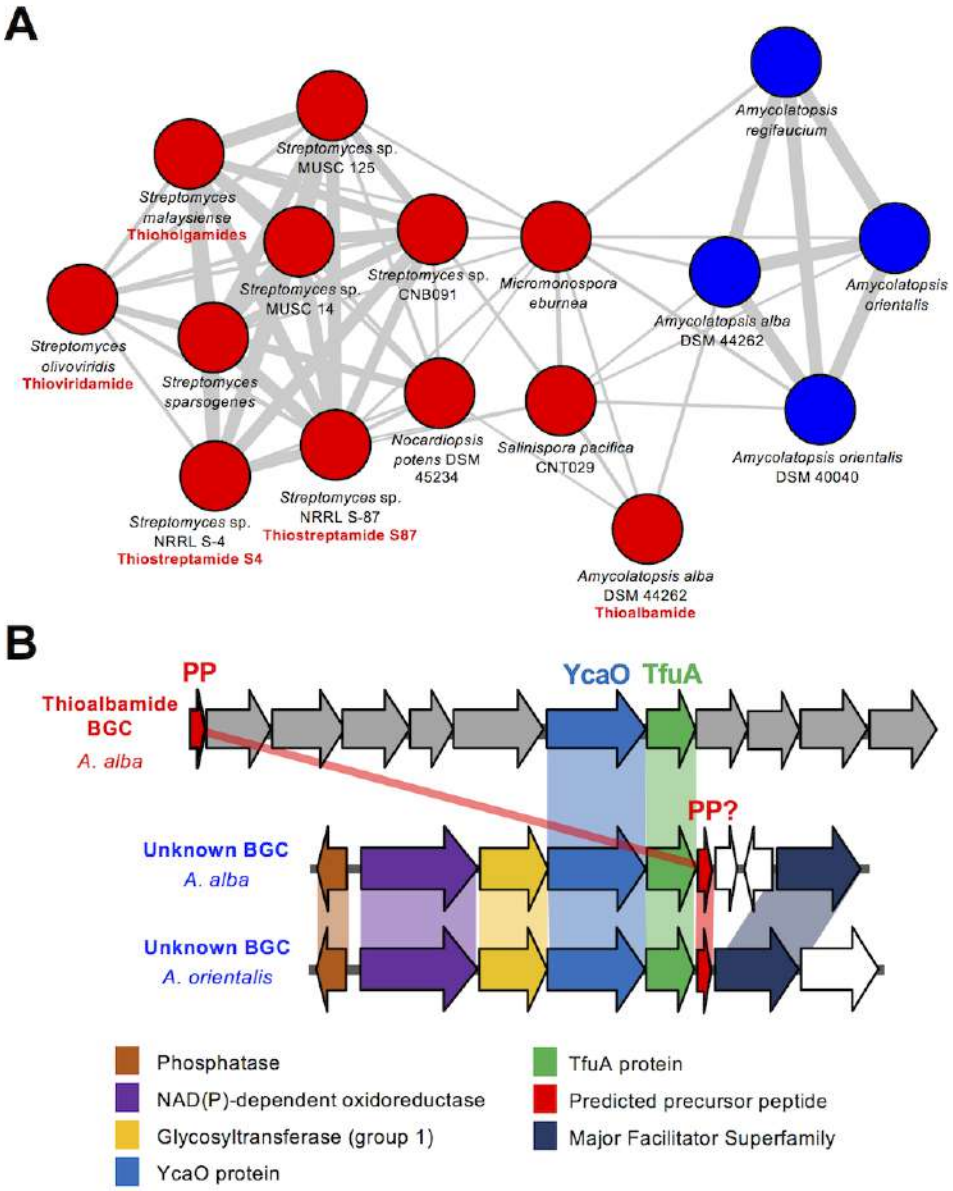
A
Streptomyces sp.
MUSC 125
Streptomyces
malaysiense
Thioholgamides
Streptomyces sp.
MUSC 14
Streptomyces sp.
CNB091
Micromonospora
eburnea
Amycolatopsis
regifaucium
Amycolatopsis
orientalis
Amycolatopsis alba
DSM 44262
Streptomyces
olivoviridis
Thioviridamide
Streptomyces
sparsogenes
Nocardiopsis
potens DSM
45234
Salinispora pacifica
CNT029
Amycolatopsis orientalis
DSM 40040
Streptomyces sp.
NRRL S-87
Thiostreptamide S87
Streptomyces sp.
NRRL S-4
Thiostreptamide S4
Amycolatopsis alba
DSM 44262
Thioalbamide
B
PP
YcaO
TfuA
Thioalbamide
BGC
A. alba
PP?
Unknown BGC
A. alba
Unknown BGC
A. orientalis
Phosphatase
NAD(P)-dependent oxidoreductase
Glycosyltransferase (group 1)
YcaO protein
TfuA protein
Predicted precursor peptide
Major Facilitator Superfamily

Figure 3

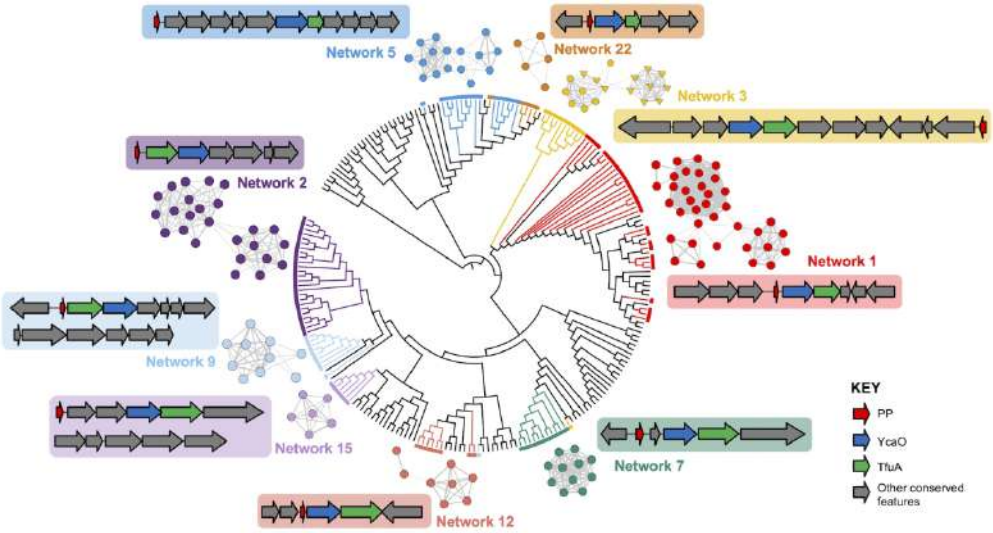
Network 5
Network 22
Network 3
Network 2
Network 1
Network 9
Network 15
Network 7
Network 12
KEY
PP
YcaO
TfuA
Other conserved features

Figure 4

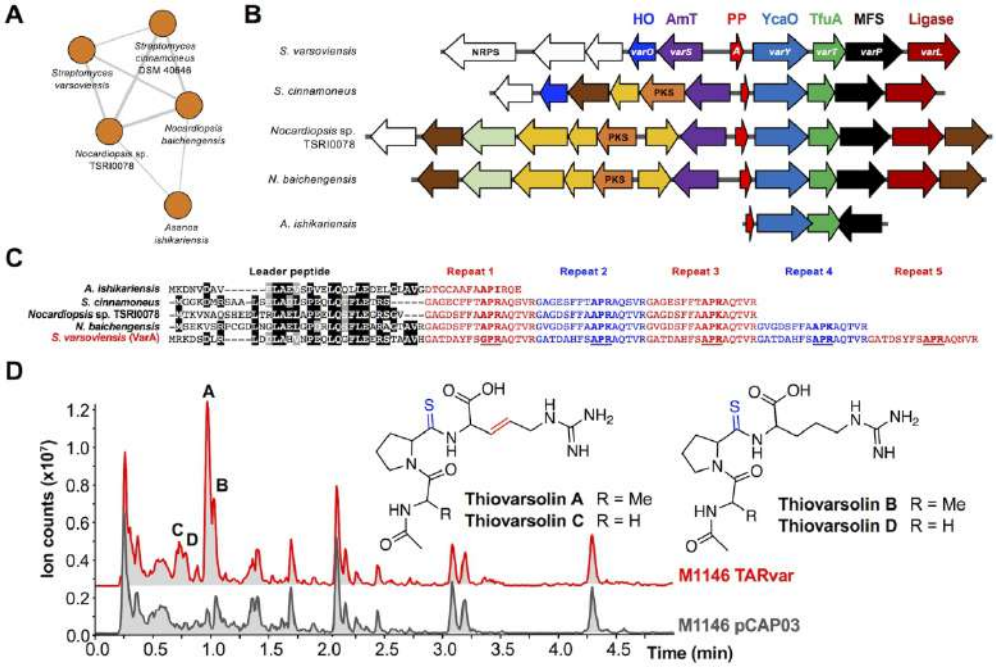
A
Streptomyces cinnamoneus DSM 40646
Streptomyces varsoviensis
Nocardiopsis baichengensis
Nocardiopsis sp. TSRI0078
Asanoa ishikariensis
B
HO AmT PP YcaO TfuA MFS Ligase
S. varsoviensis
S. cinnamoneus
Nocardiopsis sp. TSRI0078
N. baichengensis
A. ishikariensis
NRPS
PKS
varO
varS
varT
varP
varL
C
Leader peptide
Repeat 1
Repeat 2
Repeat 3
Repeat 4
Repeat 5
A. ishikariensis
S. cinnamoneus
Nocardiopsis sp. TSRI0078
N. baichengensis
S. varsoviensis (VarA)
D
Ion counts (x10^7)
Time (min)
M1146 TARvar
M1146 pCAP03
Thiovarsolin A R = Me
Thiovarsolin C R = H
Thiovarsolin B R = Me
Thiovarsolin D R = H

Figure 5

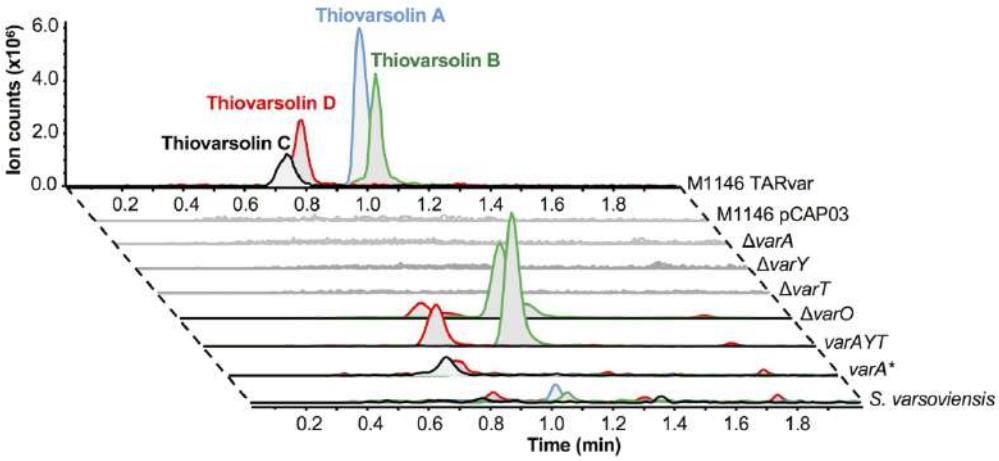
Thiovarsolin A
Thiovarsolin B
Thiovarsolin D
Thiovarsolin C
Ion counts (x10⁶)
6.0
4.0
2.0
0.0
0.2
0.4
0.6
0.8
1.0
1.2
1.4
1.6
1.8
M1146 TARvar
M1146 pCAP03
ΔvarA
ΔvarY
ΔvarT
ΔvarO
varAYT
varA*
S. varsoviensis
Time (min)

Figure 6

International Journal of Nutritional Sciences

Open Access

Austin Publishing Group

Mini Review

Polyunsaturated Fatty Acids and their Role in the Diet of Cancer Patients: An Overview

Frattaruolo L[1], Aiello F[1], Carullo G[1], Fiorillo M[1], Brindisi M[1], Cappello MS[2], Pilco G[1] and Cappello AR[1]*

[1]Department of Pharmacy, Health and Nutritional Sciences, University of Calabria, Italy

[2]CNR, Institute of Science of Food Production (ISPA), Lecce, Italy

***Corresponding author:** Cappello AR, Department of Pharmacy, Health and NutritionalSciences, University of Calabria, Edificio Poli Funzionale, Via P. Bucci, 87040 Arcavacata di Rende, Cosenza, Italy

Received: June 25, 2018; **Accepted:** August 13, 2018; **Published:** August 20, 2018

Abstract

Polyunsaturated Fatty Acids (PUFAs) are a class of natural compounds with interesting biochemical effects on human health. Indeed, in addition to their beneficial effects in brain and cardiovascular disorders, ω-3 LC-PUFA supplementation can exert antineoplastic activity by triggering cell death in human cancer cells, either alone or in combination with conventional therapies. The aim of this review is, by analyzing the recent scientific literature, to highlight the molecular mechanisms of Omega-3Polyunsaturated Fatty Acids (ω-3 PUFAs) in antineoplastic events, and the effects of supplementing diets with them during chemotherapy regimens. This analysis may provide specific information to carry out future pre-clinical and clinical studies aimed at a better use of omega-3polyunsaturated fatty acids in cancer therapy.

Keywords: Polyunsaturated fatty acids; Anti tumor activity; Cancer therapy; Diet in chemotherapy regimen

Introduction

Polyunsaturated fatty acids, also known as PUFAs, are molecules chemically characterized by a long carbon chain, starting with a Carboxyl Group (COOH) followed by a series of carbon atoms and ending with a methyl group (CH_3), held together by simples and at least two double bonds. The nomenclature of fatty acids involves assigning a Greek letter to each carbon atom according to its distance from the carboxylic end, and the terminal carbon atom is indicated with the last letter in the Greek alphabet, i.e. omega (ω). PUFAs can be classified as "omega-6" or "omega-3" on the basis of the position of the first double bond with respect to the methyl terminal portion. A secondary classification, important from a biochemical point of view, could be made to distinguish short- and long-chain polyunsaturated fatty acids. Short-chain PUFAs, Alpha-Linolenic Acid (ALA, 18:3 n-3) and Linoleic Acid (LA, 18:2 n-6), are defined as Essential (EFAs) because animals are unable to synthesize them ex-novo, so they must be obtained *via* the diet. The cell desaturation systems are in fact unable to introduce double bonds into the proximity of the methyl terminal, and these systems are just able to extend the fatty acid chain and to increase the number of unsaturations on it. The cellular desaturation/elongation pathway is thus responsible for the conversion of ALA into ω-3 long-chain PUFAs, such as Eicosa Pentaenoic Acid (EPA, 20:5 n-3) and Docosa Hexaenoic Acid (DHA, 22:6 n-3), and LA into ω-6 long-chain PUFAs, such as Arachidonic Acid (AA, 20:4 n-6) (Figure 1) [1]. The conversion efficiency in humans, however, is not high [2]. And consumption of long-chain ω-6 and ω-3 PUFAs containing food help keep them at optimal levels for cellular functions. ω-6 and ω-3 PUFAs are, indeed, essential components of the plasma membrane and precursors of eicosanoids, such as prostaglandins, thromboxanes and leukotrienes. All of them derive from ω-6 and ω-3 fatty acid metabolism through reactions catalyzed by the enzymes cyclooxygenase and lipoxygenase, and is important mediators of many physiological and pathological functions.

Oily fish, such as salmon, herring, mackerel, anchovies and sardines, as well as other fish and seafood are the main sources of long-chain ω-3 PUFAs, while eggs and lean red meat provide smaller amounts. Moreover, an interesting vegetarian source of DHA is marine algae, responsible for making fish a rich source of long-chain ω-3 PUFAs. On the other hand, cereals and vegetable oils provide high levels of ALA but are poor sources of long-chain ω-3 PUFAs [3,4].

ω-3Pufas in human health

Polyunsaturated fatty acids are essential molecules in human health. They are involved in various biological pathways and are beginning to play a significantrole in the treatment of several diseases [5-8]. For example, it is well known that a ω-3 PUFA-based diet is a good way of treating the hyper lipidemia associated with junk food consumption, which is rich in saturated fatty acids, responsible for atherosclerotic plaque formation, particularly around heart tissue. Various food supplements and nutraceuticals are based on ω-3 PUFAs and are used to promote positive cardiovascular health. Substantial (2 g/day) intakes of ω-3 PUFAs efficiently reduce plasma Triacylglycerol (TG) concentrations. This is the most relevant effect of ω-3 PUFAs on plasma lipids and has been explained by different mechanisms such as decreased TG synthesis due to reduced substrate availability subsequent to lipogenesis inhibition and β-oxidation stimulation and a shift in lipid synthesis toward phospholipids rather than TG [5]. Moreover, DHA is a constituent of retinal tissue and ω-3 PUFAs have shown cytoprotective and cytotherapeutic actions, contributing to several anti-angiogenic and neuroprotective mechanisms within the retina [6]. DHA also contributes to the formation of phospholipids in brain tissue, and several studies and clinical trials in healthy individuals indicate that long-chain ω-3 Poly Unsaturated Fatty Acid (ω-3 LC-PUFAs) intake may be associated with increased functional activation of the prefrontal cortex in children, and greater gray matter volume and white matter integrity during aging. However, its effects on cognition are not clear and, at the moment there is

Citation: Frattaruolo L, Aiello F, Carullo G, Fiorillo M, Brindisi M, Pilco G , et al. Polyunsaturated Fatty Acids and their Role in the Diet of Cancer Patients: An Overview. Int J Nutr Sci. 2018; 3(2): 1024.

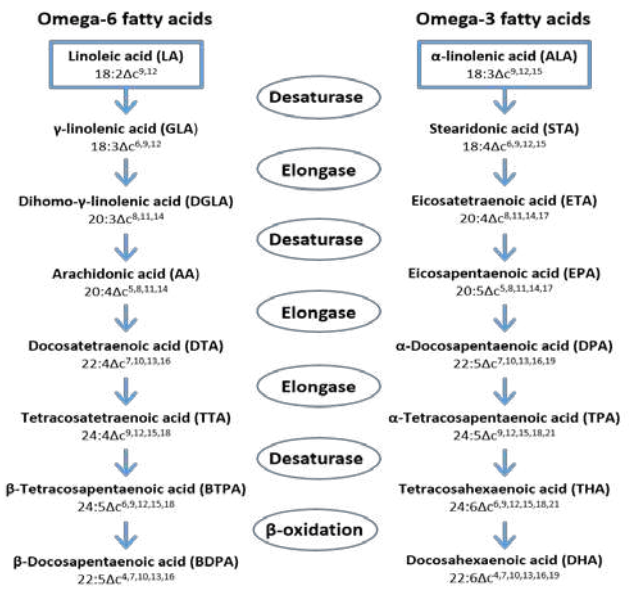

Figure 1: Biosynthesis of long-chain PUFAs, through elongation/desaturation system.

only limited evidence to support the hypothesis that ω-3 LC-PUFA supplementation is beneficial in brain disorders, such as Alzheimer's disease, attention deficit/hyperactivity disorder, major depressive disorder and schizophrenia [7].

A report by a FAO/WHO expert panel supported the hypothesis that high PUFA intake is a 'probable' beneficial factor for diabetes; although further experimental data demonstrated that the relations between fatty acid intake and markers of type 2 diabetes risk may depend on the dietary sources of the fatty acids [8].

Fatty acids, moreover, are versatile molecules which can be conjugated to various substrates with the aim of improving the biological activity of the substrate itself and, in this field, several examples are present in literature. For example, unsaturated fatty acids have been conjugated with hormones for androgen-requiring therapy [9]. Or with flavonoids to improve antioxidant capacity [10,11].

ω-3PUFA antitumor activity

In vitro and *in vivo* studies have highlighted ω-3 PUFAs' antitumor activity. These molecules are indeed able to induce cancer cell death by intrinsic and extrinsic apoptotic pathways. Over the years, various studies have been carried out, aiming to identify the molecular mechanism by which ω-3 PUFAs perform their activity. The results have shown that these molecules are characterized by a complex action mode and that their anti tumoral effect seems to be the consequence of different coexistent mechanisms, such as lipid raft alterations, PPARγ alterations and oxidative stress induction (Figure 2).

Alteration of Lipid Rafts Composition and Function

ω-3 PUFAs are incorporated into phospholipids of biological membranes. The presence of ω-3 PUFAs in the plasma membrane changes its chemical-physical properties such as permeability, fluidity and the activity of proteins associated with it. For example, ω-3 PUFAs are able to alter specific micro domains of the lipid membrane, termed lipid rafts. These domains are characterized by high cholesterol and sphingolipid content and include proteins that mediate different signal-transduction processes, such as those involved in the proliferative stimulus and cell survival. Several studies performed on T-cells and different tumor cell lines have shown that the incorporation of ω-3 PUFAs into membranes leads to an imbalance in phospholipid composition and in the amount of cholesterol in lipid rafts. This structural alteration evolves towards displacement of several raft-associated onco-proteins, including Epidermal Growth Factor Receptor (EGFR), protein a superficial di membrane c-erbB-2 (c-erbB-2), heat shock protein 90 (Hsp90), protein-chinasi B (Akt), and proto-oncogene tyrosine-protein kinase (Src), over expressed or functionally alternated in several tumor cell lines and responsible for uncontrolled tumor proliferation [12-16].

Pparγ activation and gene expression regulation

ω-3 PUFAs are able to interact with the family of Peroxisome Proliferator-Activated Receptors (PPARs), several studies having shown that ω-3 PUFAs are able to activate the PPARγ receptor. PPARs bind to a specific DNA sequence termed Peroxisome Proliferator Response Element (PPRE). Most known target genes of PPARγ regulate lipid metabolism and transport, but some of its targets are cancer-related genes, involved in different ways in cellular growth and survival. *In vitro* and *in vivo* studies, performed on breast and prostatic cancer and lymphocytic leukemia models, have demonstrated that PPARγ targets related to the anticancer effect of ω-3 PUFAs include the promoters of protein tumor suppressor p^{53}, Fas ligand and syndecan 1, which are involved in cell cycle arrest and in the triggering of extrinsic and intrinsic apoptotic processes [17-20].

Lipid Peroxidation and Oxidative Stress

The antineoplastic activity of ω-3 PUFAs has also been associated with their ability to stimulate ROS production at cellular level and to induce oxidative stress [21,22]. This seems to be due to the susceptibility to peroxidation processes of ω-3 PUFAs incorporated in plasma and mitochondrial membranes; thus, the highly reactive products generated by these oxidative mechanisms are able to react with biological macromolecules and to form DNA adducts [23]. Further studies have shown that the ability of these molecules to increase Reactive Oxygen Species (ROS) levels is responsible for sensitizingcancer cells to the activity of different anticancer agents, in combined treatments [24]; the pro-oxidant nature at the base of this latter synergistic activity has been confirmed by investigations in which loss of activity has been evidenced after administration of antioxidant agents [25].

Enzymatic Oxydation Metabolites

At cellular level, ω-3 PUFAs may undergo oxidative metabolism catalyzed by Cyclooxygenase (COX) and Lipoxygenase (LOX) enzymes. ω-3 PUFAs compete with ω-6 PUFAs, such as arachidonic acid, as substrates for the two enzymes, and the products that are obtained from the metabolism of these two classes of PUFAs are very different from a biological potential point of view.

EPA can be hydroxylated by 15-Lipoxygenase (15-LOX) and

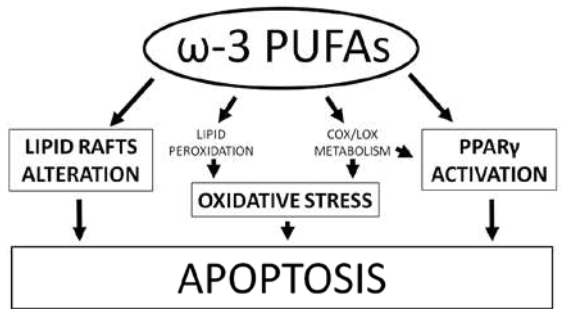

Figure 2: Mechanisms underlying the antitumor effect of ω-3 PUFAs.

Acetylated Cyclooxygenase-2 (acetylated-COX-2) to form 18(R/S)-HEPA, Precursors of E-Series Resolvins (RvE). DHA, similarly, is hydroxylated to form 17S-HDHAand 17R-HDHA, Precursors of D-Series Resolvins (RvD) and protectins. The involvement of resolvins and protectins in the antitumor action of ω-3 PUFAs is unclear. Conversely, these mediators play anti-inflammatory and pro-resolving roles, leading to cellular protection [26]. However, the oxidative metabolism of ω-3 PUFAs is different in cancer cells than in normal cells and this may explain the different effects (cytoprotective-cytotoxic) of these compounds in different cell types. Recent studies have in fact shown that the toxic action of DHA on neuroblastoma cells is due to its conversion to 17-hydroperoxydocosahexaenoic acid (17HpDHA) by 15-LOX activity. This molecule, strongly cytotoxic *via* pro-oxidant mechanisms, is an intermediate in the synthesis of resolvins and protectins, and is quickly metabolized in healthy cells. In neuroblastoma cells, the production of resolvins and protectins is blocked and this is reflected in 17HpDHA accumulation and cytotoxicity [27].

Another bioactive metabolite involved in the antitumor activity of ω-3 PUFAs is Prostaglandin E3 (PGE3), generated from EPA by COX-2. It has shown anti-proliferative, pro-apoptotic and anti-angiogenic activity on human lung cancer cells, through alteration of Epidermal Growth Factor Receptor (EGFR) and Mitogen-Activated Protein Kinases (MAPK) pathways [28].

ω-3PUFA Supplementation in Chemotherapy: Clinical Trials

In cancer, there is a close relationship between malnutrition and disease itself. It is known that undernourished individuals report decreased quality of life, and present increased risks of therapy failure and sideeffects, besides a higher mortality rate [29].

Several recent clinical trials have shown improved chemotherapy tolerability and patient outcomes associated with adjuvant ω-3 PUFA supplementation [28-30].

A clinical study has shown that addition of DHA to chemotherapy is devoid of adverse side effects and may improve the outcome of metastatic breast cancer patients. For example, patients with high incorporation of supplemented DHA experienced longer time to disease progression (8.7 months *vs* 3.5 months) and significantly longer survival (median survival time: 34 months *vs* 18 months) compared to patients with lower incorporation of supplemented DHA [28]. These results suggest that DHA has the potential to specifically chemo sensitive tumors.

Additionally, lung cancer patients receiving platinum-based chemotherapy with fish oil supplementation received more chemotherapy cycles and showed significantly higher tumor response rates (60% *vs* 25.8%), clinical benefits (80% *vs* 42%) and one-year survival rates (60.0% *vs* 38.7%), compared to the control group, proving that ω-3 PUFA supplementation can increase the efficacy of chemotherapy without affecting the toxicity profile [29].

A randomized clinical trial demonstrated that dietary supplementation of ω-3 PUFAs in patients with advanced cervical cancer may help to reduce the inflammatory status, enhancing tumor response to radiation therapy [30].

Moreover, it has been reported that fish oil supplementation (2g/day) for the first 9 weeks of chemotherapy contributes to a delay in tumor progression in colorectal cancer patients, with a significantly longer time to tumor progression in the supplemented chemotherapy group [593 days (±211.5) vs 330 days (±135.1)] [31].

Chemotherapy is commonly associated both with nutritional impact symptoms, which may alter the intake of important nutrients, and with chemotherapy-induced toxicities, leading to lower quality of life, worse outcomes and interruption of prescribed treatment.

Recent clinical trials have shown that ω-3 PUFA supplementation, during chemotherapy, can reduce nutritional impact symptoms such as nausea, vomiting and appetite loss, increasing nutrient consumption and decreasing lean body mass depletion and loss of weight [32-41]. This improvement in nutritional status may be related to the better chemotherapy tolerability and overall patient outcomes, demonstrated in clinical trials. Furthermore, ω-3 PUFA supplementation was reported to significantly reduce the pro-inflammatory status induced by chemotherapy, and other therapy-related toxicities, such as anemia, thrombocytopenia and neuropathy, in colorectal [37,38], lung [39,40], and breast [28,42], cancer patients. Moreover, ω-3 PUFA adjuvant therapy ameliorates methotrexate-induced hepatotoxicity in children and adolescents with acute lymphoblastic leukemia [43].

Conclusion

According to *in vitro* and *in vivo* pre-clinical studies, ω-3 PUFAs are characterized by interesting antitumor activity, due to their ability to interfere with different pathways in cancer cells, through direct action or cell metabolism derivatives. Clinical trials have confirmed the usefulness of ω-3 PUFA nutritional supplementation to improve chemotherapy efficiency and tolerability. Therefore, today, despite the widespread belief that a good nutritional state improves tolerability to chemotherapy, there is not much experimental evidence that closely links feeding with response to chemotherapy treatments; further investigations will be needed to firmly establish this correlation.

References

1. Berg JM, Tymoczko JL, Stryer L. Biochemistry. 7th edition. New York: W. H. Freeman. 2002.
2. Burdge GC, Calder PC. Conversion of α-linolenic acid to longer-chain polyunsaturated fatty acids in human adults. ReprodNutr Dev. 2005; 45: 581-597.
3. Meyer BJ, Mann NJ, Lewis JL, Milligan GC, Sinclair AJ, Howe PR, et al .

Dietary intakes and food sources of omega-6 and omega-3 polyunsaturated fatty acids. Lipids. 2003; 38: 391-398.

4. Wall R, Ross R, Fitzgerald G, Stanton C. Fatty acids from fish: the anti-inflammatory potential of long-chain omega-3 fatty acids. Nutr Rev. 2010; 68: 280-289.

5. Richard D, Bausero P, Schneider C, Visioli F. Polyunsaturated fatty acids and cardiovascular disease. Cell Mol Life Sci. 2009; 66: 3277-3288.

6. SanGiovanni JP, Chew EY.The role of omega-3 long-chain polyunsaturated fatty acids in health and disease of the retina. Progress in retinal and eye research. 2005; 24: 87-138.

7. Bos DJ, van Montfort SJT, Oranje B, Durston S, Smeets PAM. Effects of omega-3 polyunsaturated fatty acids on human brain morphology and function: What is the evidence? Eur. Neuro psycho pharmacol. 2016; 26: 546-561.

8. Wanders AJ, Alssema M, de Koning EJP, le Cessie S, de Vries JH, Zock PL, et al. Fatty acid intake and its dietary sources in relation with markers of type 2 diabetes risk: The NEO study. Eur J ClinNutr. 2016; 1-7.

9. Aiello F, Garofalo A, Aloisi AM, Lamponi S, Magnani A, Petroni A. Synthesis of esters of androgens with unsaturated fatty acids for androgen requiring therapy. Endocrinol Invest. 2013; 36: 390-395.

10. Ziaullah Z, Bhullar KS, Warnakulaasuriya SN, VasanthaRupasinghe HP. Biocatalytic synthesis, structural elucidation, antioxidant capacity and tyrosinase inhibition activity of long chain fatty acid acylated derivatives of phloridzin and isoquercitrin. Bioorg Med Chem. 2013; 21: 684-692.

11. Tundis R, Frattaruolo L, Carullo G, Armentano B, Badolato M, Loizzo MR, et al. An ancient remedial repurposing: synthesis of new pinocembrinfatty acid acyl derivatives as potential anti microbial/anti-inflammatory agents.Nat Prod Res. 2018; 1-7.

12. Stillwell W, Shaikh SR, Zerouga M, Siddiqui R, Wassall SR. Docosahexaenoic acid affects cell signaling by altering lipid rafts. Reproduction Nutrition Development. 2005; 45: 559-579.

13. Schley PD, Brindley DN, Field CJ. (n-3) PUFA alter raft lipid composition and decrease epidermal growth factor receptor levels in lipid rafts of human breast cancer cells. The Journal of nutrition. 2007; 137: 548-553.

14. Rogers KR, Kikawa KD, Mouradian M, Hernandez K, McKinnon KM, Alwah SM, et al. Docosahexaenoic acid alters epidermal growth factor receptor-related signaling by disrupting its lipid raft association. Carcinogenesis. 2010; 31: 1523-1530.

15. Lee EJ, Yun UJ, Koo KH, Sung JY, Shim J, Ye SK, et al. Down-regulation of lipid raft-associated onco-proteins *via* cholesterol-dependent lipid raft internalization in docosahexaenoic acid-induced apoptosis. Biochimicaet Biophysica Acta (BBA)-Molecular and Cell Biology of Lipids. 2014; 1841: 190-203.

16. Ravacci GR, Brentani MM, Tortelli T, Torrinhas RS, Saldanha T, Torres EAF, et al. Lipid raft disruption by docosahexaenoic acid induces apoptosis in transformed human mammary luminal epithelial cells harboring HER-2 overexpression. The Journal of nutritional biochemistry. 2013; 24: 505-515.

17. Bonofiglio D, Gabriele S, Aquila S, Qi H, Belmonte M, Catalano S, et al. Peroxisome proliferator-activated receptor gamma activates fas ligand gene promoter inducing apoptosis in human breast cancer cells. Breast cancer research and treatment. 2009; 113: 423-434.

18. Zand H, Rhimipour A, Bakhshayesh M, Shafiee M, Mohammadi IN,Salimi S. Involvement of PPAR-γ and p53 in DHA-induced apoptosis in Reh cells. Molecular and cellular biochemistry. 2007; 304: 71-77.

19. Sun H, Berquin IM, Owens RT, O'Flaherty JT, Edwards IJ. Peroxisome Proliferator-Activated Receptor γ–Mediated Up-regulation of Syndecan-1 by n-3 Fatty Acids Promotes Apoptosis of Human Breast Cancer Cells. Cancer research. 2008; 68: 2912-2919.

20. Edwards IJ, Sun H, Hu Y, Berquin IM, O'Flaherty JT, Cline JM, et al. *In vivo* and *in vitro* regulation of syndecan 1 in prostate cells by n-3 polyunsaturated fatty acids. Journal of Biological Chemistry. 2008; 283: 18441-18449.

21. Gavino VC, Miller JS, Ikharebha SO, Milo GE, Cornwell DG. Effect of polyunsaturated fatty acids and antioxidants on lipid peroxidation in tissue cultures. Journal of Lipid Research. 1981; 22: 763-769.

22. Pan J, Keffer J, Emami A, Ma X, Lan R, Goldman R, et al. Acrolein-derived DNA adduct formation in human colon cancer cells: its role in apoptosis induction by docosahexaenoic acid. Chemical research in toxicology. 2009; 22: 798-806.

23. Siddiqui RA, Harvey KA, Xu Z, Bammerlin EM, Walker C, Altenburg JD. Docosahexaenoic acid: a natural powerful adjuvant that improves efficacy for anticancer treatment with no adverse effects. Biofactors. 2011; 37: 399-412.

24. Colas S, Germain E, Arab K, Maheo K, Goupille C,Bougnoux P. α-tocopherol suppresses mammary tumor sensitivity to anthracyclines in fish oil-fed rats. Nutrition and cancer. 2005; 51: 178-183.

25. Serhan CN, Chiang N. Endogenous pro-resolving and anti-inflammatory lipid mediators: a new pharmacologic genus. British journal of pharmacology. 2008; 153: S200-S215.

26. Gleissman H, Yang R, Martinod K, Lindskog M, Serhan CN, Johnsen JI, et al. Docosahexaenoic acid metabolome in neural tumors: identification of cytotoxic intermediates. The FASEB Journal. 2010; 24: 906-915.

27. Pan Y, Efuet E, Cartwright C, Fischer SM, Yang P. EPA derived PGE3 inhibits proliferation and angiogenesis of non-small cell lung cancer A549 cells through the EGFR and MAPKinase pathways. Cancer Research. 2012; 72: 600-600.

28. Bougnoux P, Hajjaji N, Ferrasson MN, Giraudeau B, Couet C, Le Floch O. Improving outcome of chemotherapy of metastatic breast cancer by docosahexaenoic acid: a phase II trial. British journal of cancer. 2009; 101: 1978-1985.

29. Murphy RA, Mourtzakis M, Chu QS, Baracos VE, Reiman T,Mazurak VC. Supplementation with fish oil increases first-line chemotherapy efficacy in patients with advanced nonsmall cell lung cancer. Cancer. 2011; 117: 3774-3780.

30. Wuryanti S, Andrijono A, Susworo S,Witjaksono F. The Effect of High Poly Unsaturated Fatty Acid (PUFA) Dietary Supplementation on Inflammatory Status of Patients with Advanced Cervical Cancer on Radiation Treatment. Indonesian Journal of internal Medicine. 2015; 47.

31. Camargo CDQ, Mocellin MC, Pastore Silva JDA, Fabre MEDS, Nunes EA, Trindade EBSDM. Fish oil supplementation during chemotherapy increases posterior time to tumor progression in colorectal cancer. Nutrition and cancer. 2016; 68: 70-76.

32. Bauer JD, Capra S. Nutrition intervention improves outcomes in patients with cancer cachexia receiving chemotherapy-a pilot study. Supportive care in cancer. 2005; 13: 270-274.

33. Bonatto SJ, Oliveira HH, Nunes EA, Pequito D, Iagher F, Coelho I, et al. Fish oil supplementation improves neutrophil function during cancer chemotherapy. Lipids. 2012; 47: 383-389.

34. Trabal J, Leyes P, Forga M, Maurel J. Potential usefulness of an EPA-enriched nutritional supplement on chemotherapy tolerability in cancer patients without overt malnutrition. Nutr Hosp. 2010; 25: 736-740.

35. Van der Meij BS, Langius JAE, Spreeuwenberg MD, Slootmaker SM, Paul MA, Smit EF, et al. Oral nutritional supplements containing n-3 polyunsaturated fatty acids affect quality of life and functional status in lung cancer patients during multimodality treatment: an RCT. European journal of clinical nutrition. 2012; 66: 399-404.

36. Murphy RA, Mourtzakis M, Chu QS, Baracos VE, Reiman T, Mazurak VC. Nutritional intervention with fish oil provides a benefit over standard of care for weight and skeletal muscle mass in patients with nonsmall cell lung cancer receiving chemotherapy. Cancer. 2011; 117: 1775-1782.

37. Read JA, Beale PJ, Volker DH, Smith N, Childs A, Clarke SJ. Nutrition intervention using an Eicosapentaenoic Acid(EPA)-containing supplement in patients with advanced colorectal cancer. Effects on nutritional and inflammatory status: a phase II trial. Supportive Care in Cancer. 2007; 15: 301-307.

38. Mocellin MC, de Silva, JDAP, de QuadrosCamargo C, de SouzaFabre ME, Gevaerd S, Naliwaiko K, et al. Fish oil decreases C-reactive protein/albumin ratio improving nutritional prognosis and plasma fatty acid profile in colorectal cancer patients. Lipids. 2013; 48: 879-888.

39. Finocchiaro C, Segre O, Fadda M, Monge T, Scigliano M, Schena M, et al. Effect of n-3 fatty acids on patients with advanced lung cancer: a double-blind, placebo-controlled study. British Journal of Nutrition. 2012; 108: 327-333.

40. Sánchez-Lara K, Turcott JG, Juárez-Hernández E, Nuñez-Valencia C, Villanueva G, Guevara P, et al. Effects of an oral nutritional supplement containing eicosapentaenoic acid on nutritional and clinical outcomes in patients with advanced non-small cell lung cancer: Randomised trial. Clinical Nutrition. 2014; 33: 1017-1023.

41. Mocellin MC, de QuadrosCamargo, C, de SouzaFabre ME, de MoraesTrindade EBS. Fish oil effects on quality of life, body weight and free fat mass change in gastrointestinal cancer patients undergoing chemotherapy: A triple blind, randomized clinical trial. Journal of Functional Foods. 2017; 31: 113-122.

42. Ghoreishi Z, Esfahani A, Djazayeri A, Djalali M, Golestan B, Ayromlou H, et al. Omega-3 fatty acids are protective against paclitaxel-induced peripheral neuropathy: a randomized double-blind placebo controlled trial. BMC cancer. 2012; 12: 355.

43. Elbarbary NS, Ismail EAR, Farahat RK, El-Hamamsy M. ω-3 fatty acids as an adjuvant therapy ameliorates methotrexate-induced hepatotoxicity in children and adolescents with acute lymphoblastic leukemia: A randomized placebo-controlled study. Nutrition. 2016; 32: 41-47.

Int J Nutr Sci - Volume 3 Issue 2 - 2018
Submit your Manuscript | www.austinpublishinggroup.com

Citation: Frattaruolo L, Aiello F, Carullo G, Fiorillo M, Brindisi M, Pilco G , et al. Polyunsaturated Fatty Acids and their Role in the Diet of Cancer Patients: An Overview. Int J Nutr Sci. 2018; 3(2): 1024.

J. Biochem. 2018;164(4):313–322 doi:10.1093/jb/mvy054

JB THE JOURNAL OF BIOCHEMISTRY

Functional characterization of the partially purified Sac1p independent adenine nucleotide transport system (ANTS) from yeast endoplasmic reticulum

Received March 6, 2018; accepted June 6, 2018; published online June 8, 2018

Yuan Li[1,2], Anna Rita Cappello[1,†], Luigina Muto[1], Emanuela Martello[1], Marianna Madeo[1], Rosita Curcio[1], Paola Lunetti[3], Susanna Raho[2], Francesco Zaffino[1], Luca Frattaruolo[1], Rosamaria Lappano[1], Rocco Malivindi[1], Marcello Maggiolini[1], Donatella Aiello[4], Carmela Piazzolla[2], Loredana Capobianco[3,‡], Giuseppe Fiermonte[2] and Vincenza Dolce[1,*]

[1]Department of Pharmacy, Health, and Nutritional Sciences, University of Calabria, 87036 Arcavacata di Rende, Cosenza, Italy; [2]Laboratory of Biochemistry and Molecular Biology, Department of Biosciences, Biotechnologies and Biopharmaceutics, University of Bari, 70125 Bari, Italy; [3]Department of Biological and Environmental Sciences and Technologies, University of Salento, 73100 Lecce, Italy and [4]Department of Chemistry and Chemical Technology, University of Calabria, 87036 Arcavacata di Rende, Cosenza, Italy

*Vincenza Dolce, Department of Pharmacy, Health, and Nutritional Sciences, University of Calabria, 87036 Arcavacata di Rende, Cosenza, Italy. Tel.: +39-0-984493119, Fax: +39-0-984493107, email: vincenza.dolce@unical.it

†Anna Rita Cappello, Department of Pharmacy, Health, and Nutritional Sciences, University of Calabria, 87036 Arcavacata di Rende, Cosenza, Italy. Tel.: +39-0-984493177, Fax: +39-0-984493107, email: annarita.cappello@unical.it

‡Loredana Capobianco, Department of Biological and Environmental Sciences and Technologies, University of Salento, 73100 Lecce, Italy. Tel.: +39-0-832298864, Fax: +39-0-832298626, email: loredana.capobianco@unisalento.it

Several ATP-depending reactions take place in the endoplasmic reticulum (ER). Although in *Saccharomyces cerevisiae* ER the existence of a Sac1p-dependent ATP transport system was already known, its direct involvement in ATP transport was excluded. Here we report an extensive biochemical characterization of a partially purified adenine nucleotide transport system (ANTS) not dependent on Sac1p. Highly purified ER membranes from the wild-type and Δ*sac1* yeast strains reconstituted into liposomes transported ATP with the same efficiency. A chromatography on hydroxyapatite was used to partially purify ANTS from Δ*sac1* ER extract. The two ANTS-enriched transport activity eluted fractions showed essentially the presence of four bands, one having an apparent MW of 56 kDa, similar to that observed for ANTS identified in rat liver ER. The two fractions reconstituted into liposomes efficiently transported, by a strict counter-exchange mechanism, ATP and ADP. ATP transport was saturable with a Km of 0.28 mM. The ATP/ADP exchange mechanism and the kinetic constants suggest that the main physiological role of ANTS is to catalyse the transport of ATP into ER, where it is used in several energy-requiring reactions and to export back to the cytosol the ADP produced.

Keywords: adenine nucleotide transport system; endoplasmic reticulum; HTP purification; Sac1p; transport.

Abbreviations: AAC, ADP/ATP carrier; ANTS, adenine nucleotide transport system; COX, cytochrome oxidase subunit III; DIDS, 4, 4′-diisothiocyano-2,2′-stilbenedisulfonic acid; DPM1, anti-dolichol phosphate mannose synthase; ER, endoplasmic reticulum; PLP, pyridoxal 5′-phosphate; RER, rough ER; SER, smooth ER; TX-100, Triton X-100; TX-114, Triton X-114.

The endoplasmic reticulum (ER) is a membrane network (*1*) found in every nucleated cell. The morphologically distinct smooth and rough ER (SER and RER, respectively) are formed by the same continuous membrane as the nuclear envelope. Its internal compartment, the ER lumen, is completely separated from the cytosol. This compartmentation often narrows the specificity of luminal enzymes (*2*) because several potential substrates cannot pass the barrier. The transport of selected substrates across the ER membrane is an additional point where enzyme activity can be potentially regulated. It is, therefore, doubtless that ER functions cannot be properly revealed without understanding the related transport processes which, in turn, require the characterization and identification of the participating membrane proteins.

The lumens of the ER and Golgi apparatus are the subcellular sites where dissociation of chaperones-proteins complexes, disulphide bridge formation, protein polymerization, glycosylation and phosphorylation of proteins, proteoglycans or lipids occur (*3*–*9*). It is known that ATP is utilized in the RER lumen in all reactions listed above as energy source (*2*). Furthermore, the degradation of misfolded or overexpressed proteins, a process that requires ATP, has been postulated to occur within the ER lumen (*10*, *11*). ATP is synthesized in cytosol during glycolysis and oxidative phosphorylation within the mitochondria, where is exchanged with the cytosolic ADP by the action of the mitochondrial ADP/ATP carrier (AAC) (*12*, *13*).

Cytoplasmic ATP is imported by a different transport system in various organelles such as peroxisomes (*14*, *15*) and ER (*16*–*18*).

The existence of an ATP transport system inhibited by 4,4'-diisothiocyano-2,2'-stilbenedisulfonic acid (DIDS) was demonstrated in ER-derived vesicles prepared from rat liver and canine pancreas (*16*).

In rat liver ER a saturable transport, highly specific for ATP, was measured in a reconstituted system (*19*), successively a 56-kDa protein was identified as an ATP transporter by photoaffinity labelling and partial purification (*20*). In a more recent study (*21*) an ATP transporter from rat liver RER was solubilized and reconstituted into phosphatidylcholine liposomes, ATP transport was time and temperature dependent, and inhibited by DIDS, but it was unaffected by carboxyatractyloside, a specific inhibitor of the mitochondrial AAC (*13*, *22*).

An ATP transport system and its inhibition by DIDS was also demonstrated in *Saccharomyces cerevisiae* ER (*17*). In yeast ER a 68-kDa protein (Sac1p) was identified as a carrier responsible for ATP transport during protein translocation (*23*). However, it turned out that Sac1p was not an ATP transporter itself, since purified Sac1p reconstituted into proteoliposomes did not catalyse any ATP uptake (*24*), rather it acted as an important regulator of the transport process, probably by controlling ER phosphoinositides. The absence of Sac1p resulted in a defect in microsomal ATP transport; however, microsomes from *sac1*Δ strain retained 15% of ATP transport rate suggesting that another ATP transporter Sac1p independent was present in the microsomal membranes (*23*).

Here we report the biochemical characterization and the partial purification of a Sac1p independent adenine nucleotide transport system (ANTS) in yeast ER.

Materials and Methods

Yeast strains and growth

BY4742 (wild-type), *sac1*Δ (YKL212W), *aac1*Δ (YMR056C), *aac3*Δ (YBR085W), *mme1*Δ (YMR166C), *ymc2*Δ (YBR104W), *ndt2*Δ (YEL006W), *leu5*Δ (YHR002W), *mrs3*Δ (YJL133W), *mrs4*Δ (YKR052C), *mtm1*Δ (YGR257C), *flx1*Δ (YIL134W), *YFR045W*Δ and *ant1*Δ (YPR128C) yeast strains were provided by the EUROFAN resource Centre EUROSCARF (Frankfurt, Germany). Yeast strains were grown in YPD (1% Bacto yeast extract, 2% Bacto peptone and 2% glucose) fermentable medium, the final pH was adjusted to 4.5.

Isolation of yeast organelles

Mitochondria/peroxisomes and microsomes were isolated from the wild-type and deletion strains grown in YPD until the early exponential phase (optical density between 1.0 and 1.5) was reached. The cells were pelleted by centrifugation at 3,000 × g for 5 min at room temperature and washed with distilled water, then they were suspended in 2 ml/g cells (v/w) DTE buffer (100 mM Tris–H_2SO_4, pH 9.4, 10 mM 1, 4-dithioerythritol) and shaken slowly for 10 min at 30°C. The pellet was washed with zymolyase buffer (1.2 M sorbitol, 20 mM potassium phosphate, pH 7.4) and then incubated in 7 ml/g of zymolyase buffer with the addition of 4 mg/g (w/w) Zymolyase-20T (Seikagaku Kogyo Co.) for 45 min at 30°C for conversion into spheroplasts. Homogenization was carried out by 30 strokes in a glass–Teflon potter in 14 ml/g (v/w) ice-cold homogenization buffer (0.6 M sorbitol, 10 mM Tris–HCl, pH 7.4, 1 mM PMSF, 0.2% BSA). This homogenate was diluted with 1 volume of ice-cold homogenization buffer, then cell debris and nuclei were removed by centrifugation at 3,000 × g for 5 min at 4°C. The supernatant was centrifuged twice at 12,000 × g for 15 min at 4°C to recover the mitochondrial/peroxisomal fraction, which was suspended in ST buffer (0.25 M sucrose, 10 mM Tris–HCl, pH 7) to a final concentration of 10 mg of protein/ml. The supernatant was centrifuged at 100,000 × g for 60 min at 4°C, and the resulting microsomal fraction was suspended in ST buffer to a final concentration of 10 mg of protein/ml. About 1 or 10 mg of mitochondrial/peroxisomal and microsomal fractions were stored at −80°C as pellet until use.

Partial purification of ANTS

About 10 mg of frozen microsomes were suspended at a final concentration of 10 mg protein/ml in a solubilization buffer containing 2.5% Triton X-100, 30 mM NaCl, 10 mM PIPES pH 7 and 10 mg/ml asolectin. After 30 min at 4°C the mixture was centrifuged at 100,000 × g for 30 min to obtain a clear supernatant referred to as extract, then 800 µl of extract (5–6 mg protein) were applied on cold hydroxyapatite (HTP) columns (a Pasteur pipette containing 600 mg of dry material) and the elution was performed using the solubilization buffer. Two consecutive fractions, each of 600 µl were collected, 100 µl of each fraction were reconstituted into liposomes.

Reconstitution of ANTS

When microsomal membrane extracts were reconstituted, 1 mg of frozen microsomes was solubilized for 30 min at 4°C in 1 ml of a solubilization buffer containing 2.5% Triton X-100, 30 mM NaCl, and 10 mM PIPES pH 7 and centrifuged for 30 min at 100,000 × g. The microsomal extracts and the HTP eluates were reconstituted into liposomes by the cyclic detergent removal procedure (*25*). In this procedure, the mixed micelles containing detergent, protein and phospholipids were repeatedly passed through a column filled with Bio-Beads SM-2 resin (Bio-Rad Milan, Italy) to remove the detergent. The composition of the initial mixture used for reconstitution was: 100 µl of extracts or HTP eluates (about 80–100 µg and 70–90 ng of proteins, respectively), 70 µl of 10% Triton X-114 (TX-114), 100 µl of liposomes (10 mg of L-α-phosphatidylcholine from egg yolk), prepared as described previously (*26*), 2.4 mg of asolectin, 20 mM PIPES pH 7.0 and, when present, 10 mM internal substrate, in a final volume of 700 µl. After vortexing, this mixture was passed 13 times through the same Bio-Beads SM-2 column (0.5 × 3.5 cm) equilibrated with a buffer containing 10 mM PIPES pH 7.0. All the operations were performed at 4°C, except the passages through Bio-Beads SM-2 column that were performed at room temperature (*27*).

Transport measurements

Approximately 600 µl of proteoliposomes were passed through a Sephadex G-75 column (0.7 × 15 cm) pre-equilibrated with 50 mM NaCl/10 mM PIPES/NaOH pH 7.0 (buffer A). The first 600 µl of the turbid eluate from the Sephadex column were collected, transferred to reaction vessels (100 µl each), and used for transport measurements by the inhibitor stop method (*28*, *29*). Transport was started by adding external labelled substrate at the concentrations indicated in the figure legends. After the required time interval, the reaction was stopped by adding 80 mM pyridoxal 5′-phosphate (PLP); in control samples, the inhibitor was added together with the labelled substrate at time zero. The assay temperature was 25°C. Finally, each sample of proteoliposomes (100 µl) was passed through a Sephadex G-75 column (0.6 × 13 cm) to separate the external from the internal radioactivity. The liposomes eluted with 3 ml of 50 mM NaCl were collected in 4 ml of scintillation mixture, vortexed and counted. For the determination of the [^{14}C]ATP uptake, the experimental values were corrected by subtracting the respective controls (samples inhibited at time zero). For kinetic determinations, the initial transport rate was evaluated from the radioactivity taken up by the proteoliposomes in 1 min, i.e. within the initial linear range of the substrate uptake. Specific transport was referred to the amount of protein in the proteoliposomes (*30*–*32*). For efflux measurements, proteoliposomes containing 2 mM ATP were labelled with 0.01 µM [^{14}C]ATP by carrier-mediated exchange equilibration (*33*, *34*). After 40 min, external radioactivity was removed by passing the proteoliposomes through Sephadex G-75 column. Efflux was initiated by adding unlabelled external substrate or buffer A alone and terminated by the addition of the inhibitor above indicated.

Mass spectrometry and gel digestion

In gel digestion: isolate protein band was destained with a freshly prepared destaining solution (20 ml) that contained 30 mM potassium ferricyanide and 50 mM sodium thiosulfate. The destaining solution was removed, and the gel pieces were washed with 50 μL water (5–7 times) until the yellow colour disappeared. The gel pieces were washed (two times) with 50 μl of 50% acetonitrile (ACN): 50% 200 mM ammonium bicarbonate for 5 min, dehydrated with 50 μL of 100% ACN until the gel turned opaque white and dried in a vacuum centrifuge for 30 min. The gel pieces were rehydrated in 5–10 μl of 50 mM ammonium bicarbonate (37°C, 4 min), an equivalent volume (2–5 μl) of trypsin (Sigma Aldrich) solution (4 pmol/μL) was added. After digestion peptides were recovered by sonication (10 min) in 50 μL of solution, 60% ACN in 5% TFA (vol/vol). The supernatants were pooled and dried by Concentrator Plus system.

Mass spectrometer: MALDI MS and MS/MS analysis. Linear MALDI-TOF spectra were acquired using a 5800 MALDI-TOF/TOF analyser (AB SCIEX, Darmstadt, Germany) equipped with a neodymium: yttrium-aluminium-garnet laser (laser wavelength: 349 nm). About 1 μl portion of a premixed solution of sample and α-CHCA (0.3% in TFA) was spotted on the matrix target, dried at room temperature and analysed in the mass spectrometer.

Spectra were acquired in default calibration mode averaging 2,500 laser shots with a mass accuracy of 50 ppm. Besides, MS and MS/MS analyses were performed with a 5800 MALDI-TOF/TOF analyser in reflectron positive-ion mode. About 1 μl of sample matrix mixed solution was spotted on a MALDI plate and dried. MS spectra were acquired with a laser pulse rate of 400 Hz and at least 4,000 laser shots, while CID-MS/MS experiments were performed at a collision energy of 1 kV, using ambient air as collision gas with a medium pressure of 10^{-6} Torr. CID-MS/MS spectra required up to 5,000 laser shots and a pulse rate of 1,000 Hz.

Database searching and bioinformatics. Proteins were identified by searching a comprehensive protein database using Mascot programs (www.matrixscience.com). Peak harvesting was done automatically using Data Explorer software (Applied Biosystems). Peak resolution was calculated using the Data Explorer software. The query was made for '*Saccharomyces cerevisiae* (baker's yeast) (134,049 sequences)'' taxonomy allowing maximum mass tolerance of 50 ppm and at most two missed cleavages for tryptic peptides. MS/MS interrogation was carried out, with the same parameters as described previously for the PMF research. Peptide sequences were automatically identified by database searching of the MS/MS spectra against the NCBIprot 20180429 (152462470 sequences; 55858910152 residues) database using the MASCOT search program (http://www.matrixscience.com). However, all spectra were manually checked to verify the validity of the MASCOT results. The mass tolerance of the fragments for MS/MS data search was set at 0.25 Da. All MS/MS spectra of peptides were manually processed.

Others methods

Proteins were analysed by SDS-PAGE (*35*) and stained with Coomassie Blue dye or staining (*36*). The amount of protein incorporated into liposomes was measured as described previously (*37*, *38*). Western blot analysis was carried out as described formerly (*39–41*) using an anti-complex IV subunit III (anti-COX) (Invitrogen Milan, Italy) and an anti-dolichol phosphate mannose synthase (DPM1) antibodies (Invitrogen Milan, Italy), specific for the mitochondrial and microsomal fractions, respectively. The antibody against yeast Aac2p was kindly provided by Pelosi (*42*).

Results

Optimization of the solubilization procedure

In order to functionally characterize and to identify the microsomal ANTS, we purified the mitochondrial/peroxisomal and microsomal fractions from wild-type and *sac1*Δ yeast strains by differential centrifugation from yeast homogenate; the latter was used to unravel the role of Sac1p in the transport of ATP across the ER membrane. The two fractions were chromatographed on SDS-PAGE and tested for their purity by western blot analysis. The yeast anti-COX antibody immunodecorated a single band with an apparent molecular mass of about 26 kDa only in the mitochondrial/peroxisomal fractions (Fig. 1A, lane M/P); whereas the yeast anti-DPM1 antibody immunodecorated a single band with an apparent molecular mass of about 30 kDa only in microsomal fractions (Fig. 1A, lane ER).

Initially the transport measurements were carried out on microsomal fractions purified from both wild-type and *sac1*Δ yeast strains. No difference was found between the two fractions concerning their efficiency to transport ATP and their sensitivity to the inhibitors DIDS and carboxyatractyloside, in all the initial reconstitution conditions tested (Fig. 1B). Once excluded a possible involvement of Sac1p in the ER ATP transport, the remaining transport experiments were carried out only on the microsomal fraction purified from *sac1*Δ yeast strain.

In order to better understand the mechanism of functioning of this transport system, we first optimized the reconstitution procedure of the microsomal fraction. This aim was reached by adjusting the main parameters able to affect the percentage of the active transporter extracted by the detergent from the microsomal membranes and the efficiency of its incorporation into liposomes, i.e. the detergent/lipid ratio, the number of passages through the same Bio-Beads SM-2 column and the pH of the reconstitution mixture (*38*). The solubilization of membrane proteins by detergents is a critical step to obtain active extracted proteins suitable for the further successful biochemical characterization (*43*). The same amount of microsomal membranes (about 1 mg) was solubilized for 20 min at 4°C with a buffer containing TX-100 or TX-114, two non-ionic detergents, 30 mM NaCl and 10 mM PIPES, pH 7. On the basis of our previous experience on membrane proteins solubilization, two different detergent concentrations were chosen, 1, 5 and 2, 5% (w/v) (*38*, *43*). Once removed the residual unsolubilized material by centrifugation, the supernatant (80–100 μg of proteins) was incorporated into liposomes. In all tested conditions, no significant difference was observed in the measured transport activities, even though the highest activity was found in extracts solubilized in the presence of TX-100 (2, 5% w/v) (Fig. 2A). In order to verify the efficacy of our solubilization procedure in term of amount of transport activity recovered per μg of microsomal membrane proteins used, we solubilized the same amount of ER membranes using 3% TX-100, 150 mM Na_2SO_4 and 10 mM Tris–HCl pH 7, as described previously by Mayinger *et al.* (*23*); in four independent experiments only 20% of the ATP/ATP exchange activity reported in Fig. 1 was found (data not shown). Several detergent/phospholipid ratios were tested in order to optimize the reconstitution procedure. In such experiments, the [^{14}C]ATP/ATP exchange rate was measured, and the optimal transport activity was obtained by reconstituting the microsomal extracts in the presence of 7 mg of Triton X-114 (1% w/v), 10 mg of L-α-phosphatidylcholine (1, 42% w/v) and 2, 4 mg of

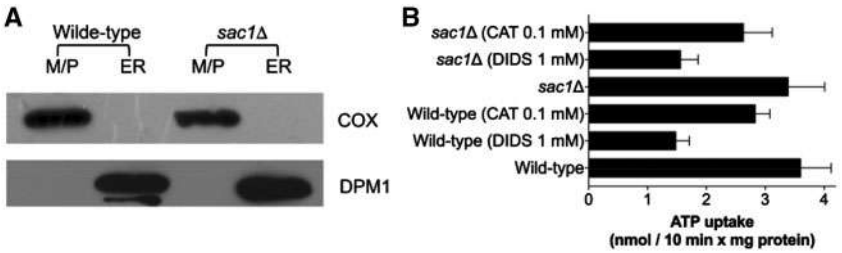

Fig. 1 Subcellular fractionation analysis. (**A**) The mitochondrial/peroxisomal (M/P) and ER fractions were isolated by differential centrifugation from the wild-type and *sac1*Δ yeast strains homogenate, subjected to SDS-PAGE (50 μg/lane) and tested for their purity by western blot analysis. The subcellular fractions were transferred to nitrocellulose and immunodecorated with antibodies raised against COX or DPM1, top and bottom panels, respectively. (**B**) Purified ER membranes from the wild-type and sac1Δ yeast strains, were solubilized by TX100 detergent and reconstituted into proteoliposomes in the presence of 10 mM ATP. Transport was started by external adding 0.1 mM [^{14}C]ATP and stopped after 10 min; the inhibitors, carboxyatractyloside (CAT) or DIDS were added together with the labelled substrate. Values are means ± S.D. of at least three independent experiments.

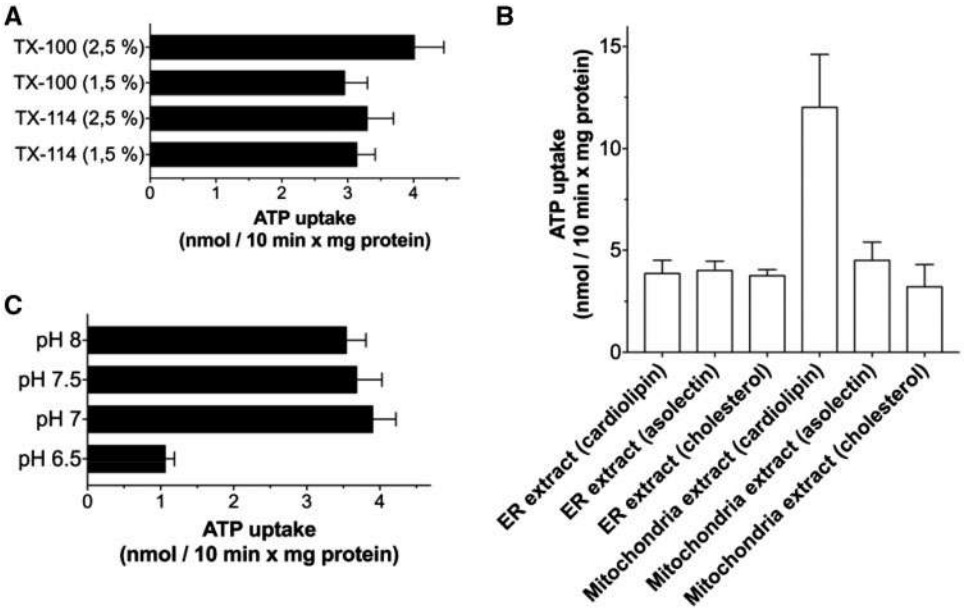

Fig. 2 Optimisation of ANTS transport activity. (**A**) Effect of detergent solubilisation on ANTS transport activity. Microsomal membranes were solubilized for 30 min in a buffer containing different concentrations of TX-100 or TX-114. (**B**) Dependence of ANTS and mitochondrial ADP/ATP carrier transport activities on different lipids added to the reconstitution mixture. Microsomal membranes (ER) and mitochondria were solubilized with TX-100 (2.5% w/v), both extracts were reconstituted into liposomes in the presence cardiolipin (0, 2 mg/ml), asolectin (3, 4 mg/ml) and cholesterol (5 mg/ml). (**C**) Effect of pH on ANTS reconstitution. All the experimental procedures from the reconstitution to the transport measurements (see Materials and Methods) were performed in 20 mM PIPES/HEPES buffer at the indicated pH. (A–C). The solubilized material was reconstituted into liposomes containing saturating concentration of ATP. Transport was started by external adding 0.1 mM [^{14}C]ATP and stopped after 10 min. Values are means ± SD of at least three independent experiments.

asolectin (0, 34% w/v), with an optimal detergent/phospholipid ratio of 0.56 w/w (data not shown). Asolectin was required in the reconstitution mixture to get a functional active transporter. The addition in the reconstitution mixture of cardiolipin, (20–200 μg/ml), which was essential to reconstitute in a more active form the mitochondrial AAC carrier (*44*, *45*) (Fig. 2B) or of cholesterol (1–5 mg/ml), used to assay the ER Sac1p-dependent ATP transport (*23*), did not exert any ameliorative effect on the ATP/ATP exchange activity (Fig. 2B). The influence of different pH values in the solubilization buffer and reconstitution mixture on the [^{14}C]ATP/ATP exchange rate was also investigated. The highest transport rates were measured in a range of pH between 7 and 8, even though at pH 7 a higher reproducibility of the maximal transport activity was observed. At pH values lower than 7, the rate of ATP transport drastically decreased (Fig. 2C).

Partial purification of the microsomal ANTS on HTP

In order to identify the putative protein responsible for the [^{14}C]ATP/ATP transport activity measured in the reconstituted microsomal extract, the TX-100 extract of ER membranes was applied on a HTP column and several fractions were recovered by eluting the column with the same solubilization buffer. Only in the first 2 fractions some bands were visible on silver-staining

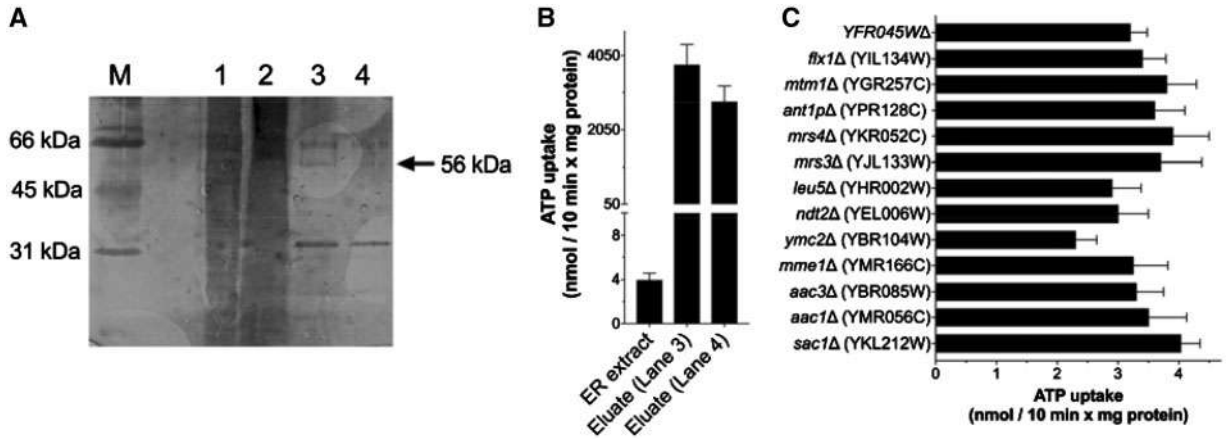

Fig. 3 Partial purification of ANTS from *sac1*Δ yeast ER. (**A**) SDS/PAGE of fractions obtained by hydroxyapatite chromatography. Lane M, marker proteins (BSA, ovalbumin and carbonic anhydrase); lane 1, SDS ER extract; lane 2, TX-100 ER extract; lanes 3 and 4, first and second fraction eluted from the HTP column loaded with TX-100 ER extract, respectively. (**B**) About 80–100 μg and 70–90 ng of proteins from TX-100 ER extract (lane 2) and HTP eluates (lanes 3 and 4), respectively, were reconstituted into liposomes in the presence of 10 mM internal ATP. Transport was initiated by adding 0.1 mM [^{14}C]ATP and terminated after 10 min. (**C**) TX-100 ER extracts (about 80–100 μg of proteins) from different yeast deletion strains were reconstituted into liposomes and assayed as reported in (B). Values are means ± S.D. of at least three independent experiments (A and B).

SDS-PAGE (Fig. 3A, lanes 3 and 4), 100 μl of each fractions were reconstituted into liposomes. Both reconstituted fractions catalysed an efficient [^{14}C]ATP/ATP exchange reaction (Fig. 3B). By comparing the [^{14}C]ATP/ATP exchange activity catalysed by the reconstituted extract (Fig. 3A, lanes 2) with those of the two fractions (Fig. 3A, lanes 3 and 4), it was evident that the purification step increased ANTS-specific activity by about 950-fold (Fig. 3B). Interestingly, the two HTP fractions showed essentially four bands with apparent molecular weights of 30, 56, 64 and 65 kDa, respectively. Since many members of the mitochondrial carrier family (MCF) have a molecular weight of about 30 kDa, in order to exclude that the 30 kDa band could derive from the presence of one of the functionally unknown or biochemically not characterized mitochondrial carrier (MC) in the ER membrane, we reconstituted the ER membrane extracts of the following deletion strains: *aac1*Δ (*Y*MR056C), *aac3*Δ (YBR085W), *mme1*Δ (YMR166C), *ymc2*Δ (YBR104W), *ndt2*Δ (YEL006W), *leu5*Δ (YHR002W), *mrs3*Δ (YJL133W), *mrs4*Δ (YKR052C), *mtm1*Δ (YGR257C), *flx1*Δ (YIL134W), *YFR045W*Δ and *ant1*Δ (YPR128C). The last strain was tested since Ant1p, although biochemically characterized (*15*), was the only member of the yeast MCF not localized in the mitochondria but in the peroxisomal membrane. No significant difference was found between the [^{14}C]ATP/ATP exchange reaction catalysed by the *sac1*Δ ER extract and those of the various MCs deletion yeast strains (Fig. 3C). Furthermore, we excluded that the 30 kDa band could represent the yeast Aac2p, the most abundant isoform of the yeast mitochondrial adenine nucleotide carrier, since it did not react against a specific antibody (*42*) (data not shown). The tryptic digest from 56 kDa gel band was examined in MS reflection mode, whereas MS/MS experiments were used for peptide sequence discrimination. Identification of the peptides, however, was unsuccessful probably due low sample amounts (Supplementary Data).

Functional characterization of the reconstituted ANTS

The biochemical characterization of ANTS was carried out on the HTP eluates. Since the patterns of proteins eluted in the two HTP fractions (Fig. 3A, lanes 3 and 4) were similar and the highest [^{14}C]ATP/ATP exchange activity was found not only in the first fraction (Fig. 3, lane 3), but, sometimes, also in the second fraction (Fig. 3, lane 4), we decided to pool the first and second fraction before proceeding to the reconstitution step. The [^{14}C]ATP/ATP exchange activity catalysed by the reconstituted ANTS was fully inhibited by PLP, thus all the transport measurements were carried out by using PLP as stop inhibitor (*28*). No transport activity was detected when phosphate, glucose, carnitine and glutamine homoexchanges (internal concentration, 10 mM; external concentration 0.1 mM) were checked or with HTP eluates boiled before incorporation into liposomes (data not shown).

ANTS reconstituted into liposomes catalysed a counter-exchange of 0.25 mM external [^{14}C]ATP for 10 mM internal ATP following a first-order kinetic behaviour (rate constant, 0.22 min^{-1}), isotopic equilibrium being approached exponentially (Fig. 4A). Maximum uptake of [^{14}C]ATP was approached after 20 min. The corresponding value at infinite time was 8.26 μmol/mg protein. The initial rate of ATP uptake (the product of k and the maximal amount of ATP taken up at equilibrium) was 1.87 μmol/min × mg protein. In contrast, no [^{14}C]ATP uptake was observed without internal substrate (i.e. when, internal 10 mM ATP was replaced with the same internal amount of NaCl), demonstrating that the transporter did not catalyse a unidirectional transport (uniport) (Fig. 4A). This issue was further investigated by measuring the efflux of [^{14}C]ATP from pre-labelled active proteoliposomes, as this provides a more sensitive assay for unidirectional transport (*46*). In the absence of external substrate, no significant efflux was observed,

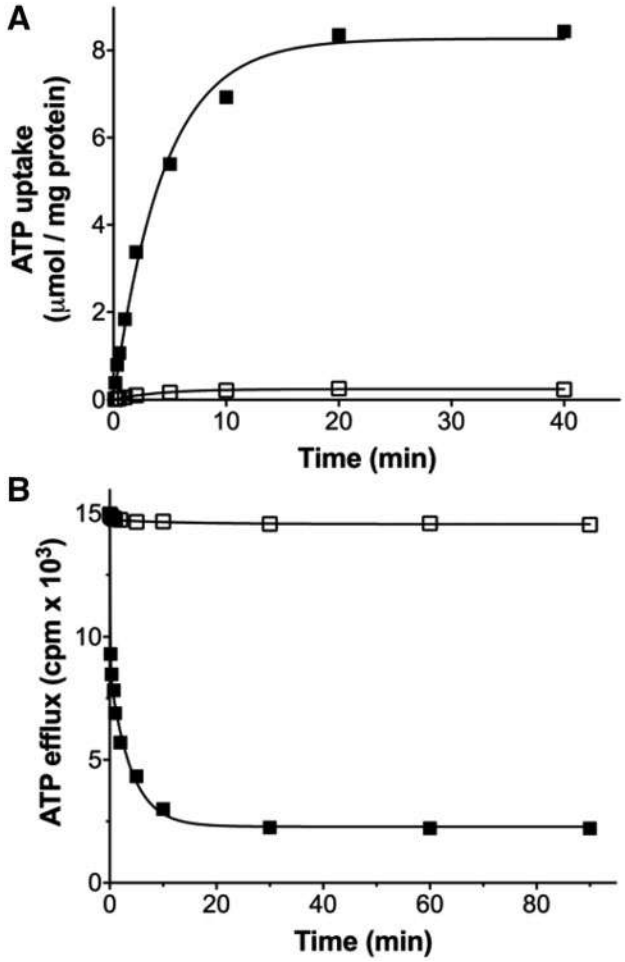

Fig. 4 Kinetics of [^{14}C]ATP transport in proteoliposomes reconstituted with partially purified ANTS. (**A**) [^{14}C]ATP (0, 25 mM) was added to proteoliposomes reconstituted with the HTP elutes (about 70–90 ng of proteins) and containing 10 mM ATP (exchange, ■) or 10 mM NaCl (uniport, □). (**B**) Efflux of [^{14}C]ATP from proteoliposomes reconstituted as reported in (A). The internal substrate pool (2 mM ATP) was labelled with [^{14}C]ATP by carrier-mediated exchange equilibration. Proteoliposomes were then passed through a Sephadex G-75 column. The efflux of [^{14}C]ATP was initiated by adding buffer A alone (□) or 10 mM ATP in buffer A (■). Similar results were obtained in three independent experiments for both uptake and efflux of ATP.

even after an incubation of 90 min (Fig. 4B). However, upon addition of external ATP, an extensive efflux of radioactivity occurred. These results showed that the reconstituted ANTS catalysed an obligatory exchange reaction of substrates.

The substrate specificity of ANTS was examined in detail by measuring the rate of [^{14}C]ATP uptake into proteoliposomes that had been pre-loaded with a variety of substrates (Fig. 5A). The highest activities were observed in the presence of internal ATP and ADP. The external [^{14}C]ATP was also exchanged at lower but significant levels with AMP, dATP, dADP, dAMP, GTP, GDP and GMP. Very low transport rates were measured using internal dGTP, dGDP, dGMP, ITP and IDP. No significant exchanges were measured with all the other internal nucleotides tested (Fig. 5A). These results clearly demonstrate that, from the internal side of the proteoliposomal membrane, the substrate specificity of the microsomal ANTS is confined essentially to adenine nucleotides and, to a lesser extent, to guanine nucleotides.

The effects of inhibitors on the [^{14}C]ATP/ATP exchange reaction catalysed by the reconstituted yeast ANTS were also examined (Fig. 5B). The lysine reagent, PLP, chosen as stop inhibitor (*28*, *47*), caused the complete inhibition of ANTS function. As many other transport proteins, it was sensitive to organic mercurials, being virtually completely blocked by 0.1 mM $HgCl_2$ and 0.1 mM mersalyl and highly inhibited by 0.1 mM N-ethylmaleimide and 0.1 mM p-chloromercuribenzoate. DIDS, the well-known and powerful inhibitor of the Sac1p-dependent RE ATP transporter (*17*), markedly decreased the ATP/ATP exchange activity when it was used at 1 mM concentration. Bongkrekic acid and carboxyatractyloside (*13*, *22*) are known to be specific inhibitors of the mitochondrial AAC. The use of 10 μM bongkrekic acid and of carboxyatractyloside concentrations higher than 0.1 mM resulted in only slight inhibition, indicating no contamination of this fraction with mitochondrial/peroxisomal fractions (*15*, *48*).

Kinetic characteristics of the reconstituted yeast ANTS

The kinetic constants of the partially purified ANTS were determined by measuring the initial transport rate at various external [^{14}C]ATP concentrations in the presence of a constant saturating internal concentration of 10 mM ATP. The K_m and V_{max} values calculated from 13 independent experiments at 25°C were 0.28 ± 0.02 mM and 3.98 ± 0.2 μmol/min per mg of protein, respectively. In order to measure the affinity of ANTS for some of the well transported nucleotides, we checked their ability to inhibit the [^{14}C]ATP/ATP exchange reaction when added to a fixed concentration together with various external [^{14}C]ATP concentrations. ADP, GTP and GDP were competitive inhibitors of the [^{14}C]ATP uptake because they increased the apparent K_m without changing V_{max} (not shown); the measured K_i values were 0.07 ± 0.01 mM, 0.42 ± 0.05 mM and 0.35 ± 0.03 mM, respectively (means of three experiments for each).

Discussion

The existence of an ATP transport system has already been demonstrated in eukaryotes (*23*, *24*, *49*). The transport of ATP from the cytosol to the ER lumen is essential for the protein translocation across the ER membranes since the transfer of the bound protein precursors into the translocation pore and the subsequent transport is mediated by ATP-dependent ER chaperones (*6*, *50*), as well as glycosylation or phosphorylation of many proteins, proteoglycans and lipids, occurring in the ER lumen, are all ATP-dependent reactions (*7*).

Although the presence of a Sac1p-dependent ATP/ADP exchange activity in the yeast microsomal membranes has already been reported (*23*, *24*), its function

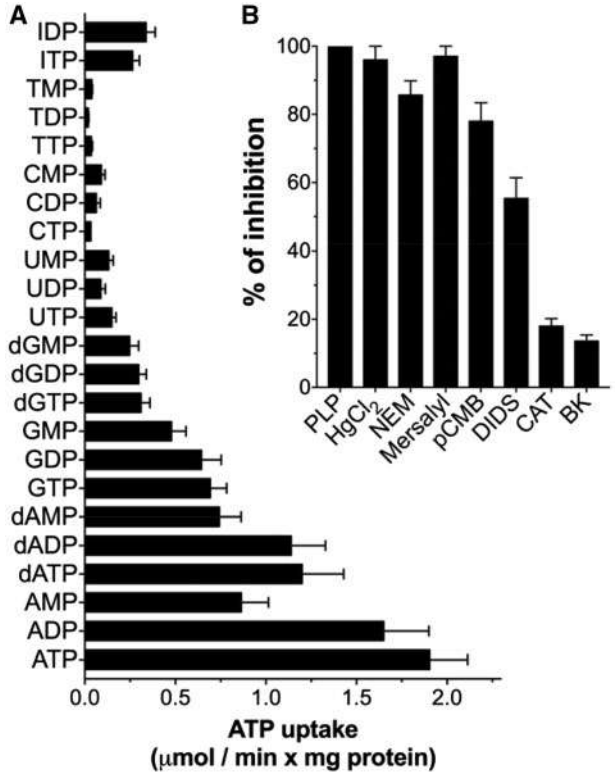

Fig. 5 Substrate specificity and inhibitor sensitivity of the partially purified ANTS. (**A**) Dependence of ANTS transport activity on internal substrate. Proteoliposomes reconstituted with the HTP eluates (about 70–90 ng of proteins) were preloaded internally with various substrates (10 mM concentration). Transport was started by adding 0.25 mM [^{14}C]ATP and stopped after 1 min. (**B**) Effect of inhibitors on the [^{14}C]ATP/ATP exchange reaction catalysed by ANTS. Proteoliposomes, reconstituted as reported in (A), were preloaded internally with 10 mM ATP; transport was initiated by adding 0.25 mM [^{14}C]ATP and terminated after 1 min. Thiol reagents were added 2 min before the labelled substrate; the other inhibitors were added together with 0.25 mM [^{14}C]ATP. The final concentrations of the inhibitors were 0.1 mM carboxyatractyloside (CAT); 10 μM bongkrekic acid (BK); 0.1 mM *p*-chloromercuribenzoate (pCMB); 0.1 mM mersalyl; 0.1 mM $HgCl_2$; 0.1 mM *N*-ethylmaleimide (NEM); 1 mM DIDS; 80 mM pyridoxal 5′-phosphate (PLP). Values are means ± S.D. of at least four independent experiments.

as a ER ATP/ADP transporter has been excluded since the reconstituted recombinant Sac1p did not catalyse any ATP/ADP exchange activity (*24*). On this basis, we have decided to shed light on this transport system. In order to unravel the role of Sac1p in the ER nucleotides transport, microsomal membranes from the wild-type and *sac1*Δ yeast strains were reconstituted into liposomes. Differently from what previously reported (*23*, *24*), in our experimental conditions both membrane extracts from wild-type and *sac1*Δ ER catalysed the same ATP/ADP exchange activity and showed the same sensitivity to CAT and DIDS (Fig. 1B). These results clearly demonstrate that Sac1p has nothing to do with the measured ER ATP/ATP exchange activity. Similar results were previously found in the functional characterization of the ATP transporter from rat liver RE (*20*), where a 56 kDa purified protein was identified as responsible for an ATP/ADP exchange activity in the RE; no band at 67 kDa, weight typical of the mammalian SAC1 (*51*), was detected in the purified fraction (*20*). In order to identify the yeast ER ANTS and to reduce the huge amount of proteins present in the ER extract which could interfere with the reconstitution of the ATP transporter into liposomes, a purification attempt was carried out. By applying TX-100-solubilized *sac1*Δ *ER extract* on an HTP column, we recovered two active fractions (Fig. 3A, lanes 3 and 4), which essentially showed the same electrophoretic pattern and a similar ATP/ATP exchange activity (Fig. 3B). The two purified fractions were about 950-fold enriched with respect to the ATP/ATP exchange activity and contained four bands, one at 30 kDa, another at 56 kDa and a double band at 65–66 kDa. The 56 kDa band could represent the putative yeast orthologue of the rat microsomal ATP transporter, since a similar purification pattern was previously obtained during the identification of the rat liver microsomal ATP transporter, with a molecular weight of 56 kDa (*20*); in that work, using a photoaffinity labelling approach, the authors established that the 30 kDa band could be due to the degradation of the 56 kDa band. Furthermore, the high degree of homology very often found between yeast and mammalian orthologues (*52*) tipped the scales in favour of the 56 kDa band, since the same MW was found for the rat liver ER ATP transporter (*20*).

Several attempts, to further purify the yeast ER transporter by using different kind of chromatography failed, most probably due to the low levels of protein recovered in the HTP fractions. For this reason, the further biochemical characterization of the yeast ER ANTS was carried out on the HTP eluates. Before proceeding with these experiments, it was important to exclude that the ATP/ATP exchange activity measured in the HTP eluates was not due to the presence of a MCF member in the microsomal membranes, since among the four bands, visible on the SDS-PAGE of the HTP eluates, the one at 30 kDa was the most abundant and many members of the MCF have a MW ranging from 30 to 36 kDa (*52*). This doubt was soon ruled out, since the reconstituted microsomal membranes of the yeast strains carrying single deletions for each of the biochemically not characterized MCs showed the same ATP/ATP exchange activity as that of the *sac1*Δ ER extract (Fig. 3C). The tryptic digest from 56 kDa gel band was examined in MS reflection mode, whereas MS/MS experiments were used for peptide sequence discrimination. The human keratins originate from chemicals and/or sample handling become ubiquitous at low levels, as in the context of silver-stained gels. The pattern of keratin peptides is not predictable, thus the interrogation of the PMF (MASCOT search program), contaminants 20090624 (262 sequences; 133,770 residues) was performed as control. Keratin, type II cuticular Hb6 (Hair keratin, type II Hb6) (ghHb6)—Homo sapiens (Human) was identified using two masses corresponding to two possible sequences characterized by insignificant protein scores (score <20) (Supplementary Fig. S1). Searching the complete set of tryptic peptide masses in a NCBIprot 20180429 (152462470 sequences; 55858910152 residues), Taxonomy [*Saccharomyces cerevisiae* (baker's yeast) (134,049 sequences)], Top Score: 89 for AJV32483.1,

Imd2p [*Saccharomyces cerevisiae* YJM1342] (Supplementary Figs S2 and S3), sequence coverage of 19%. MS/MS (*53*, *54*) evaluation assigned a total of 2 peptides to the AJV32483.1, Imd2p (*Saccharomyces cerevisiae* YJM1342) (Supplementary Fig. S4). Further database searches did not retrieve any significant matches and we therefore concluded that band 56 kDa contained mainly one YJM1342. Imd2p is inosine-5'-monophosphate dehydrogenase, catalysing the conversion of inosine 5′-phosphate (IMP) to xanthosine 5′-phosphate (XMP). The identification of the band was unambiguous since the other retrieved proteins identified had significantly fewer matching tryptic peptides, a different intact molecular weight, and were from a different species. MS and MS/MS data suggest that the identification of the protein responsible for the transport activity was unsuccessful probably due to the very low amounts present in the sample.

The biochemical characterization of the partially purified ER ANTS was carried out by following a procedure successfully used to identify most of the mitochondrial transport systems (*28*, *55*) including the mitochondrial (*13*, *22*) and peroxisomal (*14*, *15*) ADP/ATP transporters.

Interestingly, ANTS efficiently exchanged ATP not only when ATP or ADP were present inside the proteoliposomes, but also in the presence of internal AMP, dATP, dADP dAMP and guanine nucleotides (Fig. 5A). A guanine nucleotides transport by ANTS had never been described up to date. Furthermore, ANTS substrate specificity is not shared with any of the functionally known MCs, ruling out, once again, that the 30 kDa band in the HTP eluates could be due to the presence of a MCF member in the microsomal membranes. Although the guanine nucleotides transport catalysed *in vitro* by ANTS may not necessarily occur *in vivo*, it should be emphasized that a GTP/ATP exchange activity was also found in the chromaffin granules (*56*).

Similarly to the yeast Sac1p-dependent ATP transporter, the partially purified ANTS showed a significant inhibitor sensitivity toward DIDS and was scarcely affected by carboxyatractyloside and bongkrekic acid, two potent inhibitors of the mitochondrial adenine nucleotide carrier (*22*, *57*) (Fig. 5B).

Lastly, it should be noted that the affinity towards ATP showed by the partially purified ANTS was about 30-fold lower than that measured for the yeast Sac1p-dependent and the rat liver microsomal ATP transporter (*20*, *23*). The Km for ATP measured in our experimental conditions was 0.28 mM whereas those previously found for the yeast and rat microsomal ATP transporter were about 10 μM. One possible explanation of this difference may reside in the different measuring conditions used to determine the kinetic constants. They are usually determined by measuring the initial transport rate at various external labelled substrate concentrations. These measurements should be taken at very short interval of time, when the transport rate is a linear function of time. Thus it is important to block all samples (having different external substrate concentrations) instantaneously, completely and at the same time in order to get reliable results, here we used the technique of the stop-inhibitor (*28*), which guarantees all these conditions; differently, the kinetic parameters previously measured for the yeast and rat liver ER transporter (*20*, *23*) were determined by blocking the exchange reactions by the filtration technique which requires some seconds. It should also be emphasized that a K_m for ATP in a millimolar range, found in this work, was also demonstrated for the ATP transporter of the chromaffin granules (*56*). Furthermore, a K_m for ATP in a millimolar range would be physiologically more relevant, since cytosolic ATP concentration is in the same range (*58*). A micromolar Km for ATP was found for the yeast mitochondrial adenine nucleotide carrier (*48*), but in this case it is physiologically relevant, since ATP concentration in the mitochondrial matrix is much lower than that of the cytosol (*59*), and it should be kept low in order to keep the oxidative phosphorylation going.

This report represents the first partial purification of the yeast ER ANTS completely independent on the presence of Sac1p. ANTS functional characterization into liposomes suggests that its main physiological role could be to transport ATP in the ER lumen in exchange for ADP, playing a crucial role in the great variety of ATP-requiring reactions occurring in the ER. Although, a 56 kDa band has been identified as the most probable candidate of the yeast ER ANTS, further studies are required to confirm its identity.

Supplementary Data

Supplementary Data are available at *JB* Online.

Funding

This work was supported by Associazione Italiana per la Ricerca sul Cancro (MM grant n. 16719/2015) and by Associazione Italiana per la Ricerca sul Cancro (FG grant n. 15404/2014).

Conflict of Interest

None declared.

References

1. Palade, G.E. (1956) The endoplasmic reticulum. *J. Biophys. Biochem. Cytol.* **2**, 85–98
2. Benedetti, A., Banhegyi, G., and Burchell, A. (2005) Endoplasmic Reticulum: A Metabolic Compartment, pp. 1–162. IOS Press, Amsterdam
3. Braakman, I., Helenius, J., and Helenius, A. (1992) Manipulating disulfide bond formation and protein folding in the endoplasmic reticulum. *EMBO J.* **11**, 1717–1722
4. Pfeffer, S.R., and Rothman, J.E. (1987) Biosynthetic protein transport and sorting by the endoplasmic reticulum and Golgi. *Annu. Rev. Biochem.* **56**, 829–852
5. Quemeneur, E., Guthapfel, R., and Gueguen, P. (1994) A major phosphoprotein of the endoplasmic reticulum is protein disulfide isomerase. *J. Biol. Chem.* **269**, 5485–5488
6. Schatz, G., and Dobberstein, B. (1996) Common principles of protein translocation across membranes. *Science* **271**, 1519–1526
7. Hirschberg, C.B., Robbins, P.W., and Abeijon, C. (1998) Transporters of nucleotide sugars, ATP, and nucleotide

sulfate in the endoplasmic reticulum and Golgi apparatus. *Annu. Rev. Biochem.* **67**, 49–69

8. Dolce, V., Cappello, A.R., Lappano, R., and Maggiolini, M. (2011) Glycerophospholipid synthesis as a novel drug target against cancer. *Curr. Mol. Pharmacol.* **4**, 167–175
9. Dolce, V., Cappello, A.R., and Capobianco, L. (2014) Mitochondrial tricarboxylate and dicarboxylate-tricarboxylate carriers: from animals to plants. *IUBMB Life* **66**, 462–471
10. Cacan, R., Villers, C., Belard, M., Kaiden, A., Krag, S.S., and Verbert, A. (1992) Different fates of the oligosaccharide moieties of lipid intermediates. *Glycobiology* **2**, 127–136
11. Stafford, F.J. and Bonifacino, J.S. (1991) A permeabilized cell system identifies the endoplasmic reticulum as a site of protein degradation. *J. Cell Biol.* **115**, 1225–1236
12. Palmieri, F. (1994) Mitochondrial carrier proteins. *FEBS Lett.* **346**, 48–54
13. Klingenberg, M. (2008) The ADP and ATP transport in mitochondria and its carrier. *Biochim. Biophys. Acta* **1778**, 1978–2021
14. Lasorsa, F.M., Scarcia, P., Erdmann, R., Palmieri, F., Rottensteiner, H., and Palmieri, L. (2004) The yeast peroxisomal adenine nucleotide transporter: characterization of two transport modes and involvement in DeltapH formation across peroxisomal membranes. *Biochem. J.* **381**, 581–585
15. Palmieri, L., Rottensteiner, H., Girzalsky, W., Scarcia, P., Palmieri, F., and Erdmann, R. (2001) Identification and functional reconstitution of the yeast peroxisomal adenine nucleotide transporter. *EMBO J.* **20**, 5049–5059
16. Clairmont, C., A., De Maio, A., and Hirschberg, C., B. (1992) Translocation of ATP into the lumen of rough endoplasmic reticulum-derived vesicles and its binding to luminal proteins including BiP (GRP 78) and GRP 94. *J. Biol. Chem.* **267**, 3983–3990
17. Mayinger, P. and Meyer, D.I. (1993) An ATP transporter is required for protein translocation into the yeast endoplasmic reticulum. *EMBO J.* **12**, 659–666
18. Leroch, M., Neuhaus, H.E., Kirchberger, S., Zimmermann, S., Melzer, M., Gerhold, J., and Tjaden, J. (2008) Identification of a novel adenine nucleotide transporter in the endoplasmic reticulum of Arabidopsis. *Plant Cell* **20**, 438–451
19. Guillen, E. and Hirschberg, C.B. (1995) Transport of adenosine triphosphate into endoplasmic reticulum proteoliposomes. *Biochemistry* **34**, 5472–5476
20. Kim, S.H., Shin, S.J., and Park, J.S. (1996) Identification of the ATP transporter of rat liver rough endoplasmic reticulum via photoaffinity labeling and partial purification. *Biochemistry* **35**, 5418–5425
21. Shin, S.J., Lee, W.K., Lim, H.W., and Park, J. (2000) Characterization of the ATP transporter in the reconstituted rough endoplasmic reticulum proteoliposomes. *Biochim. Biophys. Acta* **1468**, 55–62
22. Dolce, V., Scarcia, P., Iacopetta, D., and Palmieri, F. (2005) A fourth ADP/ATP carrier isoform in man: identification, bacterial expression, functional characterization and tissue distribution. *FEBS Lett.* **579**, 633–637
23. Mayinger, P., Bankaitis, V.A., and Meyer, D.I. (1995) Sac1p mediates the adenosine triphosphate transport into yeast endoplasmic reticulum that is required for protein translocation. *J. Cell Biol.* **131**, 1377–1386
24. Kochendorfer, K.U., Then, A.R., Kearns, B.G., Bankaitis, V.A., and Mayinger, P. (1999) Sac1p plays a crucial role in microsomal ATP transport, which is distinct from its function in Golgi phospholipid metabolism. *EMBO J.* **18**, 1506–1515
25. Rocca, B.M.D., Rocca, B.M.D., Miniero, D.V., Tasco, G., Dolce, V., Falconi, M., Ludovico, A., Cappello, A.R., Sanchez, P., Stipani, I., Casadio, R., Desideri, A., and Palmieri, F. (2005) Substrate-induced conformational changes of the mitochondrial oxoglutarate carrier: a spectroscopic and molecular modelling study. *Mol. Membr. Biol.* **22**, 443–452
26. Iacopetta, D., Madeo, M., Tasco, G., Carrisi, C., Curcio, R., Martello, E., Casadio, R., Capobianco, L., and Dolce, V. (2011) A novel subfamily of mitochondrial dicarboxylate carriers from *Drosophila melanogaster*: biochemical and computational studies. *Biochim. Biophys. Acta* **1807**, 251–261
27. Porcelli, V., Fiermonte, G., Longo, A., and Palmieri, F. (2014) The human gene SLC25A29, of solute carrier family 25, encodes a mitochondrial transporter of basic amino acids. *J. Biol. Chem.* **289**, 13374–13384
28. Palmieri, F., Indiveri, C., Bisaccia, F., and Iacobazzi, V. (1995) Mitochondrial metabolite carrier proteins: purification, reconstitution, and transport studies. *Methods Enzymol.* **260**, 349–369
29. Carrisi, C., Madeo, M., Morciano, P., Dolce, V., Cenci, G., Cappello, A.R., Mazzeo, G., Iacopetta, D., and Capobianco, L. (2008) Identification of the *Drosophila melanogaster* mitochondrial citrate carrier: bacterial expression, reconstitution, functional characterization and developmental distribution. *J. Biochem.* **144**, 389–392
30. Bonofiglio, D., Santoro, A., Martello, E., Vizza, D., Rovito, D., Cappello, A.R., Barone, I., Giordano, C., Panza, S., Catalano, S., Iacobazzi, V., Dolce, V., and Ando, S. (2013) Mechanisms of divergent effects of activated peroxisome proliferator-activated receptor-gamma on mitochondrial citrate carrier expression in 3T3-L1 fibroblasts and mature adipocytes. *Biochim. Biophys. Acta* **1831**, 1027–1036
31. Iacopetta, D., Carrisi, C., De Filippis, G., Calcagnile, V.M., Cappello, A.R., Chimento, A., Curcio, R., Santoro, A., Vozza, A., Dolce, V., Palmieri, F., and Capobianco, L. (2010) The biochemical properties of the mitochondrial thiamine pyrophosphate carrier from *Drosophila melanogaster*. *FEBS J.* **277**, 1172–1181
32. Curcio, R., Muto, L., Pierri, C.L., Montalto, A., Lauria, G., Onofrio, A., Fiorillo, M., Fiermonte, G., Lunetti, P., Vozza, A., Capobianco, L., Cappello, A.R., and Dolce, V. (2016) New insights about the structural rearrangements required for substrate translocation in the bovine mitochondrial oxoglutarate carrier. *Biochim. Biophys. Acta* **1864**, 1473–1480
33. Lunetti, P., Damiano, F., De Benedetto, G., Siculella, L., Pennetta, A., Muto, L., Paradies, E., Marobbio, C.M., Dolce, V., and Capobianco, L. (2016) Characterization of human and yeast mitochondrial glycine carriers with implications for heme biosynthesis and anemia. *J. Biol. Chem.* **291**, 19746–19759
34. Lunetti, P., Cappello, A.R., Marsano, R.M., Pierri, C.L., Carrisi, C., Martello, E., Caggese, C., Dolce, V., and Capobianco, L. (2013) Mitochondrial glutamate carriers from *Drosophila melanogaster*: biochemical, evolutionary and modeling studies. *Biochim. Biophys. Acta* **1827**, 1245–1255
35. Aiello, D., Casadonte, F., Terracciano, R., Damiano, R., Savino, R., Sindona, G., and Napoli, A. (2016) Targeted proteomic approach in prostatic tissue: a panel of potential biomarkers for cancer detection. *Oncoscience* **3**, 220–241

36. Napoli, A., Aiello, D., Di Donna, L., Prendushi, H., and Sindona, G. (2007) Exploitation of endogenous protease activity in raw mastitic milk by MALDI-TOF/TOF. *Anal. Chem.* **79**, 5941–5948
37. Parisi, O.I., Fiorillo, M., Scrivano, L., Sinicropi, M.S., Dolce, V., Iacopetta, D., Puoci, F., and Cappello, A.R. (2015) Sericin/poly(ethylcyanoacrylate) nanospheres by interfacial polymerization for enhanced bioefficacy of fenofibrate: in vitro and in vivo studies. *Biomacromolecules* **16**, 3126–3133
38. Kurauskas, V., Hessel, A., Ma, P., Lunetti, P., Weinhaupl, K., Imbert, L., Brutscher, B., King, M.S., Sounier, R., Dolce, V., Kunji, E.R.S., Capobianco, L., Chipot, C., Dehez, F., Bersch, B., and Schanda, P. (2018) How detergent impacts membrane proteins: atomic-level views of mitochondrial carriers in dodecylphosphocholine. *J. Phys. Chem. Lett.* **9**, 933–938
39. Bartella, V., De Francesco, E.M., Perri, M.G., Curcio, R., Dolce, V., Maggiolini, M., and Vivacqua, A. (2016) The G protein estrogen receptor (GPER) is regulated by endothelin-1 mediated signaling in cancer cells. *Cell. Signal.* **28**, 61–71
40. Elia, G., Fiermonte, G., Pratelli, A., Martella, V., Camero, M., Cirone, F., and Buonavoglia, C. (2003) Recombinant M protein-based ELISA test for detection of antibodies to canine coronavirus. *J. Virol. Methods* **109**, 139–142
41. Zara, V., Dolce, V., Capobianco, L., Ferramosca, A., Papatheodorou, P., Rassow, J., and Palmieri, F. (2007) Biogenesis of eel liver citrate carrier (CIC): negative charges can substitute for positive charges in the presequence. *J. Mol. Biol.* **365**, 958–967
42. De Marcos Lousa, C., Trezeguet, V., Dianoux, A.C., Brandolin, G., and Lauquin, G.J. (2002) The human mitochondrial ADP/ATP carriers: kinetic properties and biogenesis of wild-type and mutant proteins in the yeast *S. cerevisiae*. *Biochemistry* **41**, 14412–14420
43. Madeo, M., Carrisi, C., Iacopetta, D., Capobianco, L., Cappello, A.R., Bucci, C., Palmieri, F., Mazzeo, G., Montalto, A., and Dolce, V. (2009) Abundant expression and purification of biologically active mitochondrial citrate carrier in baculovirus-infected insect cells. *J. Bioenerg. Biomembr.* **41**, 289–297
44. Klingenberg, M. (2009) Cardiolipin and mitochondrial carriers. *Biochim. Biophys. Acta* **1788**, 2048–2058
45. Hoffmann, B., Stockl, A., Schlame, M., Beyer, K., and Klingenberg, M. (1994) The reconstituted ADP/ATP carrier activity has an absolute requirement for cardiolipin as shown in cysteine mutants. *J. Biol. Chem.* **269**, 1940–1944
46. Vozza, A., De Leonardis, F., Paradies, E., De Grassi, A., Pierri, C.L., Parisi, G., Marobbio, C.M., Lasorsa, F.M., Muto, L., Capobianco, L., Dolce, V., Raho, S., and Fiermonte, G. (2017) Biochemical characterization of a new mitochondrial transporter of dephosphocoenzyme A in *Drosophila melanogaster*. *Biochim. Biophys. Acta* **1858**, 137–146
47. Carrisi, C., Antonucci, D., Lunetti, P., Migoni, D., Girelli, C.R., Dolce, V., Fanizzi, F.P., Benedetti, M., and Capobianco, L. (2014) Transport of platinum bonded nucleotides into proteoliposomes, mediated by *Drosophila melanogaster* thiamine pyrophosphate carrier protein (DmTpc1). *J. Inorg. Biochem.* **130**, 28–31
48. Knirsch, M., Gawaz, M.P., and Klingenberg, M. (1989) The isolation and reconstitution of the ADP/ATP carrier from wild-type *Saccharomyces cerevisiae*. Identification of primarily one type (AAC-2). *FEBS Lett.* **244**, 427–432
49. Csala, M., Marcolongo, P., Lizak, B., Senesi, S., Margittai, E., Fulceri, R., Magyar, J.E., Benedetti, A., and Banhegyi, G. (2007) Transport and transporters in the endoplasmic reticulum. *Biochim. Biophys. Acta* **1768**, 1325–1341
50. Agarraberes, F.A. and Dice, J.F. (2001) Protein translocation across membranes. *Biochim. Biophys. Acta* **1513**, 1–24
51. Nemoto, Y., Kearns, B.G., Wenk, M.R., Chen, H., Mori, K., Alb, J.G., Jr., De Camilli, P., and Bankaitis, V.A. (2000) Functional characterization of a mammalian Sac1 and mutants exhibiting substrate-specific defects in phosphoinositide phosphatase activity. *J. Biol. Chem.* **275**, 34293–34305
52. Palmieri, F., Pierri, C.L., De Grassi, A., Nunes-Nesi, A., and Fernie, A.R. (2011) Evolution, structure and function of mitochondrial carriers: a review with new insights. *Plant J.* **66**, 161–181
53. Napoli, A., Aiello, D., Di Donna, L., Sajjad, A., Perri, E., and Sindona, G. (2006) Profiling of hydrophilic proteins from *Olea europaea* olive pollen by MALDI TOF mass spectrometry. *Anal. Chem.* **78**, 3434–3443
54. Aiello, D., Materazzi, S., Risoluti, R., Thangavel, H., Di Donna, L., Mazzotti, F., Casadonte, F., Siciliano, C., Sindona, G., and Napoli, A. (2015) A major allergen in rainbow trout (*Oncorhynchus mykiss*): complete sequences of parvalbumin by MALDI tandem mass spectrometry. *Mol. bioSyst.* **11**, 2373–2382
55. Cappello, A.R., Guido, C., Santoro, A., Santoro, M., Capobianco, L., Montanaro, D., Madeo, M., Ando, S., Dolce, V., and Aquila, S. (2012) The mitochondrial citrate carrier (CIC) is present and regulates insulin secretion by human male gamete. *Endocrinology* **153**, 1743–1754
56. Bankston, L.A. and Guidotti, G. (1996) Characterization of ATP transport into chromaffin granule ghosts. Synergy of ATP and serotonin accumulation in chromaffin granule ghosts. *J. Biol. Chem.* **271**, 17132–17138
57. Klingenberg, M., Aquila, H., and Riccio, P. (1979) Isolation of functional membrane proteins related to or identical with the ADP, ATP carrier of mitochondria. *Methods Enzymol.* **56**, 407–414
58. Ozalp, V.C., Pedersen, T.R., Nielsen, L.J., and Olsen, L.F. (2010) Time-resolved measurements of intracellular ATP in the yeast *Saccharomyces cerevisiae* using a new type of nanobiosensor. *J. Biol. Chem.* **285**, 37579–37588
59. Imamura, H., Nhat, K.P., Togawa, H., Saito, K., Iino, R., Kato-Yamada, Y., Nagai, T., and Noji, H. (2009) Visualization of ATP levels inside single living cells with fluorescence resonance energy transfer-based genetically encoded indicators. *Proc. Natl. Acad. Sci. U.S.A.* **106**, 15651–15656

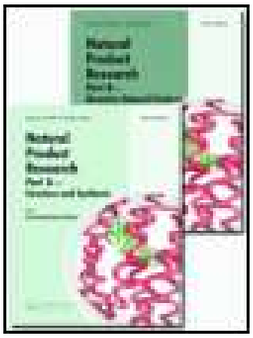

Natural Product Research

Formerly Natural Product Letters

ISSN: 1478-6419 (Print) 1478-6427 (Online) Journal homepage: http://www.tandfonline.com/loi/gnpl20

An ancient remedial repurposing: synthesis of new pinocembrin fatty acid acyl derivatives as potential antimicrobial/anti-inflammatory agents

R. Tundis, L. Frattaruolo, G. Carullo, B. Armentano, M. Badolato, M. R. Loizzo, F. Aiello & A. R. Cappello

To cite this article: R. Tundis, L. Frattaruolo, G. Carullo, B. Armentano, M. Badolato, M. R. Loizzo, F. Aiello & A. R. Cappello (2018): An ancient remedial repurposing: synthesis of new pinocembrin fatty acid acyl derivatives as potential antimicrobial/anti-inflammatory agents, Natural Product Research, DOI: 10.1080/14786419.2018.1440224

To link to this article: https://doi.org/10.1080/14786419.2018.1440224

NATURAL PRODUCT RESEARCH, 2018
https://doi.org/10.1080/14786419.2018.1440224

Taylor & Francis
Taylor & Francis Group

An ancient remedial repurposing: synthesis of new pinocembrin fatty acid acyl derivatives as potential antimicrobial/anti-inflammatory agents

R. Tundis, L. Frattaruolo, G. Carullo, B. Armentano, M. Badolato, M. R. Loizzo, F. Aiello[§] and A. R. Cappello[§]

Department of Pharmacy, Health and Nutritional Sciences, University of Calabria, Rende, Italy

ABSTRACT

Five new pinocembrin derivatives (**MC1**-**MC5**) were synthesized by Steglich reaction, and investigated for their antimicrobial, antioxidant, and anti-inflammatory activity. **MC2** (oleoyl derivative) and **MC3** (linoleoyl derivative) have shown the highest inhibitory effects on bacterial proliferation, with MIC values of 32 µg/mL against *Staphylococcus aureus*. The docosahexaenoyl derivative **MC5** displayed the highest anti-inflammatory activity, decreasing NO production in LPS-stimulated macrophages with an IC_{50} value of 15.51 µg/mL higher than the positive control diclofenac (IC_{50} of 39.71 µg/mL). All new synthesized compounds showed no anti-proliferative effects on RAW 264.7 cells. Results demonstrated as the introduction of fatty acid substituents improved the biological profile of pinocembrin. Moreover, the chemical nature of substituents significantly affects the bioactivity. These preliminary results outline the importance to investigate the synthesis of pinocembrin fatty acids derivatives as new and safe anti-microbial/anti-inflammatory agents.

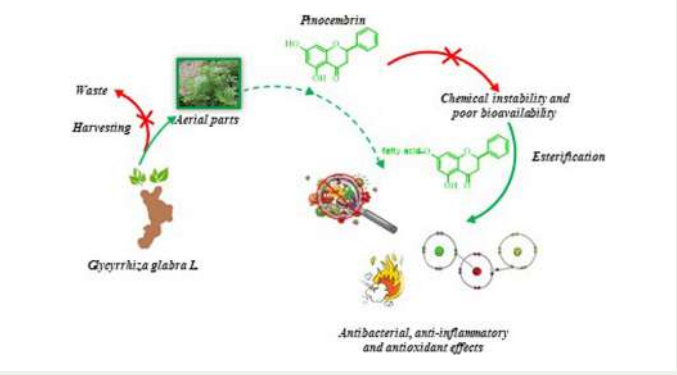

ARTICLE HISTORY
Received 23 December 2017
Accepted 3 February 2018

KEYWORDS
Pinocembrin derivatives; bacterial resistance; anti-inflammatory activity

CONTACT F. Aiello francesca.aiello@unical.it; A. R. Cappello annarita.cappello@unical.it
[§]These authors are joint senior authors.

Supplemental data for this article can be accessed at https://doi.org/10.1080/14786419.2018.1440224.

1. Introduction

During the last century, the discovery of penicillin revolutionized the treatment of bacterial infections. In this context, various antibacterial tools have been discovered and validated as antibiotic drugs (Gaynes 2017). Although several antibiotics resulted very selective vs. Gram-positive and Gram-negative bacteria, resistance phenomena were observed (Schwarz et al. 2017). From the 1980s to the early 2000s, there was a 90% decline in the approval of new antibiotics as well as the discovery of few new novel classes (Luepke et al. 2017). Therefore, there is now an urgent need to develop new and useful antibiotics to avoid returning to the 'pre-antibiotic era' (Martens and Demain 2017). Several plant extracts demonstrated good antibacterial properties due to the presence of secondary metabolites such as quinones, phenols, alkaloids, terpenoids (Rameshkumar et al. 2015; Chandra et al. 2017; Rempe et al. 2017). In this field, *Glycirrhiza glabra* (Fabaceae) (licorice) attracted our attention because it is used in traditional medicine as antibacterial agent. Indeed, hydrophobic extracts from *G. inflata* demonstrated good antimicrobial properties against *Propionibacterium acnes* and by suppressing the inflammatory and oxidative processes associated (Baumann 2007). Water Soluble Licorice Extract (WSLE) inhibited the growth of some Gram-positive and Gram-negative bacteria with MIC values of 64–512 μg/mL, due to presence of liquiritigenin and isoliquiritigenin (Furushita et al. 2005). Licorice phenols, in particular isobavachalcone, licoricidin and bakuchiol, demonstrated good antibacterial properties against *vancomycin-resistant Enterococcus* (VRE) species (Hatano et al. 2017). A recent study evaluated how the extraction solvent can influence the antibacterial activity of the extract. Chloroform, ethanol and water extracts of *G. glabra* leaves exhibited antibacterial activities against *Klebsiella pneumonia* and *Bacillus subtilis* as the most sensitive (El Kichaoui et al. 2017). In another study, the antibacterial properties of roots and leaves extracts were compared, demonstrating how in some cases leaves extracts had better activity than root extracts (Irani et al. 2010). In our previous article, we reported the chemical characterization of fractions of *G. glabra* leaves, harvested in two different periods and we have identified pinocembrin as the principal component (Aiello et al. 2017). According to the folk medicine, in which licorice had been used as an antibacterial remedy, here we decided to investigate the antibacterial properties of the obtained extracts. On the other hand, pinocembrin attenuated α-haemolysin-mediated cell injury and protected mice from *Staphylococcus aureus* pneumonia but did not show a good antibacterial activity per se (Bremner and Meyer 1998; Soromou et al. 2013). Thus, we decided to synthesize new fatty acid-based derivatives of pinocembrin, in order to evaluate if the hybrid molecules have antioxidant, antimicrobial and potential anti-inflammatory activities that could represent new drug candidates.

2. Results and discussion

G. glabra extracts and fractions were subjected to antibacterial and antifungal tests in order to appreciate their potential health applications. The obtained results (Table 1) showed a weak antibacterial activity of the total extract against the Gram positive bacterium *S. aureus*, and a slightly more active antibacterial profile in its methanol-soluble fraction, containing pinocembrin as major component. Surprisingly, the *n*-hexane-soluble fraction showed a good antibacterial activity with a minimal inhibitory concentration (MIC) value of 128 μg/mL against *S. aureus*. In order to investigate the role of pinocembrin in the antibacterial

Table 1. MIC and MBC/MFC values (µg/mL) of *G. glabra* leaves extracts and fractions.

	S. aureus		*E. coli*		*K. pneumoniae*		*P. aeruginosa*		*C. albicans*	
	ATCC 25923		ATCC 25922		ATCC 13883		ATCC 27853		ATCC 10231	
Compound	MIC	MBC	MIC	MBC	MIC	MBC	MIC	MBC	MIC	MFC
E-May	128	>512	512	>512	512	>512	512	>512	512	>512
M-May	512	>512	512	>512	512	>512	512	>512	512	>512
T-May	512	>512	>512	>512	>512	>512	>512	>512	>512	>512
E-October	128	>512	512	>512	512	>512	512	>512	512	>512
M-October	512	>512	512	>512	512	>512	512	>512	512	>512
T-October	512	>512	>512	>512	>512	>512	>512	>512	>512	>512
Pinocembrin	256	>512	256	>512	256	>512	512	>512	512	>512
F1	256	>512	512	>512	512	>512	512	>512	512	>512
F1-Pinocembrin	256	>512	>512	>512	>512	>512	>512	>512	>512	>512
Positive control										
Miconazole	–	–	–	–	–	–	–	–	2	4
Ciprofloxacin	0.25	1	0.03	0.06	0.06	0.12	0.12	0.25	–	–

Notes: *G. glabra* total extract from May (T-May); methanol-soluble fraction from May (M-May); *n*-hexane-soluble fraction from May (E-May); total extract from October (T-October); methanol-soluble fraction from October (M-October); *n*-hexane-soluble fraction from October (E-October).

activity of *G. glabra* extract, fraction F1 (chromatographic fraction containing pinocembrin) and F1-pinocembrin (in which pinocembrin was removed) were tested on the same panel of microorganisms. The two fractions showed a different profile, demonstrating how the presence of pinocembrin is essential to guarantee this moderate antibacterial activity, as the antimicrobial test of purified pinocembrin has confirmed. The pure compound turned out to be quite active against the Gram positive strain of *S. aureus* and the Gram negative strains of *Escherichia coli* and *Klebsiella pneumoniae* (MIC values of 256 µg/mL), showing a weaker activity against *Pseudomonas aeruginosa* and the fungus *Candida albicans* (MIC values of 512 µg/mL). On the other hand, minimal bacterticidal/fungicidal concentrations (MBC/MFC) resulted higher than 512 µg/mL in all the cases (Table 1). Since *n*-hexane soluble fraction of *G. glabra* leaves extracts, containing fatty acids (FAs) and related esters, exerted an interesting antibacterial activity, and according to studies in which hybrid molecules showed a better biological profile compared to native compounds (Aiello et al. 2012; Badolato et al. 2017), we decided to merge pinocembrin with a small series of fatty acids (FAs), including a saturated fatty acid, behenic acid also known as docosanoic (C_{22}:0), a monounsaturated fatty acid, oleic acid (C_{18}:1), and three polyunsaturated fatty acids such as linoleic acid (C_{18}:2), linolenic acid (C_{18}:3) and docosahexaenoic acid (DHA) (C_{22}:6), which demonstrated a good antibacterial profile in previous studies (Beck et al. 2007).

The choice of the wide chemical diversity of FAs has been made since the power of antibacterial activity of FAs changes according to the length of the carbon chain, in the presence of double bonds and their conformation (Shin et al. 2007; Desbois and Smith 2009; Huang et al. 2010). The chemical approach used to prepare esters was a classical Steglich reaction. All the ester derivatives **MC1-MC5** were obtained in good yields. Spectroscopic data demonstrated the formation of the ester in position 7 on the A ring of pinocembrin. This is also justified by the fact that OH in C-5 position forms an H-bond with the carbonyl group of the C ring (Figure 1) (see SUPPLEMENTARY MATERIAL S1–S10). In order to evaluate the influence of substituents on the antimicrobial activity of pinocembrin derivatives, compounds have been tested against Gram positive (*S. aureus*) and Gram negative (*E. coli*, *K. pneumoniae* and *P. aeruginosa*) bacterial strains, and against the fungus *Candida albicans*. According to CLSI

Table 2. Antimicrobial activity of synthesized compounds **MC1**–**MC5**.

	S. aureus		*E. coli*		*K. pneumoniae*		*P. aeruginosa*		*C. albicans*	
	ATCC 25923		ATCC 25922		ATCC 13883		ATCC 27853		ATCC 10231	
Compound	MIC	MBC	MIC	MBC	MIC	MBC	MIC	MBC	MIC	MFC
Pinocembrin	>128	>128	>128	>128	>128	>128	>128	>128	>128	>128
MC1	128	>128	>128	>128	>128	>128	>128	>128	>128	>128
MC2	32	128	>128	>128	>128	>128	>128	>128	>128	>128
MC3	32	128	>128	>128	>128	>128	>128	>128	>128	>128
MC4	64	256	>128	>128	>128	>128	>128	>128	>128	>128
MC5	128	>128	>128	>128	>128	>128	>128	>128	>128	>128
Positive control										
Miconazole	–	–	–	–	–	–	–	–	2	4
Ciprofloxacin	0.25	1	0.03	0.06	0.06	0.12	0.12	0.25	–	–

Note: Data are presented as MIC and MBC/MFC values (µg/mL).

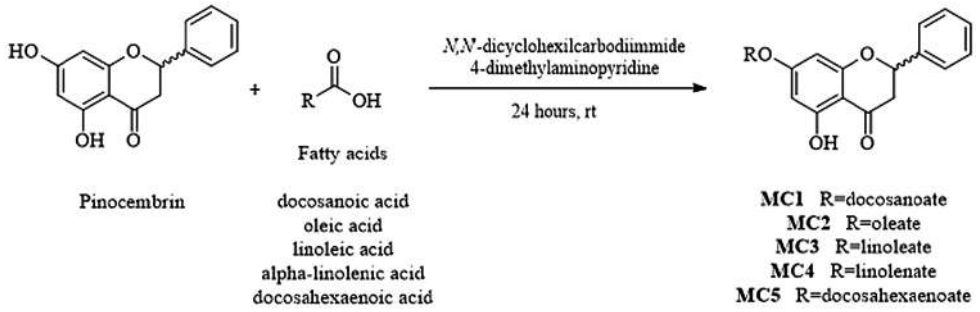

Figure 1. Synthesis of compounds **MC1-MC5**.

standards guidelines, MIC, MBC and minimal fungicidal concentration (MFC) have been determined (Table 2) (As pinocembrin, the new compounds showed no interesting activity on Gram negative bacteria and fungus growth. On the other hand, all the compounds have shown a higher inhibitory activity against *S. aureus* growth than pinocembrin. This activity seems to be highly influenced by the chemical nature of substituents. In particular, **MC2** (oleoyl derivative) and **MC3** (linoleoyl derivative) have shown the highest inhibitory effect on bacterial proliferation, with MIC values of 32 µg/mL, followed by **MC4** (linolenoyl derivative) with a MIC value of 64 µg/mL and **MC1** (docosanoyl derivative) and **MC5** (docosahexaenoyl derivative) with MIC values of 128 µg/mL. These data confirmed how the complexity of the carbon chain could influence the activity. The best compounds resulted **MC2** and **MC3** with a MIC value of 32 µg/mL, containing one and two unsaturations, respectively, in the carbon chain of FA substituents. These data could be due to the possible conformation assumed by the FA in the pinocembrin hybrid. Always a bacterial infection is associated to an inflammatory process. For this reason, the ability of the new pinocembrin derivatives to modulate the inflammatory condition was investigated by monitoring their ability to inhibit the production of nitric oxide (NO), an important chemical mediator of the inflammatory process, in LPS-stimulated RAW 264.7 cells. As shown in Figure 2, all the fatty acid-derivatives of pinocembrin exhibited a significant concentration-dependent inhibitory activity on nitrite production (Table 4). The best anti-inflammatory compound was **MC5** with an IC_{50} value of 15.5 µg/mL, followed by **MC4** (IC_{50} of 19.19 µg/mL), and **MC3** (IC_{50} of 26.26 µg/mL). All

Table 3. Antioxidant profile (IC_{50} value µg/mL) of pinocembrin derivatives **MC1**-**MC5**.

	DPPH	β-carotene bleaching test[a]	
		30 min	60 min
Compound			
MC1	24.9 ± 2.2	509.2 ± 4.4	933.4 ± 5.2
MC2	35.2 ± 2.7	26.6%	20.4%
MC3	133.6 ± 3.9	43.7%	21.8%
MC4	210.0 ± 3.0	36.8%	22.7%
MC5	38.7 ± 2.8	18.4%	13.6%
Positive control			
Ascorbic acid	5.0 ± 0.8		
Propyl gallate		1.0 ± 0.1	1.0 ± 0.1

Notes: [a]Percentages are obtained at 1 mg/mL. Differences within and between groups were evaluated by one-way analysis of variance test (ANOVA) followed by a multicomparison Bonferroni's test. DPPH: One-way ANOVA ***$p < 0.0001$ ($F = 1990$, $R_2 = 0.998$) Dunnet's Multiple Comparison Test **$p < 0.001$; β-carotene bleaching test 30 min: One-way ANOVA ***$p < 0.0001$ ($F = 160{,}100$, $R_2 = 1.0$) Dunnet's Multiple Comparison Test **$p < 0.001$; β-carotene bleaching test 60 min: One-way ANOVA ***$p < 0.0001$ ($F = 290{,}300$, $R_2 = 1.0$) Dunnet's Multiple Comparison Test **$p < 0.001$.

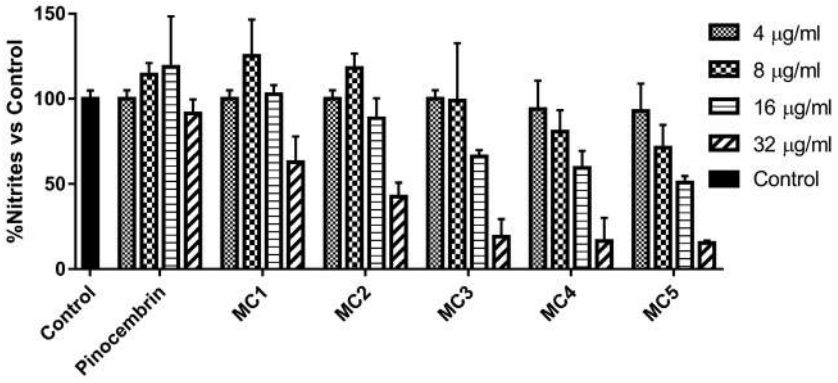

Figure 2. Anti-inflammatory activity of tested compounds. Nitrites production assessment after treatment of LPS-induced RAW 264.7 cell line with different concentrations of tested compounds for 24 h. Results, quantified by Griess assay, are expressed as percentage of nitrites production vs control (cells treated with DMSO). Values represent mean ± S.D. of three independent experiments, each one performed with triplicate samples (*$p < 0.05$, one-way ANOVA test).

synthesized compounds showed higher activity than pinocembrin (IC_{50} 203.6 µg/mL) and surprisingly **MC3**, **MC4** and **MC5** displayed higher anti-inflammatory activity compared to the commercially available drug diclofenac (IC_{50} of 39.71 µg/mL). Nowadays, it is increasingly clear the connection between cellular oxidative stress and inflammation pathways (Carullo et al. 2017). Therefore, synthesized compounds have been tested *in vitro* to evaluate their antioxidant activity. The most active in DPPH test is **MC1** with an IC_{50} value of 24.9 µg/mL, followed by **MC2** and **MC3** with IC_{50} values of 35.2 and 38.7 µg/mL, respectively (Table 3). A moderate antioxidant activity in the β-carotene bleaching test was found. The most active was compound **MC1** that showed IC_{50} values of 509.2 and 933.2 µg/mL after 30 and 60 min of incubation, respectively.

To evaluate any cytotoxic effects of pinocembrin derivatives (at concentrations ranging from 4 to 128 µg/mL) on RAW 264.7 cells, a cell viability assay has been performed. After

Table 4. Inhibition of NO production in LPS-stimulated RAW 264.7 cells by tested compounds.

Compound	IC_{50} (μg/mL)	95% confidence interval
Pinocembrin	203.60	101.30–569.31
MC1	106.82	55.41–277.20
MC2	59.58	29.35–178.42
MC3	26.26	13.56–57.13
MC4	19.19	11.82–32.16
MC5	15.51	10.38–23.45
Positive control		
Diclofenac	39.71	25.13–60.82

Notes: Data are presented as IC_{50} values (μg/mL) and 95% confidence intervals, obtained by nonlinear regression analysis of three independent experiments. Diclofenac has been used as positive control.

24 h of treatment, no cytotoxic effects have been observed. Unlike what has been observed for antimicrobial activity, an increment of anti-inflammatory activity has been noticed with the increase of the number of unsaturations in the chain of fatty acids substituents. These results showed the difficulty to maximize one of the two activities without affection of the other one. **MC2** and **MC3** resulted the best antimicrobial pinocembrin derivatives, while **MC4** and **MC5** the best anti-inflammatory ones. Overall, **MC3** and **MC4** demonstrated to have a good balance of the two activities, and represent interesting candidates for further investigations.

3. Conclusion

The aim of this work was to synthesize new pinocembrin derivatives endowed with antibacterial activity. The molecules have been realised starting from the observation that the *n*-hexane soluble fraction of *G. glabra* leaves extract, containing FAs and related FAs esters, exerted an interesting antibacterial activity. Molecules, tested to evaluate their double antibacterial/anti-inflammatory activity, demonstrated a good biological profile and higher activity compared to pinocembrin and licorice extracts. We proved how the length and the number of unsaturations of FAs chain influence the activity. Rationally modifying pinocembrin, choosing the FA substituent appropriate to selectively improve its antimicrobial (**MC2**, **MC3**) or anti-inflammatory activities (**MC4**, **MC5**), an optimal compromise of the two effects can be obtained. Additionally, results evidenced two new interesting balanced double-action bioactive compounds, **MC3** and **MC4**.

Disclosure statement

No potential conflict of interest was reported by the authors.

ORCID

R. Tundis http://orcid.org/0000-0002-3713-4403
L. Frattaruolo http://orcid.org/0000-0002-7018-8454
G. Carullo http://orcid.org/0000-0002-1619-3295
B. Armentano http://orcid.org/0000-0002-7138-0798
M. Badolato http://orcid.org/0000-0002-5892-9635
M. R. Loizzo http://orcid.org/0000-0002-6050-9357
F. Aiello http://orcid.org/0000-0001-6846-5582
A. R. Cappello http://orcid.org/0000-0001-7824-3561

References

Aiello F, Garofalo A, Aloisi AM, Lamponi S, Magnani A, Petroni A. 2012. Synthesis of esters of androgens with unsaturated fatty acids for androgen requiring therapy. J Endocrinol Invest. 36(6):390–395.

Aiello F, Armentano B, Polerà N, Carullo G, Loizzo MR, Bonesi M, Cappello MS, Capobianco L, Tundis R. 2017. From vegetable waste to new agents for potential health applications: antioxidant properties and effects of extracts, fractions and pinocembrin from *Glycyrrhiza glabra* L. aerial parts on viability of five human cancer cell lines. J Agric Food Chem. 65(36):7944–7954.

Badolato M, Carullo G, Perri M, Cione E, Manetti F, Di Gioia ML, Brizzi A, Caroleo MC, Aiello F. 2017. Quercetin/oleic acid-based G-protein-coupled receptor 40 ligands as new insulin secretion modulators. Future Med Chem. 9:1873–1885.

Baumann LS. 2007. Less-known botanical cosmeceuticals. Dermatol Ther. 20:330–342.

Beck V, Jabůrek M, Demina T, Rupprecht A, Porter RK, Ježek P, Pohl EE. 2007. Polyunsaturated fatty acids activate human uncoupling proteins 1 and 2 in planar lipid bilayers. Faseb J. 21:1137–1144.

Bremner PD, Meyer J. 1998. Pinocembrin chalcone: an antibacterial compound from *Helichrysum trilineatum*. Planta Medica. 64:777.

Carullo G, Cappello AR, Frattaruolo L, Badolato M, Armentano B, Aiello F. 2017. Quercetin and derivatives: useful tools in inflammation and pain management. Future Med Chem. 9:79–93.

Chandra H, Bishnoi P, Yadav A, Patni B, Mishra A, Nautiyal AR. 2017. Antimicrobial resistance and the alternative resources with special emphasis on plant-based antimicrobials–a review. Plants. 6:16.

Desbois AP, Smith VJ. 2009. Antibacterial free fatty acids: activities, mechanisms of action and biotechnological potential. Appl Microbiol Biotechnol. 85:1629–1642.

El Kichaoui A, Abdelmoneim A, Elbaba H, El Hindi M. 2017. The Antimicrobial Effects of *Boswellia carterii*, *Glycyrrhiza glabra* and *Rosmarinus officinalis* some Pathogenic Microorganisms. IUGNS. 25:208–213.

Furushita M, Maeda T, Shiba T, Ohno H, Yamamoto M, Tamura Y. 2005. The history of licorice applications in Maruzen Pharmaceuticals Co., Ltd. Gekkan Aqua Culture. 42:76–77.

Gaynes R. 2017. The Discovery of Penicillin - New Insights After More Than 75 Years of Clinical Use. Emerging Infectious Diseases. 23(5):849–853.

Hatano T, Eerdunbayaer Cui Y, Kuroda T, Shimozu Y. 2017. Licorice as a resource for pharmacologically active phenolic substances: antioxidant and antimicrobial effects. In: Sakagami H, editor. Biological activities and action mechanisms of licorice ingredients. London: In Tech. Chapter 4, pp 59–75.

Huang CB, George B, Ebersole JL. 2010. Antimicrobial activity of n-6, n-7 and n-9 fatty acids and their esters for oral microorganisms. Arch Oral Biol. 55:555–560.

Irani M, Sarmadi M, Bernard F, Ebrahimi pour GH, Bazarnov HS. 2010. Leaves antimicrobial activity of *Glycyrrhiza glabra* L. Iran J Pharm Res. 9:425–428.

Luepke KH, Suda KJ, Boucher H, Russo RL, Bonney MW, Hunt TD, Mohr JF III. 2017. Past, present, and future of antibacterial economics: increasing bacterial resistance, limited antibiotic pipeline, and societal implications. Pharmacotherapy. 37:71–84.

Martens E, Demain AL. 2017. The antibiotic resistance crisis, with a focus on the United States. J Antibiot. 70:520–526.

Rameshkumar KB, Alan Sheeja DB, Nair MS, George V. 2015 N. atural Product Research Curcuma ecalcarata – new natural source of pinocembrin and piperitenone. Nat Prod Res. 29:1276–1279.

Rempe CS, Burris KP, Lenaghanb SC, Neal Stewart C, Jr. 2017. The Potential of Systems Biology to Discover Antibacterial Mechanisms of Plant Phenolics. Front Microbiol. 8:422.

Schwarz S, Loeffler A, Kadlec K. 2017. Bacterial resistance to antimicrobial agents and its impact on veterinary and human medicine. Vet Dermatol. 28:e19.

Shin SY, Bajpai VK, Kim HR, Kang SC. 2007. Antibacterial activity of eicosapentaenoic acid (EPA) against foodborne and food spoilage microorganisms. LWT Food science and technol. 40:1515–1519.

Soromou LW, Zhang Y, Cui Y, Wei M, Chen N, Yang X, Huo M, Baldé A, Guan S, Deng X, et al. 2013. Subinhibitory concentrations of pinocembrin exert anti-Staphylococcus aureus activity by reducing α-toxin expression. J Appl Microbiol. 115:41–49.

ACS chemical biology

Articles

Cite This: ACS Chem. Biol. XXXX, XXX, XXX-XXX

pubs.acs.org/acschemicalbiology

A Genomics-Based Approach Identifies a Thioviridamide-Like Compound with Selective Anticancer Activity

Luca Frattaruolo,[†,‡] Rodney Lacret,[†] Anna Rita Cappello,[‡] and Andrew W. Truman*[,†]

[†]Department of Molecular Microbiology, John Innes Centre, Colney Lane, Norwich, NR4 7UH, United Kingdom

[‡]Department of Pharmacy, Health and Nutritional Sciences, University of Calabria, Rende, Italy

Supporting Information

ABSTRACT: Thioviridamide is a structurally novel ribosomally synthesized and post-translational modified peptide (RiPP) produced by *Streptomyces olivoviridis* NA005001. It is characterized by a structure that features a series of thioamide groups and possesses potent antiproliferative activity in cancer cell lines. Its unusual structure allied to its promise as an anticancer compound led us to investigate the diversity of thioviridamide-like pathways across sequenced bacterial genomes. We have isolated and characterized three diverse members of this family of natural products. This characterization is supported by transformation-associated recombination cloning and heterologous expression of one of these compounds, thiostreptamide S4. Our work provides an insight into the diversity of this rare class of compound and indicates that the unusual *N*-terminus of thioviridamide is not introduced biosynthetically but is instead introduced during acetone extraction. A detailed analysis of the biological activity of one of the newly discovered compounds, thioalbamide, indicates that it is highly cytotoxic to cancer cells, while exhibiting significantly less activity toward a noncancerous epithelial cell line.

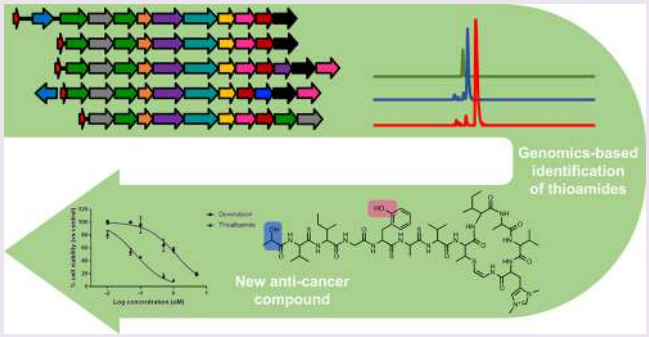

Ribosomally synthesized and post-translationally modified peptides (RiPPs) are a class of natural products with high chemical diversity, which results from the wide array of maturation processes that the genetically encoded precursor peptide may undergo.[1,2] This diversity is reflected in the wide variety of biological activities that these compounds possess. Due to their broad pharmacologic potential, this rapidly growing class of natural products is currently a focus of biotechnology and pharmaceutical research.[3,4] Thioviridamide (**1**, Figure 1a) is a RiPP biosynthesized by *Streptomyces olivoviridis* NA005001 and is characterized by potent antiproliferative and pro-apoptotic activity in several cancer cell lines.[5] This novel peptidic compound features an *N*-terminal 2-hydroxy-2-methyl-4-oxopentanoyl group, a β-hydroxy-N_1,N_3-dimethylhistidinium (hdmHis) residue, and a *S*-(2-aminovinyl)-cysteine (AviCys) residue[6] that forms part of a macrocycle.[7] A very unusual feature of **1** is the presence of five thioamide groups[8] in place of backbone amide groups. Recently, the thioviridamide (*tva*) biosynthetic gene cluster (BGC) was identified and confirmed by heterologous expression.[9] This demonstrated the ribosomal origin of this molecule, which derives from a 13 amino acid core peptide at the C terminus of the TvaA precursor peptide (Figure 1b). An additional 11 proteins encoded by this gene cluster (TvaB−TvaL) are predicted to be involved in the maturation of the precursor peptide into **1**, although little is known about individual steps in this pathway. The promising antitumor activity, unprecedented structure, and poorly understood biosynthesis of thioviridamide led us to investigate the extent and diversity of this new family of natural products.

Here, we report the identification and characterization of three new thioviridamide-like pathways. Chemical and biological characterization of these new thioviridamide-like molecules (TLMs) demonstrates the diversity of this type of RiPP, which is likely to be a subclass of a wider thioamide family of RiPPs.[10] Our work indicates that the reported thioviridamide structure may be an unnatural derivative of the true pathway product. Gene inactivation and heterologous expression of a transformation-associated recombination (TAR) cloned gene cluster supported this characterization. Finally, we show that a TLM produced by *Amycolatopsis alba* DSM 44262 is highly cytotoxic toward various tumor cell lines and yet is 6-fold less active toward a noncancerous epithelial cell line, thus exhibiting medicinally promising selectivity toward cancerous cells.

RESULTS AND DISCUSSION

Genome Mining to Identify Thioviridamide-Like Pathways. A BLAST search using the YcaO domain protein TvaH yielded 22 proteins with over 50% identity. The genomic regions surrounding their respective genes were then analyzed by a MultiGeneBlast[11] homology search using the *tva* BGC as

Received: August 7, 2017
Accepted: October 2, 2017
Published: October 2, 2017

DOI: 10.1021/acschembio.7b00677
ACS Chem. Biol. XXXX, XXX, XXX−XXX

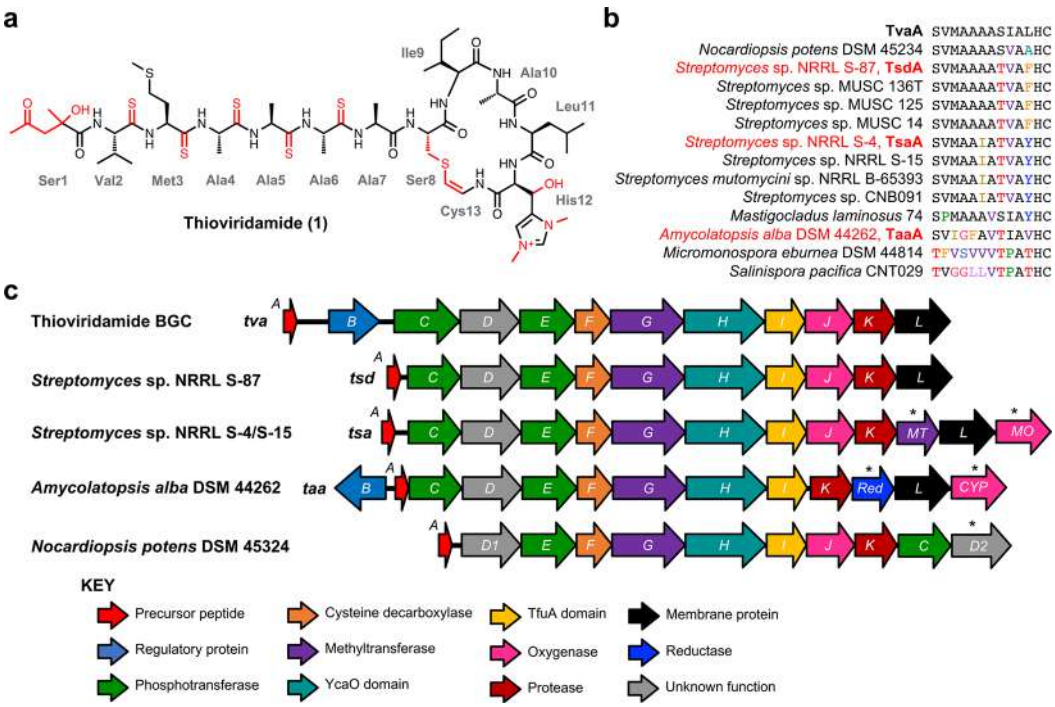

Figure 1. Identification of thioviridamide-like pathways. (a) Structure of thioviridamide with each post-translational modification highlighted red. (b) Alignment of the core peptides from every sequenced thioviridamide-like BGC. All residues that differ from TvaA are colored. (c) Comparison of the gene clusters investigated in this study (MT = methyltransferase; MO = flavin-dependent oxygenase; Red = reductase; CYP = P450; * = putative new biosynthetic enzymes). A comparison of all 14 BGCs is provided in Figure S1.

the query, which identified 14 closely related TLM-like BGCs in bacterial genomes. All were in Actinobacteria, with the intriguing exception of the cyanobacterium *Mastigocladus laminosus*. These all encode putative precursor peptides (Figure 1b) with high sequence homology to TvaA and feature a partially conserved set of tailoring genes (Figure 1c and Figure S1). We selected five publicly available strains that we predicted would collectively provide much of the diversity in this family of compounds: *A. alba* DSM 44262, *Streptomyces* sp. NRRL S-4, *Streptomyces* sp. NRRL S-15, *Streptomyces* sp. NRRL S-87, and *Nocardiopsis potens* DSM 45234. These gene clusters have homologues of most of the genes involved in thioviridamide maturation (from TvaC to TvaL), except for the *A. alba* cluster, which lacks a hydroxylase-encoding *tvaJ*-like gene (Figure 1c). In addition, only the *A. alba* BGC encodes a putative homologue of TvaB, a regulatory protein encoded in the *tva* BGC. Intriguingly, the gene clusters in *Streptomyces* sp. NRRL S-4/S-15 and *A. alba* DSM 44262 contain additional genes that could be involved in further post-translational modification steps (Figure 1c).

Production of Thioviridamide-Like Molecules. The putative core peptide sequences and associated set of tailoring enzymes allowed us to predict candidate masses for each TLM. Therefore, each strain was fermented in multiple culture conditions and screened by liquid chromatography−mass spectrometry (LC-MS) for TLM production. While the production medium reported[5] for **1** provided no candidate molecules, a solid version of bottromycin production medium[12] (BPM) yielded compounds with masses compatible with TLMs derived from the respective precursor peptides (Figure 2a), with the exception of *N. potens* DSM 45234. *A. alba* DSM 44262 produced a compound (thioalbamide, **2**, Figure 2b) with *m/z* 1329.6349 (Figure 2a), corresponding to the molecular formula $C_{61}H_{97}N_{14}O_{11}S_4^+$ (calculated M^+: 1329.6339). High-resolution (HR) MS^2 analysis of this molecule provided a fragmentation pattern that supported a thioviridamide-like structure, including the presence of thioamides (and associated losses of H_2S, −33.99 Da), fragmentation consistent with the predicted linear portion of the molecule, and an MS^2 fragment (*m/z* 607.3376, Figure 2 and Figure S2) that correlated with a (2-aminovinyl)-3-methyl-cysteine (AviMeCys) containing macrocycle (predicted *m/z* 607.3385).

The gene clusters for *Streptomyces* sp. NRRL S-4 and *Streptomyces* sp. NRRL S-15 are effectively identical, and each strain produced a compound (thiostreptamide S4, **3**, Figure 2b) with *m/z* 1377.55 that eluted at an identical retention time (Figure S3), corresponding to the molecular formula $C_{60}H_{93}N_{14}O_{11}S_6^+$ (*Streptomyces* sp. NRRL S-4 product *m/z* 1377.5479; calculated M^+ = 1377.5467). As with **2**, $HRMS^2$ analysis of this molecule provided a fragmentation pattern that supported a thioviridamide-like structure, including multiple thioamides and a putative AviMeCys-containing macrocycle fragment (obsd. *m/z* 687.3260, pred. *m/z* 687.3283, Figure 2b and Figure S4). This preliminary analysis indicated that the S-4 and S-15 pathways produce identical compounds, although differences in stereochemistry cannot be ruled out. *Streptomyces* sp. NRRL S-87 produced a compound (thiostreptamide S87, **4**, Figure 2b) with *m/z* 1305.4871, corresponding to the molecular formula $C_{56}H_{85}N_{14}O_{10}S_6^+$ (calculated M^+: 1305.4892). As before, $HRMS^2$ analysis provided thioviridamide-like fragments that were consistent with the predicted precursor peptide (Figure 2b and Figure S5).

The most striking structural feature of thioviridamide is a contiguous sequence of five thioamide-containing residues, which subtly differs from the TLMs that we isolated. Instead, exact mass and MS^2 data signified three noncontiguous thioamide linkages in **2**, and four in **3** and **4** (Figure 2b). UV absorption spectra of each compound provided maxima of

DOI: 10.1021/acschembio.7b00677
ACS Chem. Biol. XXXX, XXX, XXX−XXX

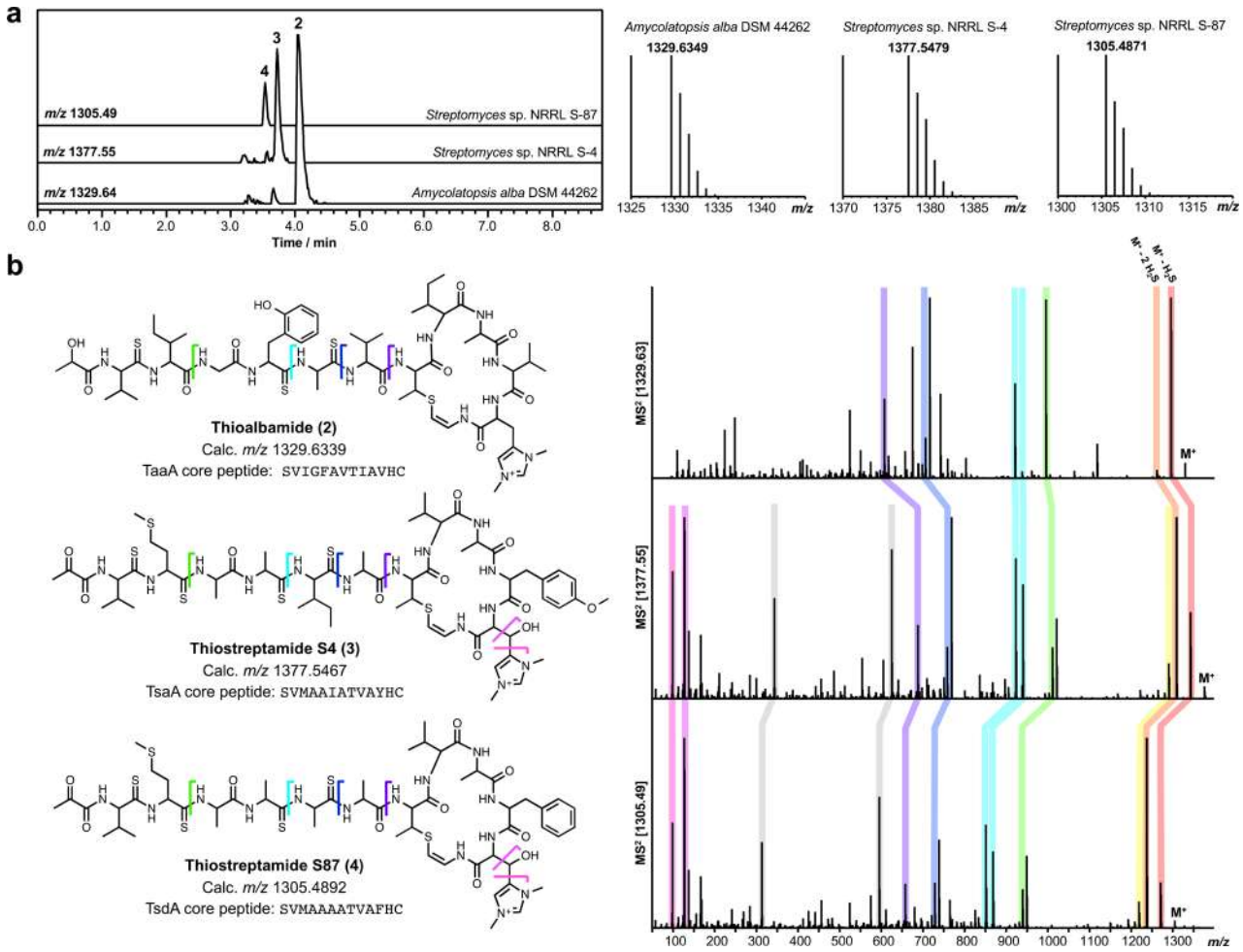

Figure 2. Identification of novel TLMs. (a) Extracted ion chromatograms from *A. alba* DSM 44262, *Streptomyces* sp. NRRL S-4, and *Streptomyces* sp. NRRL S-87 showing relative levels of production and exact masses for each compound. (b) Structures of each compound alongside MS^2 data indicating analogous fragments from each compound (gray shading indicates abundant common fragments that could not be annotated). The core peptide sequences for each compound are also shown. The structures of **2** and **3** were confirmed by NMR, while the structure of **4** is a proposal that correlates with MS^2 data, the core peptide sequence, and predicted post-translational modifications.

270−272 nm (Figure S6), which is characteristic of thioamides.[13] Notably, the MS^2 data were consistent with *N*-terminal lactyl (**2**) or pyruvyl (**3** and **4**) moieties, rather than the 2-hydroxy-2-methyl-4-oxopentanoyl group of **1**.

Cloning and Heterologous Expression of the Thiostreptamide S4 Gene Cluster. To confirm that these molecules were indeed produced by thioviridamide-like pathways, we employed two different genetic approaches: gene disruption in a native producer strain and heterologous expression of a gene cluster. These approaches could both be achieved for the *tsa* cluster predicted to make **3** in *Streptomyces* sp. NRRL S-4. Gene cluster disruption was achieved by single crossover recombination between the *tsaH* gene (encoding a YcaO domain protein[14]) and its truncated sequence cloned in pKC1132[15] to generate *Streptomyces* sp. NRRL S-4 Δ*tsaH*. Production of **3** was abolished in this mutant strain (Figure 3), indicating that the gene cluster does indeed make this TLM. To support this result, we employed transformation associated recombination (TAR) cloning[16−19] to generate a plasmid for heterologous expression of the *tsa* cluster. Here, a 19 kbp sequence from *Streptomyces* sp. NRRL S-4 containing the putative thioviridamide-like gene cluster, as well as flanking regions up- and downstream, was cloned into the ΦC31

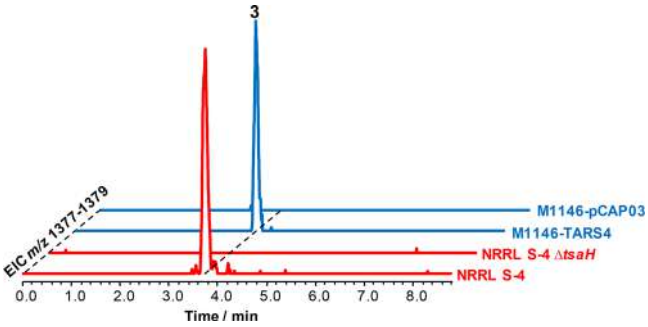

Figure 3. Production of thiostreptamide S4 in *Streptomyces* sp. NRRL S-4 and in *S. coelicolor* M1146-TARS4. Control strains unable to produce the compound are also shown.

integrative vector pCAP03[20] using TAR in *Saccharomyces cerevisiae* VL6-48N.[21] A successful clone (TARS4) was verified by PCR and restriction analysis and was introduced into *Streptomyces coelicolor* M1146[22] by intergeneric conjugation.[23] *S. coelicolor* M1146-TARS4 was cultured on solid BPM, and its LC-MS production profile was compared with a control strain containing an empty pCAP03 vector and wild type *Streptomyces* sp. NRRL S-4 as a positive control (Figure 3). *S. coelicolor*

DOI: 10.1021/acschembio.7b00677
ACS Chem. Biol. XXXX, XXX, XXX−XXX

M1146-TARS4 produced a compound with m/z 1377.55 that had an identical retention time and MS^2 spectrum to those of **3** (Figure 3 and Figure S7), thereby proving that the cloned region is sufficient for thiostreptamide S4 biosynthesis.

Detailed Structural Analysis Reveals the Diversity within the Thioviridamide Family. To confirm the MS^2 data and to pinpoint the location of additional post-translational modifications, fermentation cultures of the native producing strains were scaled up, and each compound was purified for structural elucidation by NMR. Compounds **2** and **3** were obtained in yields of 2 and 0.38 mg per liter of solid culture from their respective native producers, and 1D and 2D NMR experiments (^{1}H, ^{13}C, COSY, HSQC, HMBC, Figures S12–S24, Table S6) allowed us to establish their chemical structures. The ^{13}C NMR spectrum for thioalbamide (**2**, Figure 4) showed three downfield signals at δ_C 206.7, 207.0, and 207.5

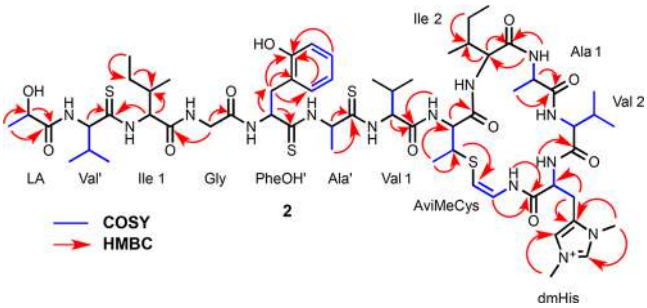

Figure 4. COSY and HMBC correlations identified for the structural characterization of **2**.

corresponding to nonprotonated carbons and indicating the presence of thioamide groups. These signals and their associated HMBC data correlate with the MS^2 data for this compound, proving that the molecule has three thioamide linkages in the linear portion of the molecule. HMBC and COSY correlations also confirmed that the molecule has an AviMeCys-containing macrocycle, consistent with a Thr8 residue in the core peptide of TaaA instead of the Ser8 residue of the core peptide of **1**. NMR analysis of the N_1,N_3-dimethylhistidinium residue showed that its β-carbon is a CH_2 group (δ_C 22.6) and therefore lacks the β-hydroxy group present in **1**. This is in agreement with the lack of a TvaJ-like 2-oxoglutarate/Fe(II)-dependent hydroxylase in the thioalbamide pathway.

MS^2 data indicated that Phe5 is hydroxylated in **2**, but the precise location of this modification could not be determined by MS^2. The ^{1}H NMR spectrum of **2** showed the presence of four nonequivalent aromatic protons at δ_H 6.83 (1H, ddd, 8.1, 8.0, 1.6), 6.87 (1H, dd, 8.0, 1.6), 7.12 (1H, ddd, 8.1, 8.0, 1.6), and 7.19 (1H, dd, 8.0, 1.6), corresponding to protons on the 1, 2, 3, and 4 positions of the phenyl group, and indicating that it is hydroxylated at the 5-position of the ring. Alongside the absence of a β-hydroxy group on histidine, this suggests that a cytochrome P450 (TaaCYP) encoded in the *taa* cluster does not functionally replace the hydroxylase absent from this pathway and instead catalyzes aromatic hydroxylation, thereby generating additional structural diversity within the TLM family. The predicted *N*-terminal lactate moiety of **2** was also confirmed based on the HMBC correlations between the methyl group at δ_H 1.38 (3H, d, 6.8) with carbon signals at δ_C 69.2 and 177.6. Interestingly, this is analogous to the *N*-terminus of JBIR-140, which is produced when the thioviridamide BGC is expressed in *Streptomyces avermitilis* SUKA17.[24] We propose that a NAD(P)H-dependent reductase (TaaRED) catalyzes this reduction in the thioalbamide pathway, whereas it is likely that the reduction to generate JBIR-140 is catalyzed by a promiscuous reductase from *S. avermitilis*.

We were also able to pinpoint the post-translational modifications of **3** by analysis of the MS^2 and NMR data. While it was not possible to establish full 2D NMR correlations throughout **3**, four thioamide linkages were identified by HMBC data (δ_C 200.6, 201.2, 202.2, and 204.6). HMBC correlations between a methyl group at δ_H 2.35 (3H, s) with carbon signals at δ_C 160.4 and 197.0, along with HMBC correlations between an amide proton at δ_H 8.22 with carbon signals at δ_C 160.4 and 63.1, allowed us to confirm the *N*-terminal pyruvyl group attached to Val′ (Figure S8). The MS^2 fragment predicted to be the AviMeCys-containing macrocycle (m/z 687.33) matches a mass calculated from the core peptide and expected post-translational modifications if the macrocycle features a methyl group in addition to a hdmHis residue. Accordingly, the ^{1}H NMR spectrum displayed a singlet at δ_H 3.71 and two equivalent aromatic protons at δ_H 6.79 (2H, d, 8.7) and 7.03 (2H, d, 8.7) that were consistent with *O*-methylation of Tyr11, presumably catalyzed by the additional methyltransferase (TsaMT, pfam08242) encoded in the *tsa* gene cluster. The lack of any further oxidative modifications indicated that the flavin-dependent monooxygenase at the end of the gene cluster (TsaMO) is not involved in thiostreptamide S4 biosynthesis. Along with characteristic NMR signals, the presence of a hdmHis residue was supported by an MS^2 fragment of m/z 125.07 for **3** that concurs with retro-aldol fragmentation of the hdmHis residue (Figure S4) and was not present in the MS^2 spectrum of **2**.

We were unable to obtain sufficient **4** for detailed NMR characterization, but its exact mass and MS^2 spectrum (Figure S5) were fully consistent with the structure reported in Figure 2. This is in agreement with a lack of any additional tailoring enzymes encoded in the S-87 *tsd* gene cluster compared to the *tva* gene cluster (Figure 1c). MS^2 data for **4** provided a macrocycle mass (m/z 657.31) that fits with the core peptide sequence assuming AviMeCys formation and the presence of the hdmHis residue. This is supported by MS^2 fragmentation to generate m/z 125.07, which was also seen for **3** and is indicative of the hdmHis residue. Notably, the y fragments of **4** signified an *N*-terminal pyruvyl group. In some fermentation trials, compounds of m/z 1393.5427 and m/z 1321.4813 were produced by *Streptomyces* sp. NRRL S-4 and *Streptomyces* sp. NRRL S-87, respectively (Figures S9 and S10). These masses indicated the addition of one oxygen (calcd. m/z 1393.5416 and m/z 1321.4841) to **3** and **4**, respectively. MS^2 fragmentation of these molecule demonstrated that the side-chain sulfur on the Met3 residues on each compound are oxidized, shown by y fragments that are identical to their parent TLMs and the loss of methanesulfenic acid (CH_3SOH, 64.00 Da) from the parent ion, which is characteristic of oxidized methionine.[25,26] The late onset and inconsistent production of these molecules indicates that they are generated by non-enzymatic oxidation during purification rather than being true pathway products.

A Nonenzymatic Origin of the Unusual *N*-Terminus of Thioviridamide. One significant difference between the molecules reported here and **1** is at their *N*-termini, where **1** features a 2-hydroxy-2-methyl-4-oxopentanoyl group. Instead, **2**

DOI: 10.1021/acschembio.7b00677
ACS Chem. Biol. XXXX, XXX, XXX–XXX

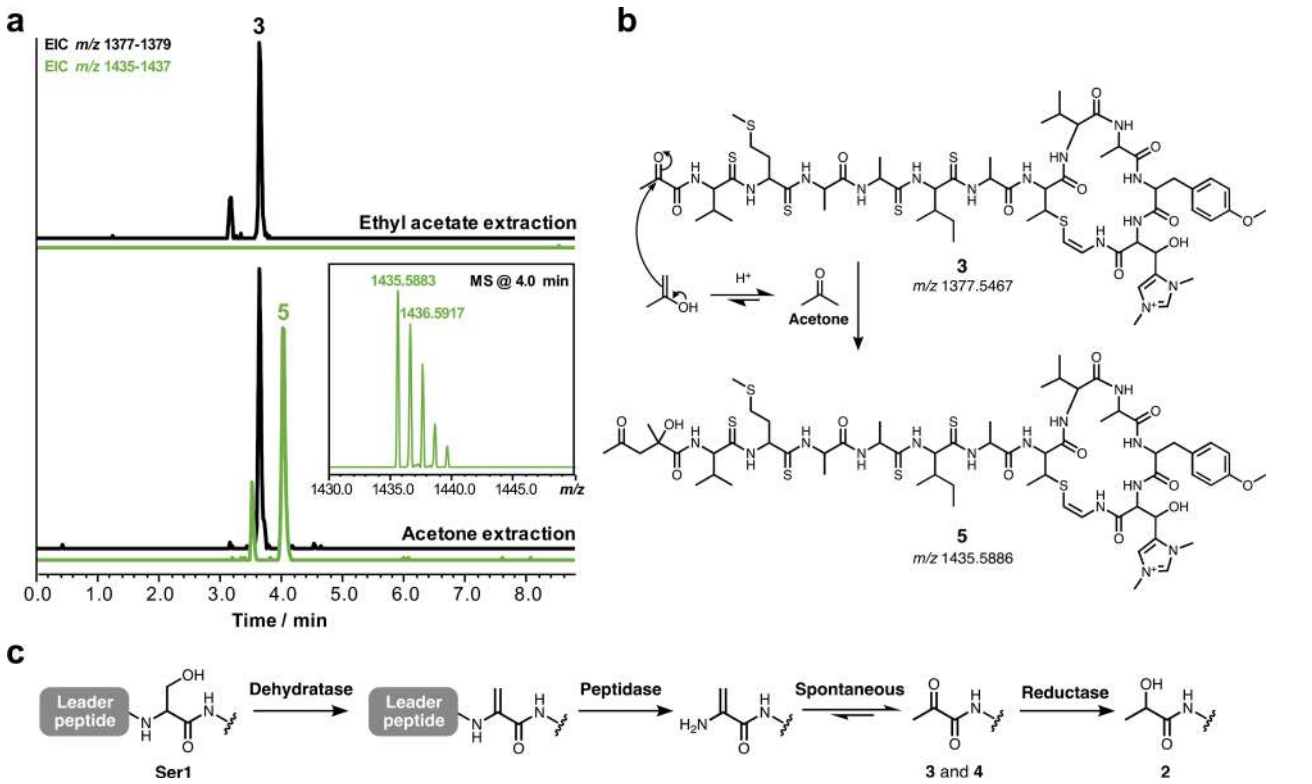

Figure 5. *N*-terminal modification of TLMs. (a) LC-MS extracted ion chromatograms of *S. coelicolor* M1146-TARS4 extracted with either ethyl acetate (top) or acetone (bottom). (b) Generation of the *N*-terminal 2-hydroxy-2-methyl-4-oxopentanoyl group *via* reaction with acetone. (c) Biosynthetic proposal for the generation of the *N*-terminal pyruvyl and lactyl moieties.

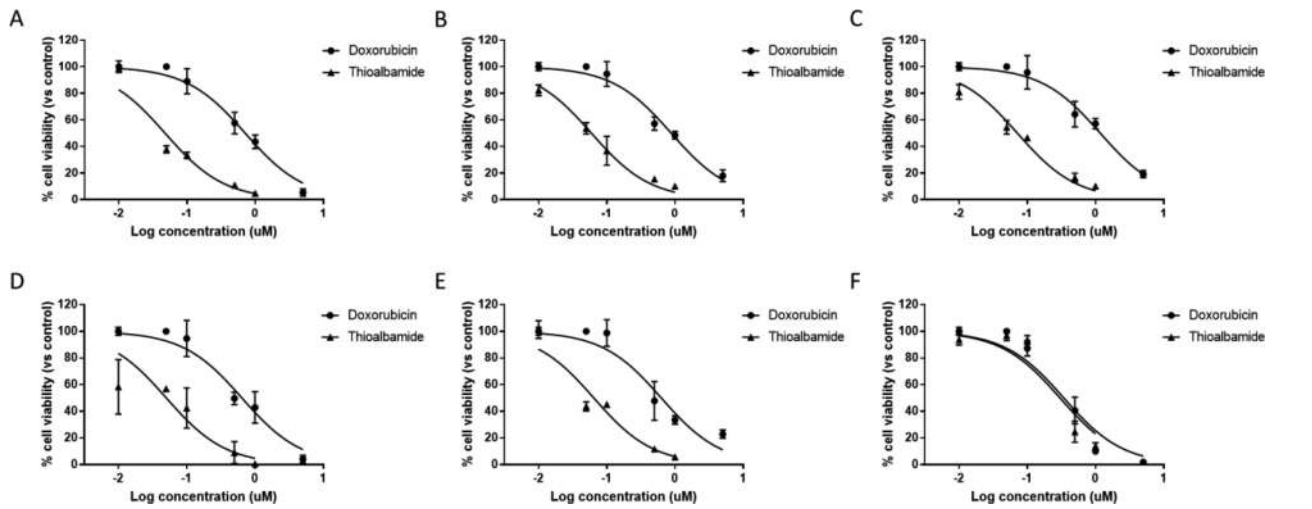

Figure 6. Effect of thioalbamide (**2**) on cell growth. Cellular growth assessment after treatment of A549 (A), MCF7 (B), MDA-MB-231 (C), HeLa (D), PA-TU-8988T (E), and MCF-10A (F) cell lines with different concentrations (0.1 to 1 μM) of **2** for 72 h. Results, quantified by the MTT assay, are expressed as a percentage of growth versus control cells treated with DMSO. Values represent mean ± SD of three independent experiments, each one performed with triplicate samples.

contains a lactyl moiety, while **3** and **4** each have pyruvyl groups. However, the *tva* gene cluster does not appear to encode any additional biosynthetic enzymes in comparison to the clusters reported here. This observation led us to speculate that the unusual *N*-terminus of thioviridamide could feasibly be generated from an aldol reaction between a pyruvyl group and acetone, which was used in the published extraction of thioviridamide.[5] In contrast, we used either methanol or ethyl acetate to extract our TLMs. We therefore used acetone to extract solid cultures of both *Streptomyces* sp. NRRL S-4 and *S. coelicolor* M1146-TARS4, which resulted in the production of a mixture of **3** (m/z 1377.55) and a comparable amount of a compound with m/z 1435.58 (**5**, Figure 5a) that was not found when other solvents were used for extraction. MS^2 data for **5** are consistent with an *N*-terminal 2-hydroxy-2-methyl-4-oxopentanoyl group (Figure S11), which implies that the true product of the thioviridamide pathway has an *N*-terminal pyruvyl group (Figure 5b). Instead of being a post-translation-

DOI: 10.1021/acschembio.7b00677
ACS Chem. Biol. XXXX, XXX, XXX−XXX

ally introduced modification, this pyruvyl group could derive from a dehydrated *N*-terminal serine, which then spontaneously tautomerizes and exchanges with water following removal of the leader peptide (Figure 5c).

This result is consistent with a conserved serine residue at this position in almost all TLM precursor peptides (Figure 1b), and a homologous reaction has been proposed to be involved in the generation of the unusual *N*-terminus of polytheonamide from threonine,[27] the *N*-terminal 2-oxobutanoyl group of lacticin 3147 A2,[28] and a pyruvyl group in a thiostrepton derivative generated by mutagenesis.[29] The serine dehydration in TLM biosynthesis could feasibly be catalyzed by the same dehydratase that introduces the 2,3-didehydrobutyrine residue required for forming the AviMeCys macrocycle. Interestingly, the TLM gene clusters do not encode any Lan-like proteins that are usually required for dehydration,[1] nor can a cypemycin-like mechanism occur, as this uses cysteine as a precursor to 2,3-didehydroalanine.[30]

Thioalbamide Is a Potent Anticancer Compound with Selective Activity. Thioviridamide has been reported to possess a potent antiproliferative effect against cancer cell lines.[5] We were therefore interested in determining whether any of our newly discovered compounds exhibited comparable bioactivity. Compound **2** was therefore subjected to a series of activity assays on various model organisms, including both prokaryotic and eukaryotic systems. A wide panel of cancer cell lines were tested, including alveolar (A549), uterine cervical (HeLa), pancreatic (PA-TU-8988T), and luminal and basal breast (MCF7 and MDA-MB-231) adenocarcinoma cell lines (Figure 6). Compound **2** showed intense antiproliferative activity on all tumor lines tested with IC_{50} values ranging from 48 to 72 nM (Table 1). Remarkably, the cytotoxic activity of **2** was found to be highly specific to tumor cells, as IC_{50} values on a nontumor breast epithelial cell line (MCF 10A) were 6 times higher than those found in cancer cells. This selectivity means that thioalbamide activity toward tumor lines is superior (>10× lower IC_{50}) to the clinically used doxorubicin but exhibits a comparable IC_{50} to doxorubicin toward the one healthy cell line we tested. In order to further investigate the specificity of the cytotoxic activity of **2**, it was tested against Gram positive (*Staphylococcus aureus*) and Gram negative (*Escherichia coli*, *Klebsiella pneumoniae*, and *Pseudomonas aeruginosa*) bacterial strains, and against the fungus *Candida albicans*. In each case, it did not inhibit the growth of the tested microorganisms, except for *S. aureus*, which was sensitive to high concentrations of **2**, with a minimum inhibitory concentration (MIC) of 24 μM (Table S7). At this concentration, however, activity was purely bacteriostatic and not bactericidal, as the minimum bactericidal concentration was over 48 μM.

Table 1. Cytotoxic Activity of 2 in Comparison to Doxorubicin[a]

cell line		doxorubicin	2
A549	IC_{50}	0.712	0.048
	95% confidence interval	0.582 to 0.872	0.035 to 0.064
MCF7	IC_{50}	0.878	0.059
	95% confidence interval	0.723 to 1.071	0.049 to 0.072
MDA-MB-231	IC_{50}	1.174	0.072
	95% confidence interval	0.938 to 1,477	0.058 to 0.088
HeLa	IC_{50}	0.644	0.050
	95% confidence interval	0.487 to 0.852	0.027 to 0.090
PA-TU-8988T	IC_{50}	0.630	0.065
	95% confidence interval	0.451 to 0.888	0.047 to 0.089
MCF 10A	IC_{50}	0.343	0.302
	95% confidence interval	0.253 to 0.464	0.206 to 0.444

[a]Data are presented as IC_{50} values (μM) and 95% confidence intervals obtained by nonlinear regression analysis of three independent experiments.

SUMMARY

We report the genomics-guided discovery of three novel thioviridamide-like molecules and show that thioalbamide possesses nanomolar antiproliferative activity with approximately 6-fold selectivity for cancer cells over healthy cells. A recent analysis indicated that the TLMs are one of the rarest families of RiPP pathways across sequenced genomes,[31] yet our work indicates that the family features a significant amount of structural diversity, both within the precursor peptide and by the array of modifying enzymes encoded in each cluster. TAR cloning was utilized to clone the thiostreptamide S4 (**3**) pathway, which was expressed in *S. coelicolor* M1146 to produce **3** at levels comparable to the wild type producing strain. This provides a promising platform for the future engineered production of novel TLMs, especially given the diversity identified across the 14 pathways that are currently sequenced. Our identification of these pathways should facilitate the characterization of the biosynthetic enzymes involved in the generation of these fascinating molecules. We propose that the reported *N*-terminus of thioviridamide is an artifact of acetone extraction and that the true pathway product features an *N*-terminal pyruvyl group derived from serine. Finally, the newly identified TLM **2** possesses remarkable antiproliferative activity on all cancer cell lines that were tested, while being significantly less active toward a healthy nonmalignant cell line. Further work is required to determine whether **2** is similarly less active toward other noncancerous cell lines. The nanomolar levels of activity of **2** are superior to the clinically used anticancer agent doxorubicin across all tumor cell lines. This result indicates the power of genome mining to discover new anticancer molecules with clinical potential, and future studies will define the molecular mechanisms underlying the high pharmacological potential of the TLMs.

ASSOCIATED CONTENT

Supporting Information

The Supporting Information is available free of charge on the ACS Publications website at DOI: 10.1021/acschembio.7b00677.

Experimental details, LC-MS and NMR spectra, and supporting figures and tables (PDF)

AUTHOR INFORMATION

Corresponding Author

*Tel.: +44(0)1603 450750. E-mail: andrew.truman@jic.ac.uk.

ORCID

Andrew W. Truman: 0000-0001-5453-7485

Notes

The authors declare no competing financial interest.

ACKNOWLEDGMENTS

We would like to thank T. Eyles (John Innes Centre, U.K.) for assistance with TAR cloning, B. Wilkinson (JIC, U.K.) for

helpful discussions and feedback on this manuscript, G. Saalbach (JIC, U.K.) for LC-MS assistance, and D. Howe and P. Grice (Department of Chemistry, University of Cambridge) for running NMR experiments. We are also very grateful to B. Moore (Scripps Institution of Oceanography, University of California San Diego, U.S.A.) for providing pCAP03, V. Larionov (National Cancer Institute, NIH, U.S.A.) for providing *S. cerevisiae* VL6-48N, and M. Bibb (JIC, U.K.) for providing *S. coelicolor* M1146. This work was supported by a Royal Society University Research Fellowship (A.W.T.) and the BBSRC MET ISP (BB/J004561/1) at the John Innes Centre (A.W.T. and R.L.).

■ REFERENCES

(1) Arnison, P. G., Bibb, M. J., Bierbaum, G., Bowers, A. A., Bugni, T. S., Bulaj, G., Camarero, J. A., Campopiano, D. J., Challis, G. L., Clardy, J., Cotter, P. D., Craik, D. J., Dawson, M., Dittmann, E., Donadio, S., Dorrestein, P. C., Entian, K.-D., Fischbach, M. A., Garavelli, J. S., Göransson, U., Gruber, C. W., Haft, D. H., Hemscheidt, T. K., Hertweck, C., Hill, C., Horswill, A. R., Jaspars, M., Kelly, W. L., Klinman, J. P., Kuipers, O. P., Link, A. J., Liu, W., Marahiel, M. A., Mitchell, D. A., Moll, G. N., Moore, B. S., Müller, R., Nair, S. K., Nes, I. F., Norris, G. E., Olivera, B. M., Onaka, H., Patchett, M. L., Piel, J., Reaney, M. J. T., Rebuffat, S., Ross, R. P., Sahl, H.-G., Schmidt, E. W., Selsted, M. E., Severinov, K., Shen, B., Sivonen, K., Smith, L., Stein, T., Süssmuth, R. D., Tagg, J. R., Tang, G.-L., Truman, A. W., Vederas, J. C., Walsh, C. T., Walton, J. D., Wenzel, S. C., Willey, J. M., and van der Donk, W. A. (2013) Ribosomally synthesized and post-translationally modified peptide natural products: overview and recommendations for a universal nomenclature. *Nat. Prod. Rep. 30*, 108−160.

(2) Truman, A. W. (2016) Cyclisation mechanisms in the biosynthesis of ribosomally synthesised and post-translationally modified peptides. *Beilstein J. Org. Chem. 12*, 1250−1268.

(3) Andes, D., Craig, W., Nielsen, L. A., and Kristensen, H. H. (2009) In vivo pharmacodynamic characterization of a novel plectasin antibiotic, NZ2114, in a murine infection model. *Antimicrob. Agents Chemother. 53*, 3003−3009.

(4) Dischinger, J., Basi Chipalu, S., and Bierbaum, G. (2014) Lantibiotics: promising candidates for future applications in health care. *Int. J. Med. Microbiol. 304*, 51−62.

(5) Hayakawa, Y., Sasaki, K., Adachi, H., Furihata, K., Nagai, K., and Shin-ya, K. (2006) Thioviridamide, a novel apoptosis inducer in transformed cells from Streptomyces olivoviridis. *J. Antibiot. 59*, 1−5.

(6) Sit, C. S., Yoganathan, S., and Vederas, J. C. (2011) Biosynthesis of Aminovinyl-Cysteine-Containing Peptides and Its Application in the Production of Potential Drug Candidates. *Acc. Chem. Res. 44*, 261−268.

(7) Hayakawa, Y., Sasaki, K., Nagai, K., Shin-ya, K., and Furihata, K. (2006) Structure of thioviridamide, a novel apoptosis inducer from Streptomyces olivoviridis. *J. Antibiot. 59*, 6−10.

(8) De Zotti, M., Peggion, C., Biondi, B., Crisma, M., Formaggio, F., and Toniolo, C. (2016) Endothioxopeptides: A conformational overview. *Biopolymers 106*, 697−713.

(9) Izawa, M., Kawasaki, T., and Hayakawa, Y. (2013) Cloning and heterologous expression of the thioviridamide biosynthesis gene cluster from Streptomyces olivoviridis. *Appl. Environ. Microbiol. 79*, 7110−7113.

(10) Nayak, D. D., Mahanta, N., Mitchell, D. A., and Metcalf, W. W. (2017) Post-translational thioamidation of methyl-coenzyme M reductase, a key enzyme in methanogenic and methanotrophic Archaea. *eLife 6*, e29218.

(11) Medema, M. H., Takano, E., and Breitling, R. (2013) Detecting sequence homology at the gene cluster level with MultiGeneBlast. *Mol. Biol. Evol. 30*, 1218−1223.

(12) Crone, W. J. K., Vior, N. M., Santos-Aberturas, J., Schmitz, L. G., Leeper, F. J., and Truman, A. W. (2016) Dissecting Bottromycin Biosynthesis Using Comparative Untargeted Metabolomics. *Angew. Chem., Int. Ed. 55*, 9639−9643.

(13) Huang, Y., Ferrie, J. J., Chen, X., Zhang, Y., Szantai-Kis, D. M., Chenoweth, D. M., and Petersson, E. J. (2016) Electronic interactions of i, i + 1 dithioamides: increased fluorescence quenching and evidence for n-to-π^* interactions. *Chem. Commun. 52*, 7798−7801.

(14) Burkhart, B. J., Schwalen, C. J., Mann, G., Naismith, J. H., and Mitchell, D. A. (2017) YcaO-Dependent Posttranslational Amide Activation: Biosynthesis, Structure, and Function. *Chem. Rev. 117*, 5389−5456.

(15) Bierman, M., Logan, R., O'Brien, K., Seno, E. T., Nagaraja Rao, R., and Schoner, B. E. (1992) Plasmid cloning vectors for the conjugal transfer of DNA from Escherichia coli to Streptomyces spp. *Gene 116*, 43−49.

(16) Larionov, V., Kouprina, N., Graves, J., Chen, X. N., Korenberg, J. R., and Resnick, M. A. (1996) Specific cloning of human DNA as yeast artificial chromosomes by transformation-associated recombination. *Proc. Natl. Acad. Sci. U. S. A. 93*, 491−496.

(17) Kouprina, N., and Larionov, V. (2008) Selective isolation of genomic loci from complex genomes by transformation-associated recombination cloning in the yeast Saccharomyces cerevisiae. *Nat. Protoc. 3*, 371−377.

(18) Kim, J. H., Feng, Z., Bauer, J. D., Kallifidas, D., Calle, P. Y., and Brady, S. F. (2010) Cloning large natural product gene clusters from the environment: piecing environmental DNA gene clusters back together with TAR. *Biopolymers 93*, 833−844.

(19) Yamanaka, K., Reynolds, K. A., Kersten, R. D., Ryan, K. S., Gonzalez, D. J., Nizet, V., Dorrestein, P. C., and Moore, B. S. (2014) Direct cloning and refactoring of a silent lipopeptide biosynthetic gene cluster yields the antibiotic taromycin A. *Proc. Natl. Acad. Sci. U. S. A. 111*, 1957−1962.

(20) Tang, X., Li, J., Millán-Aguiñaga, N., Zhang, J. J., O'Neill, E. C., Ugalde, J. A., Jensen, P. R., Mantovani, S. M., and Moore, B. S. (2015) Identification of Thiotetronic Acid Antibiotic Biosynthetic Pathways by Target-directed Genome Mining. *ACS Chem. Biol. 10*, 2841−2849.

(21) Noskov, V., Kouprina, N., Leem, S.-H., Koriabine, M., Barrett, J. C., and Larionov, V. (2002) A genetic system for direct selection of gene-positive clones during recombinational cloning in yeast. *Nucleic Acids Res. 30*, 8e.

(22) Gomez-Escribano, J. P., and Bibb, M. J. (2011) Engineering Streptomyces coelicolor for heterologous expression of secondary metabolite gene clusters. *Microb. Biotechnol. 4*, 207−215.

(23) Kieser, T., Bibb, M. J., Buttner, M. J., Chater, K. F., and Hopwood, D. A. (2000) *Practical Streptomyces Genetics*, John Innes Foundation, Norwich.

(24) Izumikawa, M., Kozone, I., Hashimoto, J., Kagaya, N., Takagi, M., Koiwai, H., Komatsu, M., Fujie, M., Satoh, N., Ikeda, H., and Shin-ya, K. (2015) Novel thioviridamide derivative−JBIR-140: heterologous expression of the gene cluster for thioviridamide biosynthesis. *J. Antibiot. 68*, 533−536.

(25) Guan, Z., Yates, N. A., and Bakhtiar, R. (2003) Detection and characterization of methionine oxidation in peptides by collision-induced dissociation and electron capture dissociation. *J. Am. Soc. Mass Spectrom. 14*, 605−613.

(26) Miles, C. O., Melanson, J. E., and Ballot, A. (2014) Sulfide oxidations for LC-MS analysis of methionine-containing microcystins in Dolichospermum flos-aquae NIVA-CYA 656. *Environ. Sci. Technol. 48*, 13307−13315.

(27) Freeman, M. F., Gurgui, C., Helf, M. J., Morinaka, B. I., Uria, A. R., Oldham, N. J., Sahl, H. G., Matsunaga, S., and Piel, J. (2012) Metagenome Mining Reveals Polytheonamides as Posttranslationally Modified Ribosomal Peptides. *Science 338*, 387−390.

(28) Cotter, P. D., Deegan, L. H., Lawton, E. M., Draper, L. A., O'Connor, P. M., Hill, C., and Ross, R. P. (2006) Complete alanine scanning of the two-component lantibiotic lacticin 3147: generating a blueprint for rational drug design. *Mol. Microbiol. 62*, 735−747.

(29) Li, C., Zhang, F., and Kelly, W. L. (2012) Mutagenesis of the thiostrepton precursor peptide at Thr7 impacts both biosynthesis and function. *Chem. Commun. 48*, 558−560.

(30) Claesen, J., and Bibb, M. (2010) Genome mining and genetic analysis of cypemycin biosynthesis reveal an unusual class of

DOI: 10.1021/acschembio.7b00677
ACS Chem. Biol. XXXX, XXX, XXX−XXX

posttranslationally modified peptides. *Proc. Natl. Acad. Sci. U. S. A. 107*, 16297−16302.

(31) Skinnider, M. A., Johnston, C. W., Edgar, R. E., Dejong, C. A., Merwin, N. J., Rees, P. N., and Magarvey, N. A. (2016) Genomic charting of ribosomally synthesized natural product chemical space facilitates targeted mining. *Proc. Natl. Acad. Sci. U. S. A. 113*, E6343−E6351.

DOI: 10.1021/acschembio.7b00677
ACS Chem. Biol. XXXX, XXX, XXX−XXX

www.impactjournals.com/oncotarget/ Oncotarget, 2017, Vol. 8, (No. 40), pp: 67457-67472

Research Paper

Mitoriboscins: Mitochondrial-based therapeutics targeting cancer stem cells (CSCs), bacteria and pathogenic yeast

Bela Ozsvari[1,2], Marco Fiorillo[1,2,3], Gloria Bonuccelli[1,2], Anna Rita Cappello[3], Luca Frattaruolo[3], Federica Sotgia[1,2], Rachel Trowbridge[5], Richard Foster[4,5] and Michael P. Lisanti[1,2]

[1] Translational Medicine, School of Environment & Life Sciences, University of Salford, Greater Manchester, UK

[2] The Paterson Institute, University of Manchester, Withington, UK

[3] The Department of Pharmacy, Health and Nutritional Sciences, The University of Calabria, Cosenza, Italy

[4] Astbury Centre for Structural Molecular Biology, University of Leeds, West Yorkshire, UK

[5] School of Chemistry, Faculty of Mathematics and Physical Sciences, University of Leeds, West Yorkshire, UK

Correspondence to: *Michael P. Lisanti,* ***email***: *michaelp.lisanti@gmail.com*

Richard Foster, ***email***: *r.foster@leeds.ac.uk*

Keywords: antibiotic, drug design, mitochondrial ribosome, mitoribosome, mitochondria

Received: *April 02, 2017* ***Accepted***: *May 17, 2017* ***Published***: *July 07, 2017*

ABSTRACT

The "endo-symbiotic theory of mitochondrial evolution" states that mitochondrial organelles evolved from engulfed aerobic bacteria, after millions of years of symbiosis and adaptation. Here, we have exploited this premise to design new antibiotics and novel anti-cancer therapies, using a convergent approach. First, virtual high-throughput screening (vHTS) and computational chemistry were used to identify novel compounds binding to the 3D structure of the mammalian mitochondrial ribosome. The resulting library of ~880 compounds was then subjected to phenotypic drug screening on human cancer cells, to identify which compounds functionally induce ATP-depletion, which is characteristic of mitochondrial inhibition. Notably, the top ten "hit" compounds define four new classes of mitochondrial inhibitors. Next, we further validated that these novel mitochondrial inhibitors metabolically target mitochondrial respiration in cancer cells and effectively inhibit the propagation of cancer stem-like cells *in vitro*. Finally, we show that these mitochondrial inhibitors possess broad-spectrum antibiotic activity, preventing the growth of both gram-positive and gram-negative bacteria, as well as *C. albicans* - a pathogenic yeast. Remarkably, these novel antibiotics also were effective against methicillin-resistant Staphylococcus aureus (MRSA). Thus, this simple, yet systematic, approach to the discovery of mitochondrial ribosome inhibitors could provide a plethora of anti-microbials and anti-cancer therapies, to target drug-resistance that is characteristic of both i) tumor recurrence and ii) infectious disease. In summary, we have successfully used vHTS combined with phenotypic drug screening of human cancer cells to identify several new classes of broad-spectrum antibiotics that target both bacteria and pathogenic yeast. We propose the new term "mitoriboscins" to describe these novel mitochondrial-related antibiotics. Thus far, we have identified four different classes of mitoriboscins, such as: *1) mitoribocyclines, 2) mitoribomycins, 3) mitoribosporins and 4) mitoribofloxins.* However, we broadly define mitoriboscins as any small molecule(s) or peptide(s) that bind to the mitoribosome (large or small subunits) and, as a consequence, inhibit mitochondrial function, i.e., mitoribosome inhibitors.

INTRODUCTION

Evidence is accumulating that increased mitochondrial biogenesis may play a critical role in the successful propagation and maintenance of the cancer stem-like cell (CSC) phenotype [1-9].

Analysis of transcriptional profiling data from human breast cancer samples ($N = 28$ patients) revealed that > 95 mRNA transcripts associated with mitochondrial biogenesis and/or mitochondrial translation are significantly elevated in cancer cells, as compared with adjacent stromal tissue [10, 11]. Remarkably, > 35 of these 95 upregulated mRNA's encode mitochondrial ribosomal proteins (MRPs) [11]. MRPs are the functional subunits of the mitochondrial ribosomes (mitoribosomes), which are responsible for the mitochondrial translation of 13 protein components of the OXPHOS complex encoded by mitochondrial DNA. In this context, MRPS gene products are used to form the small subunit of the mitoribosome, while MRPL gene products are used to generate the large subunit of the mitoribosome [12-15].

Most of these 36 mitoribosome-related mRNA transcripts were elevated between 2- to 5-fold in human breast cancer cells, including seventeen members of the MRPS gene family (S7, S11, S12, S13, S14, S15, S17, S18A, S18B, S22, S26, S27, S28, S30, S31, S33, S35) and nineteen members of the MRPL gene family (L3, L9, L15, L16, L17, L18, L20, L22, L24, L33, L39, L40, L42, L46, L48, L49, L52, L54, L57) [11].

Proteomic analysis of human breast cancer stem-like cells also revealed the significant over-expression of several mitoribosomal proteins, such as MRPL45 and MRPL17, and 6 other proteins associated with mitochondrial biogenesis (HSPA9, TIMM8A, GFM1, HSPD1 [a.k.a., HSP60], TSFM, TUFM) [1]. Importantly, functional inhibition of mitochondrial biogenesis, using the off-target effects of certain bacteriostatic antibiotics, effectively ablated the propagation of CSCs, in 12 cell lines representing 8 different tumor types (breast, DCIS, prostate, ovarian, pancreatic, lung, melanoma and glioblastoma) [3, 5]. Virtually identical results were also obtained with *bonafide* OXPHOS inhibitors (pyrvinium pamoate and atovaquone), providing additional complementary evidence that functional mitochondria are required for the propagation of CSCs [3, 16]. Taken together, these preliminary studies provide the necessary evidence that the development of novel mitoribosome inhibitors might be a beneficial approach for the more effective treatment of cancer patients.

Recently, the 3D structures of both the large (39S) and the small (28S) subunits of the mammalian mitoribosome (55S) have been resolved [17-22], allowing for the rationale molecular design of mitoribosome inhibitors.

Here, we used the known 3D structure of the large 39S mammalian mitoribosome as a target to perform virtual high-throughput screening (vHTS). We coupled this computational chemistry approach with phenotypic drug screening, allowing for the functional identification and validation of novel compounds targeting mammalian mitoribosomes. The ability of these mitochondrial inhibitors to functionally prevent oxygen-consumption and halt ATP production was also demonstrated by metabolic flux analysis. Most importantly, these mitochondrial inhibitors effectively blocked the propagation of CSC, as predicted, providing proof-of-concept.

Interestingly, we also show that these mitochondrial inhibitors behave as broad-spectrum antibiotics, which is consistent with the well-established hypothesis that mitochondria originally evolved from the engulfment of aerobic bacteria, approximately 1.5 billion years ago [23-28]. This has important implications for more effectively combating the development of antibiotic-resistance.

RESULTS

Exploiting the evolutionary relationship between bacteria and mitochondria, to drive the discovery of new antibiotics and novel anti-cancer agents

The "Endo-symbiotic Theory of Mitochondrial Evolution" states that mitochondria originally evolved from aerobic bacteria that were incorporated into eukaryotic cells [23-28], during millions of years of adaptation (Figure 1). Consistent with this theory, we have recently shown that certain classes of well-known antibiotics that inhibit bacterial protein synthesis [29-31], can also be used to successfully target mitochondrial protein translation, especially in cancer stem-like cells (CSCs) [32].

However, the converse of these observations should also be true. More specifically, new inhibitors of mitochondrial protein translation should also possess anti-microbial activity. Here, to test this hypothesis directly, we used the known 3D structure of the mammalian mitochondrial ribosome (large subunit) to identify novel compounds that bind to it, in the context of virtual high-throughput screening (i.e., *in silico* drug screening). Once potential binding partners were identified *in silico*, then these 880 compounds were subjected to phenotypic drug screening *in vitro,* to select positive hits that functionally induced ATP-depletion in MCF7 human breast cancer cells. Approximately 85% of cellular ATP is normally generated by OXPHOS in mitochondria, so ATP-depletion is a valid surrogate marker for mitochondrial inhibition. However, only compounds depleting ATP levels without prominent cytotoxicity were selected for further analysis.

These positive hits were then subjected to further validation, using the Seahorse metabolic flux analyzer, to confirm their mechanism of action as mitochondrial

inhibitors. Finally, these novel compounds were tested on six distinct bacterial and/or yeast strains to investigate if they possess anti-microbial activity. This overall experimental strategy is outlined schematically as a flow-diagram in Figure 2.

Identification and validation of novel inhibitors of the large mitochondrial ribosome

The resulting 880 compounds were first subjected to phenotypic drug screening at a concentration of 50 µM, to identify which compounds functionally induce ATP-depletion, before inducing cell death. Subsequently, positive hits were re-screened at lower concentrations (25 µM and 10 µM), to identify the top 10 compounds that most potently induced ATP-depletion.

Results from the ATP-depletion assay for the top 10 hits identified from phenotypic drug screening are shown in detail in Figure 3. Briefly, MCF7 cells were treated with the hit compounds at 10 µM for 72 hours. Hoechst staining showed cell viability based on DNA staining, while measurement of ATP content revealed the effect of compounds on metabolic activity during the very same treatments. Compounds inhibiting mitochondrial metabolism were selected for further analysis. Hoechst staining and ATP content were also normalized to controls. Results were rank-ordered, as indicated, based on their ability to effectively deplete ATP, without inducing overall cell toxicity - as reflected by maintenance of viability and cell attachment.

Comparison of the chemical structures of these top 10 compounds identified 4 different drug classes, based on structural similarities, which are summarized in Figure 4. Three compounds fall into Group 1, four compounds in Group 2, two compounds in Group 3, and one compound in Group 4.

To validate the hypothesis that these compounds also target cancer stem-like cells (CSCs), the top 7 hits were compared in parallel for their ability to inhibit mammosphere formation in MCF7 cells. Importantly, 5 of the 7 compounds tested significantly inhibited mammosphere formation, at a concentration of 5 µM

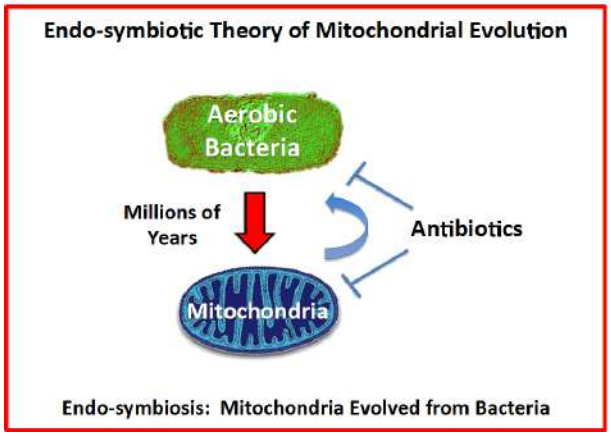

Figure 1: The endo-symbiotic theory of mitochondrial evolution: Implications for modern drug development. Note that mitochondria originally evolved from engulfed aerobic bacteria, during millions of years of adaptation. A corollary of these findings is that many antibiotics also show mitochondrial side effects and effectively behave as inhibitors of mitochondrial protein translation (e.g., chloramphenicol, the tetracyclines and the erythromycins). Conversely, if we identify inhibitors of mitochondrial protein translation using mammalian cells, these drugs should also show anti-microbial activity, behaving as novel antibiotics. This would provide a new therapeutic strategy for efficiently generating novel drugs that target both mitochondria and bacteria, as well as pathogenic yeast strains.

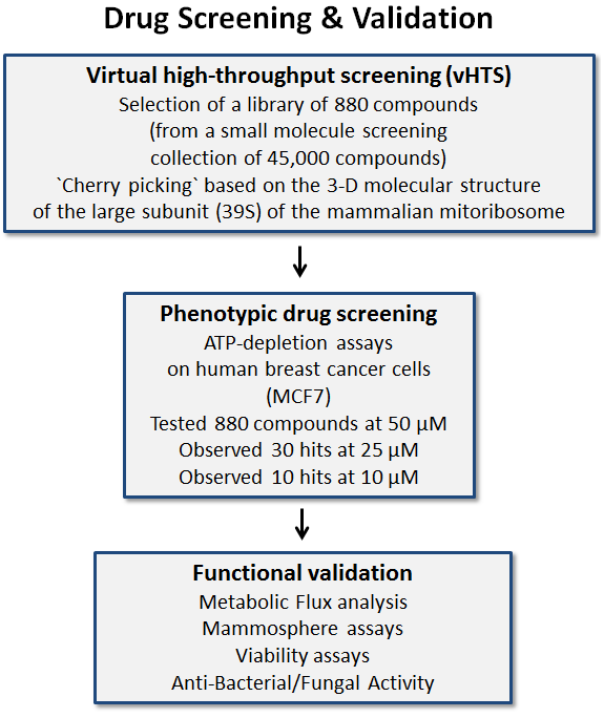

Figure 2: Schematic diagram illustrating our overall drug discovery strategy, employing both in silico drug discovery and phenotypic drug screening. 1. Virtual high-throughput screening (vHTS) - We used the 3D structure of the large mammalian mitochondrial ribosome to screen a virtual collection of 45,000 compounds and identified a subset of 880 compounds that "bind" in silico. 2. Phenotypic drug screening - The resulting 880 compounds were then subjected to phenotypic drug screening at a concentration of 50 µM, to identify which compounds functionally induce ATP-depletion, before inducing cell death. Subsequently, positive hits were re-screened at lower concentrations (25 and 10 µM), to identify the top ten compounds that most potently induced ATP-depletion. 3. Functional validation - The top hits were then further validated using metabolic flux analysis, to determine specific effects on oxygen consumption, to estimate their anti-mitochondrial activity. Mammosphere assays (for assessing potential anti-cancer stem cell activity) and cell viability assays were also carried out. Finally, the top three compounds were assessed for anti-microbial activity, to determine their minimum inhibitory concentration (MIC) and they were compared side-by-side with known antibiotics.

(Figure 5). For example, 23/G4 (Group 1) reduced mammosphere formation by 50% at this concentration. Similarly, 24/F9 (Group 2) and 24/D4 (Group 3), both reduced mammosphere formation by ~90%.

Based on this analysis, we next selected 3 top hits to assess their functional effects on overall viability in MCF7 cell monolayers and normal human fibroblasts (hTERT-BJ1 cells) (Figure 6). Interestingly, 23/G4 (Group 1) reduced the viability of MCF7 cells by 70% at a concentration of 5 µM. However, 23/G4 had no effect on

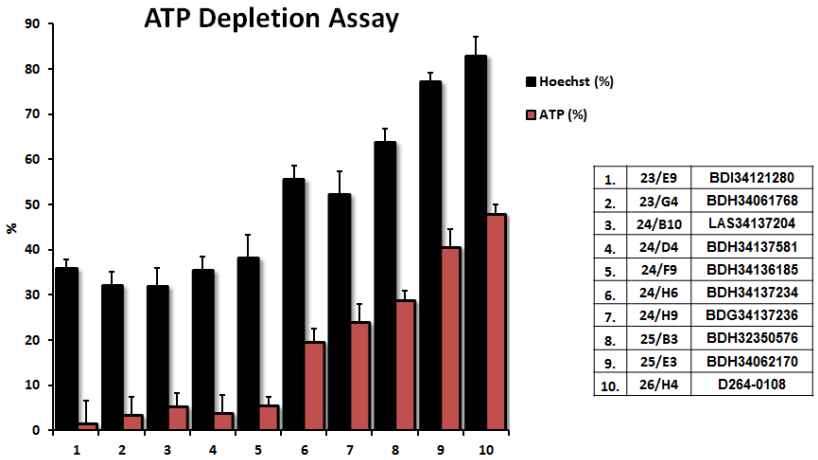

Figure 3: Comparison of the top 10 hits using the ATP-depletion assay. The top ten hits were all evaluated at a concentration of 10 µM, to determine their rank order potency, for their ability to deplete ATP levels. MCF7 cells were treated with the selected compounds of at 10µM for 72 hours. Hoechst staining showed cell viability based on DNA staining, while measurement of ATP content revealed the effects of the compounds on metabolic activity. Compounds targeting the inhibition of metabolism were selected. Hoechst staining and ATP content were normalized to controls. Results are shown as mean ± SEM (n = 4).

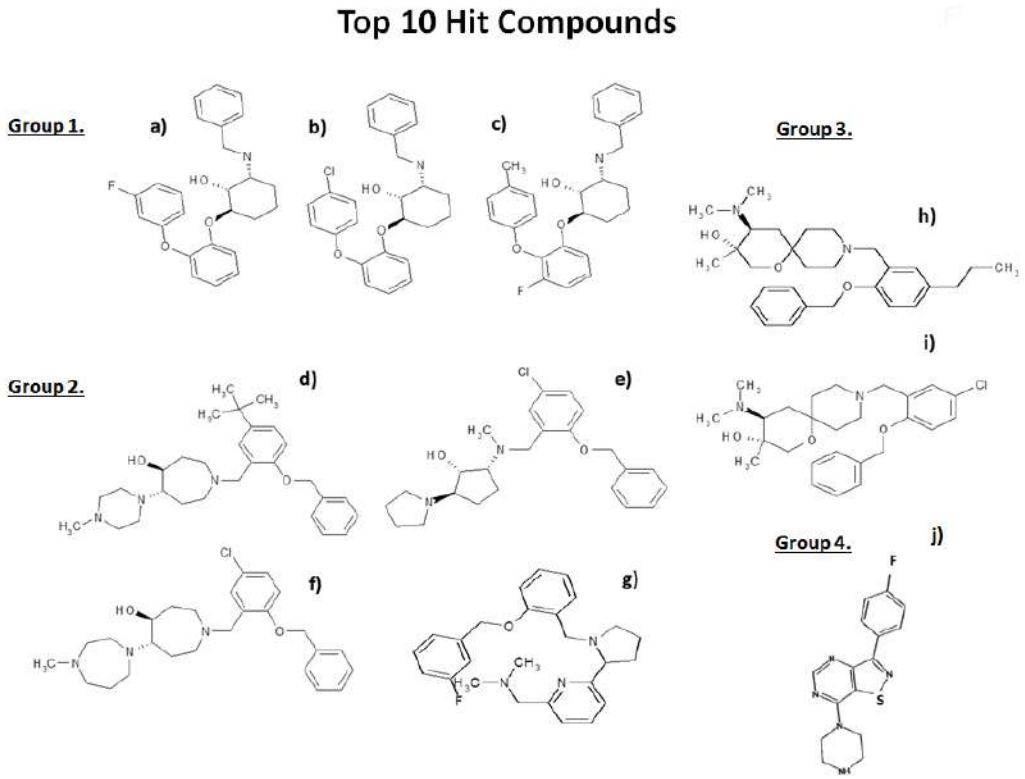

Figure 4: Chemical structures of the top 10 hits. The most promising top 10 hits of the phenotypic drug screen were organized into 4 groups based on chemical structure: Group 1: a) 23/E9 (BDI34121280); b) 23/G4 (BDH34061768); and c) 25/E3 (BDH34062170). In this group, we focused on characterizing the activity of 23/G4. Group 2: d) 24/F9 (BDH34136185); e) 24/B10 (LAS34137204); f) 24/H6 (BDH34137234); and g) 25/B3 (BDH32350576). In this group, we focused on characterizing the activity of 24/F9. Group 3: h) 24/D4 (BDH34137581) and i) 24/H9 (BDG34137236). In this group, we focused on characterizing the activity of 24/D4.Group 4: j) 26/H4 (D264-0108).

the viability of hTERT-BJ1 cells, when tested at the same concentration. Thus, it is possible to identify compounds, such as 23/G4, that preferentially target CSCs and "bulk" cancer cells, but not normal fibroblasts.

Next, we performed functional validation of the 3 top hits using the Seahorse Analyzer, to quantitatively measure oxygen consumption rate (OCR) and extracellular acidification rate (ECAR). OCR is a surrogate marker for OXPHOS and ECAR is a surrogate marker for glycolysis and L-lactate production.

As predicted, 23/G4 (Group 1), 24/F9 (Group 2) and 24/D4 (Group 3) all dose-dependently inhibited mitochondrial oxygen-consumption in MCF7 cells, with 23/G4 being the most potent (Figures 7, 8 and 9). For example, 23/G4 reduced ATP levels by > 50% at a concentration of only 500 nM. In addition, 23/G4 reduced ATP levels by ~75% at 2.5 µM (Figure 7). Remarkably, treatment with 23/G4, at the same concentrations, had little or no effect on the overall cell viability of MCF7 monolayers (Figure 6). Therefore, 23/G4 very effectively depleted ATP levels, without showing significant cytotoxicity.

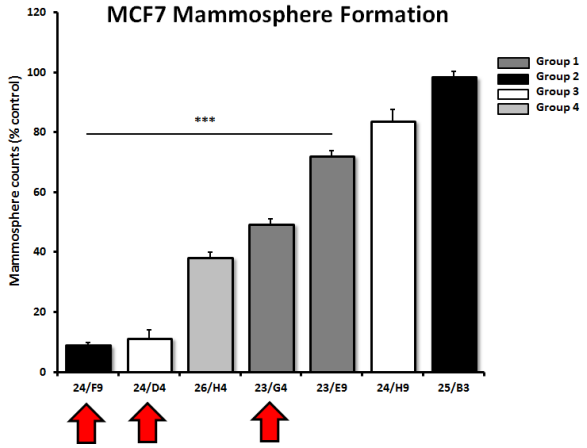

Figure 5: Effects of 7 top hit compounds on mammosphere formation, representing 4 different structural groups or classes. Note that 5 of the 7 compounds evaluated significantly inhibited mammosphere formation, a measure of cancer stem cell activity, at a concentration of 5 µM. Compounds 24/F9, 24/D4 and 23/G4 were among the most effective, with an IC-50 < 5 µM. Results are shown as the mean ± SEM ($n = 3$). *** $p < 0.001$.

Interestingly, 23/G4 induced an increase in glycolysis rates by > 1.5-fold, while 24/F9 and 24/D4 both suppressed glycolysis. This could explain why 24/F9 and 24/D4 were more potent than 23/G4 in the mammosphere assay, where 24/F9 and 24/D4 both reduced mammosphere formation by ~90% at a concentration of 5 µM (Figure 5). The rank order potency of the top 10 hits for their ability to reduce i) maximal respiration and ii) ATP production is shown in Figure 10. Note that the top 6 compounds in this regard were 23/G4, 25/B3, 24/H9, 24/F9, 23/E9 and 24/H6, with 23/G4 being the most potent, yielding a > 75% reduction in ATP levels at 5 µM.

As EMT and cell invasion are phenotypic features associated with "stemness" and distant metastasis [33-35], we also evaluated the effects of these compounds on the ability of another more aggressive breast cancer cell line, namely MDA-MB-231, to undergo cell migration. Figure 11 shows that 23/G4, 24/D4 and 24/F9 all inhibited cell migration by > 70%, at a concentration of 2.5 µM.

In summary, 23/G4 (Group 1) appears to be the most promising new lead compound, as it is more selective at targeting CSCs and cancer cells, while sparing normal

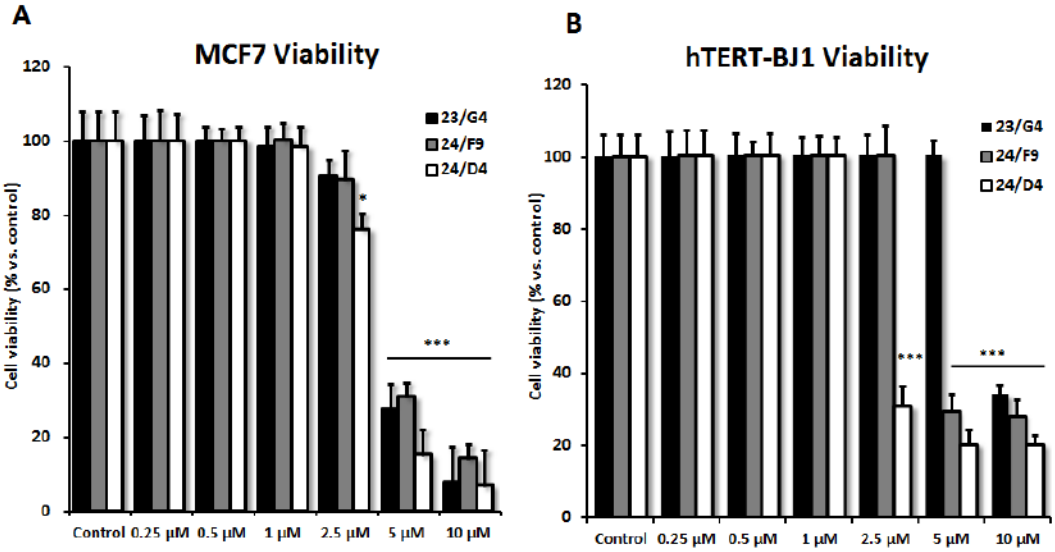

Figure 6: Effects of 3 top hit compounds on cell viability. A. MCF7 human breast cancer cells. **B.** hTERT-BJ1 normal human fibroblasts. The SRB assay was performed after 72 hours of treatment. Note that 23/G4 has no effect on normal fibroblasts at 5 µM. However, at the same concentration, 23/G4 reduces the viability of MCF7 breast cancer cells by > 70%. Thus, 23/G4 shows a degree of selectivity for cancer cells. Results are shown as mean ± SEM ($n = 6$). *** $p < 0.001$, * $p < 0.05$.

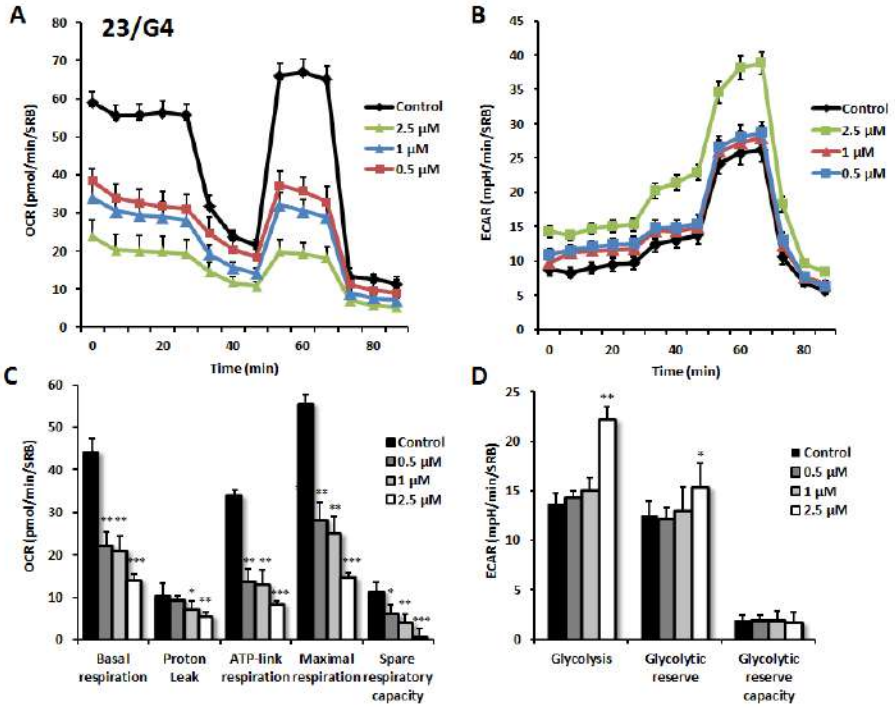

Figure 7: Effects of compound 23/G4 on the metabolic activity of MCF7 human breast cancer cells. Oxygen consumption rate (OCR) and extracellular acidification rate (ECAR) was measured using the Seahorse XFe96 Metabolic Flux Analyzer. Then data were normalized to protein content (SRB assay). Note that 23/G4 treatment reduced mitochondrial respiration significantly even at a dose as low as 500 nM (see panel **A.**) by markedly decreasing basal and maximal respiration, as well as ATP production (panel **C.**). Treatment with the highest dose (2.5 µM) resulted in increased glycolysis (panels **B.**, **D.**). MCF7 cells were treated with 23/G4 compound for 72 hours. Results are shown as mean ± SEM ($n = 6$). * $p < 0.05$, ** $p < 0.01$, *** $p < 0.001$.

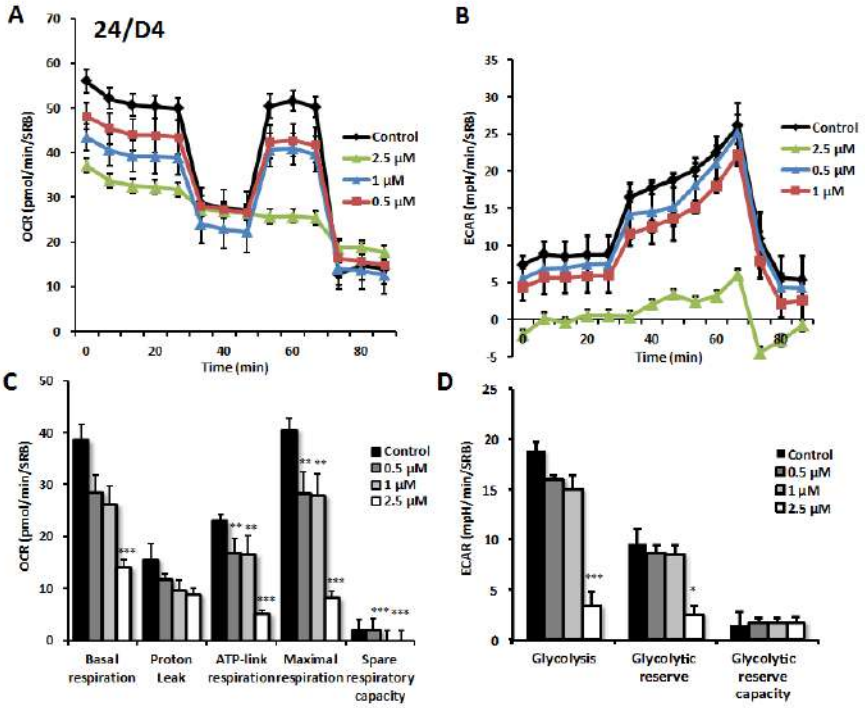

Figure 8: Effects of compound 24/D4 on metabolic activity of MCF7 human breast cancer cells. Oxygen consumption rate (OCR) and extracellular acidification rate (ECAR) was measured using the Seahorse XFe96 Metabolic Flux Analyzer. Then data were normalized to protein content (SRB assay). Note that treatment with compound 24/D4 (2.5 µM) showed a marked inhibition of mitochondrial respiration (see panels **A.**, **C.**). The same dose significantly reduced glycolysis (panels **B.**, **D.**). MCF7 cells were treated with compound 24/D4 for 72 hours. Results are shown as mean ± SEM ($n = 6$). * $p < 0.05$, ** $p < 0.01$, *** $p < 0.001$.

Table 1: Gram-Positive Bacterial Antibiotic Sensitivity.

Susceptibility Testing Gram-positive		*Staph. aureus* ATCC 25923			*Strept. pyogenes* ATCC 19615		
ANTIBIOTIC/INHIBITOR	CONTENT µg	EVALUATION					
		S	I	R	S	I	R
Ciprofloxacin	4	X			X		
Rifampicin	4	X				X	
23/G4	8	X			X		
Gentamicin	8	X			X		
Tobramycin	8	X				X	
Levofloxacin	8	X			X		
Pefloxacin	8	X			X		
Azithromycin	8	X				X	
Clarithromycin	8	X				X	
Erythromycin	8	X				X	
Miocamycin	8			X			X
Roxithromycin	8	X				X	
Co-trimoxazole	8	X			X		
Amoxicillin / Clavulanic acid	8/4		X			X	
Piperacillin	16	X			X		
24/D4	32	X			X		
Netilmicin	32	X			X		
Cefaclor	32		X			X	
Cefixime	32	X				X	
Cefonicid	32	X			X		
Ceftazidime	32	X			X		
Cefuroxime	32	X			X		
Ampicillin / Sulbactam	32/16		X		X		
24/F9	64	X			X		
Ceftriaxone	64	X			X		
Fosfomycin	200	X				X	

The anti-bacterial activity of three hit compounds (24/F9, 24/D4 and 23/G4) was compared to known antibiotics, across two different gram-positive bacterial strains (Staph. aureus and Strep. pyogenes). S, sensitive; I, intermediate; R, resistant.

cells (Figure 6). Also, 23/G4 is the most potent hit compound that effectively reduces mitochondrial ATP levels and induces glycolysis. Most importantly, our results provide the necessary proof-of-concept that new mitochondrial inhibitors can be rapidly developed, by combining *in silico* drug design with phenotypic drug screening.

Novel mitochondrial inhibitors function as broad-spectrum antibiotics

As mitochondria originally evolved from aerobic bacteria, over millions of years of evolution, we speculated that these new mitochondrial inhibitors would also behave as novel antibiotics.

To test this hypothesis directly, we selected 3 top hit compounds (24/F9, 24/D4 and 23/G4) and examined their anti-microbial activity against two gram-positive bacterial strains (*Staph. aureus and Strep. pyogenes*) and three gram-negative bacterial strains (*E. coli, P. aeruginosa, K. pneumoniae*), as well as the pathogenic yeast strain *C. albicans*.

The inhibition ratios of the selected compounds, against pathogenic strains, were calculated by serial dilution. The average of three inhibition zone diameter measurements was compared against commercial drugs, using the Kirby-Bauer method.

Table 2: Gram-Negative Bacterial Antibiotic Sensitivity.

Susceptibility Testing Gram-negative		*E. coli* ATCC 25922			*P. auriginosa* ATCC 27853			*K. pneumoniae* ATCC 13883		
ANTIBIOTIC/INHIBITOR	CONTENT µg	EVALUATION								
		S	I	R	S	I	R	S	I	R
Ciprofloxacin	4	X			X			X		
Rifampicin	4		X			X			X	
Gentamicin	8	X			X			X		
Tobramycin	8		X		X			X		
Lomefloxacin	8	X				X			X	
Levofloxacin	8	X			X			X		
Pefloxacin	8	X			X			X		
Co-trimoxazole	8	X			X			X		
24/D4	32	X			X			X		
23/G4	32		X		X			X		
Amikacin	32	X			X			X		
Ceftazidime	32	X			X			X		
Cefuroxime	32	X			X			X		
Nalidixic acid	32		X		X			X		
Teicoplanin	32	X				X			X	
Aztreonam	32	X			X			X		
Amoxicillin / Clavulanic acid	32/16		X		X			X		
Ampicillin / Sulbactam	32/16	X				X			X	
Cefotaxime	64	X			X			X		
24/F9	64	X				X		X		
Cefoperazone	64	X			X			X		
Cefotaxime	64	X			X			X		
Ceftriaxone	64	X			X			X		
Nitrofurantoin	128	X			X			X		
Piperacillin/Tazobactam	128/4	X			X			X		
Ticarcillin/Clavulanic acid	128/4	X			X			X		
Fosfomycin	200		X		X			X		

The anti-bacterial activity of three hit compounds (24/F9, 24/D4 and 23/G4) was compared to known antibiotics, across three different gram-negative bacterial strains (*E. coli*, P. aeruginosa, K. pneumoniae). S, sensitive; I, intermediate; R, resistant.

Table 3: Minimum Inhibitory Concentrations (MIC): 5 Bacterial Strains and 1 Pathogenic Yeast.

Minimum inhibitory concentration (compare with common antibiotics)	MIC µg/ml											
ANTIBIOTIC/INHIBITOR	*E. coli* ATCC 25922		*P. auriginosa* ATCC 27853		*K. pneumoniae* ATCC 13883		*Staph. aureus* ATCC 25923		*Strept. pyogenes* ATCC 19615		*C. albicans* ATCC 13883	
	50%	99%	50%	99%	50%	99%	50%	99%	50%	99%	50%	99%
24/D4	16	32	16	32	16	32	16	32	16	32	-	>64
23/G4	>16	>32	16	32	16	32	4	8	4	8	8	16
24/F9	32	64	>32	>64	32	64	32	64	32	64	-	>64
DOXYCYCLINE	0.5	2	1	2	2	4	0.5	1	0.5	1	-	>64
LINEZOLID	128	>128	64	256	128	256	1	2	1	2	-	-
AMOXICILLIN	16	>32	128	256	32	>64	4	8	4	8	-	-
MICONAZOLE	-	-	-	-	-	-	-	-	-	-	0.5	1

The anti-microbial activity of three hit compounds (24/F9, 24/D4 and 23/G4) was compared to known antibiotics, using five different bacterial strains (Staph. aureus, Strep. pyogenes, *E. coli*, *P. aeruginosa, K. pneumoniae*) and one pathogenic yeast/fungus (*C. albicans*). Note that compound 23/G4 showed the greatest broad-spectrum activity and potency, as compared with compound 24/F9 and 24/D4.

Final interpretation of the measurements enabled all of the bacterial strains tested to be grouped into three categories (Sensitive, Intermediate and Resistant) as summarized in Tables 1 and 2. No growth inhibition was seen in the control (DMSO) (data not shown). Tables 1 and 2 illustrate that all five bacterial strains tested are sensitive to the 3 hit compounds (24/F9, 24/D4 and 23/G4).

Therefore, in order to determine the minimal inhibitory concentration (MIC) for 24/F9, 24/D4 and 23/G4, the broth dilution method was performed. As expected, the MIC determination results were in good agreement with the disc-diffusion susceptibility test. Table 3 shows the MIC determination results obtained as compared to known antibiotics, against the tested bacterial strains and *C. albicans*. Importantly, note that compound 23/G4 showed the greatest broad-spectrum activity and potency, as compared with compounds 24/F9 and 24/D4.

Finally, Table 4 shows that Methicillin-resistant Staphylococcus aureus (MRSA) is also sensitive to 23/G4 and 24/D4. We confirmed that this strain of MRSA was indeed resistant to amoxicillin, as predicted. Thus, it is possible to successfully use this new drug discovery strategy employing human cancer cells, to isolate new antibiotics that can target drug-resistant bacteria, such as MRSA.

DISCUSSION

Discovery of the mitoriboscins: targeting the mitochondrial ribosome

Here, we have used state-of-the art computational chemistry to select novel compounds that bind to the 3D structure of the large subunit of the mammalian mitochondrial ribosome. Out of the 45,000 compounds tested, approximately 880 showed promising results, yielding a hit rate of 2%. To validate their functional ability to target mitochondria *in vivo*, we next performed phenotypic drug screening in human breast cancer cells (MCF7 cells). Using this approach, we selected the top

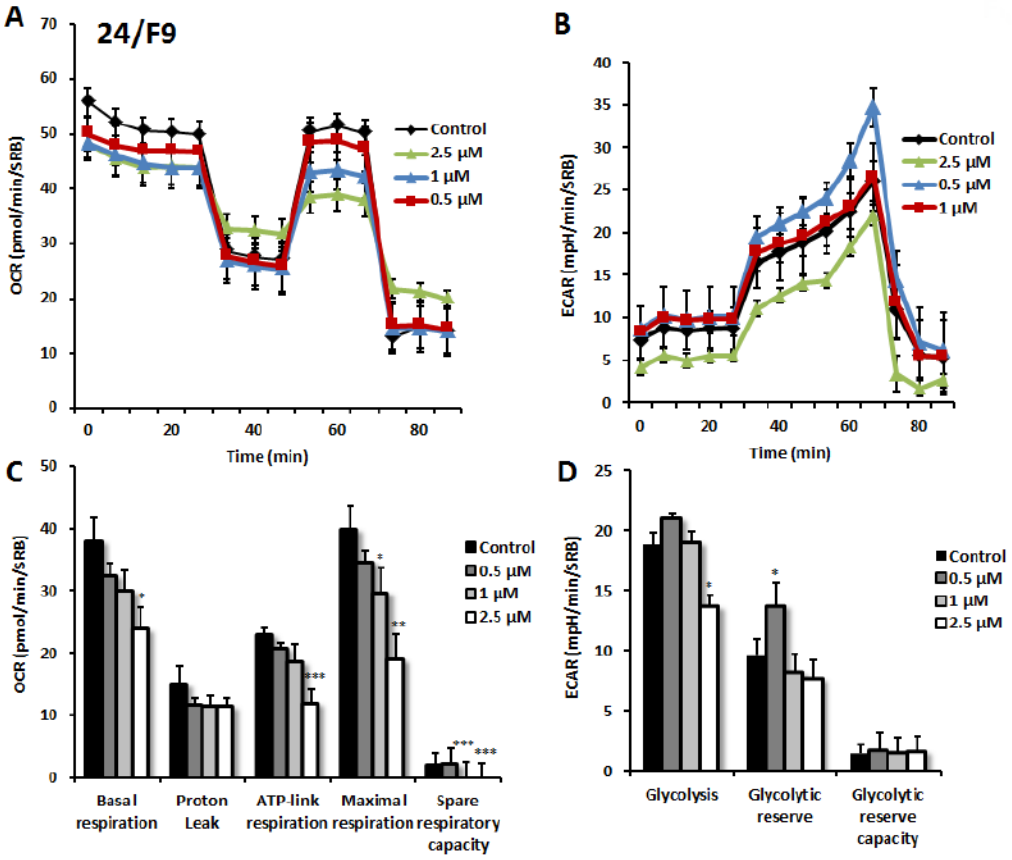

Figure 9: Effects of compound 24/F9 on metabolic activity of MCF7 human breast cancer cells. Oxygen consumption rate (OCR) and extracellular acidification rate (ECAR) was measured using the Seahorse XFe96 Metabolic Flux Analyzer. Then data were normalized to protein content (SRB assay). Treatment with compound 24/F9 showed dose-dependent reduction of mitochondrial respiration, which was highest at 2.5 µM (panels **A.**, **C.**). Inhibition of glycolysis was detected after treatment at the highest concentration (2.5 µM) of 24/F9. MCF7 cells were treated with compound 24/F9 for 72 hours. Results are shown as mean ± SEM ($n = 6$). * $p < 0.05$, ** $p < 0.01$, *** $p < 0.001$.

10 hit compounds (10/880 = 1%) that effectively depleted cellular ATP levels. These top 10 hit compounds were then subjected to further validation using the Seahorse XFe96, to measure mitochondrial oxygen consumption and glycolysis. This approach allowed us to rank-order these top 10 hits, identifying the compound 23/G4 as the most potent (1/45,000 = 0.00002 = 0.002 %). Notably, 23/G4 inhibited mitochondrial ATP production in MCF7 cells, with an IC-50 of approximately 500 nM. Remarkably, 23/G4 showed no cytotoxicity against normal human fibroblasts, even at a concentration (5 μM) that reduced cancer cell viability by > 70% (Figure 6). Importantly, the top hit compounds that we identified also potently inhibited CSC propagation and cancer cell migration, all in the low micro-molar range. Finally, we also showed that 3 of these top hit compounds also behave as antibiotics, inhibiting the growth of pathogenic bacteria and yeast. Importantly, 23/G4 and 24/D4 were also effective against MRSA.

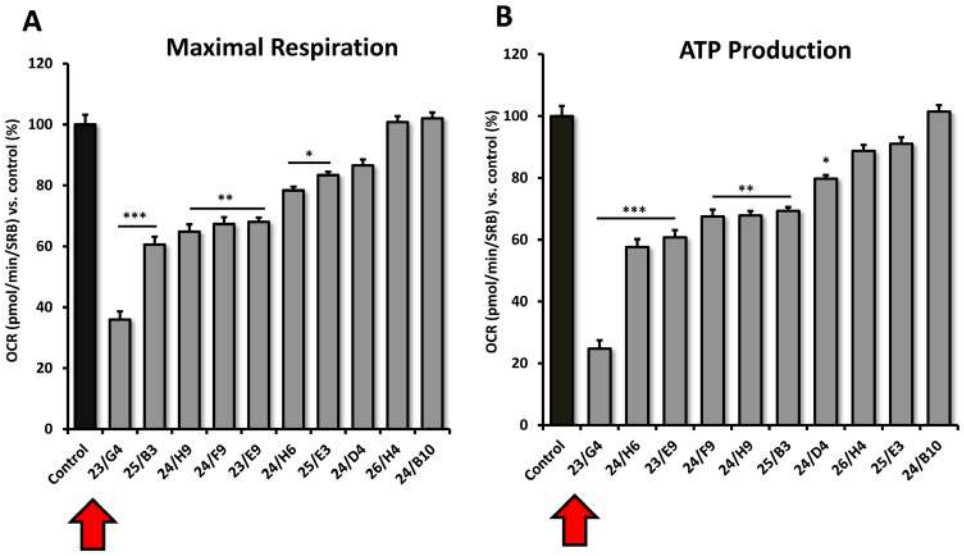

Figure 10: Comparative metabolic flux analysis of the top 10 hit compounds in MCF7 cells. A. Maximal respiration. **B.** ATP production. Measurements were made after 48 hours of treatment of MCF7 cells with a given compound, at a concentration of 5 μM. Note that compound 23/G4 most significantly reduces both i) ATP production (by > 70%) and ii) maximal respiration (by > 60%). Oxygen consumption rates (OCR) were measured using the Seahorse XFe96 and then data were normalized for protein content (SRB assay). Maximal respiration and ATP-linked respiration data were calculated, normalized to control values and were plotted as percent control. Results are shown as mean ± SEM ($n = 3$). * $p < 0.05$, ** $p < 0.01$, *** $p < 0.001$.

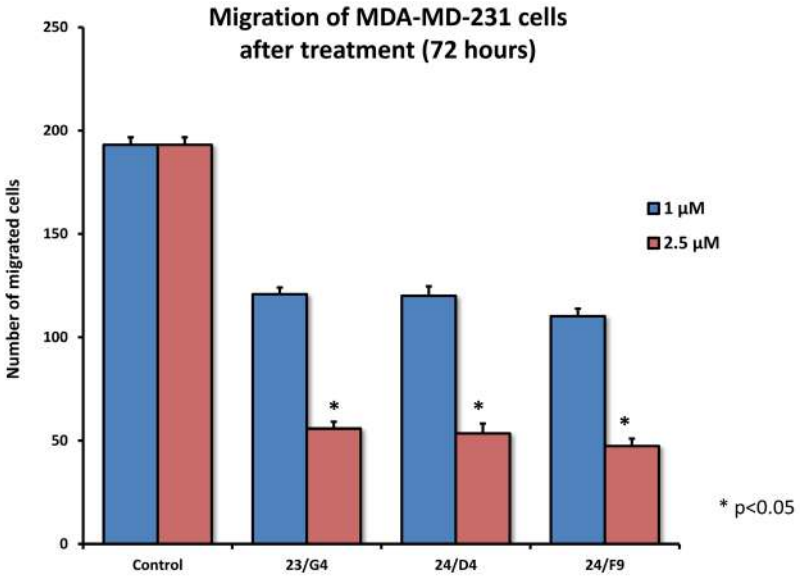

Figure 11: Effects of 3 top hit compounds on cell migration. MDA-MB-231 cells were subjected to cell migration assays. 23/G4, 24/F9 and 24/D4 all significantly reduced cell migration, at concentrations of 1 and 2.5 μM. More specifically, 23/G4, 24/D4 and 24/F9 inhibited cell migration by > 70%, at a concentration of 2.5 μM.

Table 4: Minimum Inhibitory Concentrations (MIC): MRSA versus MSSA.

Minimum inhibitory concentration (compare with common antibiotics)	MIC µg/ml			
ANTIBIOTIC/INHIBITOR	MRSA ATCC 43300		MSSA ATCC 25923	
	50%	99%	50%	99%
24/D4	16	>32	16	32
23/G4	16	>32	4	8
24/F9	64	>64	32	64
AMOXICILLIN	>64	>64	4	8

The anti-microbial activity of three hit compounds (24/F9, 24/D4 and 23/G4) was compared to known antibiotics, using two different bacterial strains of *Staph. aureus,* MRSA (methicillin-resistant *Staph. aureus)* and MSSA (methicillin-sensitive *Staph. aureus).* Note that MRSA is resistant to amoxicillin, as expected.

Thus, we propose the new term mitoriboscins, to describe these mitochondrial-related antibiotics. Moreover, the 4 classes of mitoriboscins that we describe here, we have designated as 1) mitoribocyclines, 2) mitoribomycins, 3) mitoribosporins and 4) mitoribofloxins (Figure 12). We generally define mitoriboscins as any small molecule that binds to the mitoribosome (large or small subunits) and, as a consequence, inhibits mitochondrial function.

Although the novel compounds that we identified here are relatively potent, we envision that further modifications will be required to better optimize their ability to i) disrupt mitochondria in CSCs and ii) to halt the growth of micro-organism(s), for the treatment of oncologic and infectious diseases respectively. Nevertheless, our results provide the necessary proof-of-principle that it is possible to identify new antibiotics to target pathogenic bacteria and yeast, by employing ATP production in human cancer cells as a simple phenotypic screening tool (Figure 13).

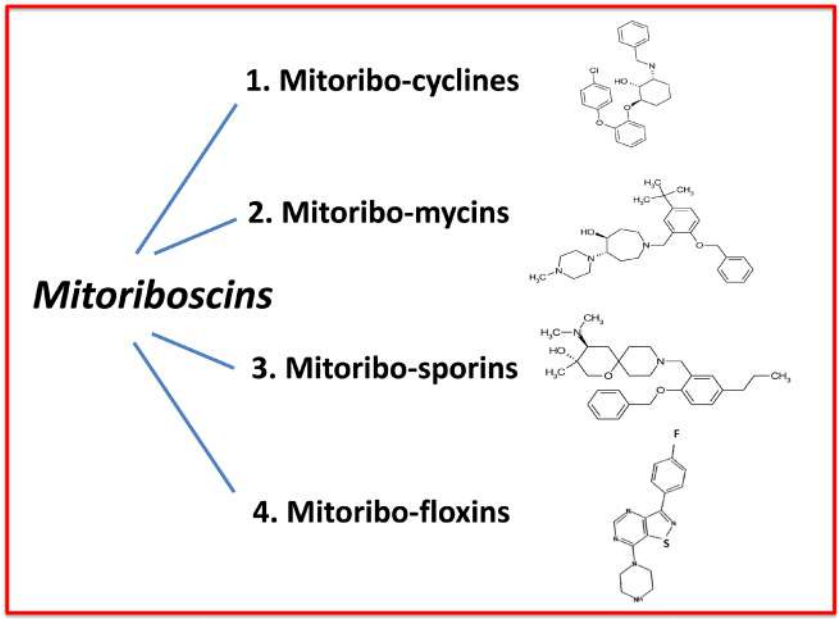

Figure 12: Mitoriboscins: Four new classes of mitochondrial inhibitors. The structures of 23/G4, 24/F9, 24/D4 and 26/H4 are shown, which now define 4 newly discovered classes of small molecules. These novel molecules were identified because of their structural and functional mitochondrial inhibitory activity in human cancer cells. As such, this convergent screening approach will undoubtedly yield other classes of new antibiotics, as well novel anti-cancer agents. We specifically define mitoriboscins as any small molecule that binds to the mitoribosome (large or small subunits); this binding activity ultimately inhibits mitochondrial function.

The mitoribosins: therapeutic use to combat ageing and extend healthspan

Interestingly, genetic inhibition of mitochondrial protein translation has also been shown to have beneficial "side-effects", such as the effective slowing of the aging process and increased lifespan in model organisms. Houtkooper et al., 2013, showed that lower steady-state levels of Mrps5 (a mitoribosomal protein) were strongly functionally correlated with longer murine lifespan, resulting in a significant increase of ~250 days [36]. In addition, selective knock-down of Mrps5 in *C. elegans* dramatically increased lifespan. Importantly, Mrps5 knock-down worms showed significant decreases in mitochondrial respiration and ATP production [36]. Similarly, knock-down of the worm homologs of mitochondrial complex I, III, IV and V, as well as several TCA cycle enzymes, all robustly extended lifespan, further implicating reduced OXPHOS activity and lower ATP levels as the mechanism [37-39]. Finally, pharmacological inhibition of mitochondrial biogenesis (using the off-target side-effects of doxycycline), also significantly increased lifespan in *C. elegans* [36]. Thus, lower doses of the mitoriboscins could potentially be used to therapeutically target the aging process, to extend healthspan (Figure 13). Further studies will be required to explore this intriguing area of investigation.

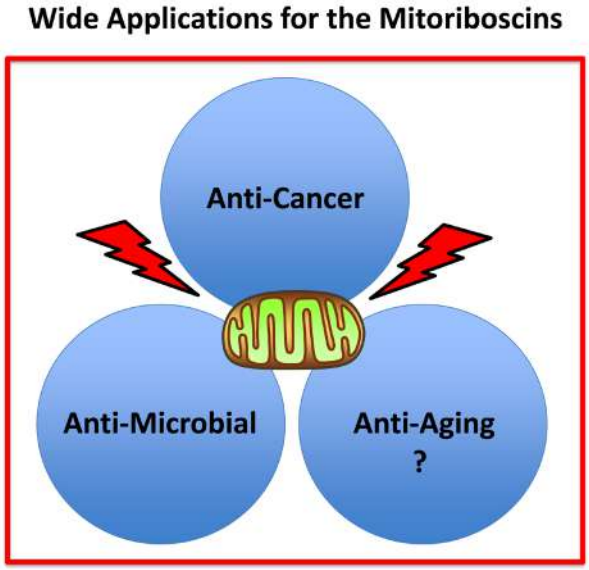

Figure 13: Practical uses of the mitoriboscins: Targeting mitochondria. We propose that mitoriboscins will be therapeutically useful for the treatment of a variety of human diseases, including cancers and infectious illnesses, caused by pathogenic bacteria and fungi. In addition, we speculate that mitoriboscins may be helpful in the context of chronological aging, for either extending lifespan or healthspan. Thus, mitoriboscins will have anti-cancer, anti-microbial and anti-aging properties.

MATERIALS AND METHODS

Materials

MCF7 and MDA-MB-231 cells were purchased from the ATCC (American Type Culture Collection). Gibco-brand cell culture media (DMEM and DMEM/F12) was purchased from Life Technologies. The top 6 hit compounds were custom-synthesized in larger quantities by ASINEX Corp., and compound D264-0108 (26/H4) was custom-synthesized by ChemDiv Inc.

Bacterial and fungus strains

The strains *Escherichia. coli* (ATCC 25922), *Klebisella pneumoniae* (ATCC 13883), *Pseudomonas aeruginosa* (ATCC 27853), *Staphylococcus aureus MSSA* (ATCC 25923), *Staphylococcus aureus MRSA* (ATCC 43300), *Streptococcus pyogenes* (ATCC 19615) and *Candida Albicans* (ATCC 13883) were provided by Remel Microbiology (Thermo Fisher). The cells were grown in Müller-Hinton broth II (MHB; Difco, Detroit, MI, USA) containing 2g/l beef infusion solids, 17.5 g/l casein hydrolysate, 1.5 g/l starch. The final pH was adjusted to 7.4.

Virtual high-throughput screening (vHTS)

Compounds were selected from a small molecule screening collection of 45,000 compounds. Initial virtual high-throughput screening (vHTS) used the eHiTS screening program [40] to identify the top 5,000 ranked compounds based on predicted binding affinity to the large subunit (39S) of the mammalian mitoribosome [21]. To efficiently perform the docking, a series of clip files was prepared spanning the entire protein structure and the virtual library docked at each of the clip files. Consensus scoring of these top 5,000 compounds was carried out using AutoDock 4.2 [41], based on using the same general binding site for each compound predicted from the eHiTS screen. A total of 880 compounds performing well in these analysis steps were then selected for phenotypic drug screening.

Phenotypic drug screening, with a metabolic ATP-depletion assay

MCF7 cells (6,000 cells/well) were plated into black clear-bottom 96-well plates and incubated overnight before treatment. The resulting 880 compounds first identified by vHTS were then subjected to phenotypic drug screening at a concentration of 50 µM, to identify which compounds functionally induce ATP-depletion, before

inducing cell death. Subsequently, positive hits were re-screened at lower concentrations (25 μM and 10 μM), to identify the top 10 compounds that most potently induced ATP-depletion. Compounds were tested after 72 hours of incubation and experiments were performed in duplicate. After treatment, media was aspirated from the wells and plates were washed with warm PBS (supplemented w/ Ca^{2+} and Mg^{2+}). Then, cells were incubated with a Hoechst 33342 (Sigma) staining solution (10 μg/ml) for 30 min and washed with PBS (to estimate cell viability). Fluorescence was read with a plate reader using excitation/emission wavelenghts at 355/460-nm. Then, the CellTiter-Glo luminescent assay (Promega) was performed to measure metabolic activity (ATP content) in the very same wells that were treated with a given compound. Assays were performed according to the manufacturer's protocol. Fluorescence intensity (Hoechst staining) and luminescence intensity (ATP content) was normalized to vehicle-alone treated controls and were displayed as percent control for comparison.

Cell viability assay

The Sulphorhodamine (SRB) assay is based on the measurement of cellular protein content. After treatment for 72h in 96-well plates, cells were fixed with 10% trichloroacetic acid (TCA) for 1h in the cold room, and were dried overnight at room temperature. Then, cells were incubated with SRB for 15 min, washed twice with 1% acetic acid, and air dried for at least 1h. Finally, the protein-bound dye was dissolved in a 10 mM Tris, pH 8.8, solution and read using the plate reader at 540-nm.

Mammosphere formation assays

A single cell suspension of MCF7 cells was prepared using enzymatic (1x Trypsin-EDTA, Sigma Aldrich) and manual disaggregation (25 gauge needle) [42]. Cells were then plated at a density of 500 cells/cm^2 in mammosphere medium (DMEM-F12/ B27 / 20-ng/ml EGF/PenStrep) in non-adherent conditions, in culture dishes coated with (2-hydroxyethylmethacrylate) (poly-HEMA, Sigma). Cells were grown for 5 days and maintained in a humidified incubator at 37°C at an atmospheric pressure in 5% (v/v) carbon dioxide/air. After 5 days in culture, spheres > 50 μm were counted using an eye-piece graticule, and the percentage of cells plated which formed spheres was calculated and is referred to as percent mammosphere formation, normalized to vehicle-alone treated controls. Mammosphere assays were performed in triplicate and repeated three times independently.

Seahorse XFe96 metabolic Flux analysis

Extracellular acidification rates (ECAR) and real-time oxygen consumption rates (OCR) for MCF7 cells were determined using the Seahorse Extracellular Flux (XF96) analyzer (Seahorse Bioscience, MA, USA). MCF7 cells were maintained in DMEM supplemented with 10% FBS (fetal bovine serum), 2 mM GlutaMAX, and 1% Pen- Strep. 5,000 cells per well were seeded into XF96-well cell culture plates, and incubated overnight at 37°C in a 5% CO2 humidified atmosphere. After 24h, cells were treated with the top three hit compounds at various concentrations (or vehicle alone). After 72h of treatment, cells were washed in pre-warmed XF assay media (for OCR measurement, XF assay media was supplemented with 10mM glucose, 1mM Pyruvate, 2mM L-glutamine and adjusted at pH 7.4). Cells were then maintained in 175 μL/well of XF assay media at 37°C, in a non-CO2 incubator for 1h. During incubation, 25 μL of of 80mM glucose, 9μM oligomycin, 1M 2-deoxyglucose (for ECAR measurement) and 25 μL of 10μM oligomycin, 9μM FCCP, 10μM rotenone, 10μM antimycin A (for OCR measurement) in XF assay media was loaded into the injection ports of the XFe-96 sensor cartridge. During the experiment, the instrument injected these inhibitors into the wells at a given time point, while ECAR/OCR was measured continuously. ECAR and OCR measurements were normalized by protein content (Sulphorhodamine B assay). Data sets were analyzed by XFe-96 software, using one-way ANOVA and Student's *t*-test calculations. All experiments were performed in triplicate.

Cell migration assay

The migration of MDA-MD-231 cells was carried out, essentially as we previously described, with minor modifications [43].

Gram (+ve) and gram (-ve) susceptibility testing

The antimicrobial susceptibilities of the novel compounds were evaluated using the Kirby-Bauer disc-diffusion method [44-46], performed according to CLSI guidelines and results were interpreted using CLSI breakpoints [47-48]. Antibiotics disks against gram(+ve) and gram(-ve) bacterias (from Oxoid™) were used as positive controls. All new componds (24/D4, 24/F9, 23/G4) were prepared by dissolving them in dimethyl sulfoxide (DMSO, from Sigma/Aldrich Company; St. Louis, MO, USA) and were utilized to impregnate the Blank Antimicrobial Susceptibility Disks (Oxoid™). Specifically, overnight cultures of bacteria tested were adjusted to a turbidity of 0.5 McFarland standards (10^6 CFU/ml) before inoculation onto agar plates with sterile

cotton swabs. A cotton swab dipped in the cell culture was streaked onto an agar plate surface in such a way as to obtain a uniform layer of bacteria across the whole surface. After 10-15 min, the antibiotics disks or novel compounds disks were laid on the inoculated surface of the agar plates; then, all agar plates were incubated at 37°C, overnight. The diameters of inhibition were measured and susceptibility was expressed in terms of resistance (R), moderate susceptibility (I) and susceptibility (S). Agar plates inoculated with bacteria tested with impregnated DMSO disks were used as controls. The result obtained on single bacteria strain was confirmed by Sensi test gram-positive and Sensi test-gram-negative kits (*Liofilchem s.r.l.*). Disc-diffusion susceptibility test was performed in triplicate and repeated three times independently.

Anti-microbial activity and MIC values determination

The minimal inhibitory concentration (MIC) of the antibacterial compounds was determined using the broth dilution method, according to CLSI guidelines [48]. Briefly, a solution content the new compounds (or several antibiotics used as positive control) was diluted, serially, with MHB medium. Then, the suspensions of the microorganisms, prepared from overnight cultures of bacteria in the MHB medium, at a concentration of 10^6 cfu x ml^{-1}, were added to each dilution in a 1:1 ratio McFarland standards were used as a reference to adjust the turbidity of microorganism suspensions. Growth (or lack thereof) of the microorganisms was determined after incubation for 24 h at 37 °C by turbidimetry (wavelength of 600 nm). MIC 50 and MIC 99 were defined as the minimum inhibitory concentration of the compound required for 50% and 99% inhibition of bacterial growth [49, 50]. The negative control tubes did not contain bacterial inoculum while the positive control tubes containing only DMSO, were antibiotics or compounds free. The susceptibility test by measurement of MIC was performed in triplicate and repeated three times independently.

Statistical analyses

Statistical significance was determined using the Student's *t*-test, values of less than 0.05 were considered significant. Data are shown as the mean ± SEM, unless stated otherwise.

Author contributions

Professor Lisanti and Dr. Sotgia conceived and initiated this project, and selected the large 39S mitochondrial ribosome (mitoribosome) as a new molecular target for drug discovery. *In silico* computational modeling was then performed by Drs. Rachel Trowbridge and Richard Foster. The phenotypic drug screening and all other wet-lab experiments described in this paper were performed by Drs. Bela Ozsvari, Gloria Bonuccelli and Marco Fiorillo, who then generated the final figures and tables for the paper. Professor Lisanti and Dr. Sotgia wrote the first draft of the manuscript, which was then further edited by all the co-authors. Professor Lisanti generated the schematic summary diagrams.

ACKNOWLEDGMENTS

We are grateful to the University of Manchester, which allocated start-up funds and administered a donation, to provide the necessary resources required to start and complete this drug discovery project (to M.P.L. and F.S.).

CONFLICTS OF INTEREST

MPL and FS hold a minority interest in Lunella, Inc.

REFERENCES

1. Lamb R, Harrison H, Hulit J, Smith DL, Lisanti MP, Sotgia F. Mitochondria as new therapeutic targets for eradicating cancer stem cells: Quantitative proteomics and functional validation via MCT1/2 inhibition. Oncotarget. 2014; 5: 11029-37. https://doi.org/10.18632/oncotarget.2789.
2. Sancho P, Burgos-Ramos E, Tavera A, Bou Kheir T, Jagust P, Schoenhals M, Barneda D, Sellers K, Campos-Olivas R, Grana O, Viera CR, Yuneva M, Sainz B Jr, Heeschen C. MYC/PGC-1alpha Balance Determines the Metabolic Phenotype and Plasticity of Pancreatic Cancer Stem Cells. Cell Metab. 2015; 22: 590-605.
3. Lamb R, Ozsvari B, Lisanti CL, Tanowitz HB, Howell A, Martinez-Outschoorn UE, Sotgia F, Lisanti MP. Antibiotics that target mitochondria effectively eradicate cancer stem cells, across multiple tumor types: Treating cancer like an infectious disease. Oncotarget. 2015; 6: 4569-84. https://doi.org/10.18632/oncotarget.3174.
4. Farnie G, Sotgia F, Lisanti MP. High mitochondrial mass identifies a sub-population of stem-like cancer cells that are chemo-resistant. Oncotarget. 2015; 6: 30472-86. https://doi.org/10.18632/oncotarget.5401.
5. Lamb R, Fiorillo M, Chadwick A, Ozsvari B, Reeves KJ, Smith DL, Clarke RB, Howell SJ, Cappello AR, Martinez-Outschoorn UE, Peiris-Pages M, Sotgia F, Lisanti MP. Doxycycline down-regulates DNA-PK and radiosensitizes tumor initiating cells: Implications for more effective radiation therapy. Oncotarget. 2015; 6:14005-25. https://doi.org/10.18632/oncotarget.4159.
6. De Luca A, Fiorillo M, Peiris-Pages M, Ozsvari B, Smith DL, Sanchez-Alvarez R, Martinez-Outschoorn UE, Cappello AR, Pezzi V, Lisanti MP, Sotgia F. Mitochondrial

biogenesis is required for the anchorage-independent survival and propagation of stem-like cancer cells. Oncotarget. 2015; 6:14777-95. https://doi.org/10.18632/oncotarget.4401.

7. Lamb R, Bonuccelli G, Ozsvari B, Peiris-Pages M, Fiorillo M, Smith DL, Bevilacqua G, Mazzanti CM, McDonnell LA, Naccarato AG, Chiu M, Wynne L, Martinez-Outschoorn UE, et al. Mitochondrial mass, a new metabolic biomarker for stem-like cancer cells: Understanding WNT/FGF-driven anabolic signaling. Oncotarget. 2015; 6: 30453-71. https://doi.org/10.18632/oncotarget.5852.
8. Lamb R, Ozsvari B, Bonuccelli G, Smith DL, Pestell RG, Martinez-Outschoorn UE, Clarke RB, Sotgia F, Lisanti MP. Dissecting tumor metabolic heterogeneity: Telomerase and large cell size metabolically define a sub-population of stem-like, mitochondrial-rich, cancer cells. Oncotarget. 2015; 6: 21892-21905. https://doi.org/10.18632/oncotarget.5260.
9. Peiris-Pages M, Martinez-Outschoorn UE, Pestell RG, Sotgia F, Lisanti MP. Cancer stem cell metabolism. Breast Cancer Research. 2016; 18: 55.
10. Casey T, Bond J, Tighe S, Hunter T, Lintault L, Patel O, Eneman J, Crocker A, White J, Tessitore J, Stanley M, Harlow S, Weaver D, et al. Molecular signatures suggest a major role for stromal cells in development of invasive breast cancer. Breast Cancer Res Treat. 2009; 114: 47-62.
11. Sotgia F, Whitaker-Menezes D, Martinez-Outschoorn UE, Salem AF, Tsirigos A, Lamb R, Sneddon S, Hulit J, Howell A, Lisanti MP. Mitochondria "fuel" breast cancer metabolism: fifteen markers of mitochondrial biogenesis label epithelial cancer cells, but are excluded from adjacent stromal cells. Cell Cycle. 2012; 11:4390-4401.
12. Goldschmidt-Reisin S, Kitakawa M, Herfurth E, Wittmann-Liebold B, Grohmann L, Graack HR. Mammalian mitochondrial ribosomal proteins. N-terminal amino acid sequencing, characterization, and identification of corresponding gene sequences. J Biol Chem. 1998; 273:34828-34836.
13. Graack HR, Wittmann-Liebold B. Mitochondrial ribosomal proteins (MRPs) of yeast. Biochem J. 1998; 329:433-448.
14. Cavdar Koc E, Burkhart W, Blackburn K, Moseley A, Spremulli LL. The small subunit of the mammalian mitochondrial ribosome. Identification of the full complement of ribosomal proteins present. J Biol Chem. 2001; 276:19363-19374.
15. Koc EC, Burkhart W, Blackburn K, Moyer MB, Schlatzer DM, Moseley A, Spremulli LL. The large subunit of the mammalian mitochondrial ribosome. Analysis of the complement of ribosomal proteins present. J Biol Chem. 2001; 276:43958-43969.
16. Fiorillo M, Lamb R, Tanowitz HB, Mutti L, Krstic-Demonacos M, Cappello AR, Martinez-Outschoorn UE, Sotgia F, Lisanti MP. Repurposing atovaquone: Targeting mitochondrial complex III and OXPHOS to eradicate cancer stem cells. Oncotarget. 2016; 7: 34084-99. https://doi.org/10.18632/oncotarget.9122.
17. Amunts A, Brown A, Toots J, Scheres SH, Ramakrishnan V. Ribosome. The structure of the human mitochondrial ribosome. Science. 2015; 348:95-98.
18. Amunts A, Brown A, Bai XC, Llacer JL, Hussain T, Emsley P, Long F, Murshudov G, Scheres SH, Ramakrishnan V. Structure of the yeast mitochondrial large ribosomal subunit. Science. 2014; 343:1485-1489.
19. Greber BJ, Bieri P, Leibundgut M, Leitner A, Aebersold R, Boehringer D, Ban N. Ribosome. The complete structure of the 55S mammalian mitochondrial ribosome. Science. 2015; 348:303-308.
20. Brown A, Amunts A, Bai XC, Sugimoto Y, Edwards PC, Murshudov G, Scheres SH, Ramakrishnan V. Structure of the large ribosomal subunit from human mitochondria. Science. 2014; 346:718-722.
21. Greber BJ, Boehringer D, Leibundgut M, Bieri P, Leitner A, Schmitz N, Aebersold R, Ban N. The complete structure of the large subunit of the mammalian mitochondrial ribosome. Nature. 2014; 515:283-286.
22. Greber BJ, Ban N. Structure and Function of the Mitochondrial Ribosome. Annu Rev Biochem. 2016; 85:103-32. doi: 10.1146/annurev-biochem-060815-014343.
23. Gray MW, Burger G, Lang BF. Mitochondrial evolution. Science. 1999; 283:1476-1481.
24. Lang BF, Gray MW, Burger G. Mitochondrial genome evolution and the origin of eukaryotes. Annu Rev Genet. 1999; 33:351-397.
25. Zimorski V, Ku C, Martin WF, Gould SB. Endosymbiotic theory for organelle origins. Curr Opin Microbiol. 2014; 22:38-48.
26. Karlberg O, Canback B, Kurland CG, Andersson SG. The dual origin of the yeast mitochondrial proteome. Yeast. 2000; 17:170-187.
27. Burger G, Lang BF. Parallels in genome evolution in mitochondria and bacterial symbionts. IUBMB life. 2003; 55:205-212.
28. Chang X, Wang Z, Hao P, Li YY, Li YX. Exploring mitochondrial evolution and metabolism organization principles by comparative analysis of metabolic networks. Genomics. 2010; 95:339-344.
29. Wilson DN. Ribosome-targeting antibiotics and mechanisms of bacterial resistance. Nat Rev Microbiol. 2014; 12:35-48.
30. Carter AP, Clemons WM, Brodersen DE, Morgan-Warren RJ, Wimberly BT, Ramakrishnan V. Functional insights from the structure of the 30S ribosomal subunit and its interactions with antibiotics. Nature. 2000; 407:340-348.
31. Moazed D, Noller HF. Interaction of antibiotics with functional sites in 16S ribosomal RNA. Nature. 1987; 327:389-394.
32. Lamb R, Harrison H, Smith DL, Townsend PA, Jackson T, Ozsvari B, Martinez-Outschoorn UE, Pestell RG, Howell A, Lisanti MP, Sotgia F. Targeting tumor-initiating cells:

eliminating anabolic cancer stem cells with inhibitors of protein synthesis or by mimicking caloric restriction. Oncotarget. 2015; 6:4585-4601. https://doi.org/10.18632/oncotarget.3278.

33. Scheel C, Eaton EN, Li SH, Chaffer CL, Reinhardt F, Kah KJ, Bell G, Guo W, Rubin J, Richardson AL,Weinberg RA. Paracrine and autocrine signals induce and maintain mesenchymal and stem cell states in the breast. Cell. 2011; 145:926-940.
34. Dang H, Ding W, Emerson D, Rountree CB. Snail1 induces epithelial-to-mesenchymal transition and tumor initiating stem cell characteristics. BMC Cancer. 2011; 11:396.
35. Scheel C, Weinberg RA. Cancer stem cells and epithelial-mesenchymal transition: concepts and molecular links. Semin Cancer Biol. 2012; 22:396-403.
36. Houtkooper RH, Mouchiroud L, Ryu D, Moullan N, Katsyuba E, Knott G, Williams RW, Auwerx J. Mitonuclear protein imbalance as a conserved longevity mechanism. Nature. 2013; 497:451-457.
37. Hamilton B, Dong Y, Shindo M, Liu W, Odell I, Ruvkun G, Lee SS. A systematic RNAi screen for longevity genes in C. elegans. Genes Dev. 2005; 19:1544-1555.
38. Hansen M, Hsu AL, Dillin A, Kenyon C. New genes tied to endocrine, metabolic, and dietary regulation of lifespan from a Caenorhabditis elegans genomic RNAi screen. PLoS Genet. 2005; 1:119-128.
39. Lee SS, Lee RY, Fraser AG, Kamath RS, Ahringer J, Ruvkun G. A systematic RNAi screen identifies a critical role for mitochondria in C. elegans longevity. Nat Genet. 2003; 33:40-48.
40. Ravitz O, Zsoldos Z, Simon A. Improving molecular docking through eHiTS' tunable scoring function. J Comput Aided Mol Des. 2011; 25:1033-1051.
41. Morris GM, Huey R, Lindstrom W, Sanner MF, Belew RK, Goodsell DS, Olson AJ. AutoDock4 and AutoDockTools4: Automated docking with selective receptor flexibility. J Comput Chem. 2009; 30:2785-2791.
42. Shaw FL, Harrison H, Spence K, Ablett MP, Simoes BM, Farnie G, Clarke RB. A detailed mammosphere assay protocol for the quantification of breast stem cell activity. J Mammary Gland Biol Neoplasia. 2012; 17:111-117.
43. Bonuccelli G, Tsirigos A, Whitaker-Menezes D, Pavlides S, Pestell RG, Chiavarina B, Frank PG, Flomenberg N, Howell A, Martinez-Outschoorn UE, Sotgia F, Lisanti MP. Ketones and lactate "fuel" tumor growth and metastasis: Evidence that epithelial cancer cells use oxidative mitochondrial metabolism. Cell Cycle. 2010; 9:3506-3514.
44. Bauer AW, Kirby WM, Sherris JC, Turck M. Antibiotic susceptibility testing by a standard single disk method. Am J Clin Pathol. 1966; 45:493-496.
45. Benson HJ (1998) Antimicrobial sensitivity testing: the Kirby-Bauer method. In: Microbiological Applications: Laboratory Manual in General Microbiology, 7th ed. McGraw-Hill, Boston, Massachusetts. pp 139-141.
46. Benson HJ (2002) Appendix A. In: Microbiological Applications: Laboratory Manual in General Microbiology, 8th edn. McGraw-Hill, Boston, Massachusetts. p 432.
47. Clinical and Laboratory Standards Institute "Performance Standard for Antimicrobial Disk Susceptibility Tests; Approved Standard". Document M02-A11 No. 1. Vol. 32. PA, USA: CLSI; 2012.
48. Clinical and Laboratory Standards Institute."Performance Standards for Antimicrobial Susceptibility Testing: Twentieth Informational Supplement M100-S23. Wayne, PA: CLSI; 2013.
49. Clinical and Laboratory Standards Institute, 2012. Methods for dilution antimicrobial susceptibility test for bacteria that grow aerobically; approved standards. 9th ed. Document M07-A9. CLSI, Wayne, PA.
50. Kalinowska-Lis U, Wojciechowski JM, Wolf WM, Ochocki J. Synthesis, Characterization, and Antimicrobial Activity of Silver(I) and Copper(II) Complexes of Phosphate Derivatives of Pyridine And Benzimidazole. ChemMedChem. 2014; 9: 169-176.

Review

For reprint orders, please contact reprints@future-science.com

Future Medicinal Chemistry

Quercetin and derivatives: useful tools in inflammation and pain management

Inflammation represents a very frequent condition in humans; it is often underestimated, making the problem an increasingly alarming phenomenon. For these reasons, conventional therapies are losing their effectiveness, leaving room for innovative therapies. In this field, natural products showed their efficacy in various diseases; and flavonoids, in particular quercetin, is known for its broad range of activities. In this review, we have highlighted its efficacy in various models of inflammation, focusing also on the activity of its semisynthetic derivatives, and those naturally present in plant extracts. Finally, the analgesic property of quercetin, intrinsically linked to its anti-inflammatory action, has been also evaluated, to investigate about an innovative approach to this interesting natural compound, such as analgesic remedial.

First draft submitted: 21 September 2016; Accepted for publication: 31 October 2016; Published online: 20 December 2016

Keywords: anti-inflammation activity • pain management • quercetin derivatives

Gabriele Carullo[1], Anna Rita Cappello[1], Luca Frattaruolo[1], Mariateresa Badolato[1], Biagio Armentano[1] & Francesca Aiello*,[1]

[1]Department of Pharmacy, Health & Nutritional Sciences, University of Calabria, Via Pietro Bucci, 87036 Rende Arcavacata, Cs, Italy

*Author for correspondence: francesca.aiello@unical.it

Phenolic compounds are one of the most important class of plants' secondary metabolites that include aglycones, glycosides and methylated derivatives. Among these, flavonoids are the most interesting for their therapeutic properties [1]; in fact, they are used as natural medicaments in several pathologies. Acting as potent antioxidants and metal chelators, flavonoids can be used to reduce oxidative stress and ameliorate or prevent numerous diseases. Furthermore, the antibacterial, antifungal, anticancer and anti-inflammatory properties of these compounds are also well known [2–4]. Quercetin (Qu), 2-(3,4-dihydroxyphenyl)-3,5,7-trihydroxy-4H-chromen-4-one (Figure 1), is the representative of the flavonols family, compounds characterized by 3-hydroxyflavone backbone. Qu is a natural compound that captured our attention, since it has numerous beneficial properties, and especially because it is easily detachable from a variety of food sources, such as cherries, apple, red wine, cappers and red onion [5]. Both Qu and its derivatives are involved in several physiological functions. Qu exerts a wide spectrum of biological effects: anti-inflammatory [6], anti-infectious [7], anticancer/chemopreventive [8,9], neuroprotective [10], antihypertensive [11,12] and blood glucose lowering properties have been reported [13]. Qu is considered a strong antioxidant [14] due to its ability to scavenge free radicals and bind transition metal ions. These properties are primarily ascribed to the presence of two antioxidant pharmacophores within the molecule. The catechol and the OH group at position C3 give Qu the optimal configuration for free radical scavenging. Despite its attractive properties, some limitations make difficult the use of Qu as a drug, in fact this molecule has a very poor oral bioavailability after a single oral dose (~2%), and its metabolism is complex, involving intestinal uptake and/or deglycosylation, glucuronidation, sulfatation, methylation, possible deglucuronidation and ring fission [15]. In this review, the

FUTURE SCIENCE part of fsg

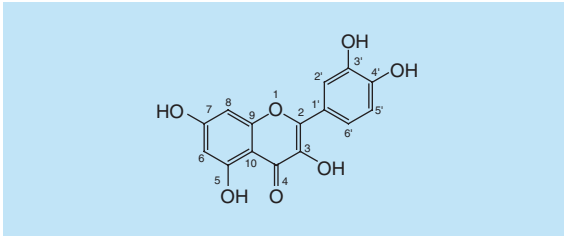

Figure 1. Quercetin.

anti-inflammatory and pain-relieving properties of Qu will be considered, taking into account the different biological pathways in which it interferes.

Inflammation & inflammatory mediators

Inflammation is a mechanism of nonspecific innate immunity, a complex biological response of body tissues to harmful physical, chemical and biological stimuli. It is a dynamic process that involves immune cells, blood vessels and molecular mediators, to eliminate the cause of harm and to initiate tissue repair. It can be classified into acute and chronic inflammation. The cardinal signs of acute inflammation are redness, swelling, heat, pain and loss of function (*rubor*, *tumor*, *calor*, *dolor* and *functio laesa*), as consequences of the different steps of the inflammatory process [16]. Acute inflammation process can be divided into a vascular phase and a cellular phase. The first one is characterized by marked vascular changes such as vasodilation, increased permeability and increased blood flow, which are induced by the actions of several inflammatory mediators. The cellular phase involves leukocytes, mainly including phagocytes and granulocytes, which move from blood into the inflamed tissue via extravasation to aid in inflammation by ingestion of pathogens and cellular debris and by releasing the toxic contents of the granules, respectively. The last ones do not discriminate between microbial and host targets, so collateral damage to host tissues is unavoidable [17]. The inflammatory response ends when the cause of harm is removed and the tissue is repaired. Chronic inflammation is a process in which active inflammation, tissue destruction and repair attempts coexist. It can be a consequence of a nonresolved acute inflammation in which the injurious agent persists, or it can begin as such. The characteristic of chronic inflammation is the prevalence of cellular phenomena rather than the vascular ones, which even may be completely absent. Inflammatory mediators have a key role in the progression of inflammation and in its resolution. They can be divided into preformed mediators and *de novo* produced mediators. The first type can be stored in the granules of blood particles (granulocytes and platelets), or they can freely circulate as inactive precursors in the plasma. Instead, *de novo* produced mediators are directly produced in response to appropriate harmful stimulation. Inflammatory mediators can be classified into several groups, according to their biochemical properties: vasoactive amines and peptides, complement components, lipid mediators, inflammatory cytokines, proteolytic enzymes, nitric oxide (NO) and reactive oxygen species (ROS) [18].

ROS include superoxide anion ($\cdot O_2^-$), H_2O_2 and the particularly reactive hydroxyl radical ($\cdot OH$), which is able to react with any biological macromolecule, including lipids, DNA and proteins, by alteration of their stability and physiological functions [19].

Nowadays, it is increasingly clear the connection between ROS and inflammation pathways. ROS is normally a minor by-product of oxidative phosphorylation and they can be neutralized by several enzymatic systems, such as superoxide dismutase enzymes, catalase, thioredoxin, glutathione peroxidase and peroxiredoxin systems [20].

During inflammation, instead, phagocytic leukocytes activation leads to the assembly of the multicomponent flavoprotein NADPH oxidase, which drastically increases ROS production. The saturation of the activity of the endogenous neutralizing systems results in ROS accumulation and, because of their high chemical reactivity, these species lead to direct nonspecific toxicity against both pathogenic and host biological systems. Moreover, increased ROS levels can also initiate and amplify inflammation through the upregulation of several genes involved in the inflammatory response. The expression of inflammation-related genes is strictly modulated by transcription factors activity. NF-κB is a ubiquitous transcription factor and a pleiotropic regulator of numerous genes involved in the immune and inflammatory responses. In quiescent cells, NF-κB is sequestered in the cytoplasm as an inactive form, associated with the inhibitor IκB, which prevents its translocation into the nucleus. Once produced, oxidant species are able to activate a redox-sensitive kinase complex, IκB kinase (IκK), which phosphorylates IκB, inducing its ubiquitination and proteasome-mediated degradation. These events result in the translocation of the active transcription factor into the nucleus, where it can amplify the inflammatory response by upregulating the production of various proinflammatory cytokines and enzymes, such as interleukins, TNF-α and inducible NOS (iNOS), which are able to continue the inflammatory signaling [21,22]. NO, generated by upregulated iNOS, mediates inflammatory vascular phase. Moreover, it can also react with superoxide anion to generate peroxinitrite ($ONOO^-$) and other reactive nitrogen species, which are able to react with lipids, DNA and proteins, potentiating ROS cytotoxic effects [23].

Because of its central role in inflammation, ROS pathway can be potential target for inflammation treat-

ment. Pathway disruption may occur through several pharmacological strategies, by reducing ROS production, by promoting their direct or enzyme-mediated neutralization or by inhibiting their downstream effect, through the activation of NF-κB modulators.

Activity of Qu in inflammation models

As already mentioned above, ROS are inflammatory mediators. Since all the flavonoids show an anti-inflammatory property, due to their intrinsic antioxidant behavior [24], they are involved in various inflammatory disorders. In particular, Qu results in the most interesting molecule, because it interferes with peculiar biological pathways [25], and recently it has been reported to be able to reduce inflammation process, involved in several models, through different mechanisms (Figure 2).

In particular, the AMPK/SIRT1 pathway results in more interesting inflammation management; so, activators of AMPK may reduce macrophage inflammation. Qu and other flavonoids, as AMPK and SIRT1 activators, may reduce inflammation by interfering with this pathway [26,27].

Nowadays it is raising the attention about the diet, mainly addressed to a progressive reduction of saturated fatty acids intake. An unbalanced diet can cause inflammation, leading to different disorders.

High-fat diet (HFD)-induced inflammatory model was used to evaluate the anti-inflammatory properties of Qu, since the consumption of HFD promotes production of ROS, which triggers inflammatory state [28]. Qu downregulates the expressions of iNOS and IFN-γ and also assuages NF-κB-mediated inflammation in HFD-fed mice within 15 days either by scavenging ROS, necessary for NF-κB activation, or by blocking TNF-α-dependent commencement of nuclear translocation of NF-κB [29].

Furthermore, the obesity status derived from an incorrect lifestyle, increases leptin levels and, when it binds to its receptor (Ob-Ra), there are high plasma leptin conditions. In human umbilical vein endothelial cells Ob-Ra expression, ERK1/2 phosphorylation and NF-κB activation increase significantly after 500 ng/ml leptin exposure, but they are reduced by addition of 125 μM Qu [30].

In obesity-induced adipose inflammation, a specific CC chemokine, MIP-1α/CCL3, induces monocyte/macrophage infiltration. Qu decreases MIP-1α release from adipocytes and macrophages; it also opposes MIP-1α-induced macrophage infiltration and activation. The inhibitory action of Qu on the MIP-1α-induced inflammatory responses of macrophages is mediated by downregulation of CCR1/CCR5, and inhibition of activation of JNK, p38 MAPK and IKK as well as IκBα degradation [31].

In HFD-fed mice, Qu also might suppress adipose tissue macrophage infiltration and inflammation through the AMPKα1/SIRT1 pathway [32].

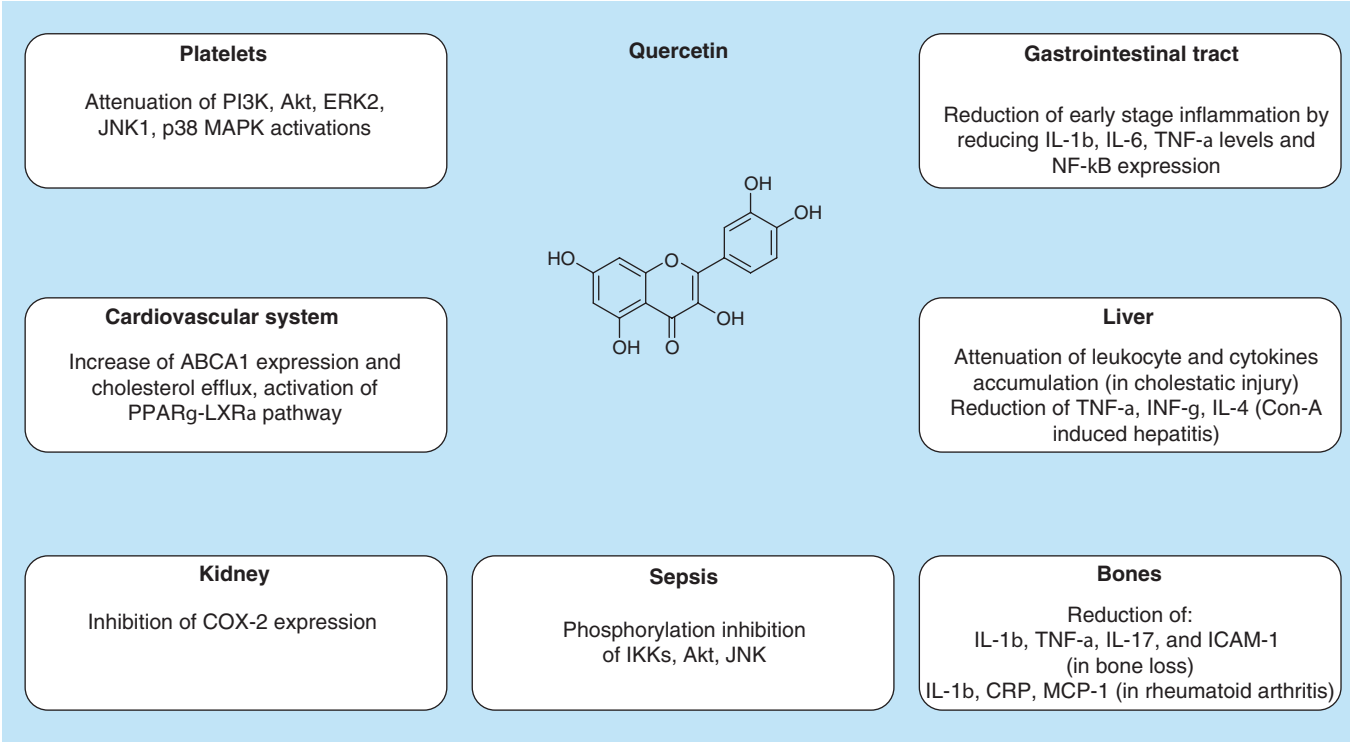

Figure 2. Anti-inflammatory activities of quercetin in experimental models.

Another very important evidence of Qu anti-inflammatory properties has been found in several models of gastrointestinal disorders. In hypertriglyceridemia-related acute pancreatitis, Qu is able to reduce early stage inflammation by reducing IL-1β, IL-6, TNF-α levels and NF-κB expression. In this context, Qu could downregulate IRE1α, sXBP1, C/EBPα, C/EBPβ expression; whose genes are involved in lipid metabolism and inflammation [33].

Qu has also been studied for its gastro-protective properties, in rats and in human intestinal epithelial cell line (Caco-2 cells). Qu prevents the nuclear translocation of Nrf2, involved in the antioxidant response, and reduces the ROS presence induced by indomethacin pretreatment. Furthermore, Qu is able to reduce myeloperoxidase and NF-κB activities as well as IL-8 production, leading to a potentiation of anti-inflammatory activity in a NSAID treatment [34].

In cholestatic liver injury, Qu attenuates leukocyte accumulation, NF-κB activation and pro-inflammatory cytokine production, through daily oral administration (25 mg/kg). Moreover, an inhibitory effect of Qu on MyD88 and TGF-β-activated kinase-1, critical for linking Toll-like receptor (TLR) and NF-κB, has been shown [35].

On the other hand, Qu has also been evaluated in bone loss and inflammation using a mouse periodontitis model, induced by *Aggregatibacter* (*Actinobacillus*) *actinomycetemcomitans* infection. In this context, subcutaneous treatment with Qu (100 mg/kg) reduces *A. actinomycetemcomitans*-induced bone loss and IL-1β, TNF-α, interleukin-17 and intercellular adhesion molecule 1 production in the gingival tissue, without affecting bacterial counts [36].

Furthermore, Qu exerts anti-inflammatory activity by inhibiting COX-2 expression in renal medullary interstitial cells and rats subjected to acute unilateral ureteral obstruction [37].

Mice undergone to heat and treated with Qu (15 mg/kg), have lower IL-6 and higher superoxide dismutase levels; heat exposure significantly elevates heat shock proteins 72 and 90, and heat shock factor-1 levels in mouse liver, heart and skeletal muscles, but no significant differences in tissue heat shock proteins and heat shock factor-1 have been found [38].

Another scenario in which Qu seems to be very efficacious is the sepsis, a condition in which Gram-negative bacteria caused an extensive inflammatory cytokine production. The employment of natural products in medicine has allowed the use of Qu to attenuate lipopolysaccharide (LPS)-induced production of TNF-α and IL-β in RAW 264.7 macrophages. Qu also inhibits phosphorylation of IKKs, Akt (PKB) and JNK. Acute administration of Qu reduces the toxicity rate of TNF-α and IL-1β in C57BL/6J mice [39].

It is well known that atherosclerosis is characterized by dysregulated cholesterol metabolism and chronic inflammation. In this field, Qu treatment induces the expression of ATP binding cassette transporter A1 in human differentiated THP-1 cells, and increases the cholesterol efflux from THP-1 cell derived foam cells. Qu also activates PPAR-γ–LXRα pathway to upregulate ABCA1 expression, through increasing protein level of PPAR-γ and its transcriptional activity. In summary, Qu reduces foam cell formation which is a critical feature in the initial stage of atherosclerosis [40].

In addition to platelets, Qu also attenuates PI3K, Akt, ERK2, JNK1 and p38 MAPK activations, which are supported by platelet-aggregation inhibition with the respective kinase inhibitors. Vasodilator-stimulated phosphoprotein stimulation is also inhibited, with the subsequent suppression of MAPK phosphorylation. In this perspective, Qu could be a good substance that involves aberrant platelet activation and inflammation [41].

In rheumatoid arthritis therapy, Qu's effects have been evaluated in a rat model of adjuvant arthritis. A daily oral dose of 150 mg/kg of Qu, for 28 days, lowers levels of IL-1β, C reactive protein (CRP), MCP-1; Qu is also able to inhibit the enzymatic activity of 12/15-lypoxigenase [42].

Finally, Qu can be considered a potential anti-inflammatory agent, in the gout treatment. It is well known that gout represents one of the most inflammatory problem in western society. The principal cause is the deposition of crystals of uric acid or its monosodium salt in human joints. Xanthine oxidase is the enzyme that catalyzes the sequential hydroxylation of hypoxanthine to uric acid, via xanthine as intermediate [43]. Its inhibition could resolve inflammation related to gout. Qu docks in the enzyme's active site, paving the way for a new set of potential anti-inflammatory agents that act on xanthine oxidase [44].

Compared with other phenolic compounds, Qu showed the best anti-inflammatory properties. In fact, in macrophages (murine J774 cells) exposed to an inflammatory stimulus (100 ng/ml LPS), Qu inhibits NO production at low concentration (IC_{50} ~ 25 μM), and significantly lowers iNOS mRNA levels. The LPS-induced activity of signal transducer and activator of transcription 1, another important transcription factor for iNOS, is nearly totally (91% inhibition) inhibited by Qu, compared with other compounds used [45].

In murine RAW264.7 macrophages, Qu and isorhamnetin **(4)** (Figure 3), but not Qu-3-glucuronide

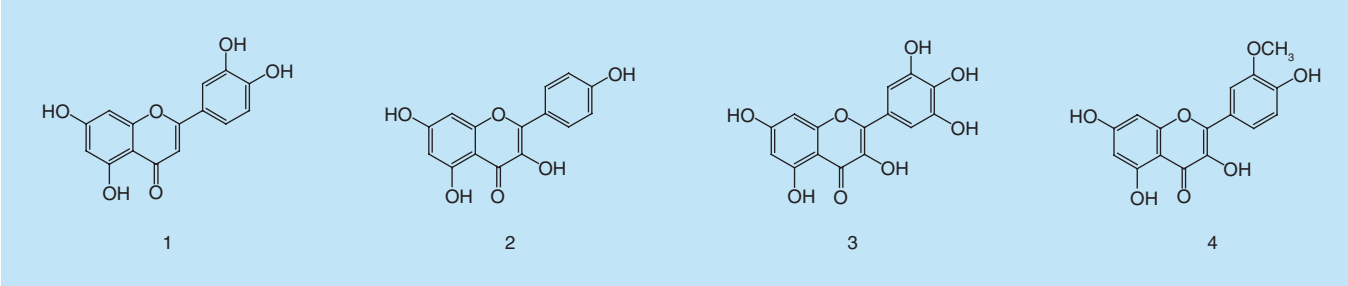

Figure 3. Chemical structures of flavonoids: (1) luteolin – (2) kaempferol – (3) myricetin – (4) isorhamnetin.

(Qu3G) decrease mRNA and protein levels of TNF-α, as well as mRNA levels of IL-β, IL-6, iNOS and MIP-1α. These inflammatory effects are ensured by an increase in heme oxygenase 1 protein levels, a target of Nrf2 pathway. miRNA 155 is a positive modulator of inflammation and its induction depends on NF-κB and JNK (c-Jun N-terminal kinase) pathway. In macrophages, its activity downregulates IkB kinase ε and receptor interacting serine-threonine kinase 1. In this context, Qu downregulates microRNA 155 levels, inhibiting NF-κB activation, which results in the anti-inflammatory effect of Qu and isorhamnetin **(4)** [46].

Furthermore, many studies have demonstrated the ability of Qu to interfere with TLRs, initiators of many inflammatory processes. Qu downregulates TLR4 signal transduction and elevates the expression of the Toll-interacting protein, a negative regulator of TLR signaling. Conversely, Qu inhibits the expression of cell surface molecules, such as clusters of differentiation 80/86 (CD80/CD86) and major histocompatibility complex class II in macrophages [47].

In detail, in the concanavalin A-induced hepatitis in mice, 50 mg/kg Qu administration reduces the concanavalin A-induced elevations in plasma aminotransferase concentrations, and also lowers the expression of TNF-α, IFN-γ, IL-4, high-mobility group box 1 protein, which induces inflammatory responses by transduction of cellular signals through its receptors, such as receptor for advanced glycation end products, TLR2, TLR4 and also involves NF-κB [48].

Treatment with Qu (40 and 80 mg/kg) of the inflammatory state in mice exposed to carbon tetrachloride results in a reduction in CYP2E1, IL-1β, iNOS, COX-2 expression. The likely mechanism involves the inhibition of TLR2 and TLR4 activation and also the MAPK phosphorylation, that blocks the NF-κB cascade [49].

Reduced levels of ROS and inflammatory biomarkers, including CRP and IL-6, with little effect on E-selectin have been observed in athletes, after ingestion of Qu with pro-oxidants, like vitamin C. Probably, the uptake of pro-oxidants may improve Qu's bioavailability through regeneration of oxidized form of Qu to parent compound [50].

Qu extracts & natural derivatives

Many total extracts are known for their anti-inflammatory properties, such as *Bryophyllum pinnatum* (Lam.) Oken ethanol extract, which is rich in anti-inflammatory flavonoids, as rutin, luteolin **(1)** (Figure 3) and often Qu [51].

Red wine polyphenolic extracts (Primitivo and Negroamaro cultivars) exhibit multiple anti-inflammatory and anti-atherosclerotic properties; in particular, flavonols such as kaempferol **(2)**, myricetin **(3)** (Figure 3) and Qu, significantly reduce the endothelial expression and release of M-CSF as well as ROS intracellular levels and the activation of NF-κB and AP-1 [52].

Careya arborea Roxb. (Lecythidaceae) methanol extract has been evaluated in its flavonoid content and also for its anti-inflammatory properties, essentially due to the presence of Qu and betulinic acid. The same extract has also been tested on carrageenan induced paw edema in rats, proving a good painkiller effect (100 mg/kg) [53].

Turkish *Scorzonera* species extracts are used to treat illnesses connected with inflammation; they show inhibitory activities on TNF-α and IL-1β production, and NF-κB nuclear translocation in THP-1 macrophages. The presence of chlorogenic acid in greater quantities and trace of Qu-3-O-β-D-glucoside (Figure 4), rutin and other flavonoids has been revealed by HPLC [54].

Butterfly pea (*Clitoria ternatea* Leguminosae) blue flower petal extract has been standardized to evaluate the presence of secondary metabolites, such as flavonols and ternatins. In this context, flavonols with a Qu moiety have been isolated and characterized; among these, manghaslin Qu 3-[2G] rhamnosylrutinoside, Qu 3-O-dirhamnoside and rutin. These flavonols show strong inhibition of COX-2 activity and partial ROS suppression. In general, *Clitoria ternatea* polyphenols show anti-inflammatory properties in LPS-induced inflammation in RAW 264.7 macrophage cells [55].

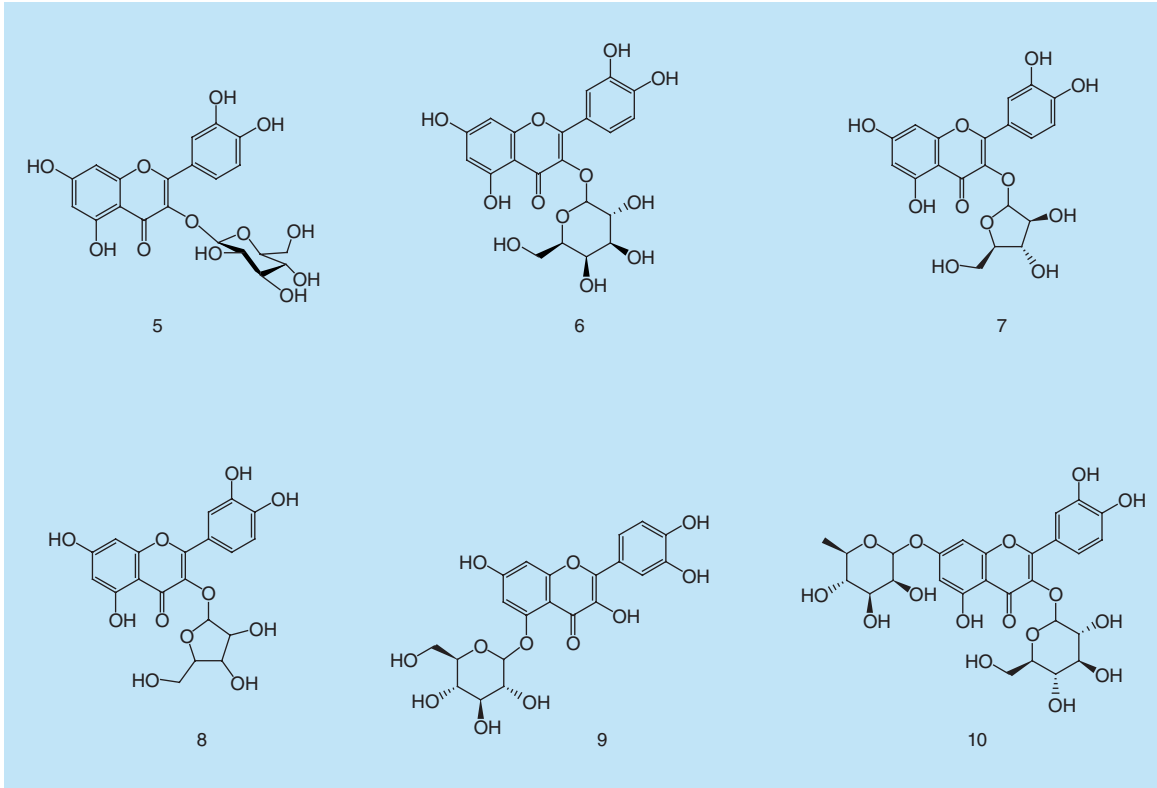

Figure 4. Quercetin glycosides. Qu-3-O-glucoside **(5)** – Qu-3-O-galactoside **(6)** – Qu-arabinoside **(7)** – Qu-O-pentoside **(8)** – Qu-5-glucoside **(9)** – Qu-3-O-glucoside-7-O-rhamnoside **(10)**.
Qu: Quercetin.

Phenolic compounds in *Nymphaea mexicana* Zucc. have been isolated and only a Qu derivative, Qu 3-(3″-acetylrhamnoside) (Figure 5) has been identified. In the inflammatory response, at 10–25 μM, it suppressed LPS-induced NO production in RAW 264.7 macrophages, although in cell viability test it showed a cytotoxic effect at 50 μM [56].

Polyphenol-rich extracts from the medicinal plants *Antirhea borbonica*, *Doratoxylon apetalum* and *Gouania mauritiana* have been characterized in their flavonoid content and rutin, kaempferol **(2)** and Qu has been found as major components. These extracts down-regulate ROS production and the secretion of IL-6 and MCP-1 pro-inflammatory markers, induced by H_2O_2, TNF-α and LPS mediators [57].

Myrica rubra sieb. et zucc. leaves contain a broad quantity of flavonoids, with Qu core, such as myricetin **(3)**, myricitrin, myricetin 3-O-(2″-O-galloyl)-α-L-rhamnopyranoside, myricetin 3-O-(2″-O-galloyl)-β-D-galactopyranoside and Qu 3-O-(2″-O-galloyl)-β-D-galactopyranoside (Figure 5). All these compounds inhibited LPS-stimulated NO, pro-inflammatory cytokines and the protein levels of iNOS and COX-2 in RAW 264.7 macrophages, in a dose-dependent way [58].

In a very interesting study, apple fruits have been genetically modified to create modified foods by means of MYB transcription factor, MYB10, fused to a constitutive promoter, Cauliflower mosaic virus 35S (MYB10 apple) [59]. This MYB transcription factor regulates biosynthetic genes in the anthocyanin-specific part of the flavonoid pathway [60]. Apples resulted enriched in anthocyanins and Qu derivatives, specifically Qu-galactoside **(6)** and Qu-arabinoside **(7)** (Figure 4); the anti-inflammatory properties regard the reduction of transcription levels of inflammation-linked genes, such as IL-2rb, Ccr2, Cxcl10 and Ccr10 [61].

In a rat model of induced colitis (by 2,4,6-trinitrobenzene sulfonic acid), Qu3G decreases mucosal myeloperoxidase activity, NO production, TNF-α expression and malondialdehyde (MDA) levels and increases total glutathione (GSH) levels, in a dose-dependent manner [62].

Qu 3,3′ dimethyl ether 7-O-β-D-glucopyranoside (Figure 5) is present, with iso-okanin (7-O-β-D-(2″,4″,6″-triacetyl) glycopyranoside), in ethyl acetate fraction of *Bidens pilosa* (Asteraceae). This extract has been evaluated for its anti-inflammatory and analgesic properties (doses 50, 100 and 200 mg/kg), showing antinociceptive effect in all four different models for nociception (acetic acid-induced writhing, hot plate test, capsaicin-induced hind paw licking, formalin-induced pain) and anti-inflammatory

properties in dextran-induced, histamine-induced, serotonin-induced rat hind paw edemas [63].

3′-O-methylated metabolite of Qu, isorhamnetin **(4)**, could reduce iNOS expression and NO production [64]. It also increases the nuclear translocation of Nrf2 in a dose- and time-dependent manner, hence the anti-oxidant response element reporter gene activity [65], the expression and synthesis of proteins such as heme-oxygenase and cysteine ligase, and the increase in intracellular GSH level. Such activities are also carried out by the Qu, suggesting a major role of OH-flavone ring, compared with the methoxyl group, although methylated derivatives are rapidly metabolized giving them a primary role in anti-inflammatory treatment [66].

Saxifragin, the 5-glucoside of the flavonoid Qu, has been found in several plants and insects. Its anti-inflammatory properties have been demonstrated in LPS-stimulated RAW 264.7 macrophages and animal models of inflammation. The flavonoid suppresses the production of NO and prostaglandin E2 and inhibits the nuclear translocation of p65 and activation of caspase-1, by NF-κB-regulated gene transcription. Saxifragin also inhibits mRNA expression of pro-inflammatory cytokines, including TNF-α, IL-6 and IL-1β. Thus, saxifragin exerts anti-inflammatory activity by inhibiting NF-κB, caspase-1 and MAPK activation [67].

Hyperoside, 3-O-galactoside of Qu, has been evaluated in the inflammatory processes induced by high glucose level in human umbilical vein endothelial cells and male C57BL/6 mice. Thus, the flavonol glycoside decreases vascular permeability, monocyte adhesion, expressions of cell adhesion molecules, ROS formation and activation of NF-κB [68].

In endothelial cells Qu, luteolin **(1)** and epigallocatechin gallate reduce ROS production and inhibit thioredoxin-interacting protein and nucleotide-binding domain-like receptor protein 3 inflammasome activation, leading to the downregulation of IL-1β expression [69].

In 3T3-L1 adipocytes, Catechin and Qu, alone and/or in association, attenuate TNF-α-induced elevated protein carbonyls, increase proinflammatory cytokine expression (MCP-1, resistin) and decrease adiponectin. These protective effects of Catechin and Qu on adipose inflammation are associated with their capacity to decrease the activation of MAPKs, JNK and p38, preventing the downregulation of PPAR-γ [70].

In palmitate-induced inflammation model, Qu and Qu3G inhibit ROS overproduction and effectively restore mitochondrial membrane potential, demonstrating their chemo-protection of mitochondrial function through antioxidative actions. Furthermore, they inhibit ROS-associated inflammation by inhibition of IL-6 and TNF-α production with suppression of IKKβ/NF-κB phosphorylation [71].

Dermatological preparations are widely used to treat inflammation of the skin surface layer. In this sense,

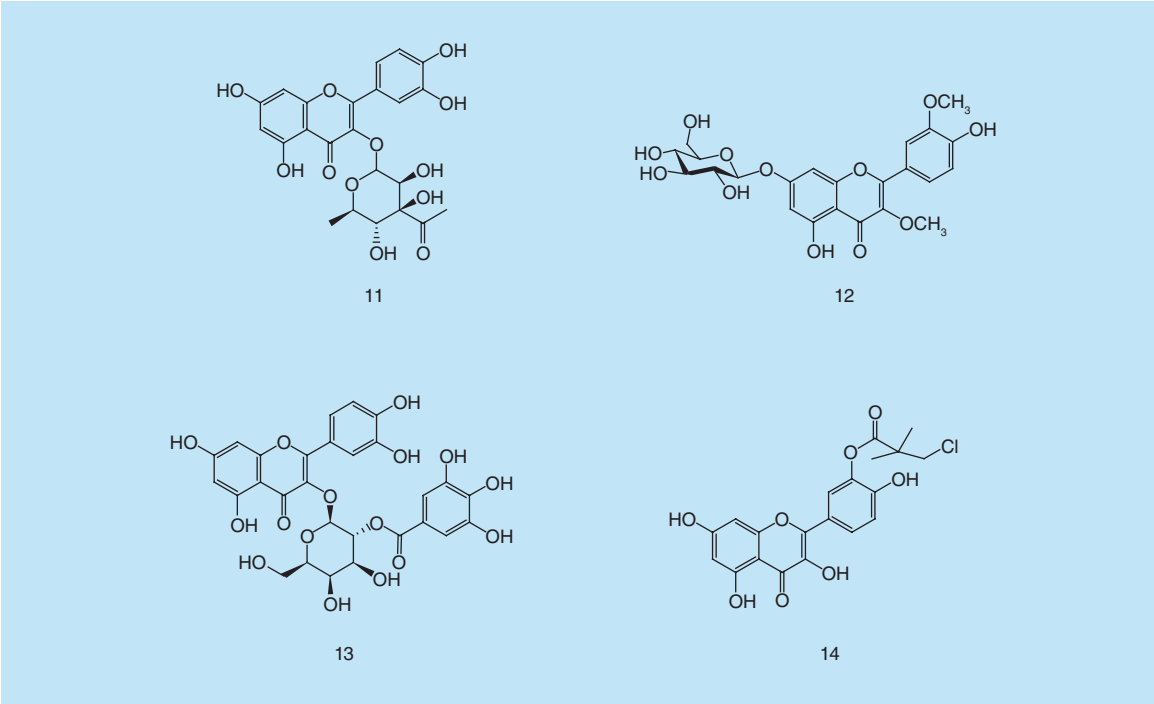

Figure 5. Quercetin derivatives. Quercetin-3–3′′ acetylrhamnoside **(11)** – Qu 3,3′ dimethylether 7-O-β-D-glucopyranoside **(12)** – Qu 3-O-(2′′ -O-galloyl) -β-D-galactopyranoside **(13)** – 3′-O-(3-chloropivaloyl) Qu **(14)**.

oil bodies are used for their pleasure sensation. The administration of reconstituted oil bodies containing a polyphenol mix of Qu and piperine efficiently inhibits LPS-mediated inflammatory responses from dendritic cells (DCs), and inhibits cytokine secretion, including IL-6, IL-23 and IL-12, while increasing IL-10 and IL-1Rα production. These reconstituted oil bodies have been tested in mice with excellent results, demonstrating their possible usage to treat acute intestinal inflammation [72].

Qu derivatives are also often used in atopic dermatitis (AD), a pediatric inflammatory skin disorder, treated with steroids for topical use. Qu, resveratrol, naringenin and tannic acid have emerged as therapeutic agents for AD treatment. In particular, a novel Qu derivative, Qu-3-O-(2″-gallate)-α-L-rhamnopyranoside, suppresses inflammatory cytokines, such as IL-4, IL-5 and IL-13, serum IgE, eosinophil levels, iNOS and COX-2 in the AD NC/Nga mouse model [73].

The anti-inflammatory action of Qu has been enhanced through nanoparticles based on Exosurf™ (containing cetyl alcohol, Burroughs-Wellcome, NC, USA) and Gelucire® 44/14 (gelucire, Gattefossė, NJ, USA); in fact, BALB/c mice treated with the aforementioned nanoparticles are less inflamed. This vehicle, which is itself anti-inflammatory, could increase the bioavailability of Qu, leading to a novel series of derivatives with better anti-inflammatory properties [74].

To evaluate anti-inflammatory properties of Qu-loaded phospholipid vesicles, 12-O tetradecanoylphorbol 13-acetate model of skin inflammation has been used. Vesicles administration results in an amelioration of the tissue damage, with a noticeable attenuation of edema and leukocyte infiltration [75].

Propionibacterium acnes-induced skin inflammation in mice has been treated with total phenolic extract (TPE) of wild bitter melon (*Momordica charantia* L. var. abbreviate Seringe), resulting in a reduction of IL-8, IL-1β, TNF-α levels. In addition, TPE suppresses matrix metalloproteinase-9 levels, blocks NF-κB activation and inactivates MAPK. These properties have been attributed to the presence of flavonoids in TPE, including Qu and its derivatives [76].

In vivo studies on mice demonstrate that, at non-toxic doses, Qu or Qu3G (0.06 or 0.15 μmol/mouse) significantly increase IL-10 secretions by macrophages of the LPS-induced septic mice. In a therapeutic manner, only Qu markedly increases IL-10 secretions. Hence, Qu is able to ameliorate systemic inflammation [77].

Isorhamnetin (4) has been evaluated in inflammation, by using ulcerative colitis-like and Crohn's disease-like models of experimental inflammatory bowel disease in mice. It abrogates inflammation through inhibition of the activity of myeloperoxidase (MPO), the levels of TNF-α and IL-6, the mRNA expression of pro-inflammatory mediators (iNOS, intercellular adhesion molecule 1, COX-2, TNF-α, IL-2 and IL-6) and the phosphorylation of IκBα and NF-κB p65 [78].

The research for new anti-inflammatory substances prompted to chemically edit Qu derivatives. In particular, acyl derivatives are more lipophilic than parent compounds. In this field, polyunsaturated fatty acids, *per se* anti-inflammatory, have been evaluated as acyl donors. The novel Qu-3-O-glucoside eicosapentaenoic acid ester (30 μg/ml) reduces IL-6 production, PGE2 and COX-2 expression, and translocation of p65 in the nucleus in THP-1 macrophages [79].

Qu has also a protective effect against inflammation caused by perfluorooctanoic acid in liver mice; in fact, it decreases IL-6, COX-2 and CRP levels [80].

Acute lung injury is an inflammatory disease characterized by excess production of inflammatory factors in lung tissue. Qu pretreatment effectively ameliorates LPS-induced acute lung injury, mainly through suppression of inflammation and oxidative stress [81].

Nickel causes injury in mice, mainly through DNA methylation. In this context, Qu induces Nrf2 nuclear translocation and heme-oxygenase activity. Moreover, Qu decreases production of pro-inflammatory markers, including TNF-α, IL-1β and iNOS. Qu significantly inhibits p38 and signal transducer and activator of transcription 1 activation, which in turn inactivates NF-κB and the inflammatory cytokines in livers [82].

Benzo(a)pyrene (BaP) is the best known and the most studied polycyclic aromatic hydrocarbon. BaP is converted to reactive species that induce inflammatory processes through various mechanisms. In particular, in adenocarcinomic human alveolar basal epithelial cells (A549 cell line) exposed to BaP and treated with 10 μM Qu, a reduction of IL-1β and TNF-α has been observed. A further reduction in OS markers such as NO, MDA, oxidative stress index, total oxidant status has been found [83].

Liver injury induced with *Tripterygium* glycosides is appeased by Qu. Particularly, it significantly inhibits alanine/aspartate transaminase, alkaline phosphatase and gamma glutamyl transferase at 20 or 40 mg/kg. A reduction of IL-10 and TNF-α expression and GSH levels has also been observed [84].

Age-related macular degeneration is a senile disorder accompanied by oxidative stress and inflammation. With the aim of preventing human retinal pigment epithelial cell line (ARPE-19 cells) inflammation, in the first time, the cells have been treated with 4-hydroxynonenal to develop peroxidation and then Qu has been added, in

concentration of 100 – 50 – 10 – 1 μM. A reduction in IL-6, IL-8 and MCP-1 expression has been observed [85].

Mitochondrial dysfunction contributes to neuron degeneration by depletion of cellular ATP, through ROS generation and development of apoptosis due to the action of MPTP and the release of cytochrome c [86]. In muscle and brain, it has been shown that Qu enhances mitochondrial biogenesis [87]; thus, mitochondrial targeted-effects appear to be a process by which Qu could prevent neurodegeneration [88].

In a rat model of spinal cord injury, Qu significantly decreases ROS production, inhibits nucleotide-binding domain-like receptor protein 3 inflammasome activation and reduces inflammatory cytokine levels [89].

In spinal cord injury, the combination of curcumin and Qu, as 'Cur(Que)min', can act 'additively and synergistically', by decreasing TNF-α and iNOS mRNA expression, Caspase-3 activity, MDA levels and lipid peroxidation [90].

Qu is able to protect neurons by inhibiting microglia activation and downregulating inflammatory genes [91]. A novel Qu derivative, 3′-O-(3-chloropivaloyl) Qu (CPQ; 1–10 μmol/l) attenuates the production of the inflammatory mediators, NO and TNF-α, in LPS-stimulated BV-2 microglial cells [92].

In mice models, macrophage-like RAW 264.7 and microglial MG6, Qu3G does not exert anti-inflammatory properties while the deconjugated forms, Qu and isorhamnetin (4), exhibit anti-inflammatory responses through attenuation of JNK pathway. It is therefore reasonable to assume that Qu3G can pass through blood–brain barrier, accumulates in macrophages and acts as an anti-inflammatory agent in the brain through deconjugation into the bioactive nonconjugated forms [93].

Atypical prostatic hyperplasia is often accompanied by inflammatory state. In this context, red onion (*Allium cepa* Linn) scale extract has been characterized and Qu and Qu-4′-β-O-D-glucoside have been found as major components. In the control of inflammation, this extract reduces IL-6, IL-8, TNF-α, IGF-1 and clusterin expression [94].

Table 1. Anti-inflammatory properties of plant extracts containing quercetin and its derivatives.

Plant extract	Quercetin derivatives	Anti-inflammatory efficacy	Ref.
Bryophyllum pinnatum ethanol extract (Lam.) Oken	Quercetin Luteolin Luteolin 7-O-β-D-glucoside Rutin	Inhibition of ear edema induced by croton oil, arachidonic acid, capsaicin, ethyl phenylpropiolate	[48]
Primitivo and Negroamaro wine polyphenolic extracts	Quercetin Kaempferol Myricetin	Reduction of endothelial expression and release of M-CSF Reduction of ROS intracellular levels Inhibition of NF-κB and AP-1	[49]
Careya arborea Roxb. methanol extract	Quercetin Betulinic acid (a steroidic derivative)	Decrease of carrageenan-induced paw edema Reduction of MDA, CRP, NO and myeloperoxidase levels Downregulation of serum TNF-α and IL-1β levels	[50]
Turkish *Scorzonera* extracts	Quercetin-3-O-β-D-glucoside	Reduction of IL-1β and TNF-α production Inhibition of carrageenan and prostaglandin E2 induced hind paw edema (aerial parts extracts)	[51]
Butterfly pea blue flower petal extract	Manghaslin quercetin 3-(2G) rhamnosyl rutinoside Quercetin 3-O-dirhamnoside Rutin	Inhibition of COX-2 ROS suppression Reduction of nuclear NF-κB translocation, iNOS protein expression and NO production (anthocyanins)	[52]
Bidens pilosa ethyl acetate fraction	Quercetin 3,3′ dimethyl ether 7-O-β-D-glucopyranoside	Anti-inflammatory activity in dextran-induced, histamine-induced, serotonin-induced rat hind paw edemas	[60]
Wild bitter melon – *Momordica charantia* L. total extract	Quercetin Apigenin Luteolin Myricetin	Reduction of IL-8, IL-1β and TNF-α production MAPK inactivation	[73]

COX-2: Cyclooxygenase 2; CRP: C reactive protein; MDA: Malondialdehyde; NO: Nitric oxide; ROS: Reactive oxygen species.

Qu & pain management

Pain conditions, only associated with inflammatory processes, are generally treated by interfering with CB1/2, TRPV1, fatty acid amide hydrolase and COX 1/2 systems. Several compounds have been synthesized and many of them act as dual inhibitors [95,96].

As an anti-inflammatory agent, Qu may exert also antinociceptive properties. In this field, a Qu-based molecule could be used as a dual anti-inflammatory/antinociceptive drug. It has been demonstrated that Qu inhibits nociceptive responses in several animal models of nociception, such as mice and rats [97–99].

Specifically, Qu (100 mg/kg) reduces both mechanical allodynia and heat hypersensitivity in chronic constriction injury applied to rats at varying degrees, resulting significantly superior to gabapentine and morphine in terms of alleviating mechanical and thermal hypersensitivity [100].

Qu significantly reduces pain score in chronic phase of formalin test at a dose of 10 mg/kg, for 6 weeks, in diabetic rats. Then, Qu treatment significantly increases tail flick latency; while brain level of MDA and nitrite have been reduced and activity of SOD slightly increased [101].

A very difficult kind of pain to treat is diabetic neuropathic pain, an important microvascular complication in diabetes mellitus. Streptozotocin-induced diabetic mice have been subjected to test thermal hyperalgesia by tail-immersion assay. Qu (100 but not 50 mg/kg) produces a marked increase in tail-flick latencies. Increase in nociceptive threshold is reversed by naloxone (2 mg/kg), an opioid receptor antagonist. These results indicate an antinociceptive activity of Qu, probably through modulation of opioidergic mechanism [102].

Intraperitoneal and oral treatments with Qu dose-dependently inhibit inflammatory nociception induced by acetic acid and phenyl-p-benzoquinone. The second phase of formalin- and carrageenan-induced mechanical hypernociception is also suppressed by Qu. Moreover, Qu inhibits the nociception induced by cytokines, by reducing carrageenan-induced IL-1β production. Probably, Qu acts as an analgesic by inhibiting pro-nociceptive cytokine production and the oxidative imbalance mediation of inflammatory pain [103].

Tilia americana var. *Mexicana* inflorescences have been evaluated in the pain-induced functional impairment model in rats. In particular, it has been seen that aqueous extract, at 30 and/or 100 mg/kg dosages, in the pain-induced functional impairment model in rats and formalin models produces a significant and dose-dependent antinociceptive response resembling that produced by a total and a partial agonist of 5-HT1A receptors like 8-OH-DPAT (8-hydroxy-2-[di-n-propylamino]tetralin hydrobromide). This activity has been attributed to the presence of flavonols such as kaempferol **(2)** and Qu derivatives, such as Qu-O-pentosylhexoside, Qu-3-O-glucoside-7-O-rhamnoside **(10)**, Qu-3-O-glucoside **(5)**, Qu-O-pentoside **(8)** (Figure 4) [104].

Diabetic rats, after 4 weeks of a single intravenous Streptozotocin injection (45 mg/kg), exhibit a significant thermal hyperalgesia and cold allodynia, along with increased plasma glucose and decreased body weights. Qu chronic treatment is able to attenuate cold allodynia as well as hyperalgesia [105].

Literature data reported that co-administration of low doses of Qu, in a dose-dependent manner, and clonidine (α_2-agonist) produces a synergistic analgesic effect. Pretreatment with yohimbine (α_2 blocker) significantly reverses Qu- as well as clonidine/Qu combination-induced effects. Therefore, Qu induces an antinociceptive effect followed by the activation of the α_2-receptor [106].

Qu (10–60 mg/kg or 100–500 mg/kg) dose dependently inhibits nociceptive behavior in the acetic acid-induced pain test. Moreover, Qu (10–60 mg/kg) inhibits both phases of formalin-induced pain, with millimolar values for the neurogenic and inflammatory phases. Qu (10–60 mg/kg) also inhibits the nociception induced by glutamate and capsaicin. Anti-nociceptive actions have been reversed by p-chlorophenylalanine methyl ester, katanserin, methysergide, bicuculline ($GABA_A$ antagonist) or baclofen ($GABA_B$ agonist). In this context, Qu exerts analgesic properties by interfering with GABAergic system [107].

As demonstrated by chronic ethanol administration in rats, Qu is also more effective in neuropathic pain. Treatment with Qu (20 and 40 mg/kg) for 10 weeks significantly attenuates allodynia, hyperalgesia as well as motor coordination and impaired nerve conduction velocity along with decreased level of membrane-bound Na^+–K^+-ATPase. It also significantly decreases elevated levels of MDA as well as pro-inflammatory mediators, such as NO [108].

Qu has also been evaluated in treating cancer pain, demonstrating a good analgesic activity in Ehrlich tumor-induced hyperalgesia. In detail, Qu exerts its analgesic properties by inhibiting IL-1β and TNF-α production [109].

Conclusion & future perspective

In this review we have described how Qu, a natural flavonoid, could be involved in many inflammatory processes and in their modulation. In addition, we evaluated anti-inflammatory properties of plant extracts containing Qu and its derivatives. Finally, because of its anti-inflamma-

tory properties, we have highlighted its analgesic activity in some experimental models of pain. This scenario could pave the way for a new class of anti-inflammatory drugs with analgesic properties that can assist NSAIDs, and even have fewer side effects in the kidneys and GI tract. Furthermore, a more lipophilic Qu-based molecule, highly antioxidant and with analgesic properties, would reach the central nervous system and, hopefully, be a potential neuroprotective agent (Table 1).

Financial & competing interests disclosure

The authors have no relevant affiliations or financial involvement with any organization or entity with a financial interest in or financial conflict with the subject matter or materials discussed in the manuscript. This includes employment, consultancies, honoraria, stock ownership or options, expert testimony, grants or patents received or pending, or royalties.

No writing assistance was utilized in the production of this manuscript.

Executive summary

Flavonoids & quercetin

- Natural products represent a great resource from the therapeutic point of view; in this sense medicinal chemists are spurred to investigate how these substances could interfere with biological pathways. Between them, flavonoids are intensely studied for their therapeutic properties due to the presence in various nutrients and plants and to the general chroman scaffold. In this family, quercetin (Qu) is the best representative because it is present in more and more fruits and vegetables; as such, it demonstrated a wide range of biological properties.

Inflammation

- Among the various physio-pathological disorders, inflammation represents a very frequent condition, or better a complex biological response of body tissues to harmful physical, chemical and biological stimuli that involves immune cells, blood vessels and molecular mediators, to eliminate the cause of harm and to initiate tissue repair. Inflammatory conditions are often underestimated, and consequently become chronic.

Qu & plant extracts in inflammation models

- All flavonoids show anti-inflammatory properties, due to their intrinsic anti-oxidant behavior. In fact, they are involved in various inflammatory disorders; in this field, Qu results in the most interesting molecule, because it interferes with peculiar biological pathways, and also it is able to reduce inflammation process, involved in several models, through different mechanisms. In particular, Qu demonstrates a good ability to reduce the expression of various interleukins such as IL-6, IL-2 and also iNOS, NF-κB, p38 MAPK and also TNF-α levels. Not only Qu, but also extracts of plants that contain it show anti-inflammatory properties. In these cases, also Qu derivatives demonstrate anti-inflammatory activities.

Looking ahead in pain management

- Qu also presents a good analgesic activity due to its anti-inflammatory properties. Specifically, it reduces mechanical allodynia and heat hypersensitivity and also pronociceptive cytokine production and the oxidative imbalance mediation of inflammatory pain. Qu chronic treatment is able to attenuate cold allodynia as well as hyperalgesia.

References

Papers of special note have been highlighted as:
• of interest; •• of considerable interest

1 Cappello AR, Dolce V, Iacopetta D *et al.* Bergamot (*Citrus bergamia* Risso) flavonoids and their potential benefits in human hyperlipidemia and atherosclerosis: an overview. *Mini Rev. Med. Chem.* 16(8), 619–629 (2016).

2 Tapas AR, Sakarkar DM, Kakde RB. Flavonoids as nutraceuticals: a review. *Trop. J. Pharm. Res.* 7(3), 1089–1099 (2008).

3 Leyva-López N, Gutierrez-Grijalva EP, Ambriz-Perez DL, Heredia JB. Flavonoids as cytokine modulators: a possible therapy for inflammation-related diseases. *Int. J. Mol. Sci.* 17 (6), 921 (2016).

4 Fürst R, Zündorf I. Plant-derived anti-inflammatory compounds: hopes and disappointments regarding the translation of preclinical knowledge into clinical progress. *Mediators Inflamm.* 2014, 146832 (2014).

5 Gharras HE. Polyphenols: food sources, properties and applications – a review. *Int. J. Food Sci. Technol.* 44, 2512–2518 (2009).

• **Flavonoids description, sources and therapeutic applications.**

6 Bischoff SC. Quercetin: potentials in the prevention and therapy of disease. *Curr. Opin. Clin. Nutr. Metab. Care* 11(6), 733–740 (2008).

7 Chirumbolo S. The role of quercetin, flavonols and flavones in modulating inflammatory cell function. *Inflamm. Allergy Drug Targets* 9(4), 263–285 (2010).

8 Hirpara KV, Aggarwal P, Mukherjee AJ, Joshi NJ, Burman AC. Quercetin and its derivatives: synthesis, pharmacological uses with special emphasis on anti-tumor properties and prodrug with enhanced bio-availability. *Anticancer Agents Med. Chem.* 9(2), 138–161 (2009).

9 Spagnuolo C, Russo M, Bilotto S, Tedesco I, Laratta B, Russo GL. Dietary polyphenols in cancer prevention: the

example of the flavonoid quercetin in leukemia. *Ann. NY Acad. Sci.* 1259(1), 95–103 (2012).

10 Ossola B, Kaariainen TM, Mannisto PT. The multiple faces of quercetin in neuroprotection. *Expert Opin. Drug Saf.* 8(4), 397–409 (2009).

11 Larson AJ, Symons JD, Jalili T. Therapeutic potential of quercetin to decrease blood pressure: review of efficacy and mechanisms. *Adv. Nutr.* 3(1), 39–46 (2012)

12 Perez-Vizcaino F, Duarte J, Andriantsitohaina R. Endothelial function and cardiovascular disease: effects of quercetin and wine polyphenols. *Free Radic. Res.* 40(10), 1054–1065 (2006).

13 Zunino S. Type 2 diabetes and glycemic response to grapes or grape products. *J. Nutr.* 139(9), S1794–S1800 (2009).

14 Boots AW, Haenen GR, Bast A. Health effects of quercetin: from antioxidant to nutraceutical. *Eur. J. Pharmacol.* 585(2–3), 325–337 (2008).

15 D'Andrea G. Quercetin: a flavonol with multifaceted therapeutic applications? *Fitoterapia* 106, 256–271 (2015).

• **Are important to understand quercetin (Qu) properties.**

16 Medzhitov R. Origin and physiological roles of inflammation. *Nature* 454, 428–435 (2008).

17 Kumar V, Abbas AK, Aster JC. Inflammation and Repair. In: *Robbins Basic Pathology (9th Edition).* Elsevier Saunders, PA, USA (2013).

18 Serhan CN, Ward PA, Gilory DW. The inflammatory response: an overiview. In: *Fundamentals of Inflammation.* Cambridge University Press, Cambridge, UK (2010).

19 Hensley K, Robinson KA, Prasad Gabbita S, Salsman S, Floyd RA. Reactive oxygen species, cell signaling and cell injury. *Free Radic. Biol. Med.* 28(10), 1456–1462 (2000).

20 Lei XG, Zhu J, Cheng W *et al.* Paradoxical roles of antioxidant enzymes: basic mechanisms and health implications. *Physiol. Rev.* 96, 307–364 (2016).

21 Morgan MJ, Liu Z. Crosstalk of reactive oxygen species and NF-κB signaling. *Cell Res.* 21, 103–115 (2011).

22 Conner EM, Grisham MB. Inflammation, free radicals and antioxidants. *Nutrition* 12(4), 274–277 (1996).

23 Dedon PC, Tannenbaum SR. Reactive nitrogen species in the chemical biology of inflammation. *Arch. Biochem. Biophys.* 423, 12–22 (2004).

• **Description of inflammation mechanisms.**

24 Koeberle A, Werz O. Multi-target approach for natural products in inflammation. *Drug Discov. Today* 19(12), 1871–1882 (2014).

25 Rathee P, Chaudhary H, Rathee S, Rathee D, Kumar V, Kohli K. Mechanism of action of flavonoids as anti-inflammatory agents: a review. *Inflamm. Allergy Drug Targets* 8, 229–235 (2009).

26 Steinberg GR, Schertzer JD. AMPK promotes macrophage fatty acid oxidative metabolism to mitigate inflammation: implications for diabetes and cardiovascular disease. *Immunol. Cell Biol.* 92, 340–345 (2014).

27 Owona Ayissi VB, Ebrahimi A, Schluesenner H. Epigenetic effects of natural polyphenols: a focus on SIRT1-mediated mechanisms. *Mol. Nutr. Food Res.* 58(1), 22–32 (2013).

28 Stern N, Osher E, Greenman Y. Hypoadiponectinemia as a marker of adipocyte dysfunction – part II: the functional significance of low adiponectin secretion. *J. Cardiometab. Syndr.* 2, 288–294 (2007).

29 Das N, Sikder K, Bhattacharjee S *et al.* Quercetin alleviates inflammation after short-term treatment in high-fat-fed mice. *Food Funct.* 4, 889–898 (2013).

30 Rasjad Indra M, Karyono S, Ratnawati R, Malik SG. Quercetin suppresses inflammation by reducing ERK1/2 phosphorylation and NF kappa B activation in leptin-induced human umbilical vein endothelial cells (HUVECs) *BMC Res. Notes* 6, 275 (2013).

31 Noh H, Kim C, Kang J *et al.* Quercetin suppresses MIP-1α-induced adipose inflammation by downregulating its receptors CCR1/CCR5 and inhibiting inflammatory signaling. *J. Med. Food.* 17(5), 550–557 (2014).

32 Dong J, Zhang X, Zhang L *et al.* Quercetin reduces obesity-associated ATM infiltration and inflammation in mice: a mechanism including AMPKα1/SIRT1. *J. Lipid Res.* 55, 363–374 (2014).

33 Zheng J, Wu J, Chen J *et al.* Therapeutic effects of quercetin on early inflammation in hypertriglyceridemia-related acute pancreatitis and its mechanism. *Pancreatology* 16(2), 200–210 (2016).

•• **Importance due to description of Qu's employment into metabolic disease.**

34 Carrasco-Pozoa C, Castillo RL, Beltránc C, Mirandac A, Fuentesd J, Gottelanda M. Molecular mechanisms of gastrointestinal protection by quercetin against indomethacin-induced damage: role of NF-κB and Nrf2. *J. Nutr. Biochem.* 27, 289–298 (2016).

35 Lin S, Wang Y, Chend W, Chuang Y, Pan P, Chen C. Beneficial effect of quercetin on cholestatic liver injury. *J. Nutr. Biochem.* 25(11), 1183–1195.

36 Napimoga MH, Clemente-Napimoga JT, Macedo CG *et al.* Quercetin inhibits inflammatory bone resorption in a mouse periodontitis model. *J. Nat. Prod.* 76, 2316–2321 (2013).

37 Carlsen I, Frøkiær J, Nørregaard R. Quercetin attenuates cyclooxygenase-2 expression in response to acute ureteral obstruction. *Am. J. Physiol. Renal. Physiol.* 308, F1297–F1305 (2015).

38 Chen Y, Islam A, Abraham P, Deuster P. Single-dose oral quercetin improves redox status but does not affect heat shock response in mice. *Nutr. Res.* 34(7), 623–629 (2014).

39 Chang Y, Tsai M, Sheu WH, Hsieh S, Chiang A. The therapeutic potential and mechanisms of action of quercetin in relation to lipopolysaccharide-induced sepsis *in vitro* and *in vivo*. *PLoS ONE* 8(11), e80744 (2013).

40 Sun L, Li E, Wang F *et al.* Quercetin increases macrophage cholesterol efflux to inhibit foam cell formation through activating PPARγ–ABCA1 pathway. *Int. J. Clin. Exp. Pathol.* 8(9), 10854–10860 (2015).

41 Oh WJ, Endale M, Park S, Cho JY, Rhee MH. Dual roles of quercetin in platelets: phosphoinositide-3-kinase and MAP kinases inhibition, and cAMP-dependent vasodilator-stimulated phosphoprotein stimulation. *Evid. Based Complement. Alternat. Med.* 2012, 485262 (2012).

42 Gardi C, Bauerova K, Stringa B *et al.* Quercetin reduced inflammation and increased antioxidant defense in rat adjuvant arthritis. *Arch. Biochem. Biophys.* 583, 150–157 (2015).

•• **animal models in which utility of Qu, such as therapeutic agent, has been validated.**

43 Hille R. Molybdenum-containing hydroxylases. *Arch. Biochem. Biophys.* 433, 107–116 (2005).

44 Cao H, Pauff JM, Hill R. X-ray crystal structure of a xanthine oxidase complex with the flavonoid inhibitor quercetin. *J. Nat. Prod.* 77, 1693–1699 (2014).

45 Chibli LA, Rodrigues KCM, Gasparetto CM. Anti-inflammatory effects of *Bryophyllum pinnatum* (Lam.) Oken ethanol extract in acute and chronic cutaneous inflammation. *J. Ethnopharmacol.* 154, 330–338 (2014).

46 Hämäläinen M, Nieminen R, Vuorela P, Heinonen M, Moilanen E. Anti-inflammatory effects of flavonoids: genistein, kaempferol, quercetin and daidzein inhibit STAT-1 and NF-κB activations, whereas flavone, isorhamnetin, naringenin and pelargonidin inhibit only NF-κB activation along with their inhibitory effect on iNOS expression and NO production in activated macrophages. *Mediators Inflamm.* 2007, 45673 (2007).

47 Boesch-Saadatmandi C, Loboda A, Wagner AE *et al.* Effect of quercetin and its metabolites isorhamnetin and quercetin-3-glucuronide on inflammatory gene expression: role of miR-155. *J. Nutr. Biochem.* 22, 293–299 (2011).

48 Byun E, Yang M, Choi H *et al.* Quercetin negatively regulates TLR4 signaling induced by lipopolysaccharide through Tollip expression. *Biochem. Biophys. Res. Commun.* 431 (4), 698–705 (2013).

49 Li X, Liu H, Yao Q, Xu B, Zhang S, Tu C. Quercetin protects mice from ConA-induced hepatitis by inhibiting HMGB1–TLR expression and down-regulating the nuclear factor Kappa B pathway. *Inflammation* 39(1), 96–106 (2016).

50 Ma JQ, Li Z, Xie WR, Liu CM, Liu SS. Quercetin protects mouse liver against CCl 4-induced inflammation by the TLR2/4 and MAPK/NF-κB pathway. *Int. Immunopharmacol.* 28(1), 531–539 (2015).

•• **Inflammation models that highlighted the positive effect of Qu.**

51 Askari G, Ghiasvand R, Feizi A, Ghanadian SM, Karimian J. The effect of quercetin supplementation on selected markers of inflammation and oxidative stress. *J. Res. Med. Sci.* 17(7), 637–641 (2012).

52 Calabriso N, Scoditti E, Massaro M *et al.* Multiple anti-inflammatory and anti-atherosclerotic properties of red wine polyphenolic extracts: differential role of hydroxycinnamic acids, flavonols and stilbenes on endothelial inflammatory gene expression. *Eur. J. Nutr.* 55(2), 477–489 (2016).

53 Begum R, Sharma M, Pillai KK, Aeri V, Sheliya MA. Inhibitory effect of Careya arborea on inflammatory biomarkers in carrageenan-induced inflammation. *Pharm. Biol.* 53(3), 437–445 (2015).

54 Bahadır Acikara Ö, Hošek J, Babula P. Turkish *Scorzonera* species extracts attenuate cytokine secretion via inhibition of NF-κB activation, showing anti-inflammatory effect *in vitro*. *Molecules* 21(1), E43 (2015).

55 Nair V, Young Bang W, Schreckinger E, Andarwulan N, Cisneros-Zevallos L. Protective role of ternatin anthocyanins and quercetin glycosides from butterfly pea (*Clitoria ternatea Leguminosae*) blue flower petals against lipopolysaccharide (LPS)-induced inflammation in macrophage cells. *J. Agric. Food Chem.* 63, 6355–6365 (2015).

56 Hsu C, Fang S, Yen G. Anti-inflammatory effects of phenolic compounds isolated from the flowers of *Nymphaea mexicana* Zucc. *Food Funct.* 4, 1216–1222 (2013).

57 Marimoutou M, Le Sage F, Smadja J, Lefebvre d'Hellencourt C, Gonthier M, Robert-Da Silva C. Antioxidant polyphenol-rich extracts from the medicinal plants *Antirhea borbonica*, *Doratoxylon apetalum* and *Gouania mauritiana* protect 3T3-L1 preadipocytes against H2O2, TNFα and LPS inflammatory mediators by regulating the expression of superoxide dismutase and NF-κB genes. *J. Inflamm. (Lond.)* 12, 10 (2015).

58 Kim HH, Kim DH, Kim MH *et al.* Flavonoid constituents in the leaves of *Myrica rubra* sieb. et zucc. with anti-inflammatory activity. *Arch. Pharm. Res.* 36(12), 1533–1540 (2013).

59 Espley RV, Hellens RP, Putterill J, Stevenson DE, Kutty-Amma S, Allan AC. Red colouration in apple fruit is due to the activity of the MYB transcription factor, MdMYB10. *Plant J.* 49, 414–427 (2007).

60 Allan AC, Hellens RP, Laing WA. MYB transcription factors that colour our fruit. *Trends Plant Sci.* 13, 99–102 (2008).

61 Espley R.V., Butts C.A., Laing W.A. Dietary flavonoids from modified apple reduce inflammation markers and modulate gut microbiota in mice. *J. Nutr.* 144, 146–154 (2014).

62 Joo M, Kim HS, Kwon TH *et al.* Anti-inflammatory effects of flavonoids on TNBS-induced colitis of rats. *Korean J. Physiol. Pharmacol.* 19, 43–50 (2015).

63 Fotso Fotso A, Longo F, Dzeufiet Djomeni PD *et al.* Analgesic and antiinflammatory activities of the ethyl acetate fraction of *Bidens pilosa* (Asteraceae). *Inflammopharmacology* 22, 105–114 (2014).

64 Seo K, Yang JH, Kim SC, Ki SH, Shin SM. The antioxidant effects of isorhamnetin contribute to inhibit COX-2 expression in response to inflammation: a potential role of HO-1. *Inflammation* 37(3), 712–722 (2014).

65 Yang JH, Shin BY, Han JY *et al.* Isorhamnetin protects against oxidative stress by activating Nrf2 and inducing the expression of its target genes. *Toxicol. Appl. Pharm.* 274(2), 293–301 (2014).

66 Chirumbolo S. Anti-inflammatory action of isorhamnetin. *Inflammation* 37(4), 1200–1201 (2014).

67 Cheon S, Chung K, Jeon E, Nugroho A, Park H, An H. Anti-inflammatory activity of saxifragin via inhibition of NF-κB involves caspase-1 activation. *J. Nat. Prod.* 78 (7), 1579–1585 (2015).

68 Ku S, Kwak S, Kwon O, Bae J. Hyperoside inhibits high-glucose-induced vascular inflammation *in vitro* and *in vivo*. *Inflammation* 37(5), 1389–1400 (2014).

69 Wu J, Xu X, Li Y *et al.* Quercetin, luteolin and epigallocatechin gallate alleviate TXNIP and NLRP3-mediated inflammation and apoptosis with regulation of

AMPK in endothelial cells. *Eur. J. Pharm.* 745, 59–68 (2014).

70 Vazquez Prieto MA, Bettaieb A, Rodriguez Lanzi C *et al.* Catechin and quercetin attenuate adipose inflammation in fructose-fed rats and 3T3-L1 adipocytes. *Mol. Nutr. Food Res.* 59(4), 622–633 (2015).

71 Guo X, Zhang D, Gao X *et al.* Quercetin and quercetin-3-*O*-glucuronide are equally effective in ameliorating endothelial insulin resistance through inhibition of reactive oxygen species-associated inflammation. *Mol. Nutr. Food Res.* 57, 1037–1045 (2013).

72 Cavalcanti E, Vadrucci E, Delvecchio FR *et al.* Administration of reconstituted polyphenol oil bodies efficiently suppresses dendritic cell inflammatory pathways and acute intestinal inflammation. *PLoS ONE* 9(2), e88898 (2014).

73 Karuppagounder V, Arumugan S, Thandavarayan RA, Sreedhar R, Giridharan VV, Watanabe K. Molecular targets of quercetin with anti-inflammatory properties in atopic dermatitis. *Drug Discov. Today* 21(4), 632–639 (2016).

74 Bi L, Wehrung D, Oyewumi MO. Contributory roles of innate properties of cetyl alcohol/gelucire nanoparticles to antioxidant and anti-inflammation activities of quercetin. *Drug Deliv. Transl. Res.* 3, 318–329 (2013).

75 Caddeo C, Díez-Sales O, Pons R, Fernàndez-Busquets X, Fadda A Ma, Manconi M. Topical anti-inflammatory potential of quercetin in lipid-based nanosystems: *in vivo* and *in vitro* evaluation. *Pharm. Res.* 31(4), 959–968 (2014).

76 Huang W, Tsai T, Huang C *et al.* Inhibitory effects of wild bitter melon leaf extract on *Propionibacterium acnes*-induced skin inflammation in mice and cytokine production in vitro *Food Funct.* 6(8), 2550–2560 (2015).

77 Liao Y, Lin J. Quercetin intraperitoneal administration ameliorates lipopolysaccharide-induced systemic inflammation in mice. *Life Sci.* 137, 89–97 (2015).

78 Dou W, Zhang J, Li H. Plant flavonol isorhamnetin attenuates chemically induced inflammatory bowel disease via a PXR-dependent pathway. *J. Nutr. Biochem.* 25(9), 923–933 (2014).

79 Sekhon-Loodu S, Ziaullah Z, Rupasinghe HPV, Wang Y, Kulka M, Shahidi F. Novel quercetin-3-*O*-glucoside eicosapentaenoic acid ester ameliorates inflammation and hyperlipidemia. *Inflammopharmacology* 23(4), 173–185 (2015).

•• **Employment of natural extract fractions, containing Qu, obtained from different sources and their implications such as therapeutic agents.**

80 Zou W, Liu W, Yang B *et al.* Quercetin protects against perfluorooctanoic acid-induced liver injury by attenuating oxidative stress and inflammatory response in mice. *Int. Immunopharmacol.* 28(1) 129–135 (2015).

81 Huang R, Zhong T, Wu H. Quercetin protects against lipopolysaccharide-induced acute lung injury in rats through suppression of inflammation and oxidative stress. *Arch. Med. Sci.* 11(2), 427–432 (2015).

82 Liu C, Ma J, Xie W *et al.* Quercetin protects mouse liver against nickel-induced DNA methylation and inflammation associated with the Nrf2/HO-1 and p38/STAT1/NF-κB pathway. *Food Chem. Toxicol.* 82, 19–26 (2015).

83 Günay E, Celik S, Sarinc-Ulasli S *et al.* Comparison of the anti-inflammatory effects of Proanthocyanidin, Quercetin and Damnacanthal on Benzo (a) pyrene exposed A549 alveolar cell line. *Inflammation* 39(2), 744–751 (2016).

84 Wang J, Miao M, Zhang Y *et al.* Quercetin ameliorates liver injury induced with *Tripterygium glycosides* by reducing oxidative stress and inflammation. *Can. J. Physiol. Pharmacol.* 93, 1–7 (2015).

85 Hytti M, Piippo N, Salminen A, Honkakoski P, Kaarniranta K, Kauppinen A. Quercetin alleviates 4-hydroxynonenal-induced cytotoxicity and inflammation in ARPE-19 cells. *Exp. Eye Res.* 132, 208–215 (2015).

•• **Other experimental models in which isolated Qu showed interesting biological activities, and confirming its utility in therapy.**

86 Olanow CW, Tatton WG. Etiology and pathogenesis of Parkinson's disease. *Annu. Rev. Neurosci.* 22, 123–144 (1999).

87 Davis JM, Murphy EA, Carmichael MD, Davis B. Quercetin increases brain and muscle mitochondrial biogenesis and exercise tolerance. *Am. J. Physiol. Regul. Integr. Comp. Physiol.* 296, R1071–R1077 (2009).

88 Dajas F, Abin-Carriquiry JA, Arredondo F *et al.* Quercetin in brain diseases: potential and limits. *Neurochem. Int.* 89, 140–148 (2015).

89 Jiang W, Huang Y, Han N *et al.* Quercetin suppresses NLRP3 inflammasome activation and attenuates histopathology in a rat model of spinal cord injury. *Spinal Cord.* 54, 592–596 (2016).

90 Kumar P, Choonara YE, Modi G, Naidoo D, Pillay V. Cur (Que) min: a neuroactive permutation of curcumin and quercetin for treating spinal cord injury. *Med. Hypotheses* 82(4), 437–441 (2014).

91 Kao TK, Ou YC, Raung SL, Lai CY, Liao SL, Chen CJ. Inhibition of nitric oxide production by quercetin in endotoxin/cytokine-stimulated microglia. *Life Sci.* 86, 315–321 (2010).

92 Mrvová N, Škandík M, Kuniaková M, Račková L. Modulation of BV-2 microglia functions by novel quercetin pivaloyl ester. *Neurochem. Int.* 90, 246–254 (2015).

93 Ishisakaa A, Mukaib R, Teraob J, Shibatac N, Kawai Y. Specific localization of quercetin-3-*O*-glucuronide in human brain. *Arch. Biochem. Biophys.* 557, 11–17 (2014).

94 Elberry AA, Mufti S, Al-Maghrabi J *et al.* Immunomodulatory effect of red onion (*Allium* cepa Linn) scale extract on experimentally induced atypical prostatic hyperplasia in Wistar rats. *Mediators Inflamm.* 2014, 640746 (2014).

95 Aiello F, Carullo G, Badolato M, Brizzi A. TRPV1–FAAH–COX: the couples game in pain treatment. *ChemMedChem* 11, 1686–1694 (2016).

96 Malek N, Starowicz K. Dual-acting compounds targeting endocannabinoid and endovanilloid systems – a novel treatment option for chronic pain management. *Front. Pharmacol.* 7, 257 (2016).

97 Cechinel Filho V, Santos AR, De Campos RO *et al.* Chemical and pharmacological studies of *Phyllanthus*

caroliniensis in mice. *J. Pharm. Pharmacol.* 48, 1231–1236 (1996).

98 Anjaneyulu M, Chopra K. Quercetin attenuates thermal hyperalgesia and cold allodynia in STZ-induced diabetic rats. *Indian J. Exp. Biol.* 42, 766–769 (2004).

99 Comalada M, Camuesco D, Sierram S *et al. In vivo* quercitrin anti-inflammatory effect involves release of quercetin, which inhibits inflammation through down-regulation of the NF-kappaB pathway. *Eur. J. Immunol.* 35, 584–592 (2005).

100 Çivi S, Emmez G, Dere ÜA, Börcek AÖ, Emmez H. Effects of quercetin on chronic constriction nerve injury in an experimental rat model. *Acta Neurochir. (Wien)* 158(5), 959–965 (2016).

101 Narenjkar J, Roghani M, Alambeygi H, Sedaghati F. The effect of the flavonoid quercetin on pain sensation in diabetic rats. *BCN* 2(3), 51–57 (2011).

102 Anjaneyulu M, Chopra K. Quercetin, a bioflavonoid, attenuates thermal hyperalgesia in a mouse model of diabetic neuropathic pain. *Prog. Neuropsychopharmacol. Biol. Psychiatry* 27(6), 1001–1005 (2003).

103 Valério DA, Georgetti SR, Magro DA *et al.* Quercetin reduces inflammatory pain: inhibition of oxidative stress and cytokine production. *J. Nat. Prod.* 72, 1975–1979 (2009).

104 Martínez AL, González-Trujano Ma E, Aguirre-Hernández E *et al.* Antinociceptive activity of *Tilia americana* var. mexicana inflorescences and quercetin in the formalin test and in an arthritic pain model in rats. *Neuropharmacology* 56(2), 564–571 (2009).

105 Anjaneyulu M, Chopra K. Quercetin attenuates thermal hyperalgesia and cold allodynia in STZ-induced diabetic rats. *Indian J. Exp. Biol.* 42(8), 766–769 (2004).

106 Kaur R, Singh D, Chopra K. Participation of α 2 receptors in the antinociceptive activity of Quercetin. *J. Med. Food* 8(4), 529–532 (2005).

107 Filho AW, Filho VC, Olinger L, de Souza MM. Quercetin: further investigation of its antinociceptive properties and mechanisms of action. *Arch. Pharm. Res.* 31(6), 713–721 (2008).

108 Raygude KS, Kandhare AD, Ghosh P, Ghule AE, Bodhankar SL. Evaluation of ameliorative effect of quercetin in experimental model of alcoholic neuropathy in rats. *Inflammopharmacology* 20, 331–341 (2012).

109 Calixto-Campos C, Corrêa MP, Carvalho TT *et al.* Quercetin reduces Ehrlich tumor-induced cancer pain in mice. *Anal. Cell. Pathol. (Amst.).* 2015, 285708 (2015).

•• **Qu involvement in pain and other neurological diseases. Discussion about emerging targets.**